Synthesis of Tubular, Belt-like and Möbius Aromatics

Von der Gemeinsamen Naturwissenschaftlichen Fakultät

der Technischen Universität Carolo-Wilhelmina

Zu Braunschweig

Zur Erlangung des Grades eines

Doktors der Naturwissenschaften

(Dr.rer.nat.)

genehmigte

Dissertation

Von

Dariush Ajami

Aus Teheran

1. Referent: Prof. Dr. Rainer Herges

2. Referent: Prof. Dr. Henning Hopf

eingereicht am: 17. October 2003

Mündliche Prüfung (Disputation) am: 07. November 2003

To my parents and Mina

Danksagung

Mein besonderer Dank für die sehr angenehme und konstruktive Atmosphäre gilt meinem Doktorvater Prof. Dr. Rainer Herges. Er hat mich während der gesamten Arbeit stets mit Interesse, Anregungen und einem immer offenen Ohr unterstützt.

Meinen Arbeitskreiskollegen Dr. Torsten Winkler, Dr. Markus Diechmann, Felix Köhler, Dr. Anke Krüger, Regina Meinlschmeit, Birtta Harbaum, Kirsten Hess, Katrin Schluze, Dietmund Peters, Monika Bayerhuber, Jan Clausen, Jörg Taubitz gebührt mein Dank für die sehr freundschaftliche Zusammenarbeit.

Beim technischen Personal in Braunschweig und Kiel möchte ich mich für die Bereitstellung der Chemikalien, die Herstellung von Glasgeräten und die Messung zahlreicher Spektren bedanken.

1. Introduction

Since the discovery of the fullerenes in 1985[1] and the generation of carbon nanotubes by Iijima in 1991[2], the synthesis of the fully conjugated non-planar hydrocarbons gained tremendous interest. The fullerenes as well as the nanotubes, so far, are prepared at very high temperatures. Under these crude conditions a number of different structures (different diameter, length, helicity etc) are formed alongside with amorphous carbon. In case of the fullerenes efficient separation techniques made it possible to isolate C_{60} and C_{70} in larger amounts and high purity, however, the purification of carbon nanotubes is still a distant prospect (except on the molecular level by single molecule manipulation in an AFM device).

The rational synthesis of carbon nanotubes obtain uniform structures with well defined physical properties is considered to be one of the "holy grails" of nanotechnology[3]. The present work is aimed at taking the first steps toward this ambitious goal.

1.1. History of Aromaticity

Fullerenes and carbon nanotubes are aromatic compounds. Aromaticity is also an important property of the belt-like compounds, which are the targets of the present study. Therefore, a short history of the development of this concept is given below:

1825 Isolation of benzene (Faraday)[4]

1865 Benzene structure (Kekule)[5]

1866 Substitution is more favourable than addition (Erlenmeyer)[6]

1910 Aromatic compounds have exalted diamagnetic susceptibilities (Pascal)[7]

1925 Electron sextet and heteroaromaticity (Armit-Robinson)[8]

1931 Theory of cyclic (4n+2)π systems (Hückel)[9]

1936 Ring current theory, free electron circulation around the benzene ring (Pauling)[10]

1937 London diamagnetism π electron current contribution to the magnetic susceptibility[11]

1956 Ring currents effects on NMR chemical shifts (Pople)[12]

1964 Möbius type conformation of annulenes (Heilbronner)[13]

1969 Modern study of diamagnetic susceptibility exaltation (Dauben)[14]

1970 Magnetic susceptibility anisotropy (Flygare)[15]

1980 IGLO quantum chemical calculation of magnetic properties: chemical shifts, magnetic susceptibilities and magnetic susceptibility anisotropies (Kutzelnigg)[16]

1985 Discovery of buckminsterfullerene, spherical aromaticity (Curl, Kyoto, Smalley)[1]

1991 Discovery of nanotubes, in-plane aromaticity (Iijima)[2]

1996 Nucleus independent chemical shifts (Schleyer)[17]

2001 Anisotropy of the induced current density (Herges)[18]

The discovery of extraordinary aromatic compounds, like fullerens and nanotubes, and their application made this area of organic chemistry, very attractive and more importantly, encouraged chemists to have wider imagination about hydrocarbon chemistry. For the design of molecular machines and their application, material scientists need a new generation of compounds. The synthesis of aromatic compounds with new topologies is one of the most promising opportunities to bring nanomachines to reality.

1.2. Spherical Aromatic Compounds

The fullerenes form a unique class of molecules containing a spherical conjugated π system. Each fullerene represents a closed network of fused hexagons and pentagons. Are fullerenes aromatic? Magnetic and NMR properties are probably the most general indicators for aromaticity, and the wealth of accumulated data clearly demonstrates that extensive cyclic delocalisation of π electrons is present in fullerenes[19]. However, complete 3D aromaticity extending over all 5- and 6-rings is not observed in neutral buckminsterfullerene C_{60}. The outer shell of electrons is incompletely filled resulting in paratropic ring current in the 5-ring (weakly antiaromatic) and a diatropic ring current in the 6-rings (aromatic). In order to completely fill the π shell, $2(N+1)^2$ electrons are necessary, which means C_{60}^{+10} (N=4) with 50 π electrons and C_{60}^{-12} (N=5) with 72 π electrons are the most aromatic C_{60} species.

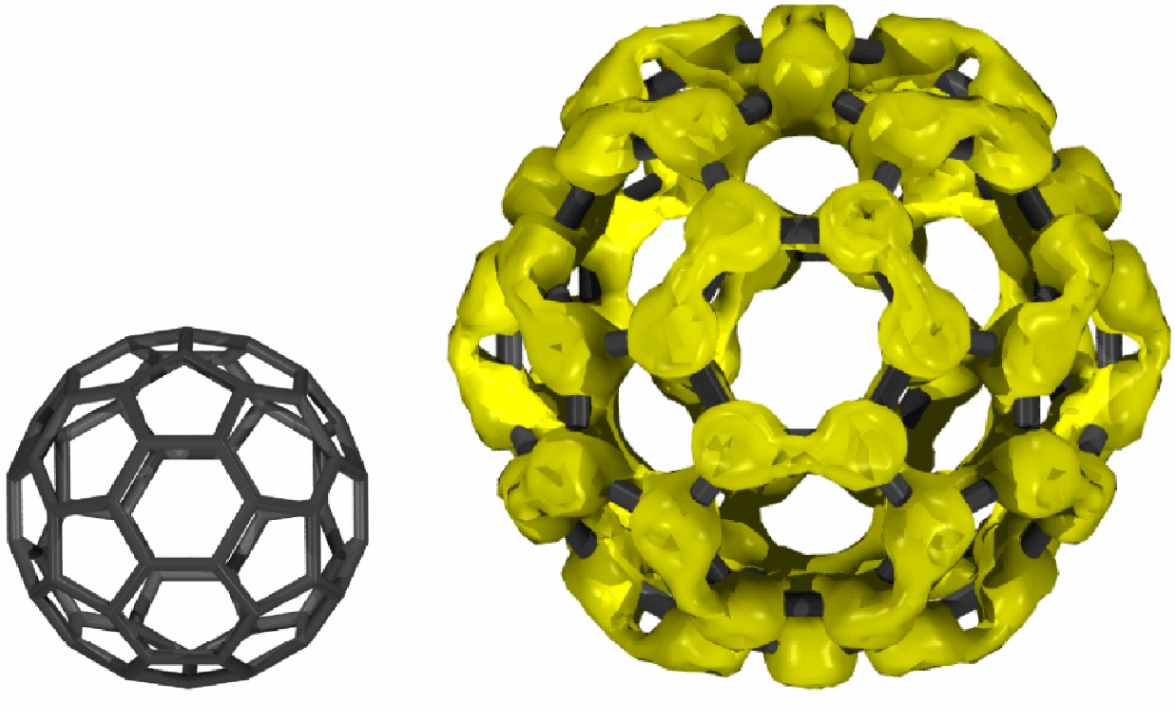

Figure 1: Buckminsterfullerene C_{60} and ACID plot of C_{60}.

Doubtlessly C_{60} and C_{70} are highlights in recent organic chemistry, however their potential of application lacks behind the beauty of their structure[20]. Under carefully controlled conditions, the vaporization of graphite generates substantial amounts of

C_{60} and C_{70}[21]. Higher fullerenes can be obtained from this source only in miniscale amounts through tedious chromatographic separations[22].

Recently Scott and coworkers[23] for first time published a rational synthesis of C60 in 12 steps (Scheme **1**)

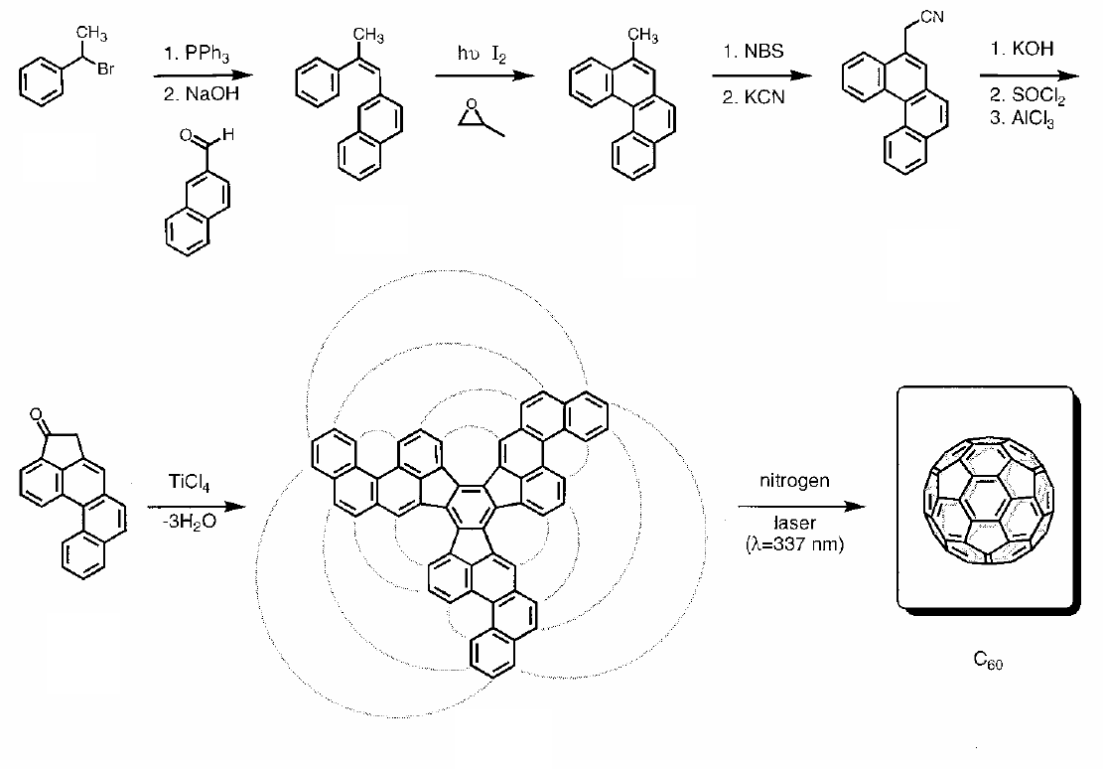

Scheme 1: Scott's rational synthesis of C_{60}

Despite the fact that the yield was lower than one percent, Scott's achievement is a remarkable point in the history of fullerenes, in which organic chemists, rather than physicists, might now take the lead in synthesizing novel fullerenes.

1.3 Tubular and Belt-like Aromatic Compounds

1.3.1 Nanotubes

In 1991, Iijima discovered long, thin cylinders of carbon, dubbed carbon nanotube in a Krätschmer/Huffman fullerene reactor. Carbon nanotubes are unique for their size, shape and remarkable physical properties and can be viewed as a sheet of graphite (a hexagonal lattice of carbon) rolled into a cylinder. These intriguing structures have sparked much excitement in the recent years and a large amount of research has been

dedicated to their synthesis and the investigation of their properties. Some milestones are:

1991 Discovery of multi-wall carbon nanotubes.

1992 Conductivity of carbon nanotubes[24].

1993 Structural rigidity of carbon nanotubes[25].

1993 Synthesis of single-wall nanotubes[26].

1995 Nanotubes as field emitters[27].

1996 Ropes of single-wall nanotubes[28].

1997 Quantum conductance of carbon nanotubes[29].

1997 Attempt to storage hydrogen in nanotubes[30].

1998 Chemical Vapour Deposition synthesis of aligned nanotube films[31].

1998 Synthesis of nanotube peapods[32].

2000 Thermal conductivity of nanotubes[33].

2000 Macroscopically aligned nanotubes[34].

2001 Integration of carbon nanotubes in logic circuits[35].

2001 Intrinsic superconductivity of carbon nanotubes[36].

2002 Synthesis of single-walled carbon nanotube with 4Å diameter[37].

1.3.1.1 Straight nanotubes

It is possible to construct cylinder by rolling up a hexagonal ghraphene sheet in different ways. Two of these are ''non helical'' and termed as ''armchair'' and ''zig-zag''. In the armchair structure, two C-C bonds on opposite sides of each hexagon are perpendicular to the tube axis, whereas in the zig-zag arrangement, these bonds are parallel to the tube axis (Fig. **2**a,b). In all other conformations, all C-C bonds lie at an angle (≠0 and ≠90°) to the tube axis and a helical structure results (Fig. **2**c,d)

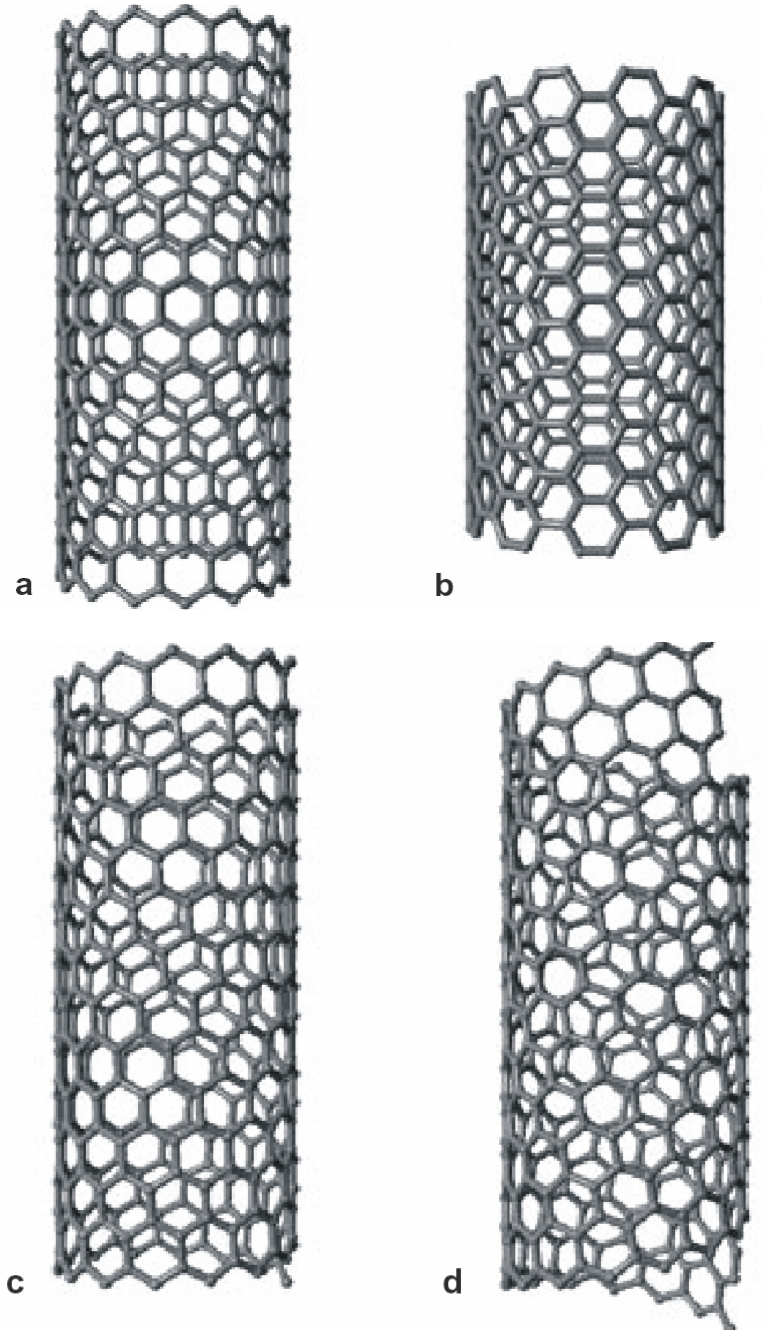

Figure 2: Molecular models of single-walled nanotubes with different helicities: **a** zig-zag arrangement, **b**-armchair configuration, **c,d**, two different helicities.

1.3.1.2 Helix-shaped and Hemitoroidal nanotube

It is possible to ''curl'' and ''twist''' graphite by the introduction of pentagon and heptagon pairs into the hexagonal graphite network. Helicoidal and toroidal nanotubes including 5- and 7- membered carbon rings were predicted theoretically and later, experimental evidence for their existence was obtained[38]. Hemitroroidal nanotube tips have been produced by passage of an arc between graphite rods.

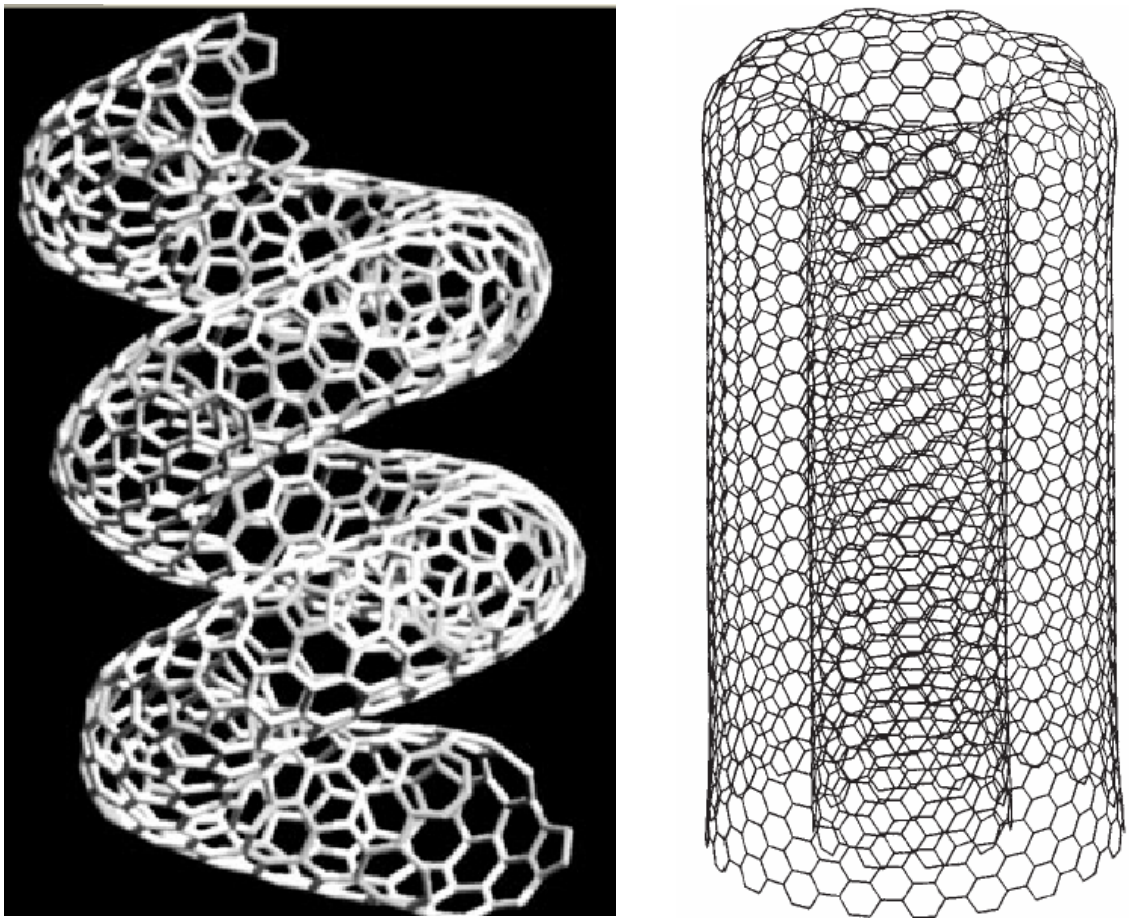

Figure 3: a helcoidal graphite, **b** a molecular model of a hemi-toroidal nanotubes cap.

Nowadays, carbon nanotubes can be produced by diverse techniques such as arc discharge[39], pyrolysis of hydrocarbons over catalysts[40], laser vaporisation of graphite[41], and by electrolysis of metal salts using graphite electrodes[42]. The products exhibit various morphologies (e.g. straight, curled, hemitoroidal, branched, spiral, helix-shaped, etc.). Carbon nanotubes behave as metallic, semiconducting or insulating nanowires depending upon their diameter and the angle of the hexagonal pattern with respect to the tube axis (helicity)[43]. However, in order to use such nanotubes or nanorods in commercial applications, it is necessary to control their growth, length, diameter, helicity, aggregation and alignment.

1.3.2 Cyclacenes, Beltenes and Collarenes

In 1983 Vöglte[44] proposed the synthesis of **1**, a molecular belt with a completely aromatic carbon skeleton. The benzenoid nuclei are fused laterally in a polyacene like manner**. 1**(n=12) may be considered as a member of the [n]cyclacenes, which gained increasing interest in the following years.

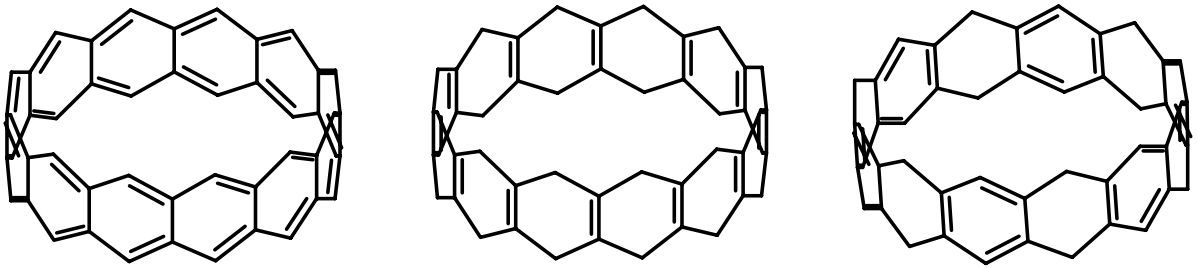

1 **2** **3**

Figure 4: 1 [12] cyclacene, **2** [12] beltene, **3** [12] collarene.

Force field calculations of Alder and Sessions[45] showed that [n]beltenes with n≥6 span a cylindrical cavity which should be suitable for including ions and small molecules. Stoddart et al.[46] put much effort towards the synthesis of the first cyclacene. They used the Diels-Alder reaction of two concave building blocks under a pressure of 9-10 Kbar to form belt-like precursors of **1**-**3**. In spite of their ingenious strategy they only succeeded to synthesize [12]collarene **3**. The full aromatization to furnish **1** failed, probably because of the large strain imposed by the nonplenarity of the benzene rings and the sensitivity towards oxidation which is know for larger acenes.

1.3.3 Picotubes

Herges et al.[47]were able to synthesize a belt– and tube- like fully conjugated molecule **4** , based on the ring enlargement metathesis reaction. The compound was

termed 'picotube' because it is a small and short substructure of the larger carbon nanotubes.

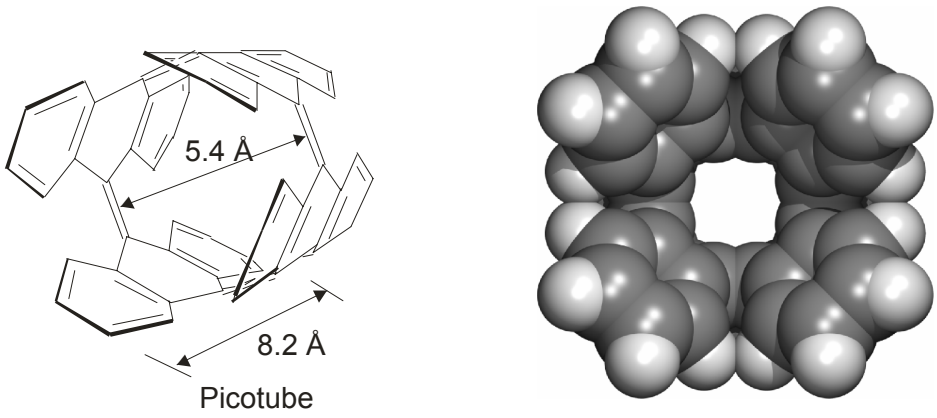

4

Figure 5: Van der Waals surface of the picotube.

Kammermeierphane **5** [48] is another example of a fully conjugated tubular compound with larger cavity.

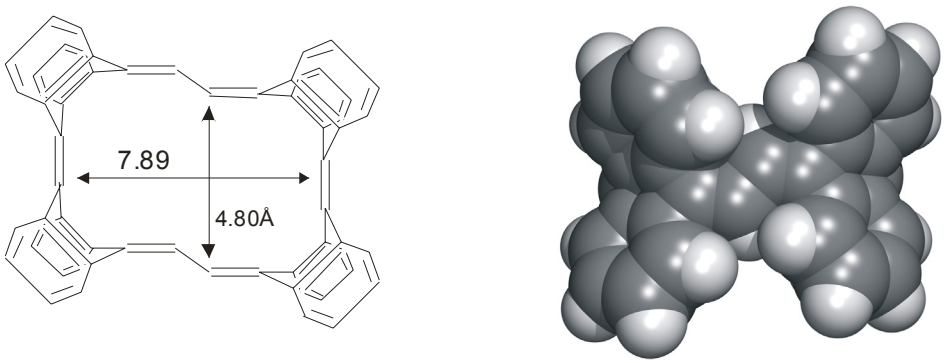

5

Figure 6: Van der Waals surface of Kammermeierphane.

1.3.4 Cylic [n]paraphenylacetylenes

Oda et al. [49]. synthesized other fully conjugated belt-like compounds. [6] and [8]Paraphenylacetylene (Figure **7**) were prepared using McMurry coupling of corresponding precursors.

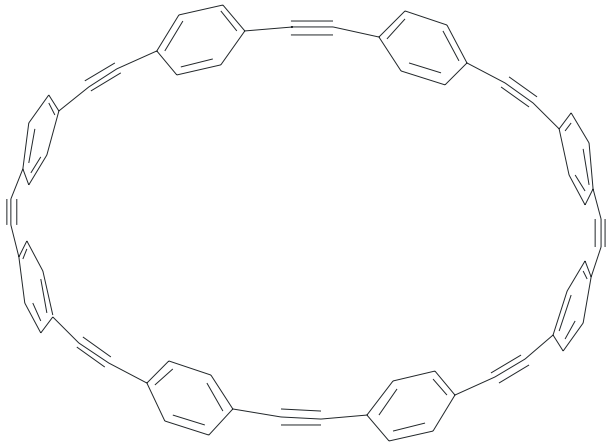

Figure 7: Structure of [8]paraphenylacetylene.

1.3.5 Bowl-shaped Benzoannulenes

Iyoda et al.[50] developed a new synthetic strategy for *all-Z*-tribenzo[12]-, tetrabenzo[16]- and pentabenzo[20] annulenes, based on the pinacol coupling of the corresponding linear poly *cis*-stilbene derivative, followed by the formation of the final *cis*-double bond using reductive dehydroxylation.

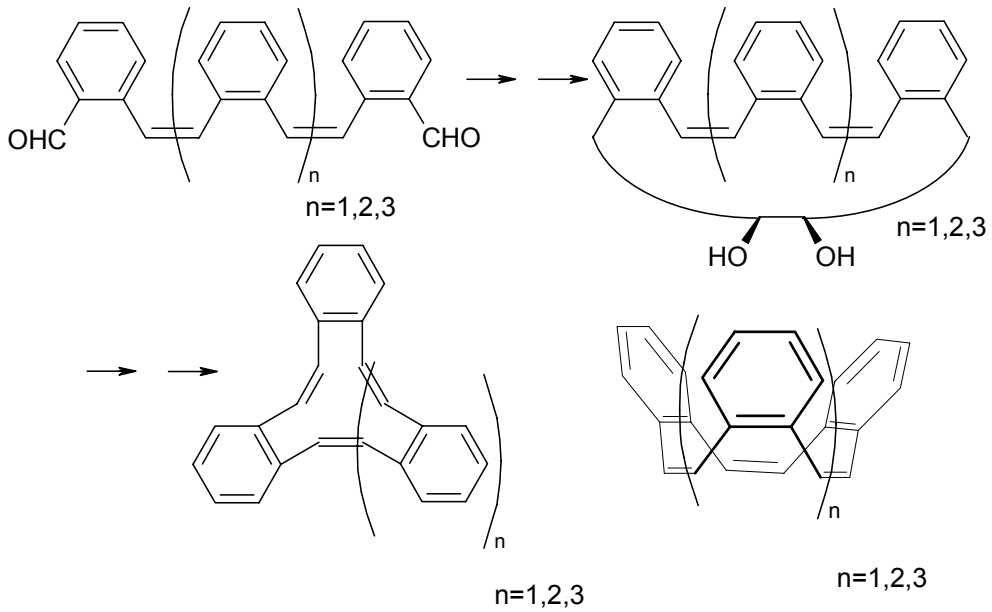

Scheme 2: Synthesis strategy of *all-Z*-tribenzo[12]-, tetrabenzo[16]- and pentabenzo[20] annulenes.

1.4 Our approach

A number of applications of carbon nanotubes were discovered during recent years. Depending on the structure (diameter, length and chirality or twist), nanotubes exhibit a very broad range of electronic, thermal and structural properties. The

potential applications spurred material scientists to develop a wide variety of routes to nanotubes, including electric arc or laser vaporization of graphite containing cobalt or other transition metals as catalysts, CVD of carbon rich gases or electrolytic techniques. In all these high temperature methods, nanotubes are generated in different diameter, length and chirality alongside with amorphous carbon and fullerenes. The isolation, purification and separation of nanotubes into samples with well-defined geometries were not achieved to date. Therefore rational synthesis of nanotubes with uniform geometry and thus well-defined properties would be an important advance in nanotechnology.

Our approach towards the rational synthesis of nanotubes is based on the ring enlargement metathesis reaction. Starting material are compounds with at least two

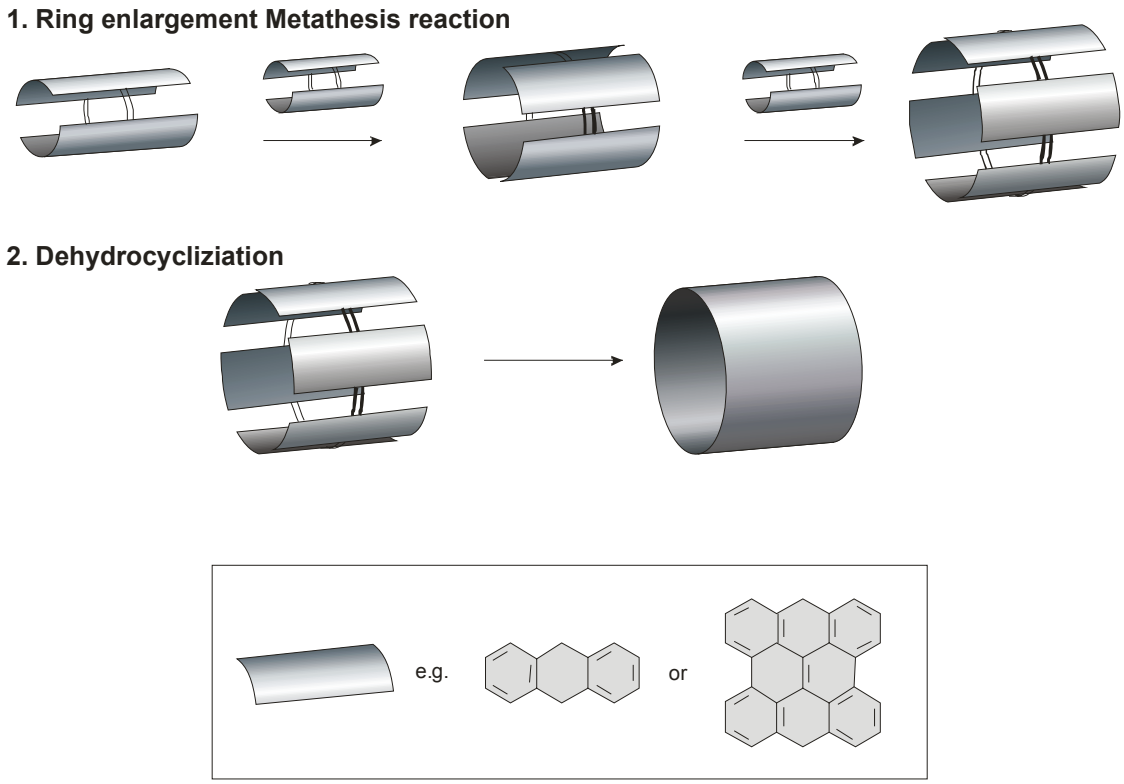

Scheme 3: Our approach toward rational synthesis of nanotubes.

aromatic "plates" (anthracene or naphtobianthrene units in Scheme **3**), which are connected by at least two quinoid double bonds conjugated to the aromatic units. Using ring enlargement metathesis larger cyclic oligomers are formed. In a second independent step the tube walls are closed by cyclodehydration and a short section of a nanotube consisting exclusively of fused benzene rings is formed (Scheme **3**).

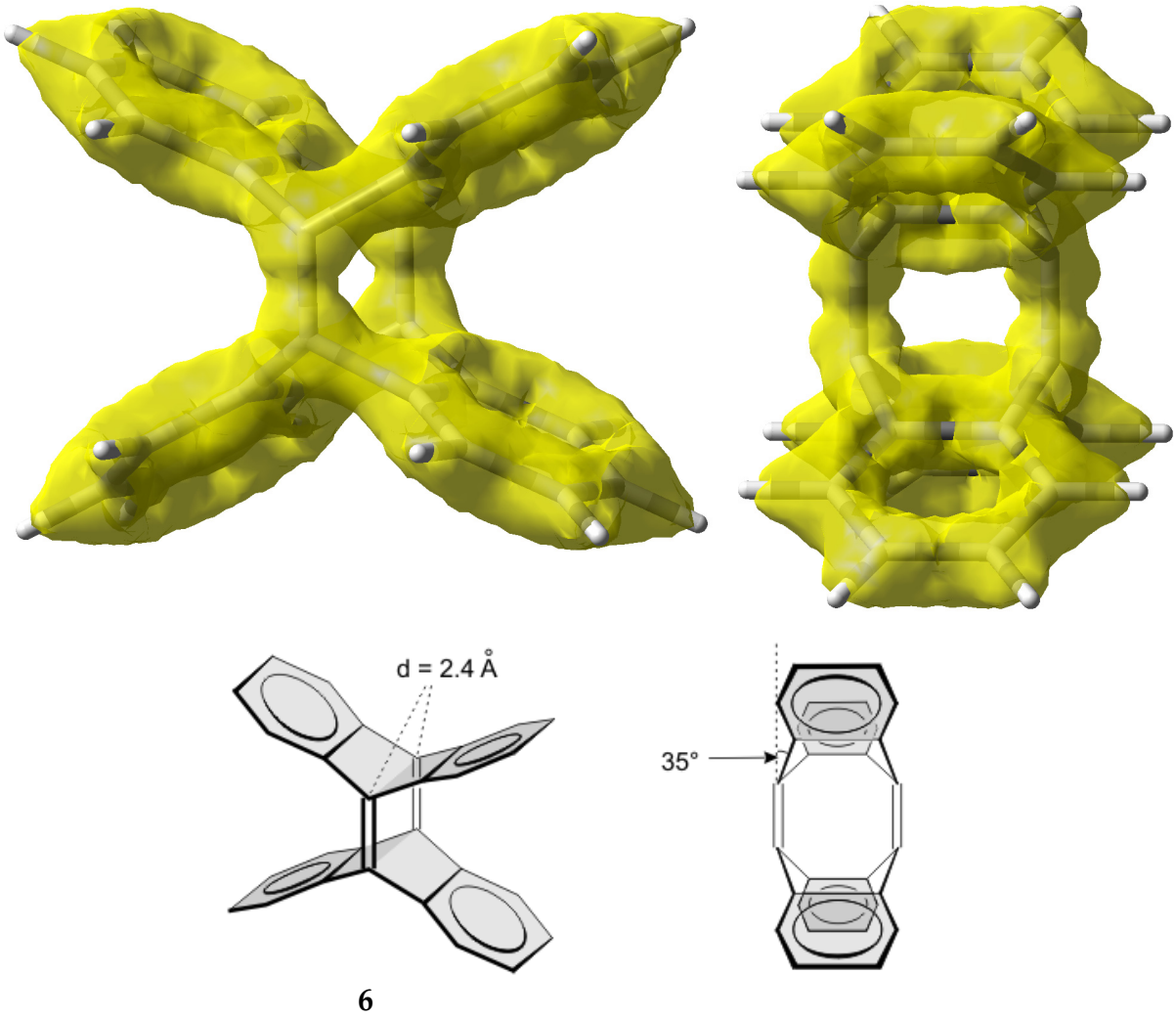

6

Figure 8: ACID plot of TDDA at isosurface value of 0.05. Pyramidalization angle of bridgehead atoms is 35° and two bridgehead double bonds make a distance of 2.4 Å.

Tetradehydrodianthracene (TDDA) **6** has been used as building block for the ring enlargement metathesis reactions. A number of new belt-like and tubular aromatic compounds were constructed by metathesis of highly reactive quinoid bridgehead double bond of TDDA with [n]annulenes or by dimerization reaction of two TDDA

units.(Scheme **4**). Targets of this study are metathesis reactions of TDDA with cyclooctatetraene, dimerization of TDDA dimer 4, to form a cyclic-octaanthracenylidene (Scheme **4**) and finally finding new building blocks to react with TDDA in metathesis reactions.

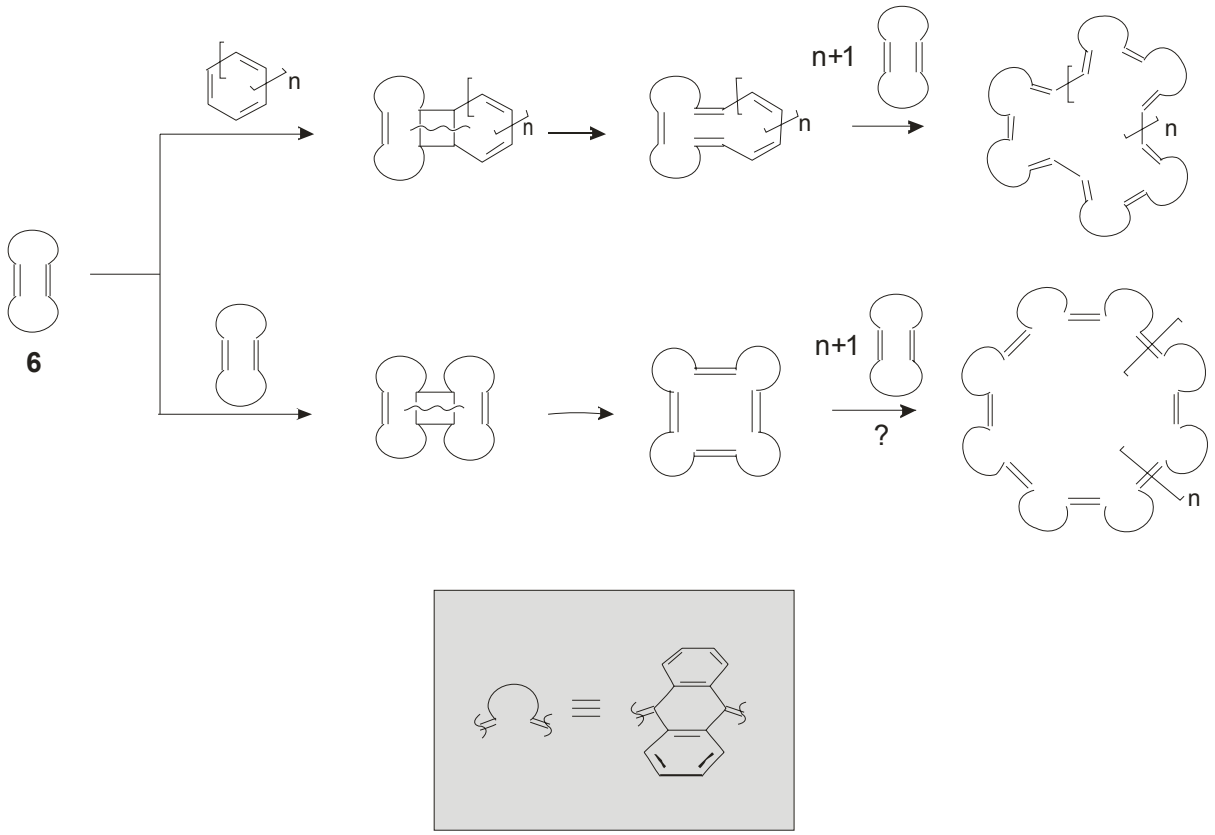

Scheme 4: Molecular unit construction system for the synthesis of molecular belts and tubes. For the sake of simplicity an arc abbreviates the 9,10-anthracenylidene units

2 9,9′,10,10′-Tetradehydrodianthracene (TDDA) as the building block of picotubes syntheses

2.1 Synthesis of TDDA

2.1.1 Greene's synthesis of TDDA

Several research groups[51] tried to synthesize TDDA **6** by HBr elimination of dibromodianthracene with different hindered bases, but they failed because of the high reactivity of the bridgehead double bond towards the base. To overcome this problem, Greene et al.[52] used a sequence of formation, protection and subsequent regeneration of the reactive double bond.

As shown in Scheme **5**, the reactive double bonds were generated by dehydrohalogenation of 9,9′-dibromodianthracene to TDDA and in situ captured with an excess of sodium azide by 1.3-dipolar cycloadditions. In a second step the triazoline was converted to the N-aminotriazoline by Carpino's reagent[53] and in the deprotection step oxidation of the N-amino triazoline with lead tetraacetate yields TDDA.

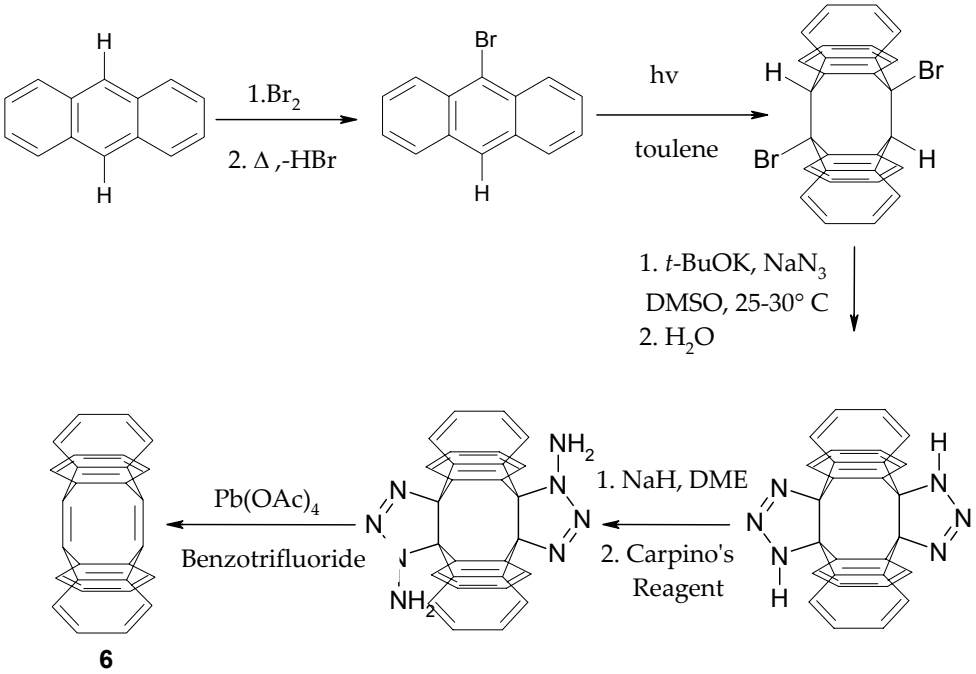

Scheme 5: Greene's synthesis of TDDA.

2.1.2 Neumann's improvement of the TDDA synthesis

In 1993, Neumann et al.[54] optimized the synthesis of TDDA to obtain a higher yield and to be able to work on a larger scale. After monitoring of the azide protection reaction Neumann found that the reaction time should be changed from 2 days to 2 weeks. In the oxidation step, dichloromethane changed with α,α,α trifluorotoluene to prevent solvent addition to TDDA and finally ultrasonic irradiation improved the yield of the last two steps.

2.1.3 Synthesis of *o*-mesitylensulfonylhydroxylamine (Carpino's reagent)

One of the difficult steps in the synthesis of TDDA is the preparation of Carpino's reagent. As shown in Scheme **6**, it is a multistep synthesis and because of its instability, it should be used freshly.[53]

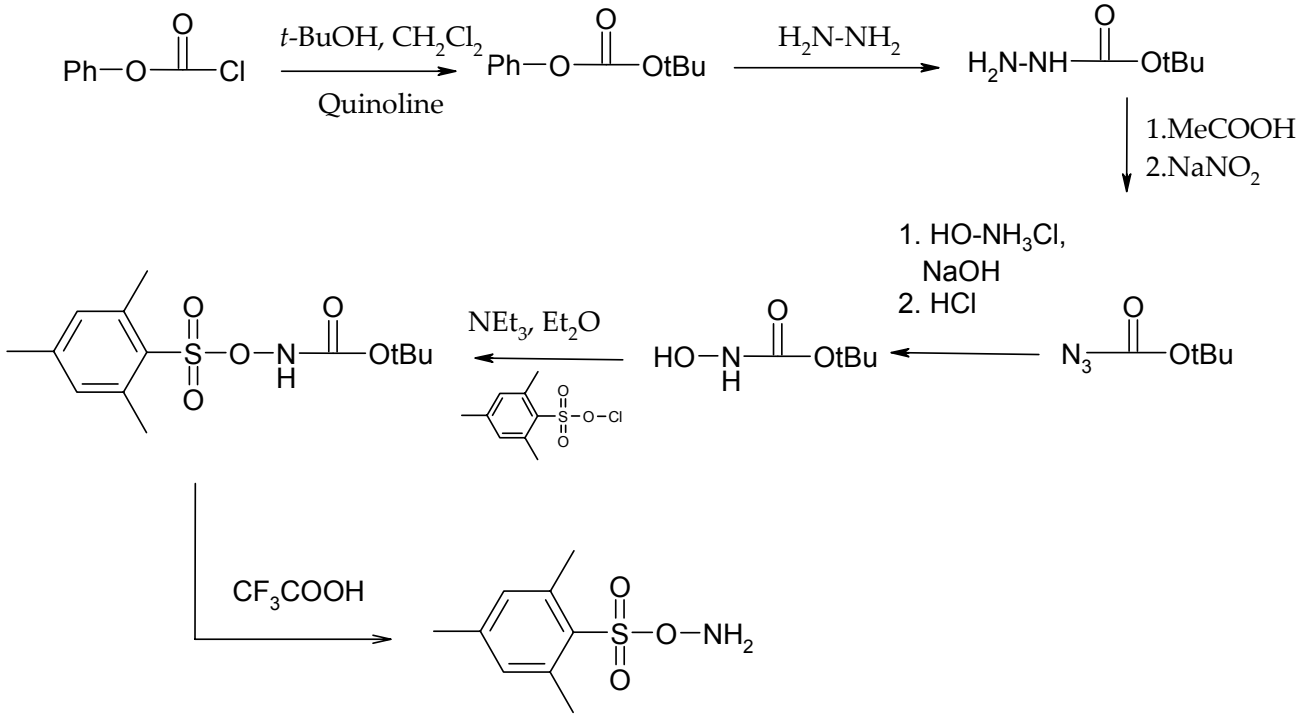

Scheme 6: Synthesis of Carpino's reagent.

Several attempts have made in order to find a shorter synthesis method but all of them failed.

2.2. Characterization

Regarding the structure of TDDA, there are four points of special interest:

(1) The bridgehead carbon-carbon double bond distance (1.35 Å).

(2) Pyramidalization angle of bridgehead atoms (35°).

(3) The distance between the double bonds (2.4 Å), which is considerably smaller than the sum of the van der Waals radii of the corresponding Sp^2 carbon atoms.

(4) The angle between the plane defined by atoms 9,9',10,10' and the plane of each of benzene rings (119,9°), that means poor conjugation between bridgehead double bonds and benzene rings.

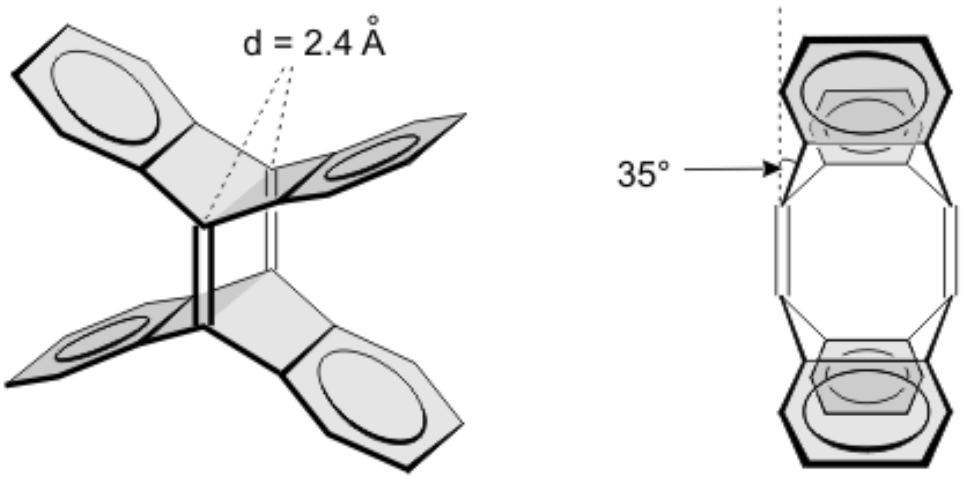

Figure 9: Structure of TDDA.

From simple MO considerations, the following assumptions can be made (Scheme **7**): Through-space interaction leads to a splitting of HOMO and LUMO each in a binding π^+ and antibonding π^- combination Through bond interaction through the benzo bridge raises the energy of the occupied π^+ and lowers the unoccupied π^+ orbitals.[55] The π^- orbital remains almost unchanged. Pyramidalization lowers the LUMO considerably and raises the HOMO.[56] Thus, an enhanced reactivity towards electrophiles and particularly towards nucleophiles can be expected. Additionally, in

Diels-Alder reactions TDDA is more reactive as an electron deficient dienophile than maleic anhydrid[57] and it should react with electron-rich and electron-poor dienes.

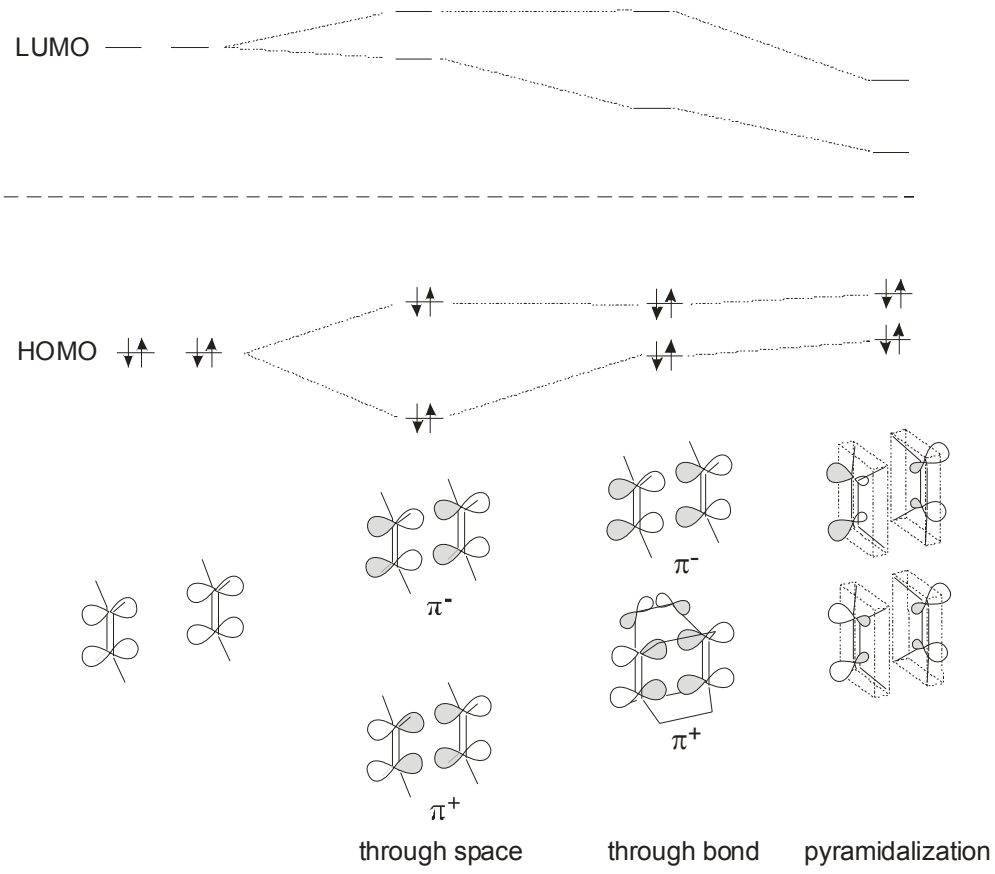

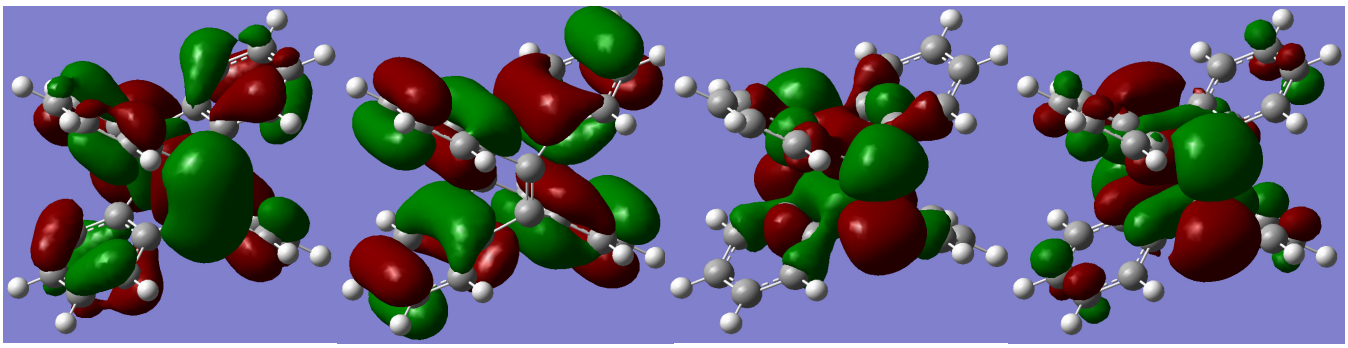

HOMO –1, **HOMO,** **LUMO,** **LUMO+1,**

Scheme 7: Quantitative MO diagram of the olefinic orbitals in TDDA and calculated frontier orbitals (B3LYP/6-31G*).

2.3 Reactivity

2.3.1 Electrophilic addition to TDDA

TDDA reacts with halogens[58] to give transannular (anti) , and ring-opened (syn) products. The product ratio shows a remarkable solvent dependence. Solvents of medium polarity favour anti addition, whereas syn addition is observed both with increasing and decreasing polarity (Scheme **8**).

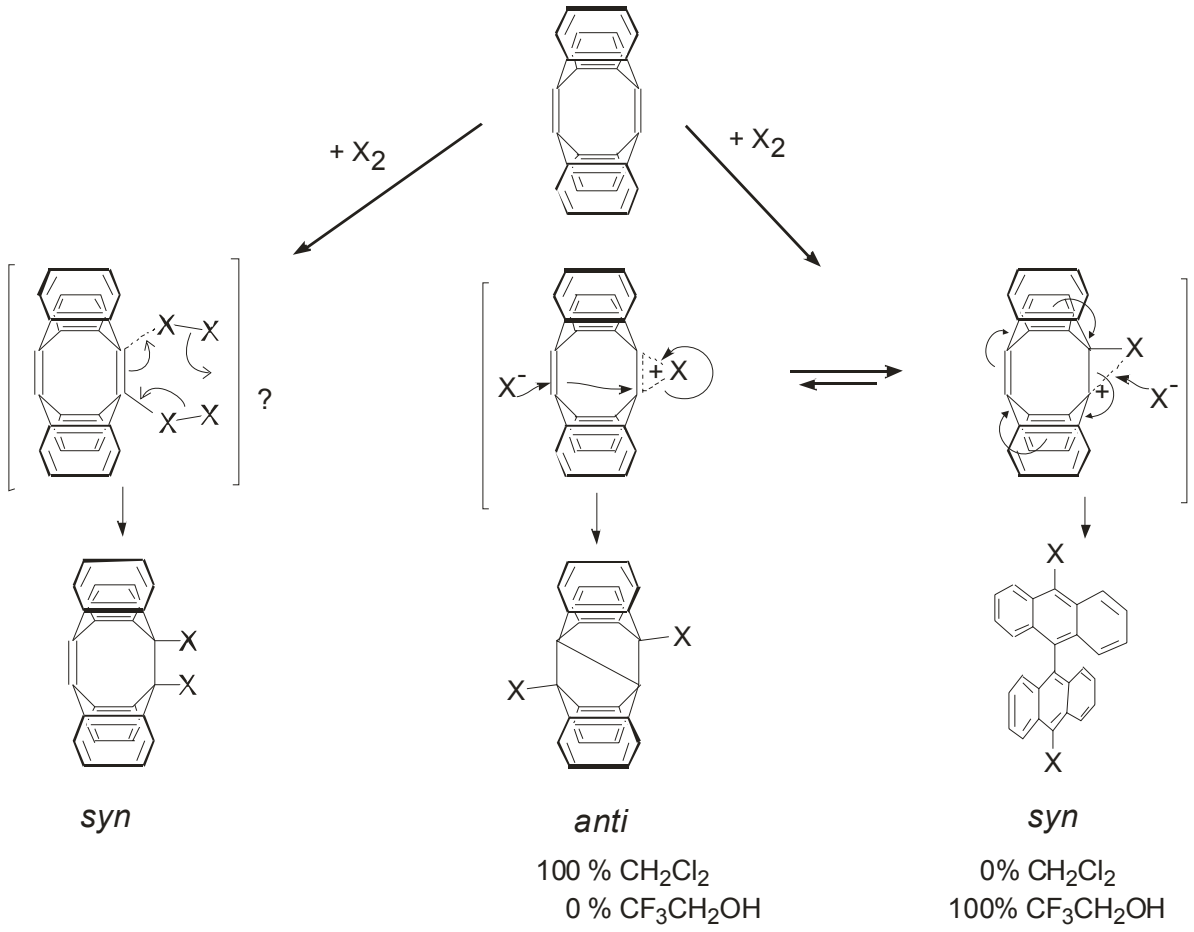

Scheme 8: Electrophilic addition to TDDA.

2.3.2 Nucleophilic addition to TDDA

Olefins that are not activated by electron withdrawing substituents usually do not react with nucleophiles.[59] Even though being a pure hydrocarbon, TDDA readily reacts with nucleophiles such as MeLi at –80° C, because of its peculiar electronic structure. Similar to the electrophilic addition syn and transannular addition

products are formed.[60] The syn products undergo electrocyclic ring opening to yield bianthryls.

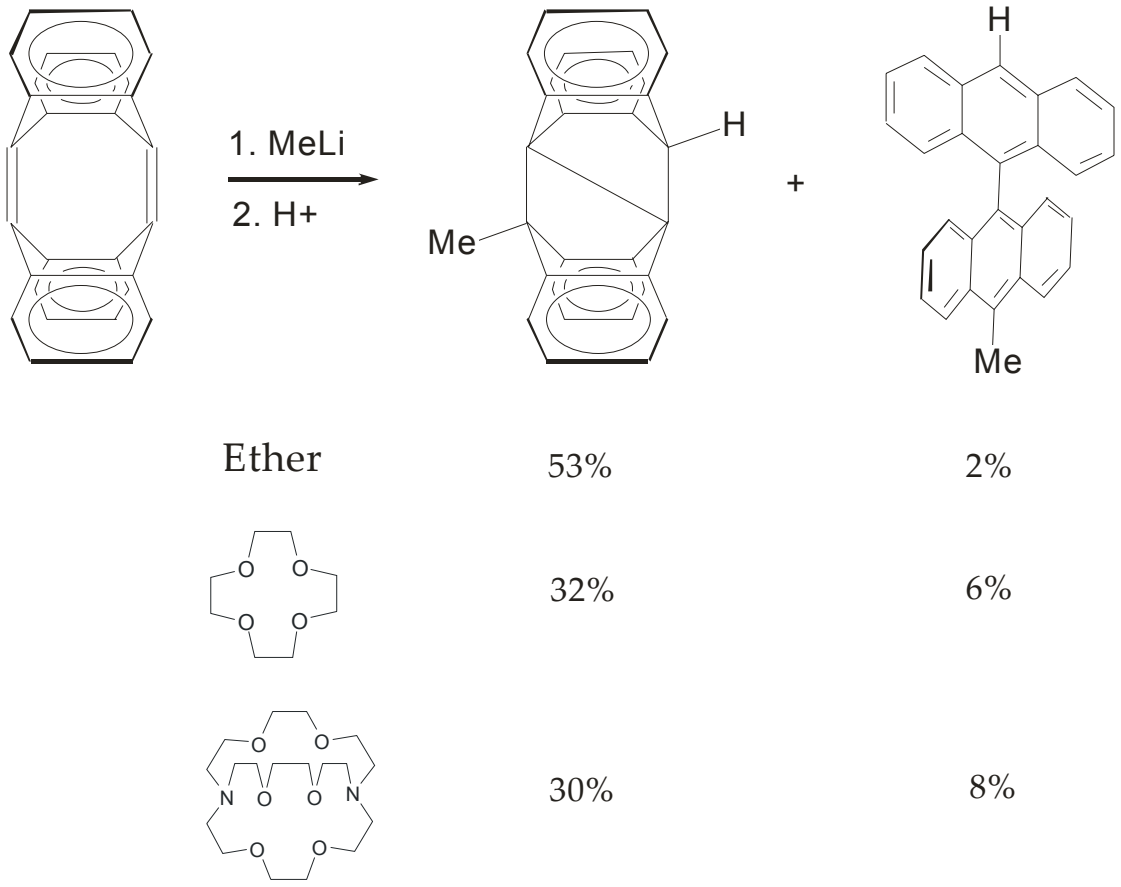

Scheme 9: Nuclophilic addition to TDDA.

2.3.3 Diels-Alder reaction of TDDA

2.3.3.1 Diels-Alder reaction with electron-rich dienes

TDDA reacts with a wide variety of electron rich dienes (Scheme **10**), under ambient conditions.[57] Only 1:1 products were observed even with a large excess of the diene and under drastic conditions (even though two strained and highly pyramidalized double bonds are available). The enhanced reactivity of TDDA compared to its mono Diels-Alder adduct is mainly due to the through-bond and through-space interaction of the two olefinic double bonds.

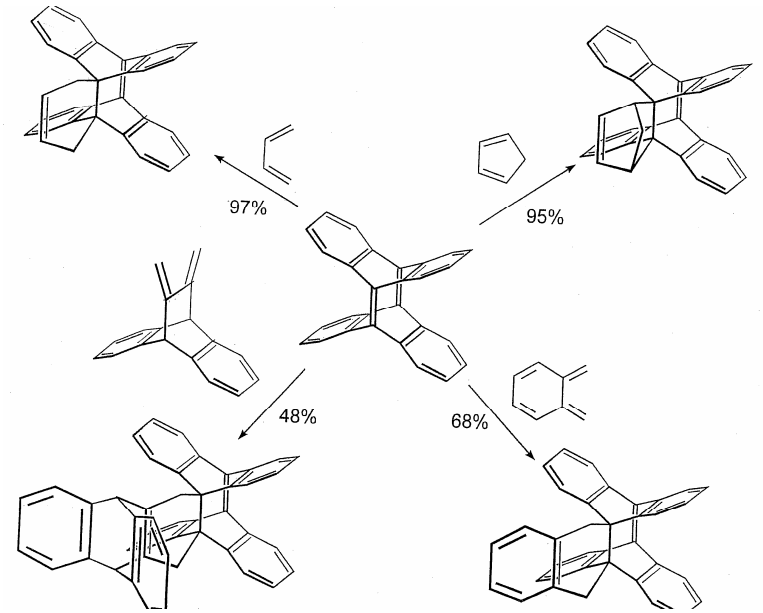

Scheme 10: Reaction of TDDA with electron rich dienes.

2.3.3.2 Diels-Alder reaction with electron-poor dienes

TDDA reacts with electron-poor dienes[61]. like α-pyrone and 1,2-diazine to give a [4+2] addition product which forms the bridged bianthraquinodimethane **7** after elimination of CO_2 or N_2 and electrocyclic ring opening of the intermediate 1,3-cyclohexadiene (Scheme **11**).

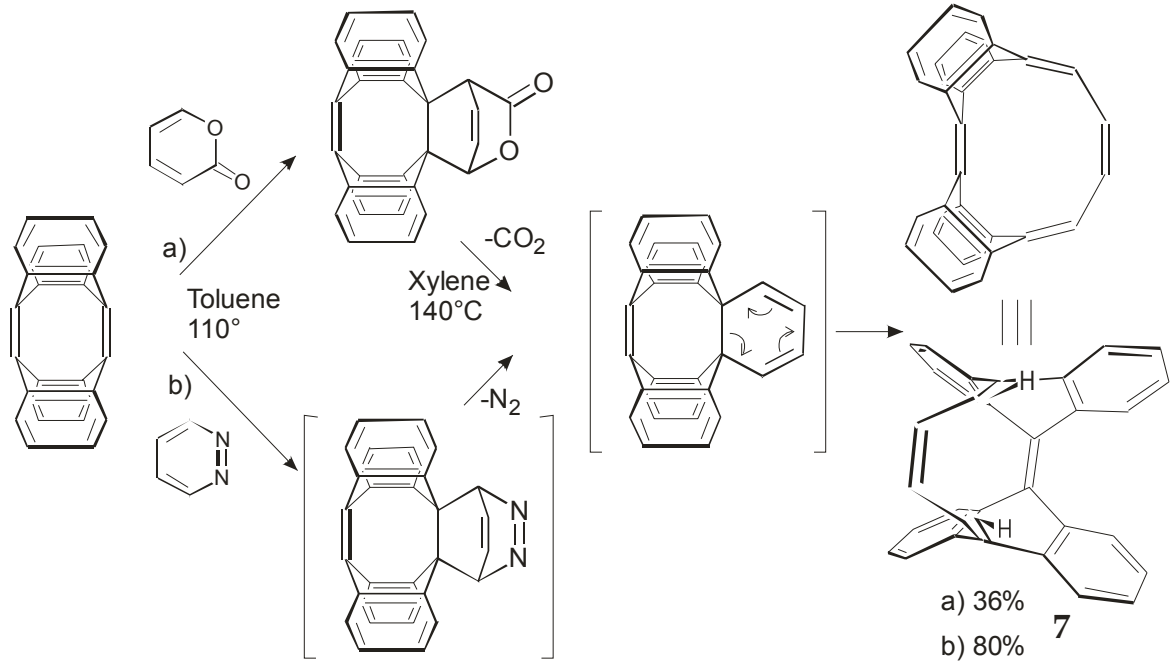

Scheme 11: Formation of 7 through Diels Alder reaction.

2.3.4 Photochemically induced metathesis reactions of TDDA

2.3.4.1 Photochemical reaction with cycloalkenes

Photochemical reactions of TDDA with cyclic olefins formed cyclophane-like bridged bianthraquinodimethanes[62] (Scheme **12**). In the first step photochemical [2+2] cycloadditions yielded unstable cyclobutane intermediates, which undergo [2+2] cycloreversions[57] to give final metathesis product.

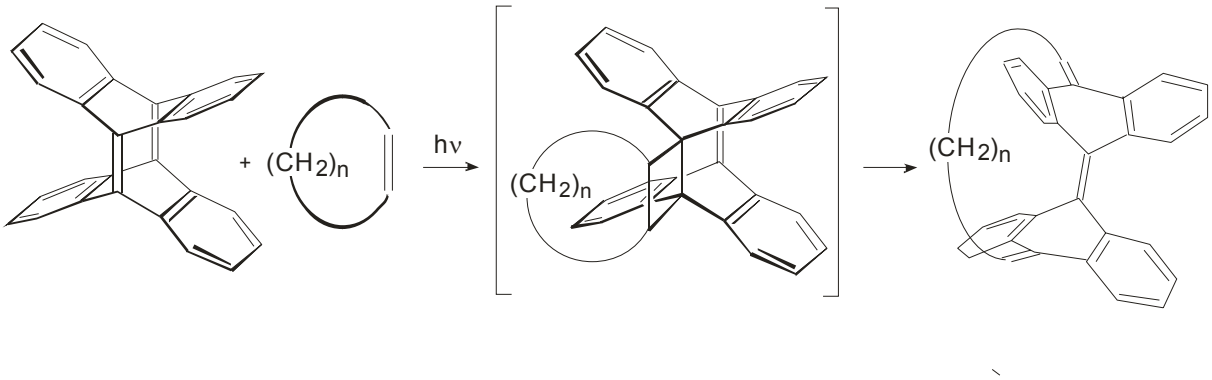

n	3	4	5	6	8	10	norbornadiene	norbornene
yield [%]	11	0	29	60	26	27	61	22

Scheme 12: Photocycloadditions of TDDA with cycloalkenes.

2.3.4.2 Photodimerization of TDDA

Photolysis of a suspension of TDDA in benzene with a high pressure mercury lamp in a quartz apparatus leads to a dimerization metathesis reaction[63] (Scheme **13**).

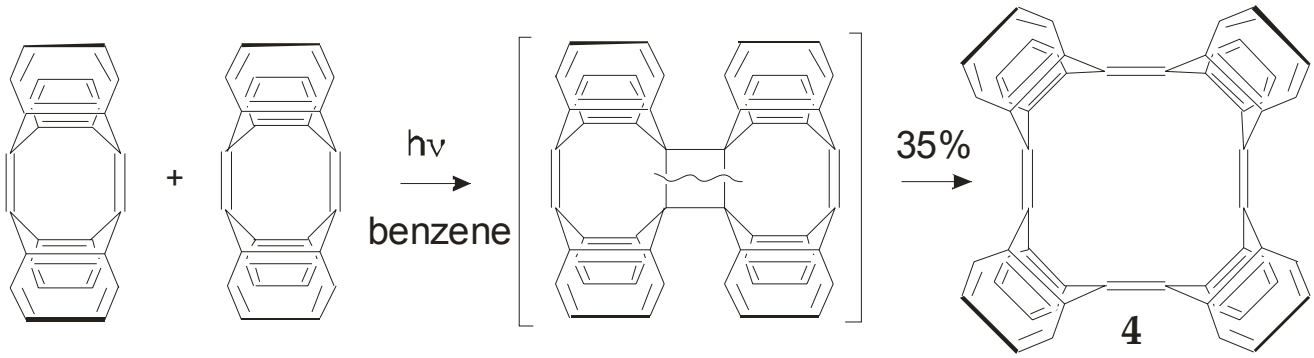

Scheme 13: Formation of picotube **4** by photodimerization of TDDA.

2.3.4.3 Synthesis of Kammermeierphane

As shown in Scheme **14**, TDDA undergoes a photochemically induced metathesis reaction with the double bond like in the cyclophane bridge of 7, to form a belt-like conjugated compound with a larger cavity.[61]

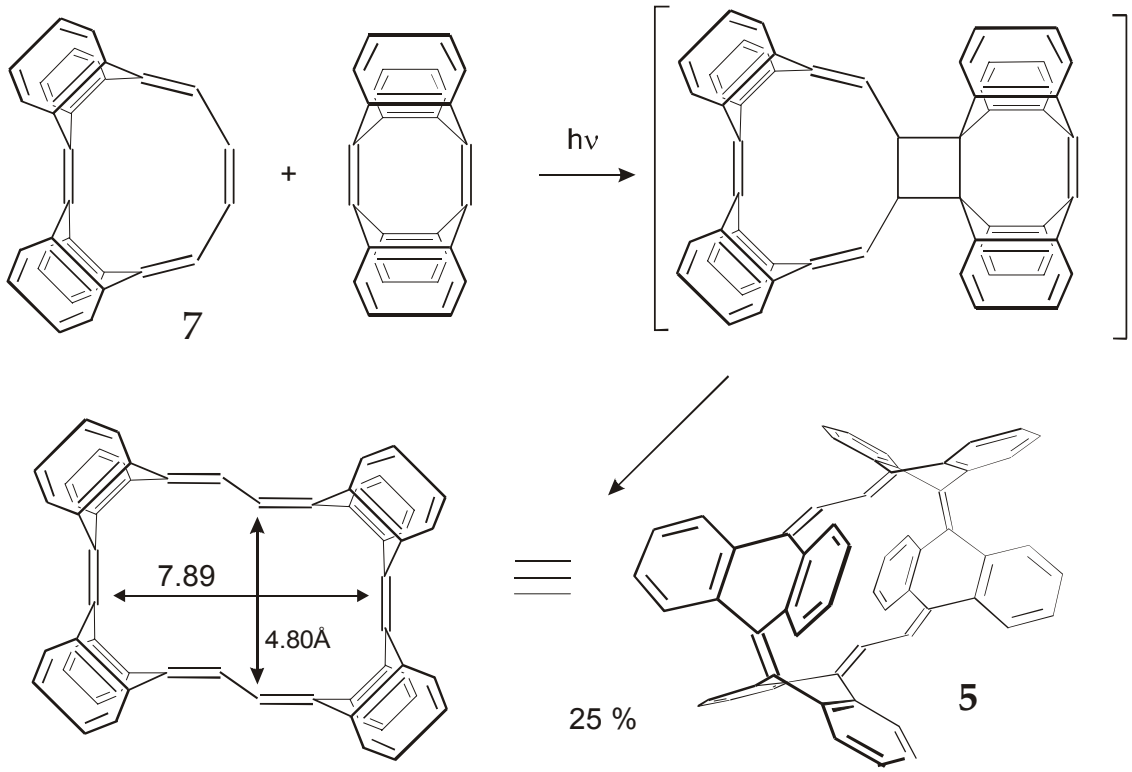

Scheme 14: Photochemically induced metathesis of TDDA with **7** forming Kammermeierphane **5**.

2.4. Conclusion:

The structure of TDDA is well suited for the synthesis of tube like molecules and its extremely high strain energy provides the driving force for metathesis reactions. The metathesis is therefore directed towards ring expansion. The general reactivity of TDDA was investigated towards electrophiles and nucleophiles and in Diels-Alder reactions with different dienes and finally with photochemically induced metathesis reactions. In the following chapters new applications of TDDA towards the synthesis of new tubular aromatic compounds will be discussed based on the reactivity described.

3 9,9′,9′′,10,10′,10′′-Hexadehydrotrianthracene (Trimer)

3.1 General

Single-walled 4 Å carbon nanotubes are the smallest carbon nanotubes have been discovered[37] so far. As predicted by theory, they are the nanotubes with the smallest diameter that are reasonably stable. Unlike larger carbon nanotubes, which can be either metallic or semiconducting, depending on their diameter and helicity, these smallest nanotubes are always metallic[64] with the highest conductivity predicted for all nanotubes.

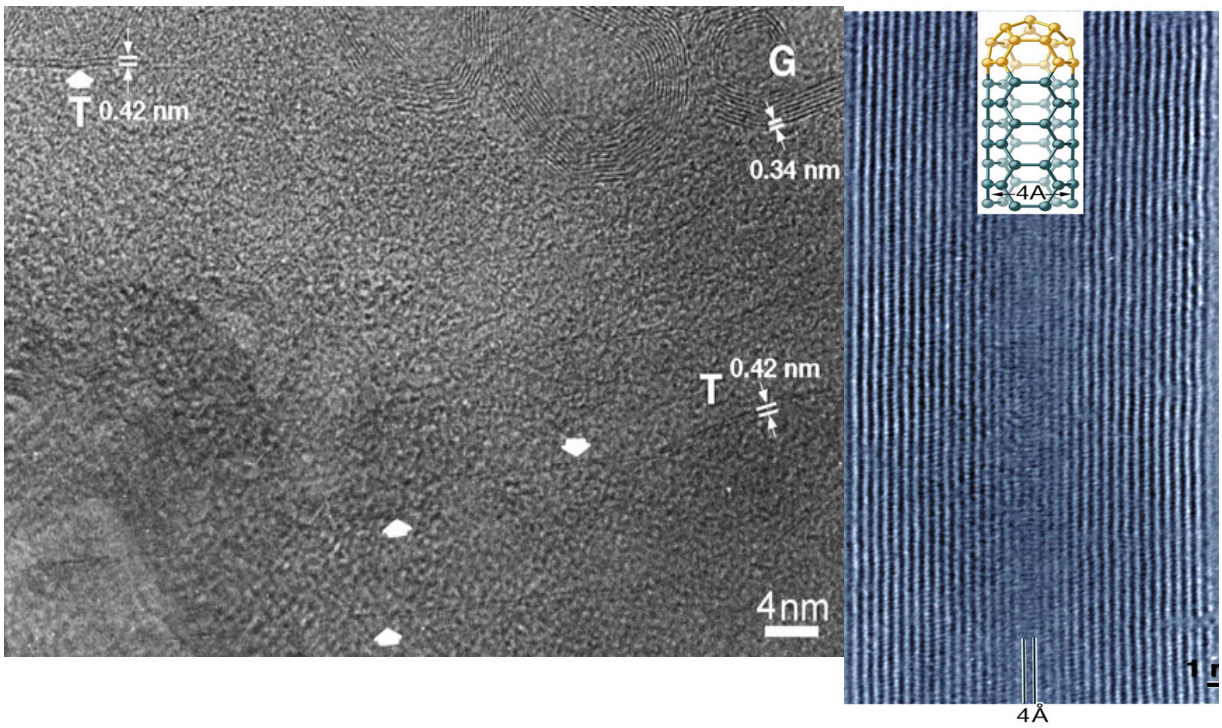

Figure 10: High-resolution transmission electron microscope image of, single-walled nanotubes (left) and a 4 Å tube confined inside an 18-shell carbon tube (right).

A rational syntheses of these nanotubes would be possible by dehydrocyclization of the 9,9′,9′′,10,10′,10′′-Hexadehydrotrianthracene (trimer). Moreover the trimer is an interesting building block for the synthesis of larger tubular aromatic compounds (e.g. pentamer, hexamer,…), which possibly can be achieved by using the photochemically induced ring enlargement metathesis reaction.

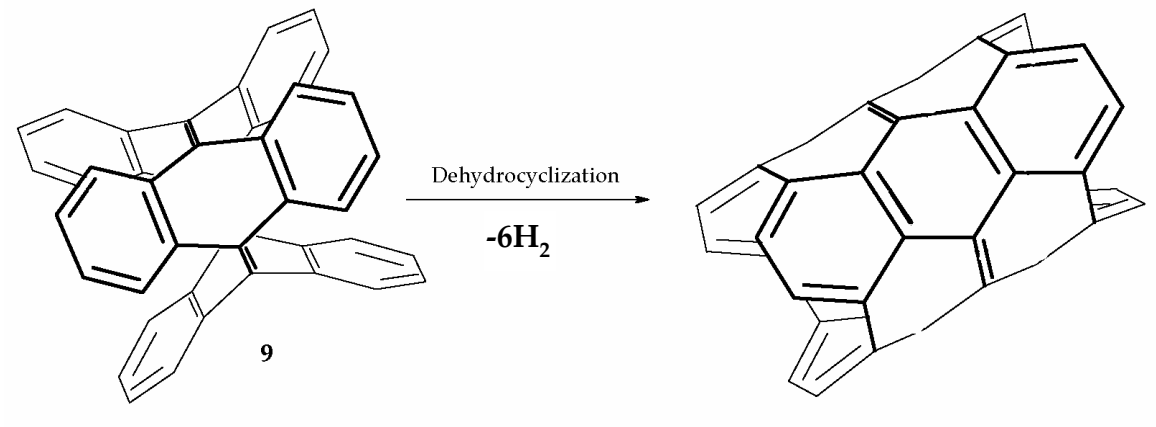

Figure 11: Hypothetical rational synthesis of 4 Å nanotubes by dehydrocyclization of the trimer **9**.

3.2 Synthesis strategy

TDDA is a reactive dienophile, which reacts with electron rich and electron poor dienes in Diels-Alder reactions. Thus, it seemed to be straightforward to react it with a 9,10-dihaloanthracene and to generate the trimer by dehalogenation of **8.**

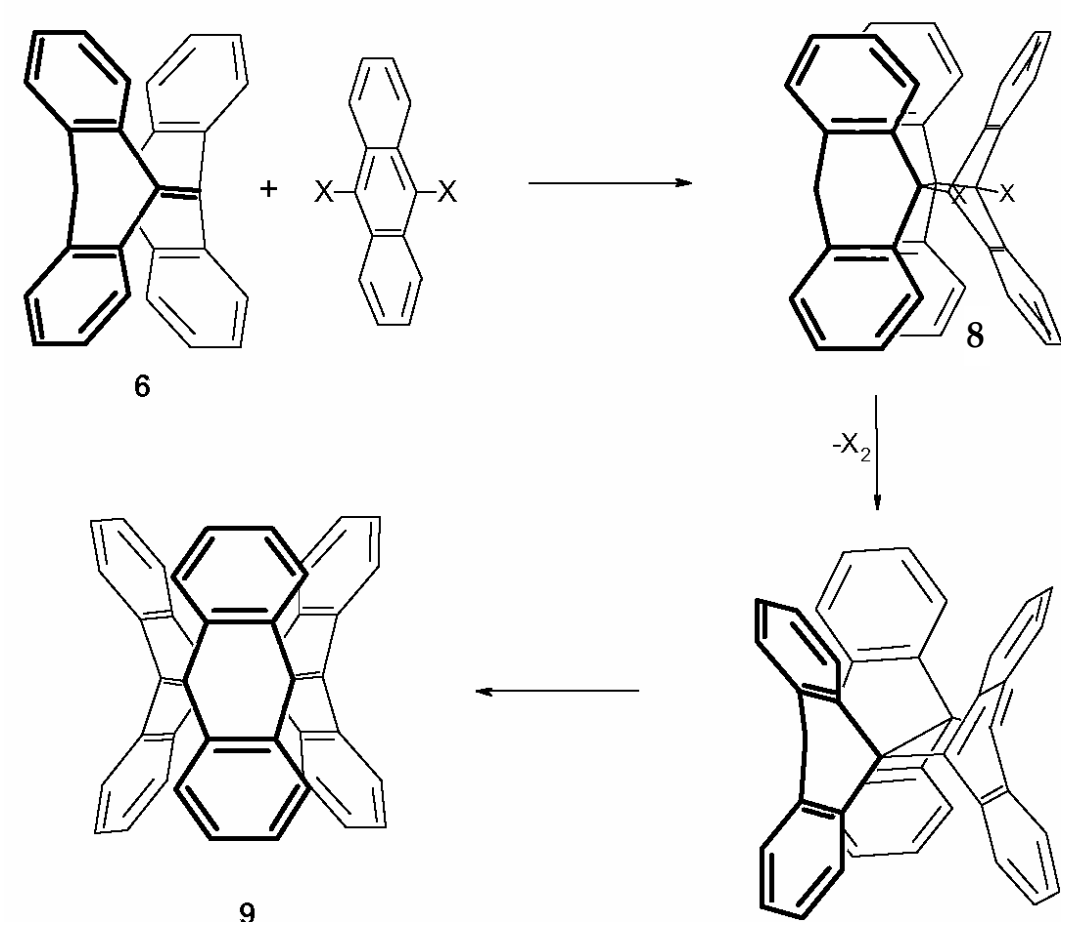

Scheme 15: Attempted trimer synthesis strategy based on Diels-Alder reaction.

Alternatively, the sequence Diels-Alder with 9 bromoanthracene, 1,4-elimination of HBr and Diels-Alder with anthracene followed by oxidation could provide access to the trimer **9**. The reaction of TDDA with anthracene has been monitored in several solvents, such as xylene, toluene, benzene and dichloromethane at room temperature or reflux conditions. Unfortunately bianthryl is the only product, which arises from ring opening of TDDA (scheme **16**).

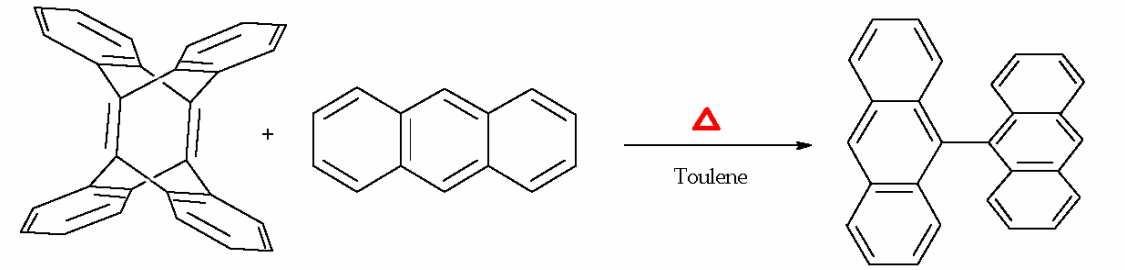

Scheme 16: The attempted Diels-Alder reaction of TDDA with anthracene affords bianthryl instead.

In order to achieve the attempted Diels-Alder reaction, ultrasonic irradiation[65], microwave irradiation[66] and high pressure conditions (12 Kbar, 120° C, 3d, toluene) were applied. However, again there was not any evidence of a Diels-Alder addition.

Lithium perchlorate in ether or THF was used to accelerate the Diels-Alder reaction[67] in several cases but in our case electrophilic addition of the solvent to TDDA was observed. The use of magnesium perchlorate in acetonitrile or benzene also was not successful.

In another attempt, a solid mixture of TDDA and anthracene was heated to 240° C. Under these conditions a mixture of more than six products was obtained. Unfortunately attempts to separate the products were not successful because of the insolubility of the products and difficulties on the chromatographic separation. The mass spectrometric analysis of the mixture of the products can be interpreted in favor of a radical addition of anthracene to TDDA and TDDA to TDDA (Scheme **17**).

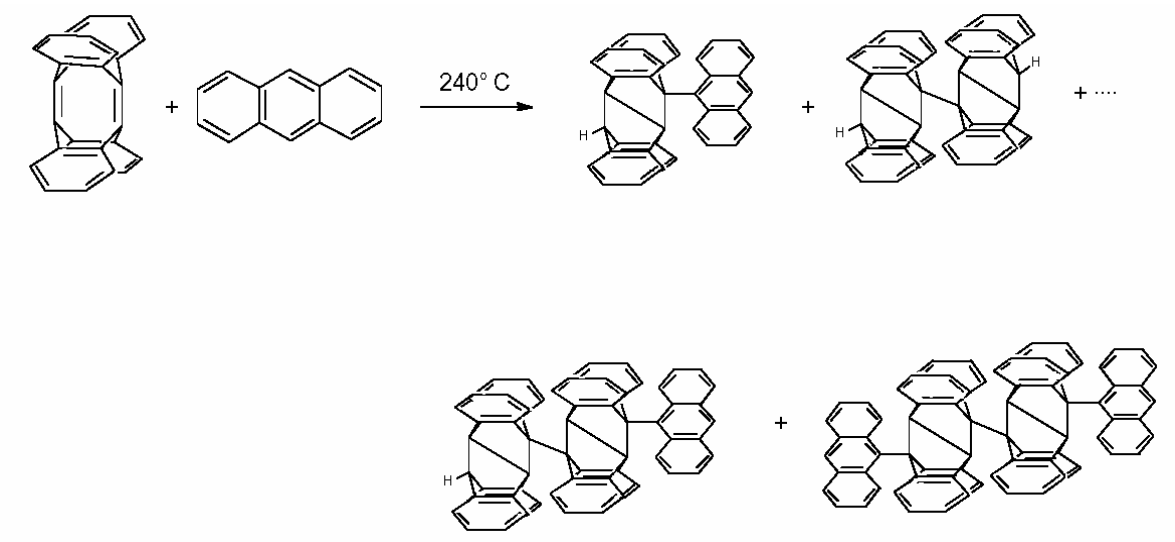

Scheme 17: Proposed products of the solid phase Diels-Alder reaction of TDDA with anthracene at 240°C.

Inorganic supports like, montmorillonite K10, silica gel and alumina can catalyze Diels-Alder reactions.[68] TDDA reacts with anthracene in toluene in the presence of montmorillonite k10 upon solvent addition to TDDA in a transannular fashion (Scheme **18**). It is interesting to know that the radical induced addition of toluene to TDDA results in compound **11**, which corresponds to a transannular addition of the benzyl radical to TDDA. The mechanism of the polar addition is base on ability of montmorillonite K10 to make radical cations[69] of TDDA. As shown in the last chapter transannular reactions in TDDA are favoured. Therefore a rearrangement to form a transannular 1,4-radical cation might occur. In the second step electrophilic aromatic substitution reaction forms the bond between TDDA and toluene.

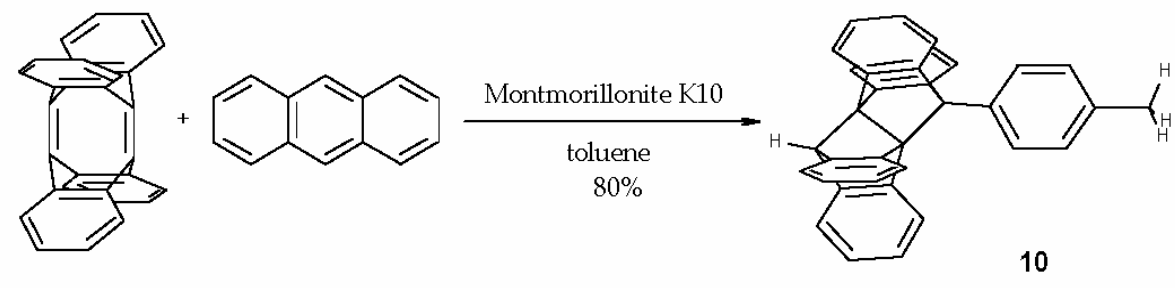

Scheme 18: Attempted **s**olid support Diels-Alder reaction of TDDA with anthracene in toluene yielding exclusively transannular addition of the solvent to TDDA.

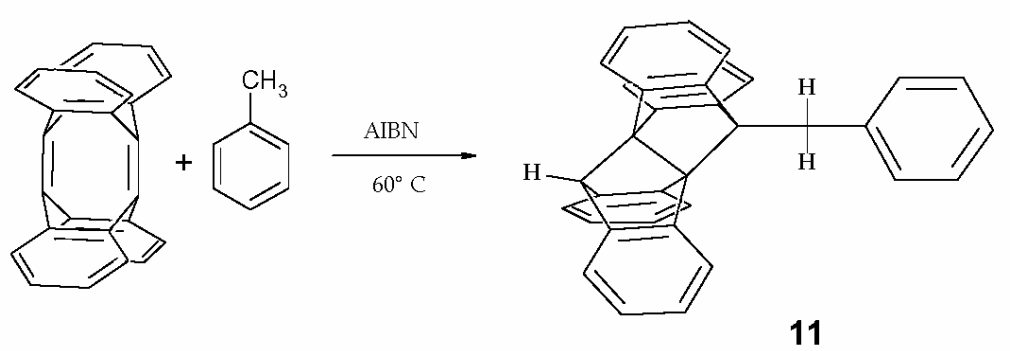

Figure 12: Product the addition of toluene to TDDA induced by a radical starter such as azobisisobutyronitrile (AIBN).

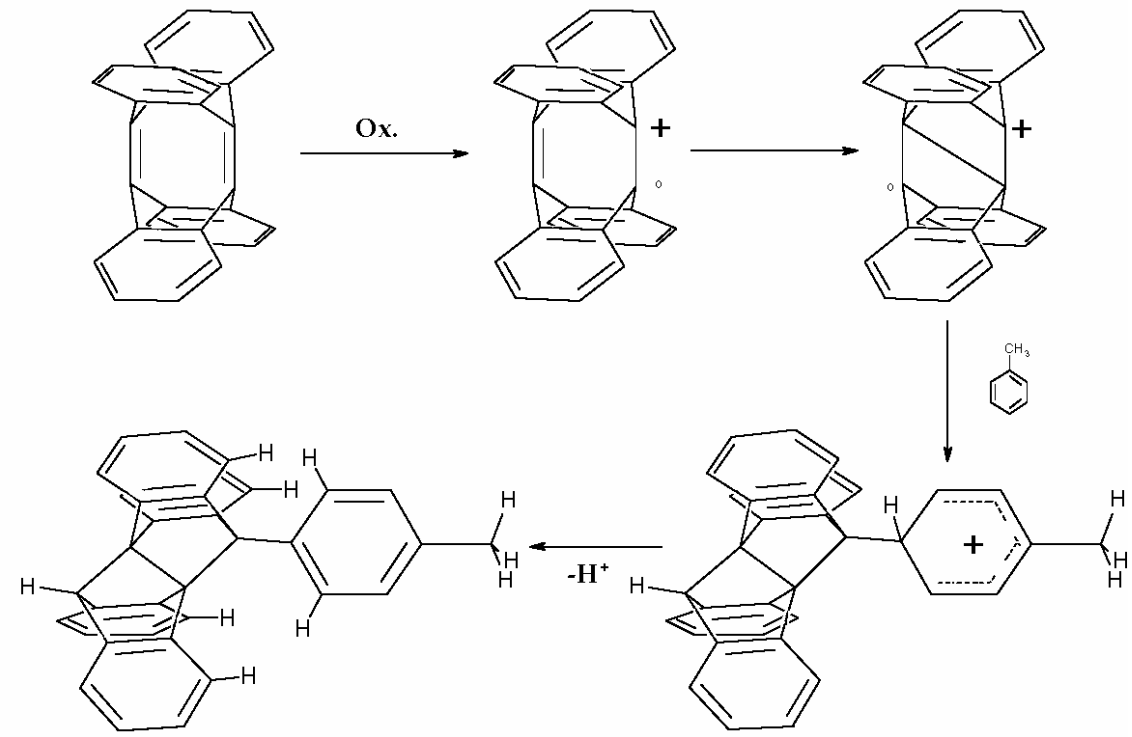

Scheme 19: Proposed mechanism of the transannular addition of toluene to TDDA.

Due to the van der Waals repulsion of the four ortho hydrogens of TDDA and two hydrogen atoms of toluene, two conformational isomers of **10** are possible. In one of them the plane of the phenyl ring of toluene is parallel with the anthracene unit **10a** and in the other conformation both units are orthogonal. Both isomers have C_s symmetry. According to DFT (density functional theory at B3LYP/6-31G*) calculations isomer **10a** is 0.82 Kcal/mol more stable than **10b**. ACID calculations of both isomers have not identified a large difference between the electronic delocalisation of both isomers (Figure **13**).

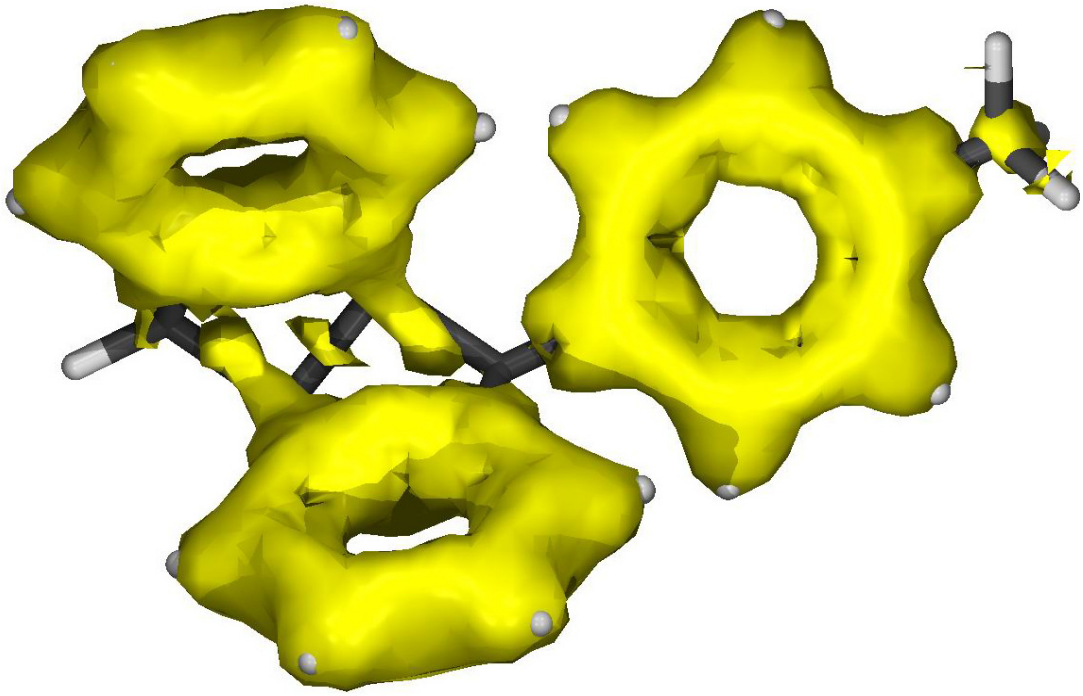

(a) **10a**

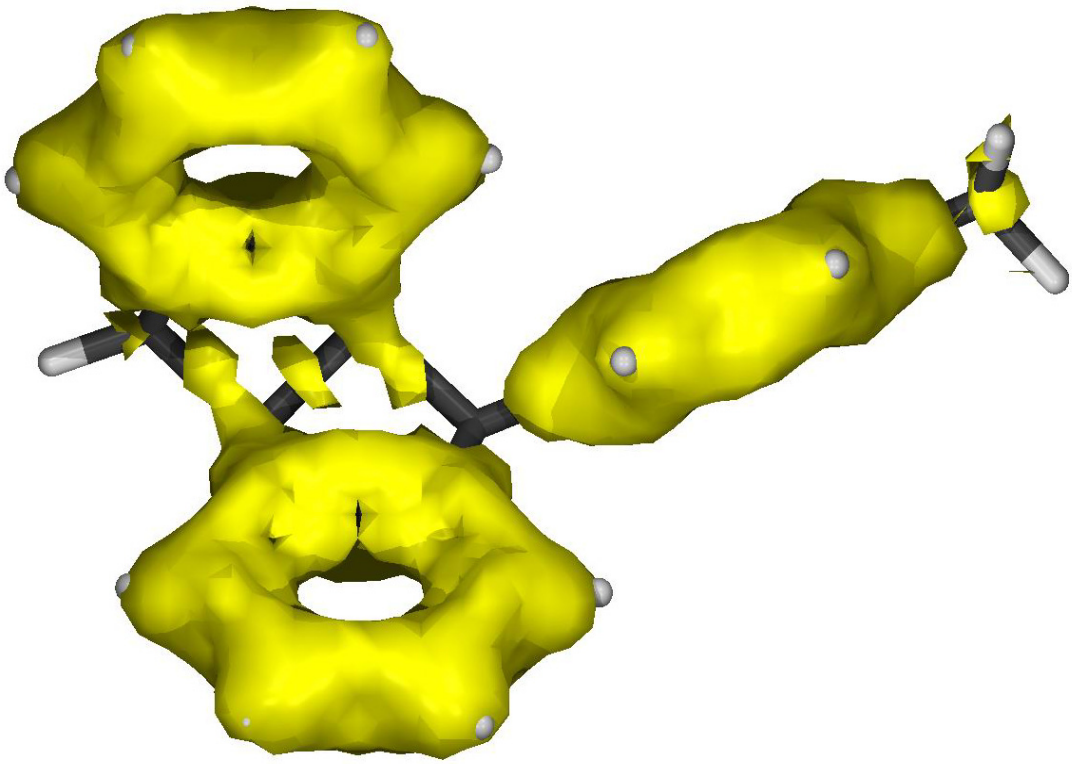

(b) **10b**

Figure 13: ACID Plot of (a) isomer 10a, (b) isomer 10b, critical isosurface value(CIV) is 0.05 at B3LYP/6-31G* level of theory.

A Single crystal of **10** was obtained from a mixture of acetonitrile and carbon disulfide as solvents. The x-ray structure analysis proved the structure of conformation **10a** in the crystal structure.

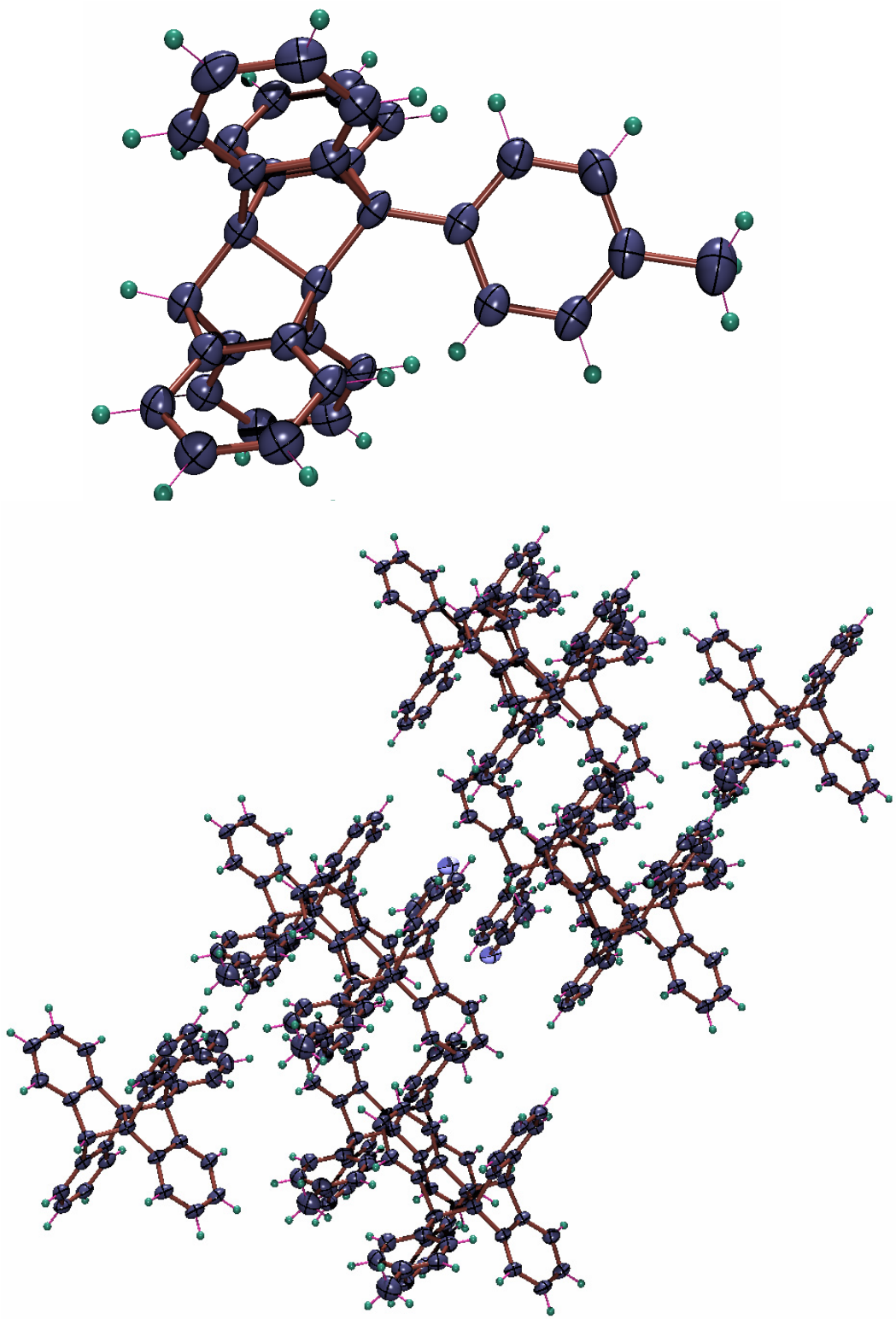

Figure 14: X-ray structure analysis of **10** and the unit cell structure in a crystal obtained from acetonitrile\CS_2.

Changing the solvent from toluene to a saturated hydrocarbon like hexane should prevent addition of the solvent to TDDA. As expected, the addition of anthracene to TDDA in the presence of montmorillonite K10 was observed in hexane. The NMR however proved that again in spite of the [4+2] Diels-Alder addition, transannular addition of anthracene to TDDA took place (Scheme **20**).

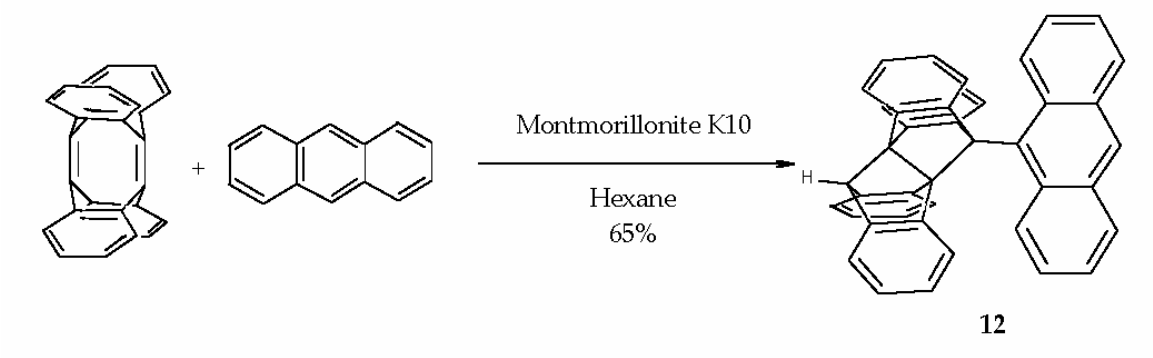

Scheme 20: Clay catalysed reaction of TDDA with anthracene in hexane.

As in the case of the toluene adduct, two conformational isomers of **12** are possible, which both have C_s symmetry. In one conformation anthracene is in the plane of the symmetry of molecule **12a** and in the other one the symmetry plane of the molecule and the anthracene ring plane are orthogonal **12b**. Compound 12a is 3.44 Kcal/mol more stable than conformation 12b according to a B3LYP/6-31G* calculation.

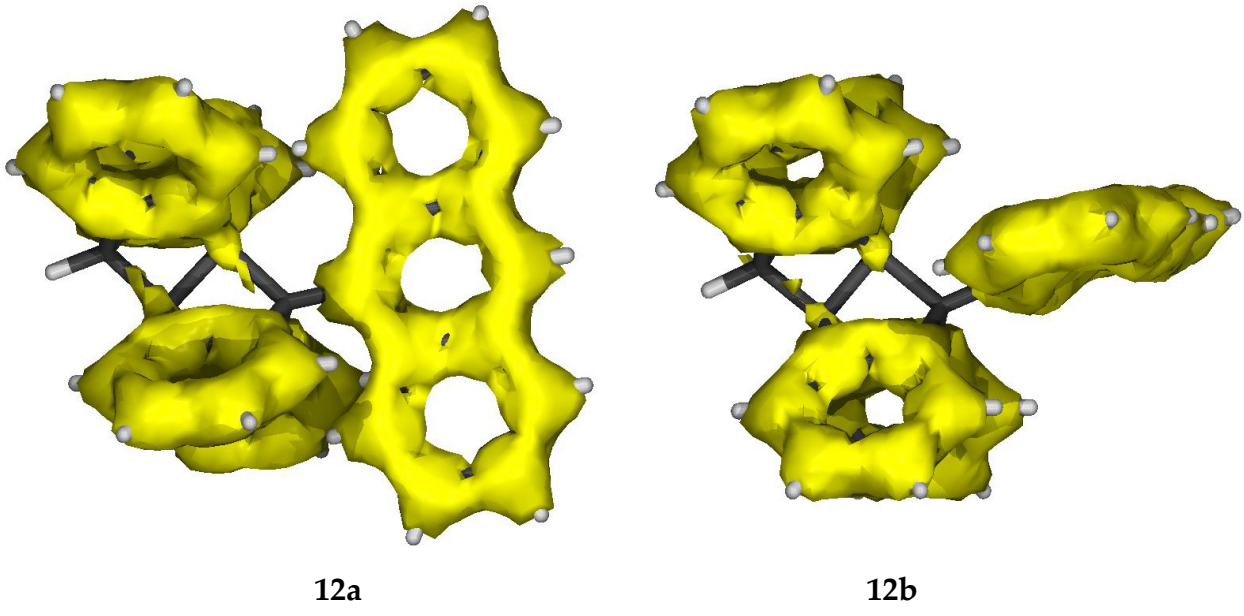

Figure 15: ACID plot of the two possible conformation of **12** at an isosurface value of 0.05 at B3LYP/6-31G* level of DFT.

Thus, unfortunately the two step synthesis of trimer through Diels Alder reaction has been failed because of sterical hindrance of four hydrogen of anthracene and four hydrogen of TDDA (figure **16**).

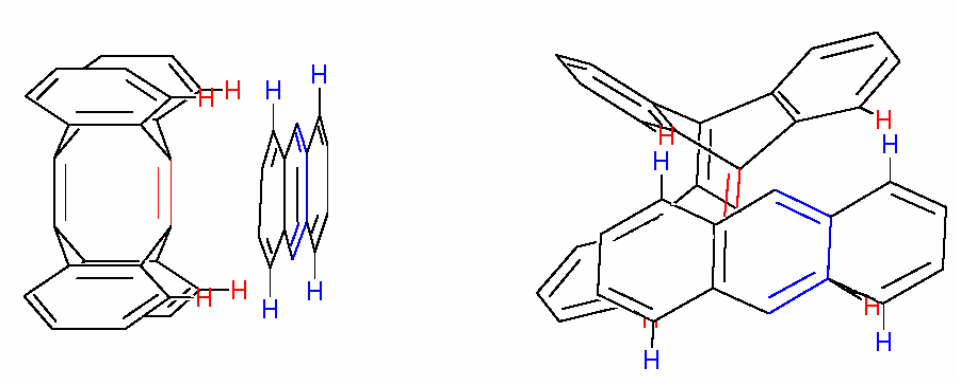

Figure 16: Sterical hindrance of four hydrogen of TDDA with four hydrogen of anthracene during Diels-Alder reaction

3.3 Synthesis of the semitrimer

In order to overcome the sterical hindrance, step by step synthesis had to be considered. In the first step half of the anthracene unit could be added and in the second step the semitrimer would be converting to the trimer. Scheme **21** depicts the retrosynthetic strategy.

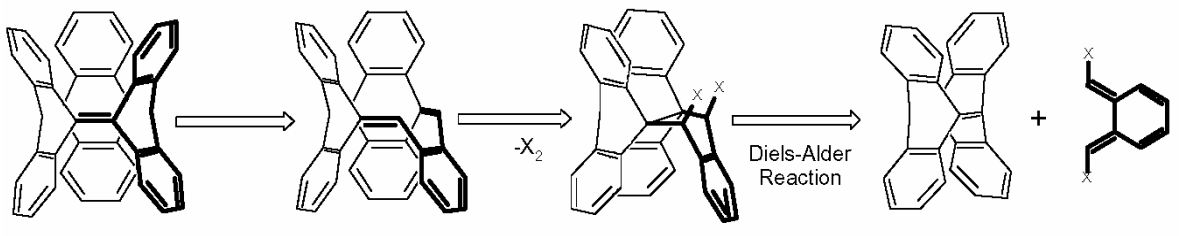

Scheme 21: Retrosynthesis of the trimer.

TDDA reacts with $\alpha,\alpha,\alpha',\alpha'$-tetrabromo-*o*-xylene **13**[70] in dimethyl formamide in the presence of sodium iodide at 70° C. The reaction product **14** was purified and isolated in 60% yield by simple column chromatography.

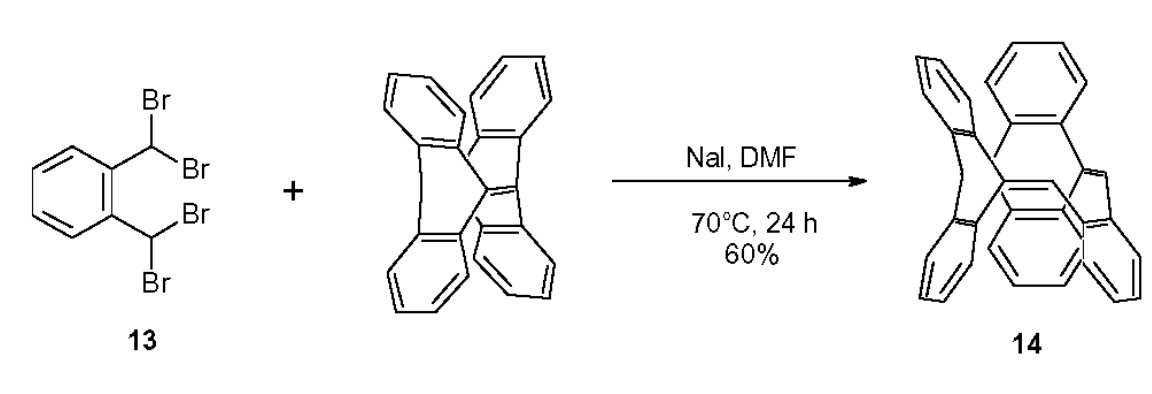

Scheme 22: TDDA reacts with α,α,α′,α′-tetrabromo-*o*-xylene to give the semitrimer **14**.

A possible mechanism for this reaction is shown in Scheme **23**. In the first step a 1,4-elimination reaction is giving rise to a highly reactive *o*-quinodimethane derivative **15**. Diels-Alder reaction of dibromo-*o*-quinodimethane **15**, with TDDA is followed by debromination and generation of the semitrimer **14**.

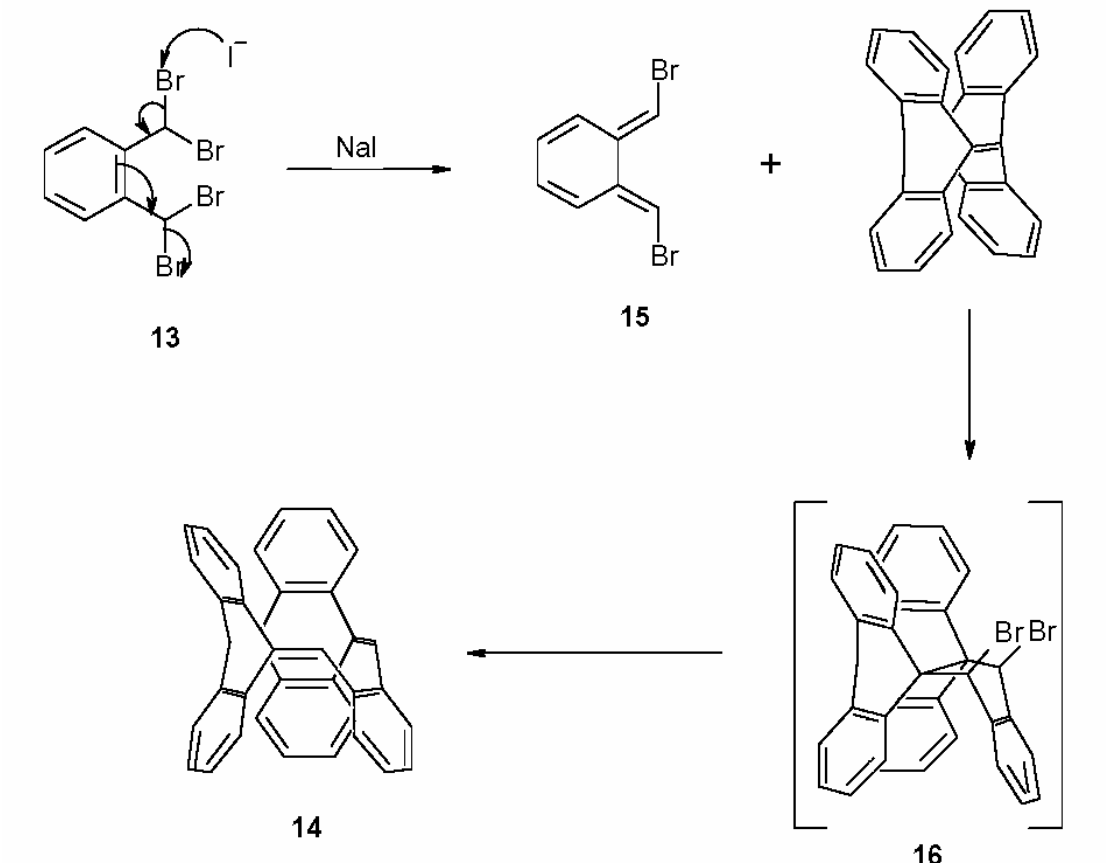

Scheme 23: Mechanism of the reaction of α,α,α′,α′-tetrabromo-*o*-xylene with TDDA and sodium iodide.

UV, MS and NMR spectral data indicate a fully conjugated tubular aromatic compound with C_s symmetry. Ever though the solubility of the semitrimer is low, single crystals were obtained from acetonitrile/carbon disulfide. The x-ray structure analysis clearly confirmed the previous structure assignment based on spectroscopic data and calculations.

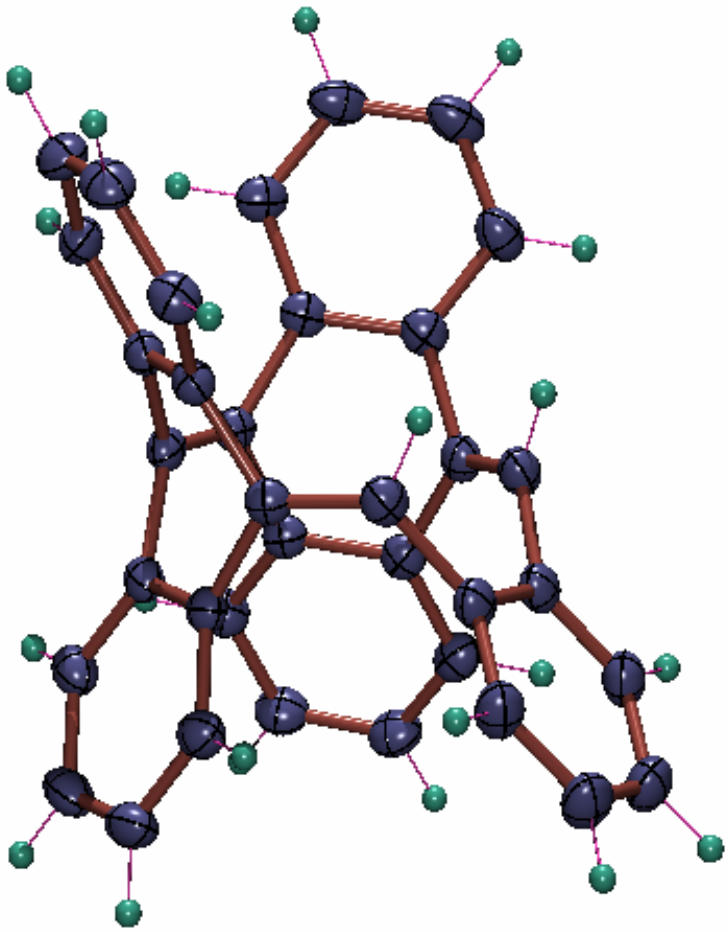

Figure 17: X-ray structure analysis of the semitrimer **14**

Even though five molecules of carbon disulfide and five molecules acetonitrile were found in the unit cell of the semitrimer, they are located outside of semitrimer structure and a close packed arrangement of semitrimer with solvent doesn't exist (Figure **18**).

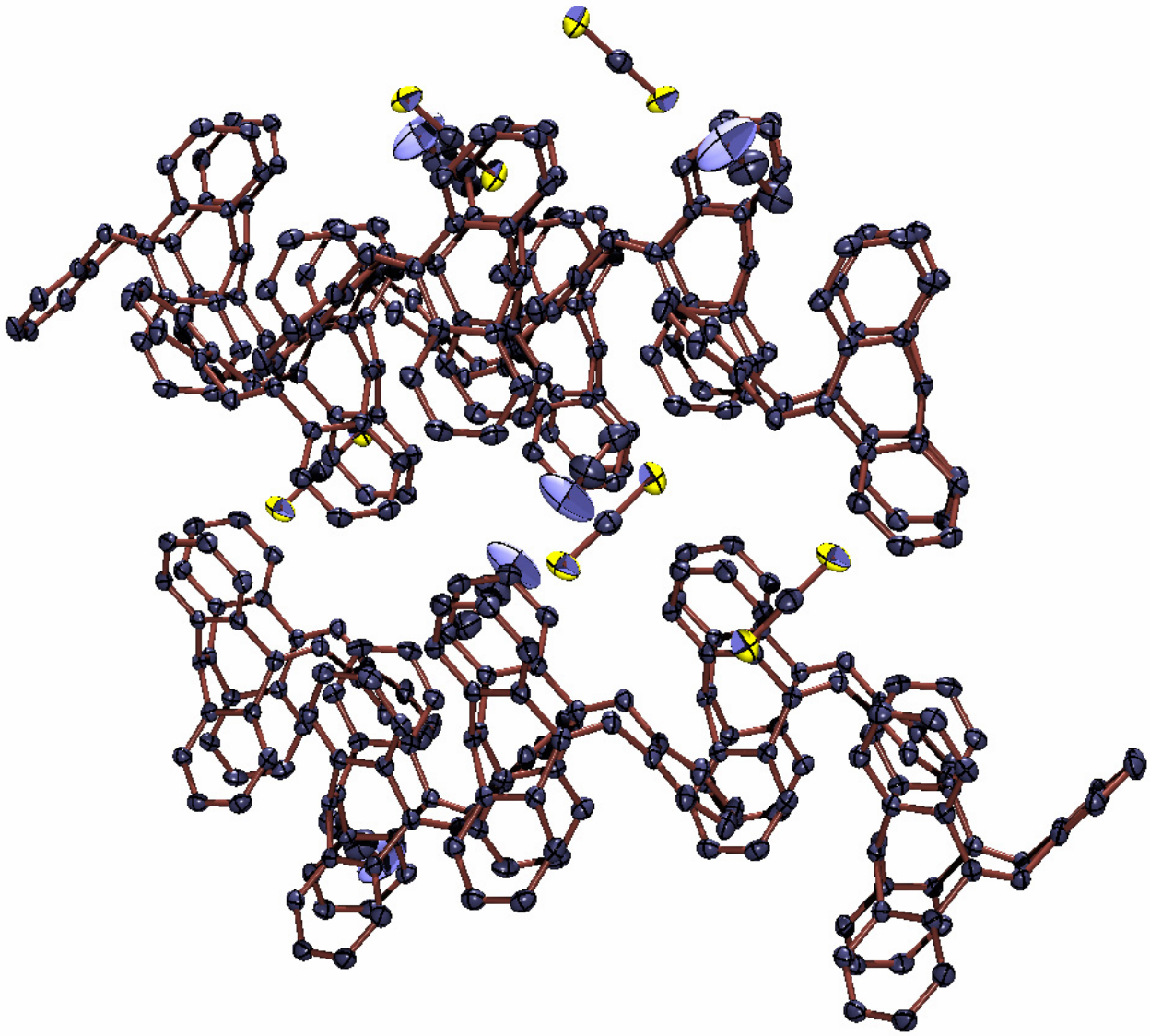

Figure 18: Unit cell structure of the semitrimer **14**. Ten molecules of solvent were found in the unit cell.

Is the semitrimer aromatic? The semitrimer consists of five conjugated benzene rings connected by three double bonds including 36 π electrons. The π-perimeter is a [12]annulene with 12 π-electron. According to the 4n+2 π Hückel rule it is

antiaromatic. The chemical shift of olefinic proton in the semitrimer is 6,41 ppm (500 Mhz, $CDCl_3$) which is in good agreement with the calculated value (6.39 ppm, GIAO, B3LYP/6-31G*) However, compared to the corresponding proton in triphenylethylene (6,96 ppm), it is considerably upfield, due to the pyramidalization of the olefinic carbon atoms in the semitrimer.

The anisotropy of the current induced density (ACID) method provides a powerful and general way to visualize the density of delocalized electrons [18] and to quantify conjugation effects. Figure **19** presents the ACID plots of the semitrimer at an isosurface value of 0.05. There is a contiguous delocalisation of π electrons including all C-C bonds of the structure. The critical isosurface value, CIV (the lowest ACID value in space between two interacting units) was defined as a measure of the strength of a conjugation. The semitrimer has a CIV of 0,0578 (between the trisubstituted double bonds and the neighbouring benzene rings), which is 0.0161 lower than CIV of benzene indicating a moderate conjugation for the semitrimer.

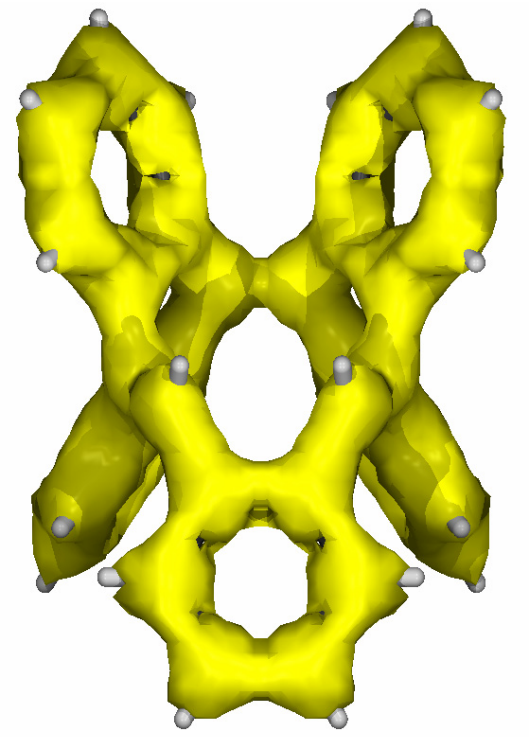

Figure 19: ACID plot of the semitrimer at an isosurface value of 0.05 at B3LYP/6-31G* level of theory.

The nucleus independent chemical shift (NICS)[17] value is defined as the absolute magnetic shielding, computed at ring centre of molecule. A negative NICS denotes aromaticity and antiaromatic compounds exhibit positive NICS value. At the B3LYP/6-31G* level of theory the semitrimer has a NICS of –1.82 which indicates a very weak or no aromaticity in the 12 electron perimeter around the "waist" of the structure.

3.4 Complexation properties of the semitrimer

In recent years, metallocyclophanes have been extensively investigated. The complexation of cyclophanes[71] with metals is important with regard to the effect on the ring current, as well as the change of the chemical properties of the arene and the coordinated metal atom. Four possible general structure types are illustrated in Figure **20**, which are based on two fundamental types of metal carbonyl- and related complex or sandwich complexes with interannularly bridged ligands or intraannularly bridged ligands.

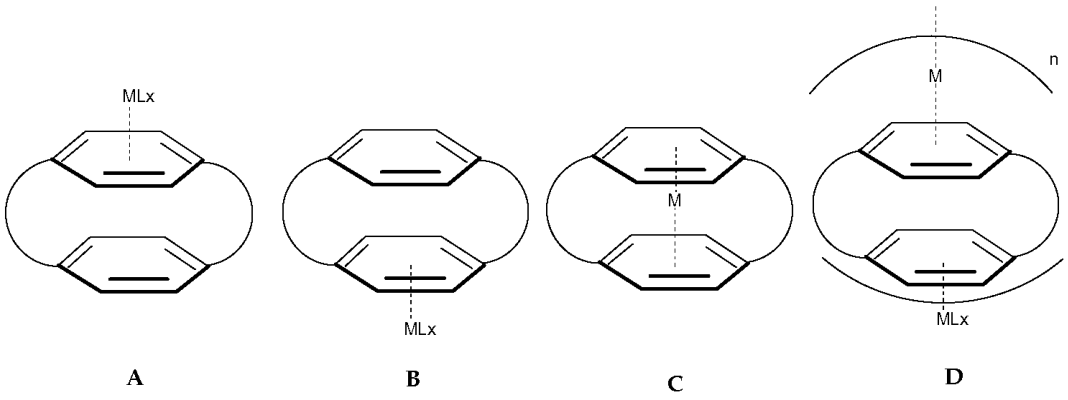

Figure 20: Four possible general metallocyclophane structures.

Iyoda et. al[72] synthesized the silver(I) and copper(I) complexes of *all*-Z-tribenzo[12]annulene which can be viewed as a simple model of the semitrimers (Figure **21**). The metal cations are complexed by the three olefinic double bonds.

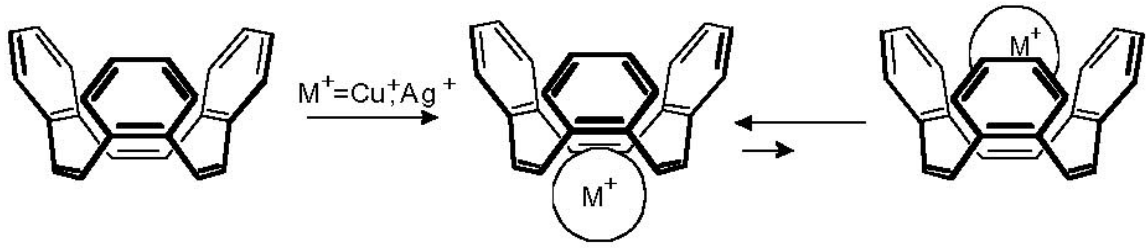

Figure 21: Structure of copper(I) and silver (I) complexes of *all*-Z-tribenzo[12]annulene.

The three quinoid double bonds of the semitrimer should provide a planar 6 π-electron ligand field similar to *all*-Z-tribenzo[12]annulene. The complexation of the semitrimer with silver(I)trifluoromethanesulfonate and copper(I)triflouromethane-sulfonate was investigated in several solvents and with different stoichiometries. There is indication that complexes were formed, however, separation from the unreacted semitrimer failed. Crystallization of the complex was not achieved because the solubility of the complexes is much higher than the solubility of the ligand. Column chromatography also could not be used for separation, because the complexes decomposed or rearranged. In one try a mixture of the silver(I)triflate complex of the semitrimer was passed through a silica gel column with dichloromethane /hexane as the mobile phase. The charged complex reacted with the solvent in the column. The structure of the main product **17** was elucidated by x-ray structure analysis (figure **22**). The X-ray data is only good enough for determination of structure and bond length and angle are not highly precise. The mechanism of this reaction is unclear. The **17** has a CH_2 group more than the semitrimer which indicate to a reaction between dichloromethane of mobile phase of chromatography and semitrimer.

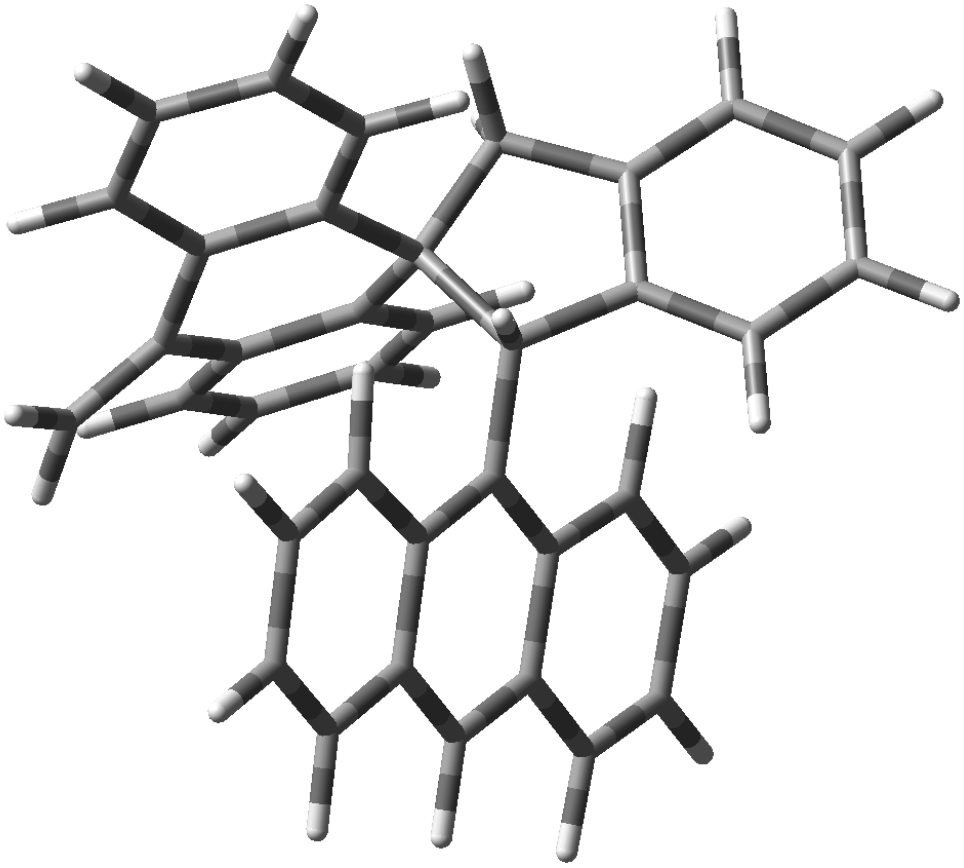

17

Figure 22: X-ray structure of the decomposition product of the silver complex upon chromatography on a silica gel column.

3.5 Epoxidation of semitrimer

The semitrimer as a solid is very stable and can be stored almost indefinitely. The solution of the semitrimer in benzene, toluene and dichloromethane is also stable. However, in THF the semitrimer oxidizes upon standing in air. Gradually the colour of the solution changes from colourless to brown. After 12 hour reaction time, two products could be isolated by, column chromatography in a combined yield of 55%. The MS, NMR, UV analysis of the products prove epoxidation of a quinoid double bond in each product. One of them keeps C_s symmetry which indicates epoxidation

at the quinoid double bond between the two anthracene units (**18**) and the other product has C_1 symmetry (**19**).

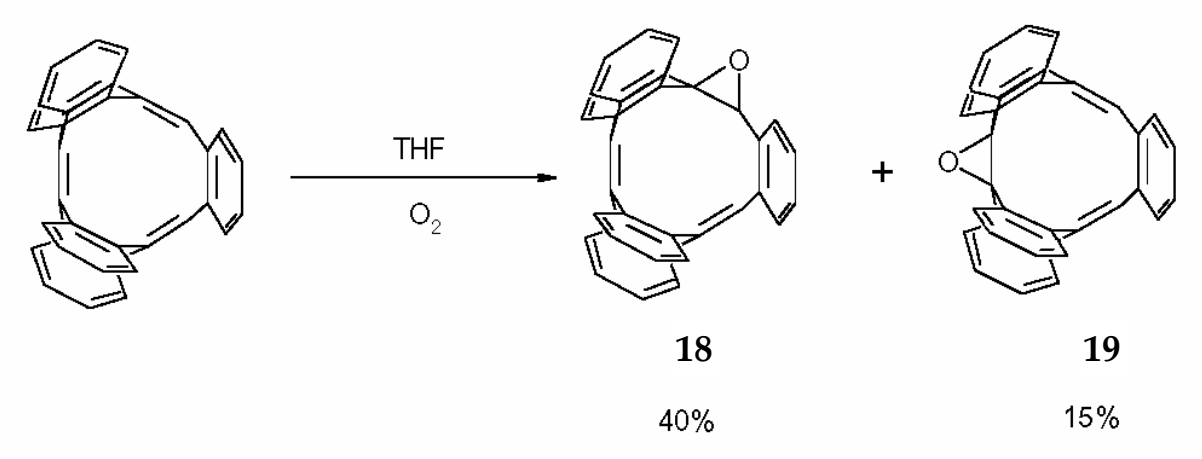

Scheme 24: Epoxidation of the semitrimer upon standing in air.

3.6 Attempted synthesis of Trimer from Semitrimer

In order to convert the semitrimer to the trimer, the two olefinic hydrogen atoms have to be replaced by the ortho carbon atoms of a benzene ring. The Heck reaction[75] now becomes a well established synthetically important method to form sp^2-sp^2 carbon-carbon bonds. A number of variations have been introduced extending the synthetic applicability of this type of reaction. In particular, tetraalkylammonium salts (phase transfer catalysis) in combination with insoluble bases have been found to be highly efficient in enhancing the reactivity and selectivity of the inter- and intramolecular Heck-type reaction[76] (Scheme **25**).

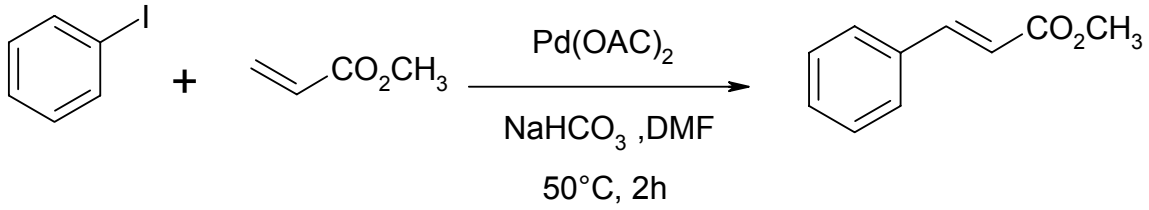

Equiv. of n-Bu_4NCl	Yield(%)
0	2
1	99

Scheme 25: The combination of tetraalkylammouim salts and insoluble bases accelerates the Heck reaction at low temperatures.

The semitrimer does not react with iodobenzene or 1,2-diiodobenzene under the above mentioned conditions. The sterical hindrance between iodobis(acetate)phenyl-palladium(II) and the semitrimer prevent the reaction.

Another way to form the trimer from the semitrimer is to replace the olefinic H atoms by bromine and to bridge the two double bonds with a benzene ring by Friedel Crafts alkylation with benzene.

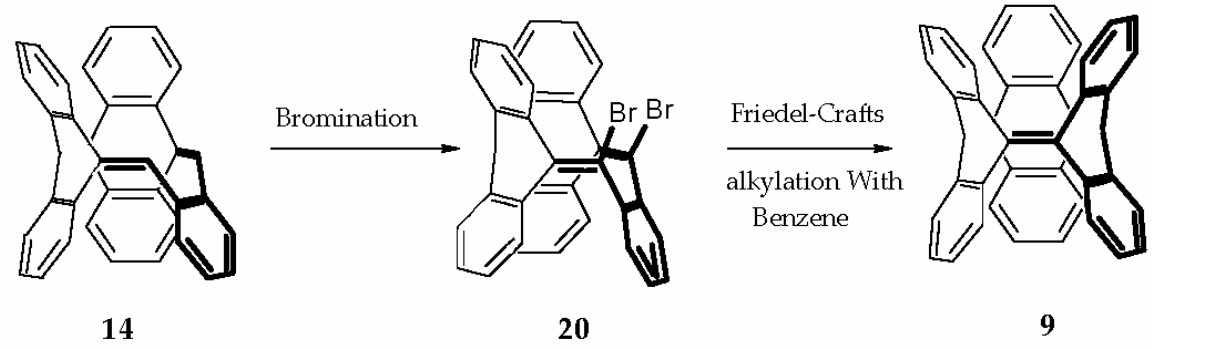

Scheme 26: Synthetic strategy to prepare the trimer by a bromination , dehydrobromination, Friedel-Crafts sequence

The bromination of the semitrimer with bromine as the brominating agent, however, unfortunately failed.

3.7 Attempted photochemically induced metathesis reactions of the semitrimer

A successful photochemically induced metathesis of TDDA with the semitrimer would give the semipentamer **21**. A suspension of TDDA and the semitrimer in benzene was irradiated with a 700-Watt high-pressure mercury lamp for 20 hours. Tetramer and unreacted semitrimer are the only detectable products.

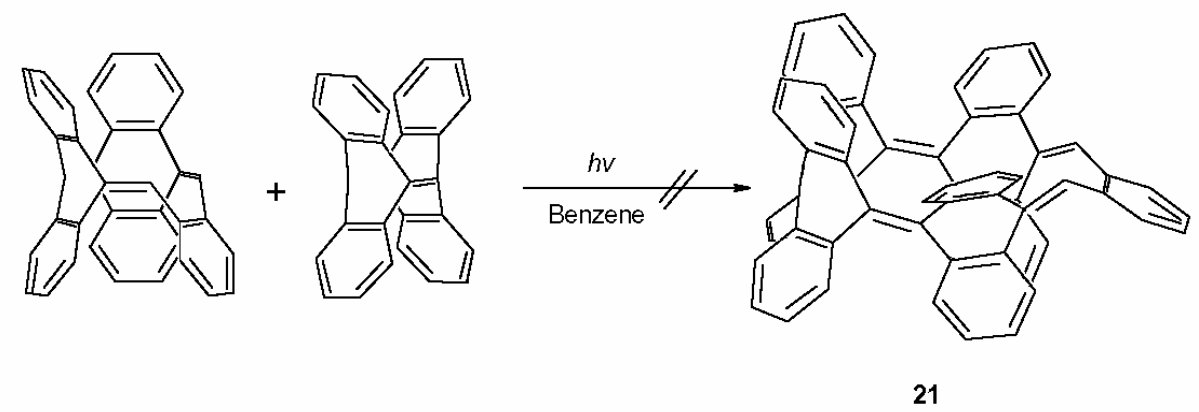

Scheme 27: Attempted photochemical reaction of TDDA with semitrimer.

3.8 Conclusion;

9,9′,9′′,10,10′,10′′-Hexadehydrotrianthracene (trimer **9**) should by an interesting building block for the synthesis of larger tubular aromatic compound (e.g. pentamer, hexamer,…), using photochemical induced ring enlargement metathesis reaction. Additionally rational synthesis of [3,3] armchair nanotubes should be possible by dehydrocyclization of the trimer. However synthesis of trimer based on Diels Alder reaction of TDDA with anthracene has been failed. In a step by step synthesis the semitrimer could be prepared.

4 Photochemically induced metathesis reaction of the tetramer

Deichmann et al.[77] have attempted to synthesize [4,4] armchair nanotubes based on the dehydrocyclization of the tetramer. Semiempirical (AM1) calculations predicted the overall elimination of eight hydrogen molecules to be endothermic by 205.9 kcal/mol^{-1}. The FVP experiments were performed at 800°C (quartz tube, 20 mm diameter, 30 cm heated length, 15 mL/min Argon, 2.5 mbar). A large number of isomers were formed under these conditions, of which an unsymmetrical compound **22** is the main product (Scheme **28**). Instead of hydrogen elimination one of the C-C single bonds neighboring the quinoid double bonds is broken in the first step and a cascade of radicaloid rearrangements driven by the release of ring strain leads to the a priori unexpected product.

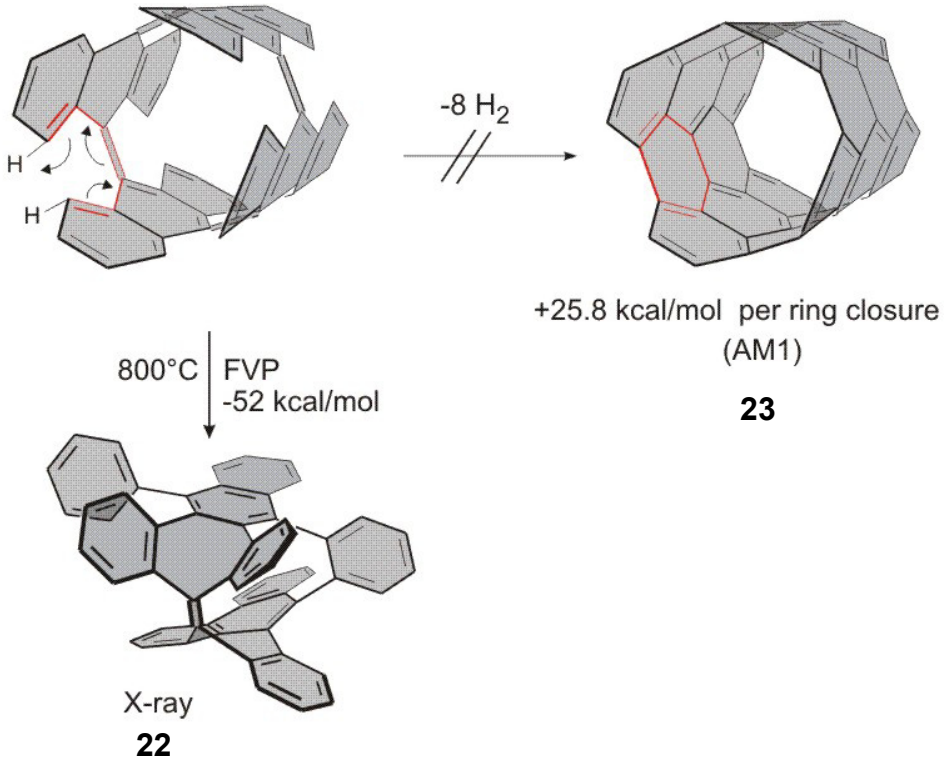

Scheme 28: Flash vapour pyrolysis of the tetramer.

Dehydrocyclization of the hexamer to a [6,6] armchair nanotube is exothermic by -5.6 kcal/mol based on semiempirical (AM1) calculations and the conversion of octamer to the [8,8] armchair nanotube at the same level of theory is even more exothermic with -62.67 kcal/mol. Hence, the tube formation is increasingly thermodynamically favored with increasing diameter of the tube (Scheme **29**). Therefore, the failed dehydrogenation of the tetramer not withstanding, the synthesis of the hexamer and the octamer is extraordinary important and their dehydrogenation still promising on the route to a rational synthesis of nanotubes.

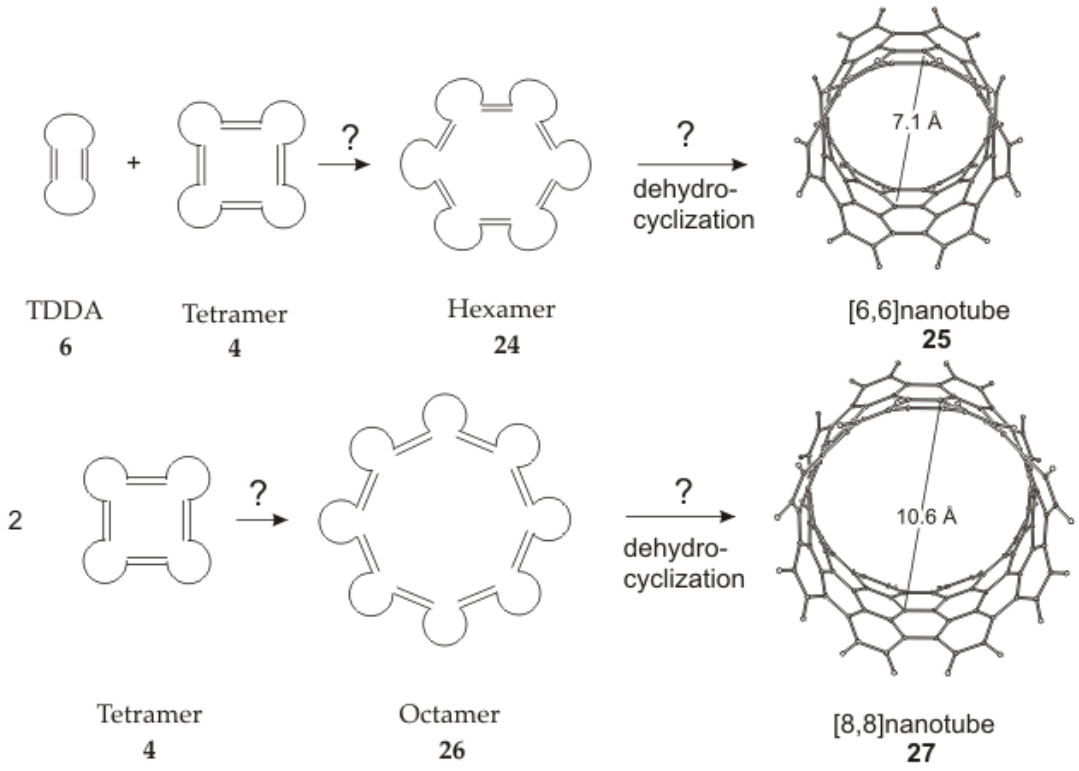

Scheme 29: Proposed methods for rational synthesis of [6,6] and [8,8] armchair nanotubes.

4.1 Improvement of the tetramer synthesis

the photochemically induced metathesis reaction of TDDA was extensively investigated. TDDA undergoes photochemically induced metathesis reaction with alkenes and cyclic alkenes and even with benzene. Dimerization metathesis of TDDA to the tetramer has been achieved after numerous variations of the reaction conditions. The metathesis product of TDDA with the solvent is the main product in homogenous solution in benzene (Scheme **30**). The tetramer has been prepared in

35% yield by irradiation of suspension of TDDA in benzene with a 700 W high-pressure mercury lamp in a quartz apparatus for 40 h.

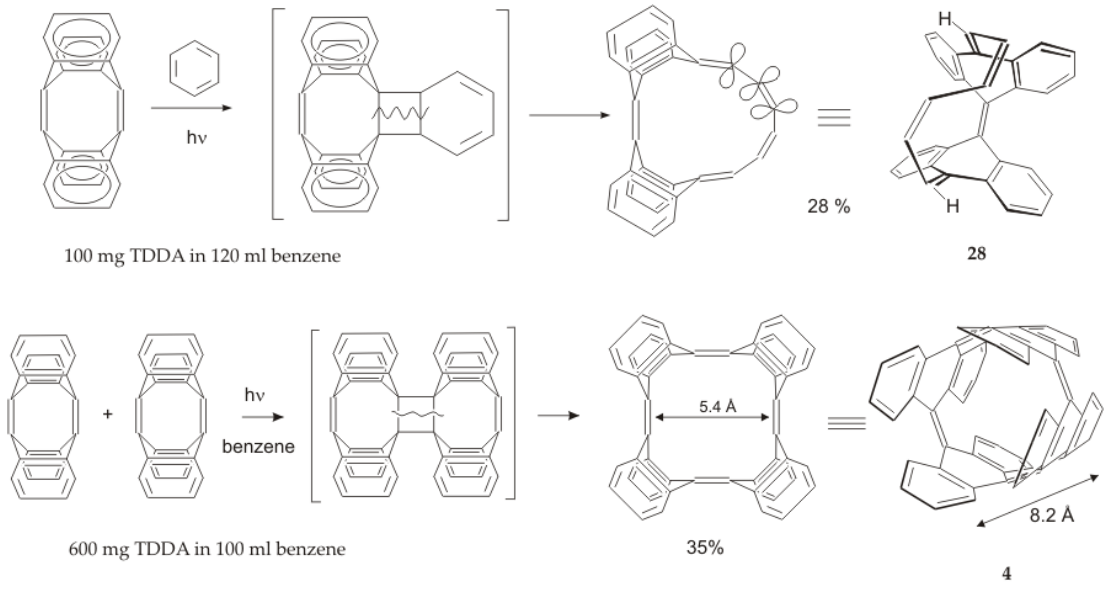

Scheme 30: Only a suspension of TDDA in benzene undergoes metathetic dimerization. In homogeneous solution TDDA react with the solvent benzene.

The long irradiation times and the lack of reproducibility are disadvantages of this method. Moreover, shortly after the beginning of the irradiation a layer of the product is deposited on the quartz tube of the lamp which prevents further irradiation of the solution. The yield of the reaction did not change with even longer irradiation times because of this contamination problem. Unreacted TDDA in the product mixture is very difficult to separate from the tetramer because both have a low solubility and similar retention times on HPLC. Therefore it is highly desirable to drive the reaction to completion. In order to avoid this problem an ultrasonic generator (cell disruptor) was used while irradiating. Surprisingly the reaction was completed after 3 hours with yield of 45%(Figure **23**).

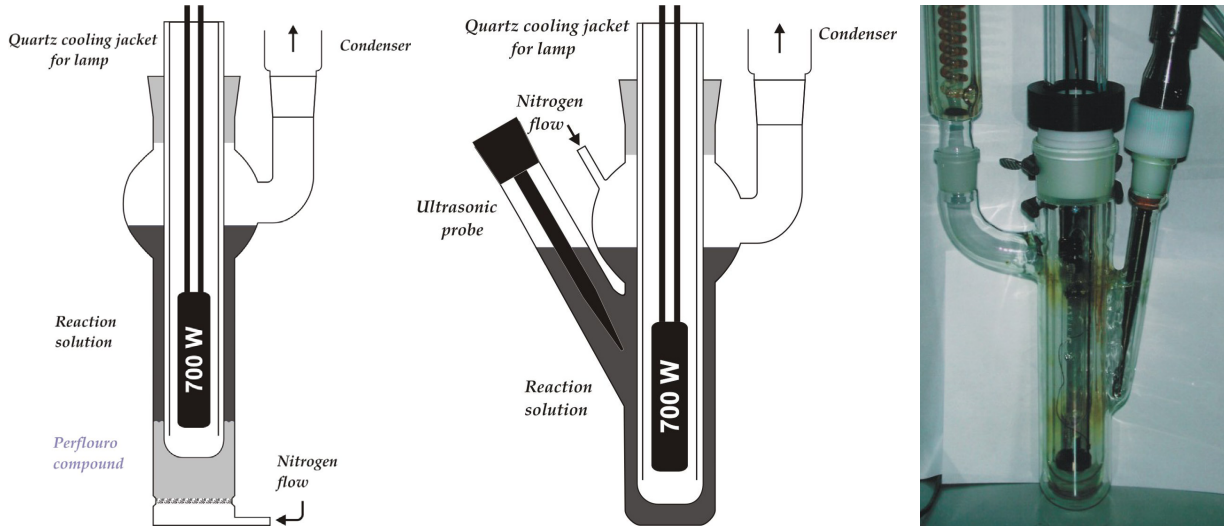

Figure 23: schematic representation of different designs of photoreactors for the preparation of the tetramer, left: use of combination of perflouro- compound and nitrogen flow to stir the reaction mixture, middle: Application of ultrasound during irradiation, right: picture of the photoreactor with the ultrasonic probe. The ultrasound generator (not shown) is located above the probe.

The crystal structure of TDDA was carefully examined to understand these results. In the crystal, the double bonds of TDDA are oriented in a favorable arrangement for a [2+2] cycloaddition with parallel π-planes and a distance of 4.31Å. The four olefinic carbons and the π-planes of the double bonds form an angle of 64° (Figure **24**). However, a solid phase photodimerization under argon atmosphere failed, probably because the crystal surface was "passivated" with layers of tetramer which has a very strong UV absorption in the range of the π-π*transition of TDDA (282nm).

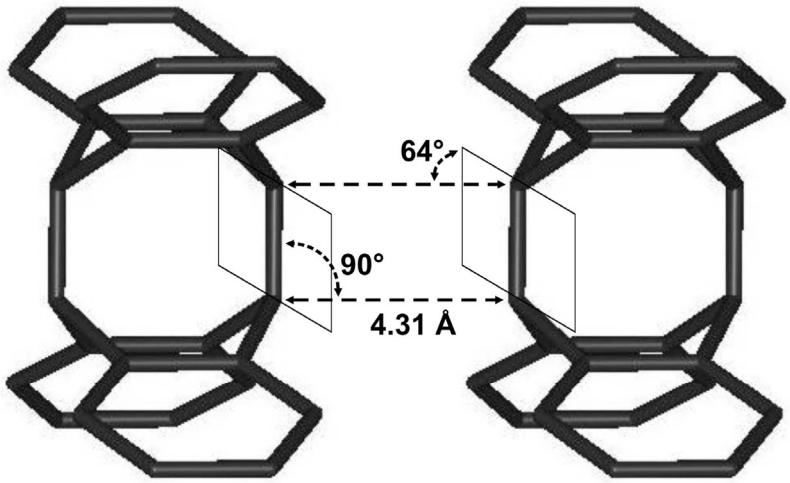

Figure 24: Arrangement of TDDA molecules in the crystal structure.

The ^{1}H NMR spectrum of the tetramer with two signals and the ^{13}C-NMR with four peaks are in agreement with a highly symmetric structure of D_{4h} symmetry. The X-ray structure analysis confirmed this assumption. Single crystals were grown in carbon disulfide/ acetonitril solution. Solvent molecules were included in the crystal. Six molecules of carbon disulfide and six molecules of acetonitril were formed in the unit cell.

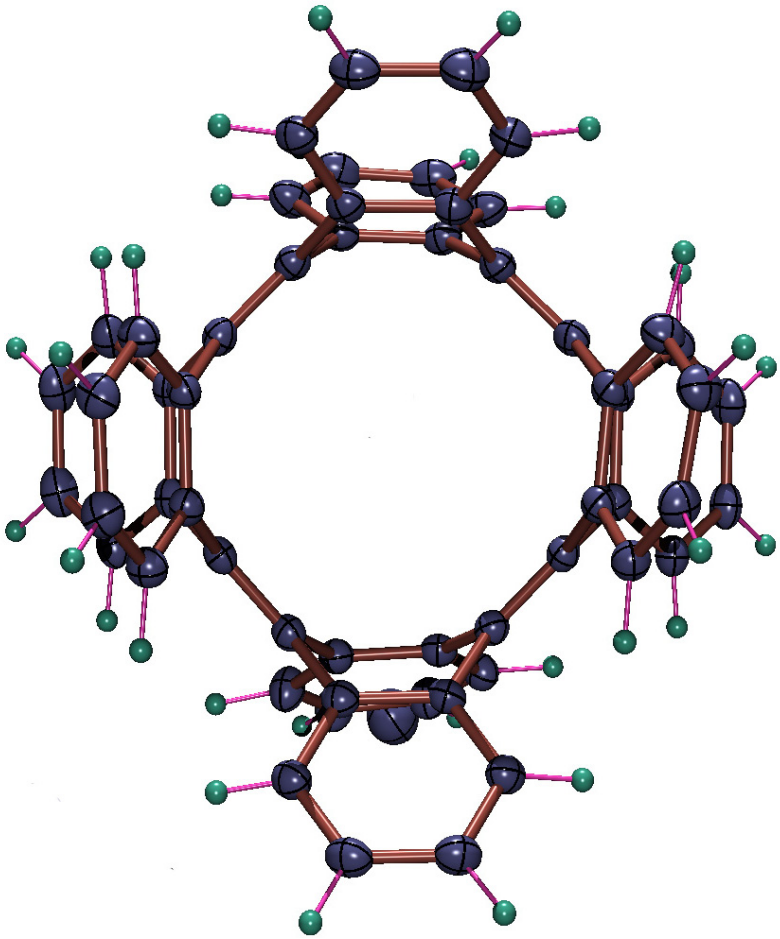

Figure 25: Ortep plot of the crystal structure of the tetramer (without solvent molecules).

There are two arrays of tetramer molecules exist in the crystal unit cell, in which their C_4 axes form an angle of 45° degrees with each other and one benzene ring of tetramer is located at the middle of the top of the adjacent tetramer (Figure **26**).

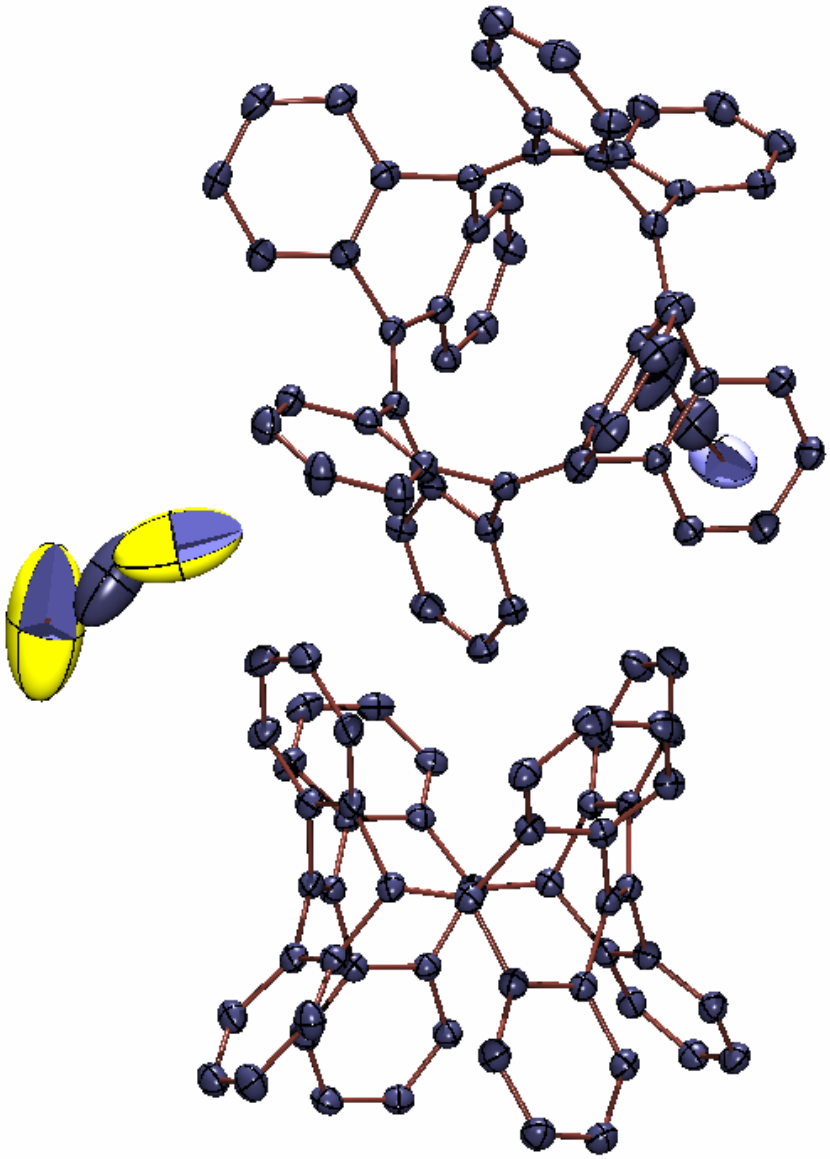

Figure 26: Arrangement of tetramers in crystal structure.

Crystal structure and NMR, which show a D_{4h} symmetric structure, are in contradiction with theoretical calculations. According to DFT calculations at the B3LYP/6-31G* level of theory the D_{2d} structure of the tetramer is 4.4 Kcal/mol lower in energy as the D_{4h} structure. This seeming contradiction can be resolved if one assumes a fast equilibrium of two D_{2d} structures, in which the D_{4h} structure is the transition state of the conformational interconversion. Comparing the matrix infrared

spectrum of tetramer with theoretically calculated spectra (B3LYP/6-31G*) proved a D_{2d} minimum structure.[78] Thus, X-ray and NMR correspond to a time-averaged D_{4h} structure.

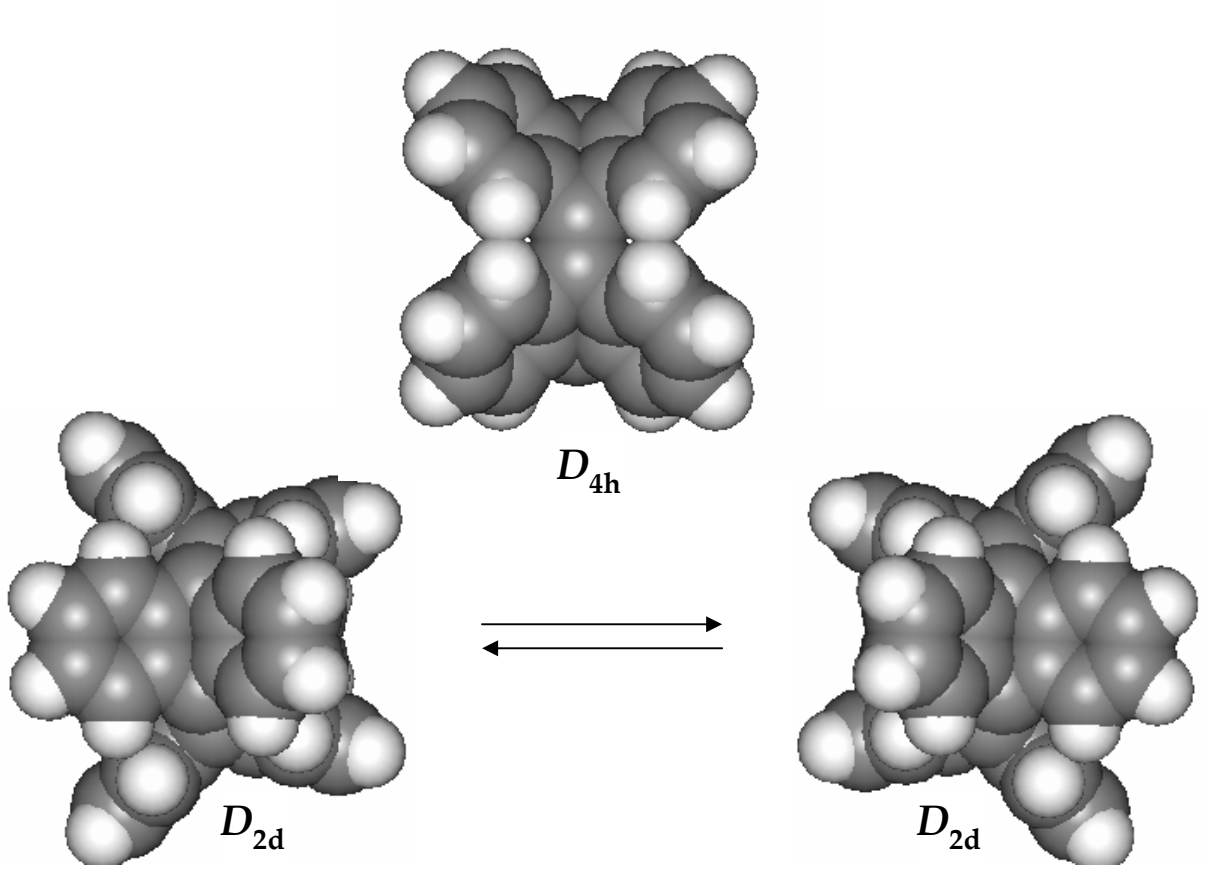

Figure 27: DFT calculation (B3LYP/6-31G*) predict an equilibrium between two D_{2d} isomers of tetramer that D_{4h} isomer is transition state.

Theoretically tetramer with an inner periphery of 16 electrons should be antiaromatic if all p-orbitals have a good overlap with each other. The gap between HOMO and LUMO is 0.149 for the D_{4h} isomer and 0.136eV for the D_{2d} isomer (B3LYP/6-31G*). The calculated NICS (0) values at B3lYP/6-31G* level of theory for the D_{2d} isomer of the tetramer is –0.7055 and –0.2102 for the D_{4h} indicate the nonaromatic property for tetramer.

4.3 Photochemically induced metathesis reaction of the tetramer

The photochemically induced metathesis of the tetramer with TDDA should give rise to the metathetic dimerization of the tetramer should furnish the octamer, which are very useful intermediate towards a rational synthesis of carbon nanotubes. Therefore the photochemical reaction of the tetramer was carefully investigated. The tetramer is extraordinarily stable and unreactive, even toward *m*-chloroperbenzoic acid and bromine at room temperature. Comparing the van der Waals surface of tetramer with TDDA shows that the bridgehead carbon-carbon double bonds in the tetramer are unavailable for further reaction because of the steric hindrance of the ortho hydrogen atoms of the neighboring benzene units (Figure **28**).

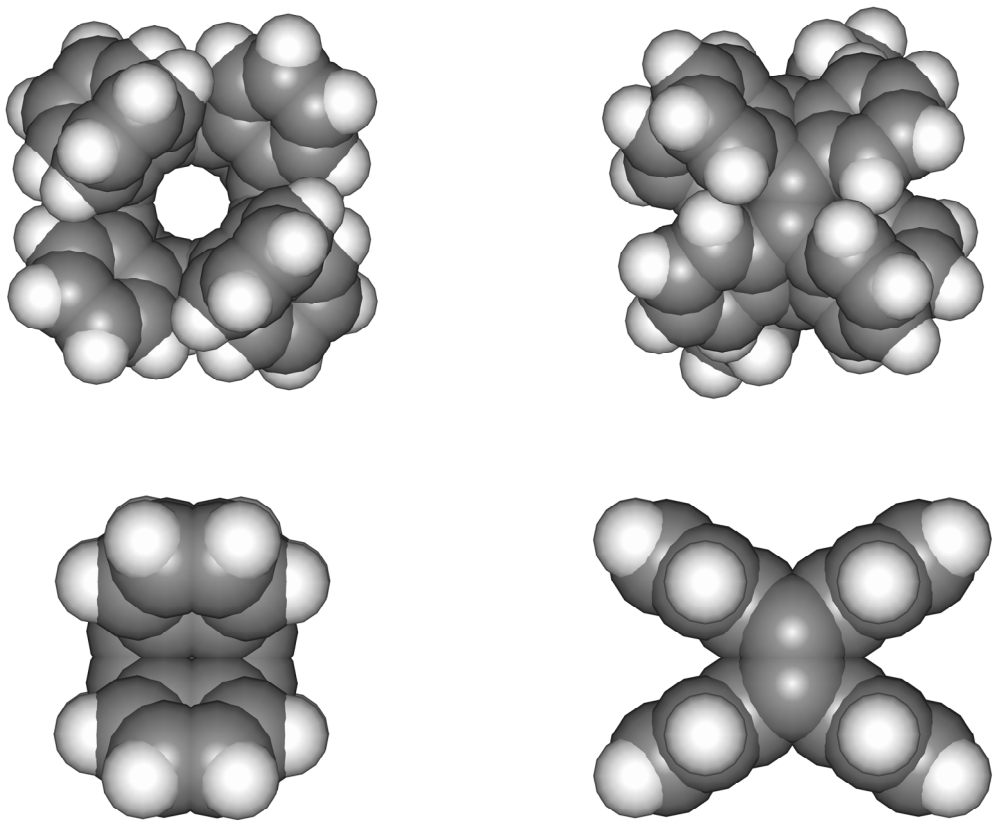

Figure 28: Comparison of the van der Waals surface of the D_{2d} tetramer (top) with TDDA (bottom).

A high concentration of the substrate is favorable in any kind of dimerization. The insolubility of the tetramer in common organic solvents is another challenge towards the dimerization reaction. Only 3 mg of tetramer dissolve in 10 ml of benzene. There was no evidence for the formation of a dimerization product after irradiation of the homogeneous solution of tetramer in benzene with a 700 W high-pressure mercury lamp in a quartz photoreactor for 20 hours. The photodimerization of a suspension of the tetramer in benzene also was not successful. Using a 250 W ultrasonic probe during irradiation (similar conditions as in the dimerization of TDDA) also failed to give the desired product. Several different photoreactors were designed to irradiate the tetramer effectively under different conditions (Figure **29**).

Figure 29: Several different quartz photoreactors designed for an effective irradiation of tetramer.

The tetramer is quite soluble in arsenic trichloride (8.8 mg/ml). Irradiation of the tetramer in arsenic trichloride ended with unreacted tetramer and dichlorotetraanthryl. The same reaction was performed in carbon disulfide but again no evidence for the formation of octamer existence was observed.

4.2 Photoreaction of tetramer in micellar solution

During the past decade aqueous micellar solutions have been extensively used as media for photochemical reactions and in many situations a dramatically change of the reaction course was found compared to the homogeneous media[79]. A surfactant or detergent is a molecule whose structure possesses both polar (or ionic) and nonpolar moieties. A typical detergent structure is RX, where R is a straight chain hydrocarbon, and X is a hydrophilic group. In aqueous solution the polar portion of the detergent is hydrophilic and the nonpolar part is hydrophobic and result of these antagonistic chemical features there is a tendency for cooperative self-association of detergent monomers to form aggregates. The term ''micelle'' refers to such aggregates of colloidal dimensions. The most relevant property of micelles in moderating reactivity is their ability to solubilize hydrophobic molecules in a bulk aqueous solution. In general, there are five common types of effects that micelles can impose on reactions: cage, local concentration, viscosity, polarity, and electrostatic effects.

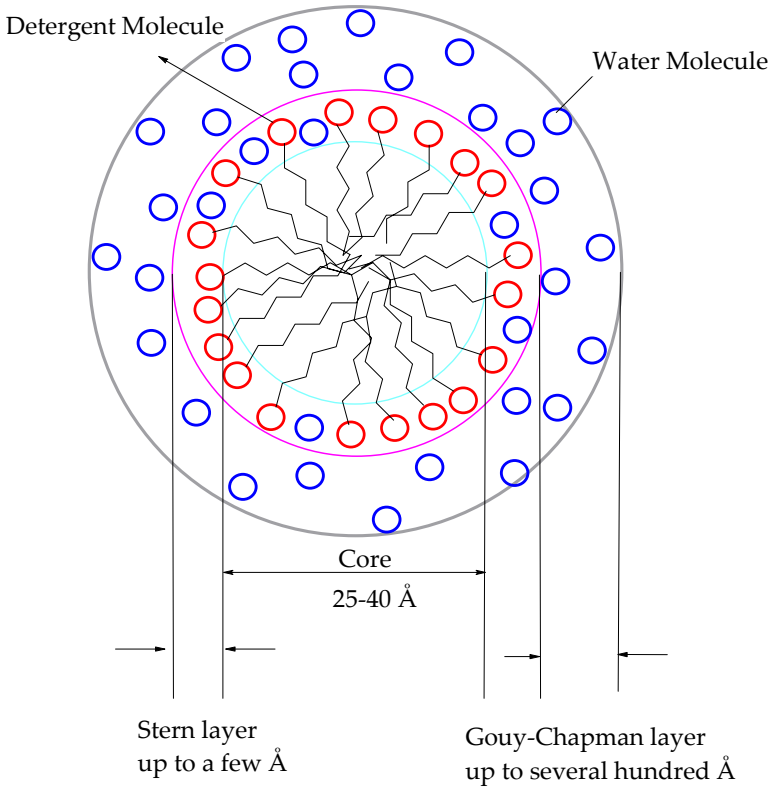

Figure 30: Schematic representation of a typical micelle.

Photodimerizations of aromatic hydrocarbons are enhanced in micellar solution over homogeneous solutions. The photodimerization of acenaphthylene is affected by the presence of micelles[80]. The yield of the reaction changed from 8% to 96.5% with leaving classical photodimerization in benzene to use an anionic micelle like sodium dodecyl sulfate (SDS). Also a change in the regioselectivily is observable and this change is slightly dependent on the nature of the surfactant. The ratio of syn to anti cycloaddition product is (0.93:1) for 10% aq. PBC-34 compared with (2.7:1) for 5% aq. SDS (Scheme **31**).

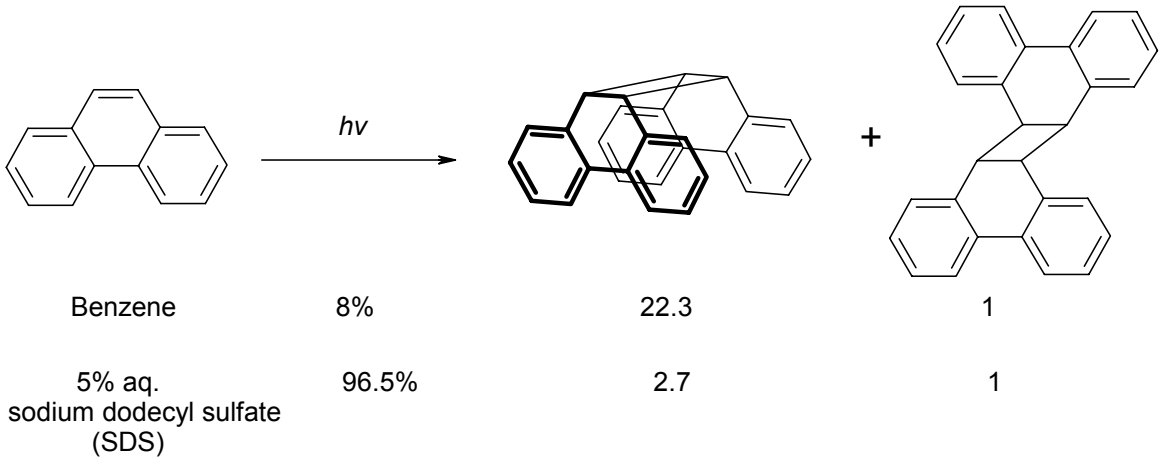

Scheme 31: Yields and ratios of products for the photochemically induced acenaphthylene dimerization.

The tetramer was irradiated in 10%, 5% and 2% aq. sodium dodecyl sulfate with a 700 Watt high-pressure lamp in a quartz apparatus. The formation of octamer was not observed even after 48 hours of irradiation. In another try a mixture of tetramer and TDDA was irradiated in different micelle concentrations but again there was no addition product detected. Finally TDDA was irradiated under the same conditions, no addition product, was observed even though the tetramer is the major product (35% yield) in the photodimerization reaction of the suspension of TDDA in benzene. Most probably TDDA and the tetramer are too big to accumulate in high concentrations inside the micelle.

4.3 Irradiation of the tetramer in aliphatic solvents

The synthesis of the tetramer was only achieved by irradiation of a suspension of TDDA in benzene. Benzene has an absorption of 254 nm and it also reacts with TDDA in a ring enlargement metathesis reaction. Changing benzene to an aliphatic hydrocarbon solvent could have several advantages, first the solvent does not adsorb within the range of the wavelength necessary for the photoreaction, and secondly it is possible to heat the reaction media while irradiating if one uses an aliphatic hydrocarbon with a higher boiling point like decane (b.p. 174°C), dodecane (215°C), or tetradecane (252°C).

A suspension of the tetramer was irradiated in dodecane with a 700 Watt high-pressure mercury lamp in a quartz apparatus under sonification with 250 Watt ultrasonic probe (cell disruptor). After 10-hours of irradiation and sonification, the tetramer was completely converted to some products. The small retention times in Gel permeation chromatography suggest that the products have a much bigger structure than the tetramer. The analysis by MS spectroscopy failed because the compounds were not volatile. There is also no chance to measure NMR spectra because the products are low soluble in common organic solvents, even NMR spectroscopy with arsenic chloride as a solvent did not give useful information. Transmission electron microscopy (TEM) or scanning electron microscopy (SEM) of the products probably could provide useful structural information.

4.4 Solid phase irradiation of the tetramer

Solid tetramer was irradiated with a 700 Watt high pressure mercury lamp and a 15 Watt low pressure mercury lamp under inert gas. The analysis of the substrate after several hours of irradiation did not give any indication of a reaction. This unreactivity of the tetramer in compared with TDDA probably is due to the arrangement of the tetramer molecules in the crystal structure, in which adjacent molecules form an angle with respect to each other. This arrangement is not

favourable for the dimerization reaction in the solid phase. Under high pressure the well defined arrangement should transform into a random amorphous orientation of the tetramer in the solid, increasing the probability of a favourable arrangement for the photodimerization. However, a pill made with a conventional IR press also did not give products after irradiation.

Finally the use of a laser as the energy source for the dimerization reaction of the tetramer in the solid state was considered. Matrix-assisted laser desorption (MALDI) mass spectrometer use a nitrogen laser source with 337 nm wavelength and this is the easiest way to investigate the behaviour of the tetramer under laser irradiation. In the MALDI-MS instrument the angle of the laser beam with respect to the sample surface can be tuned 30° and 75° and it is focused with either a single or a multielement optical system and passed through a window into the mass spectrometer. The position of the laser focus with respect to the sample surface can be changed by shifting the optical axis of the sample beneath a fixed axis.

A saturated solution of tetramer in dichloromethane used to make a thick layer of tetramer on the surface of a MALDI plate. The plate was loaded into a Bruker FlexIII™ MALDI-TOF MS instrument and it was tried to find the best combination of

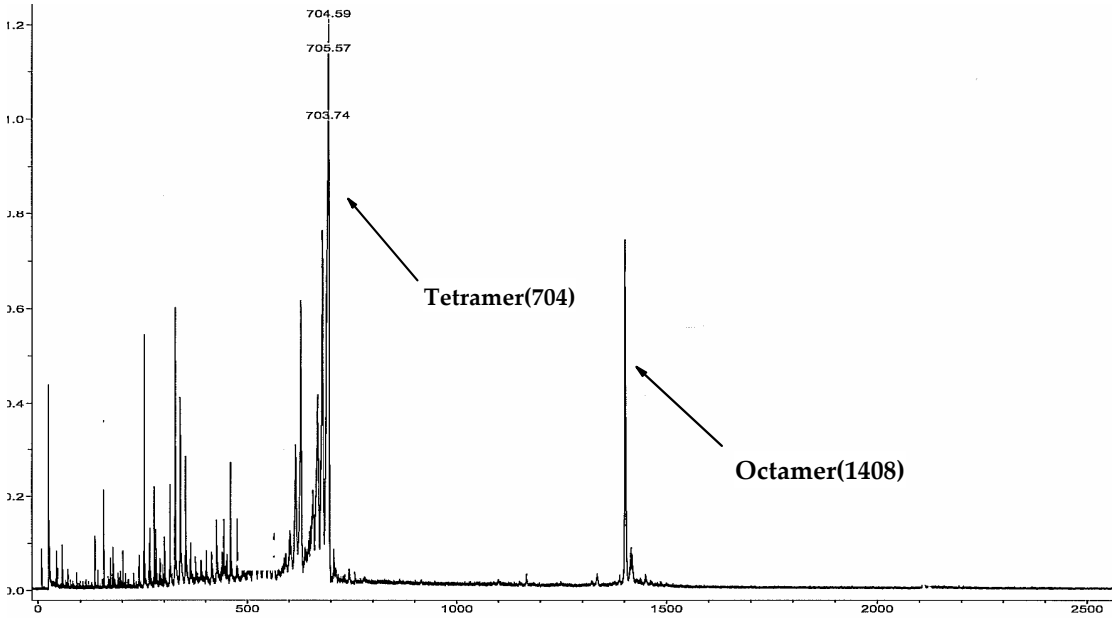

Figure 31: The Bruker FlexIII™ MALDI TOF MS spectrum for the tetramer without matrix, more than 60% laser intensity and 80 shot per run

the intensity of the laser beam in each shot, number of shots, and changing the position of laser focus during shooting. Indeed, the octamer was detected in the MALDI-MS detector if the intensity of the laser beam is larger than 60% and if 80 shots per run are applied (Figure **32**). The detected isotope distribution is in a very good agreement with the calculated one (Figure **33**).

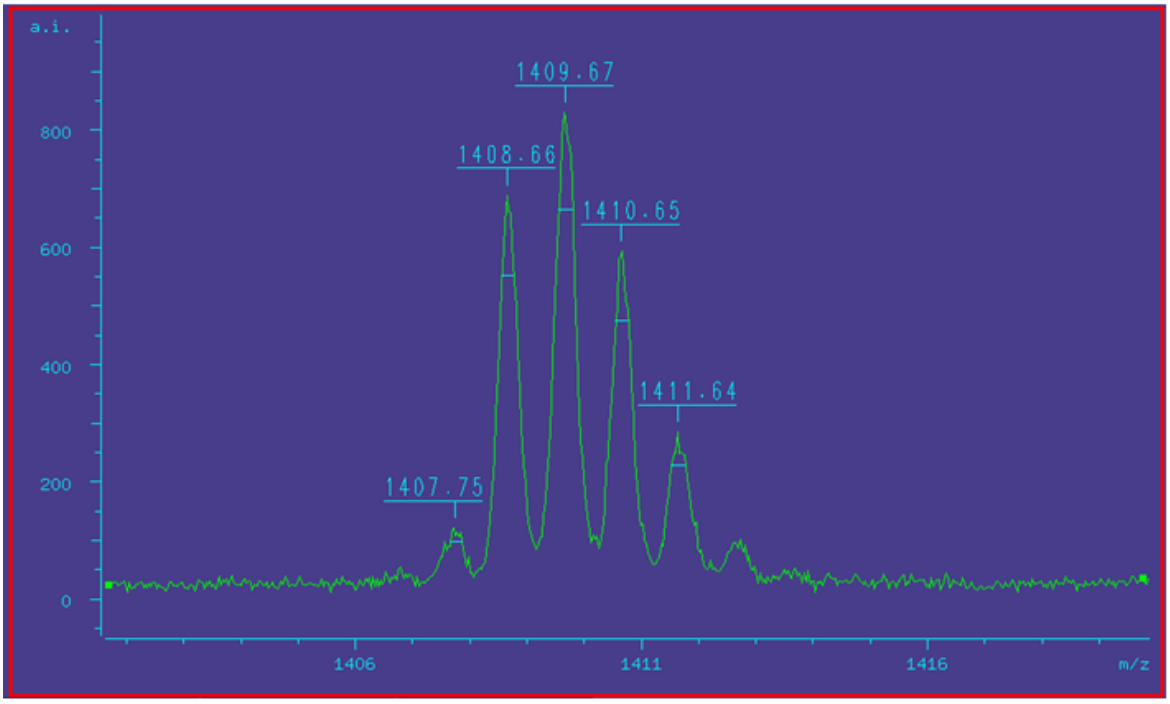

Figure 32: The isotope pattern of the assumed octamer molecular peak recorded with a Bruker FlexIII™ MALDI-TOF MS

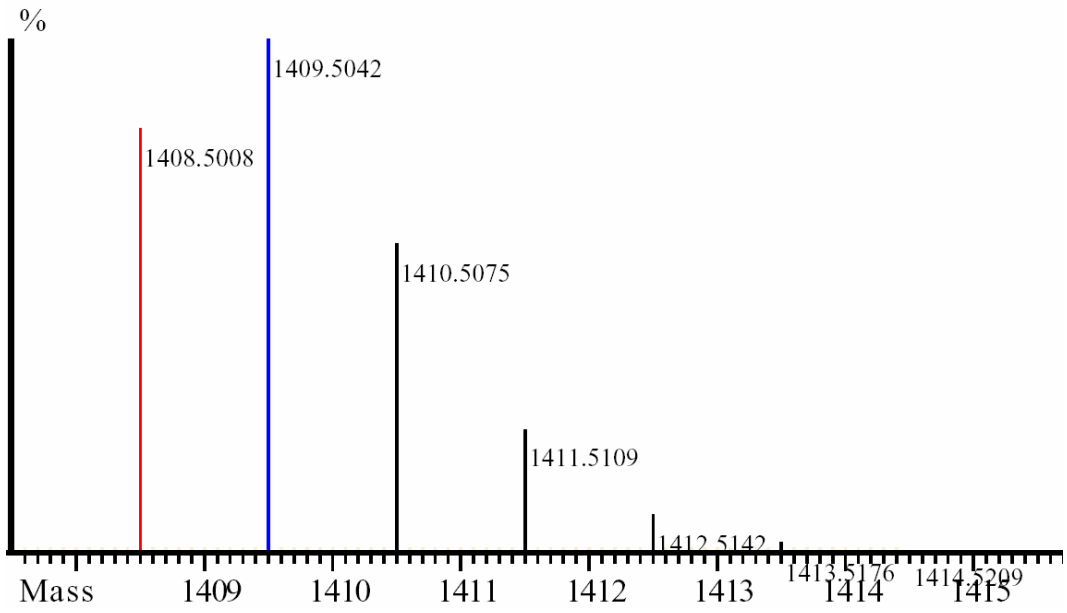

Figure 33: High-resolution calculated isotope pattern for octamer.

If a higher intensity of the laser beam (up to 90%) and suppression up to 1000 Dalton for the detector is used, it is possible to detect even the dodecamer in the MALDI-TOF MS detector (Figure **34**) in a very low yield.

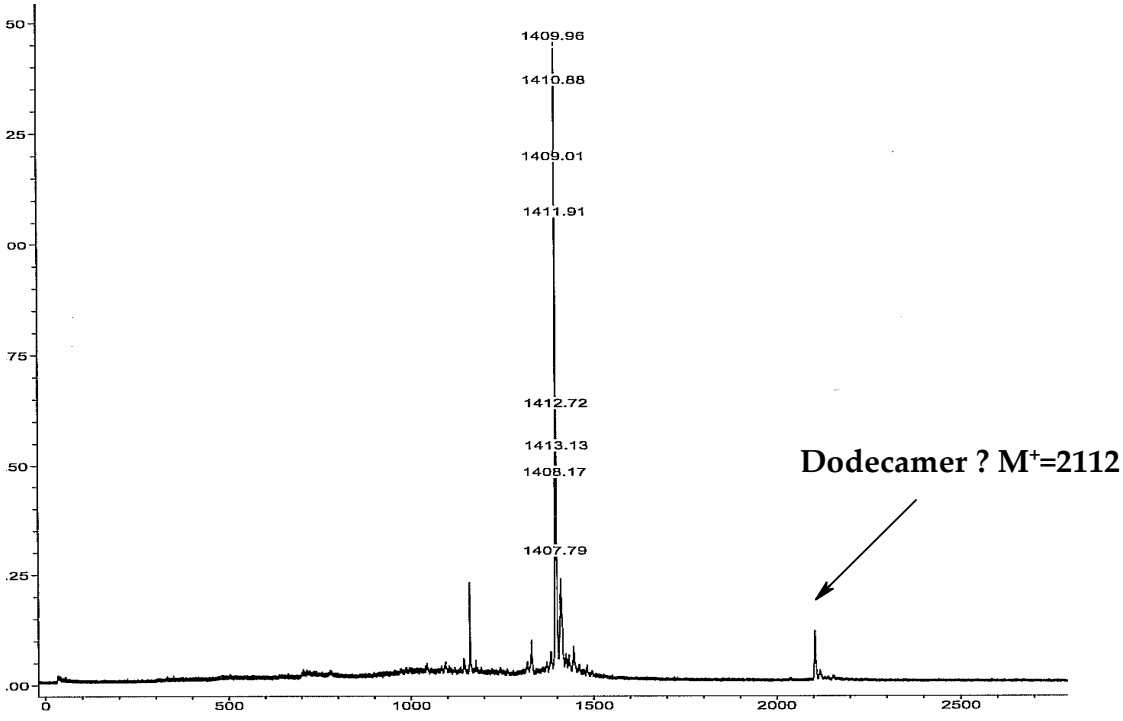

Figure 34: the Bruker FlexIII™ MALDI-TOF MS spectrum for the tetramer without matrix, with >90% laser intensity and 150 shots per run and a suppression up to 1000 dalton for the detector.

Several attempts were performed to find a possible way to irradiate tetramer with a stronger laser in larger scale. There are several parameters that should be met in order to be able to produce the octamer in a large scale. A compressed pill of tetramer (produced with a conventional IR press) was irradiated with 254 nm wavelength laser and 3 mjoule energy in a normal atmosphere. As shown in Figure **35**, due to technical problems it was not possible to change the position of the laser fast enough to avoid further decomposition reactions and probably also inert atmosphere is necessary to prevent oxidation reactions. Optimizations of the laser wavelength, laser intensity, reaction media, thickness of the pill, atmosphere of the reaction and the mechanical rotation of the sample during irradiation and irradiation time are necessary to find the best reaction conditions.

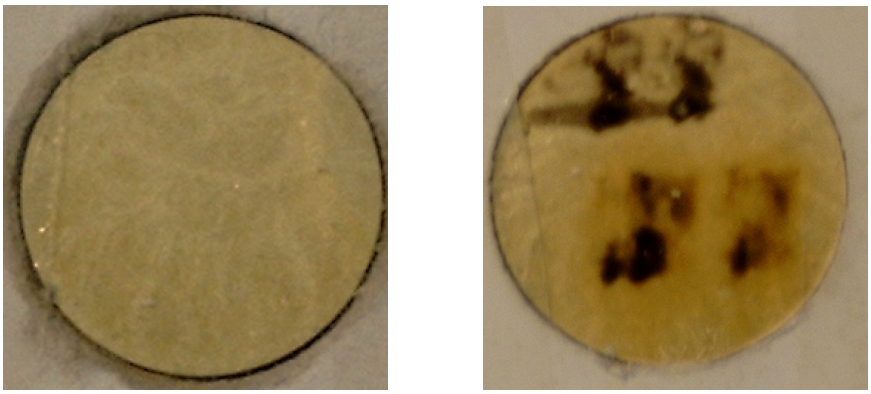

Figure 35: Comparison of compressed tetramer pill before and after laser shooting.

Not only the dimerization of the tetramer but probably also the dehydrocyclization can be achieved by laser treatment. The dehydrocyclization of the tetramer with a laser as the energy source looks promising. The fundamental experiment was done in a MALDI-TOF MS instrument in which a sample of the tetramer was treated with a nitrogen laser in a high vacuum. Some peaks were detected in the expected range for the dehydrocyclization reaction products in the MALDI-TOF MS detector.

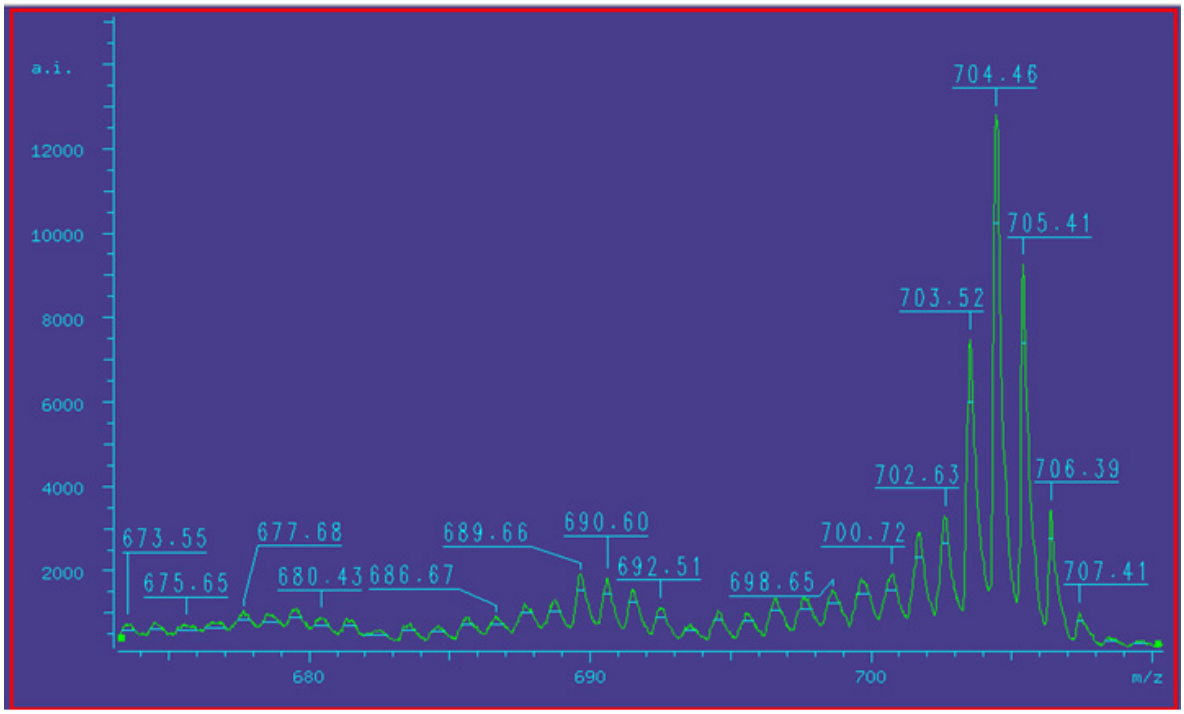

Figure 36: High resolution MS spectrum of the tetramer recorded with a Bruker FlexIII™ MALDI-TOF MS spectrum

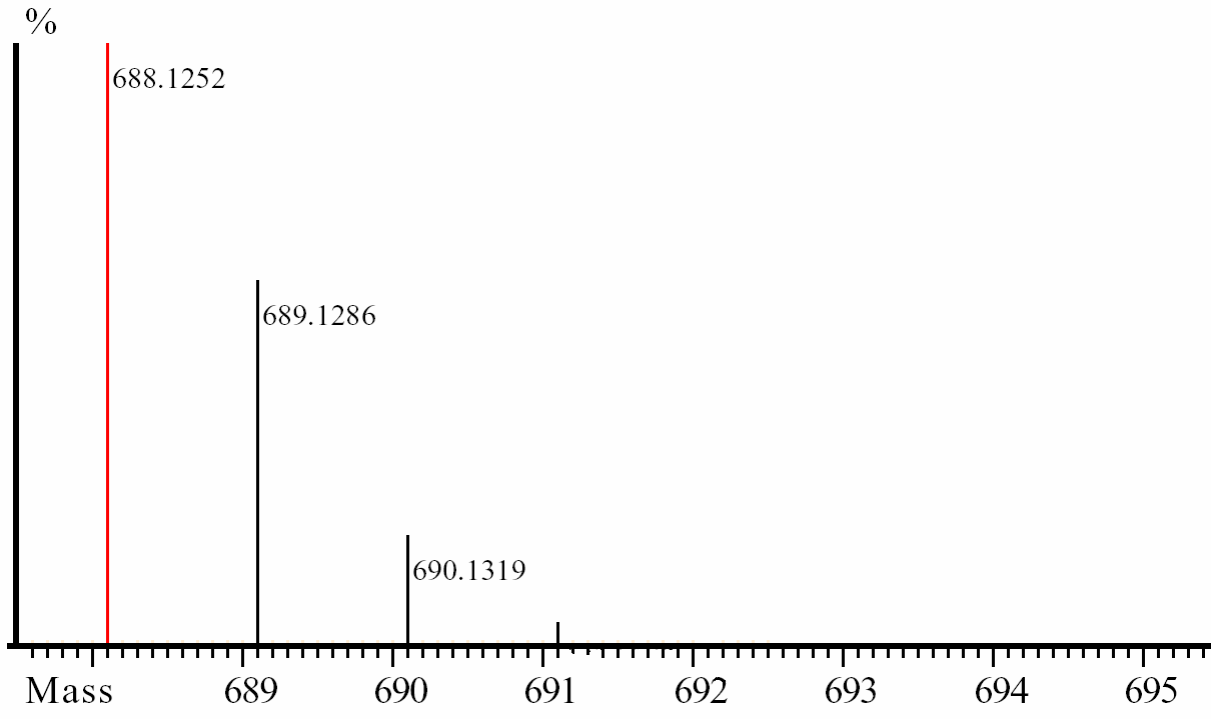

Figure 37: Calculated isotope pattern for the attempted [4,4] armchair nanotube.

4.5 Calculated structures of the hexamer and the octamer

The semiempirical (AM1) calculation of the hexamer **24** predicted a D_{3d} symmetrical structure as the global minimum. There is a fast equilibrium between two D_{3d} structures at room temperature. The D_{6h} structure was found to be the transition state of this conformational interconversion (Figure **38**).

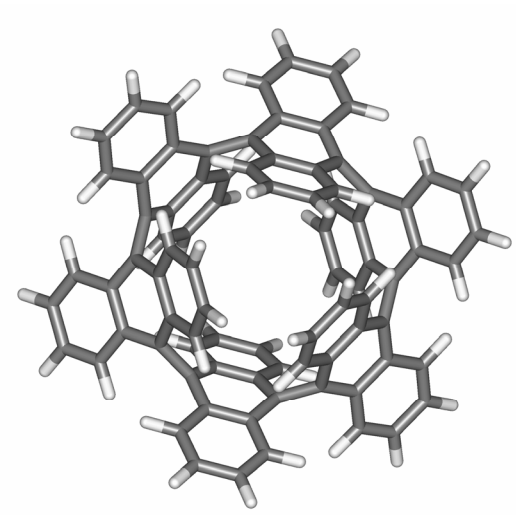

24

Figure 38: Semiempirical (AM1) calculated structure of the hexamer with D_{3d} symmetry.

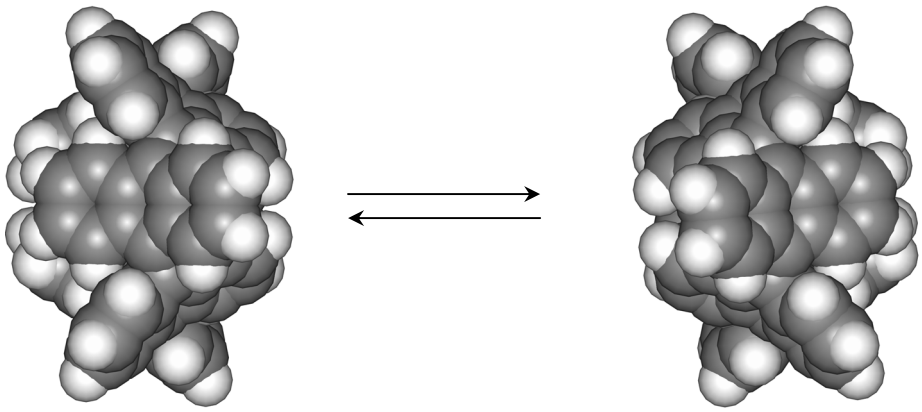

Figure 39: AM1 calculation predict a fast equilibrium between two D_{3d} conformers of the hexamer.

The twelve fold dehydrocyclization of the hexamer at the ortho positions of the benzene rings is exothermic -5.60 Kcal/mol according to the semiempirical (AM1) calculations. A [6,6] armchair carbon nanotube **25** would be formed by this dehydrocyclization. The tube has a diameter of 8.12 Å (Figure **40**)

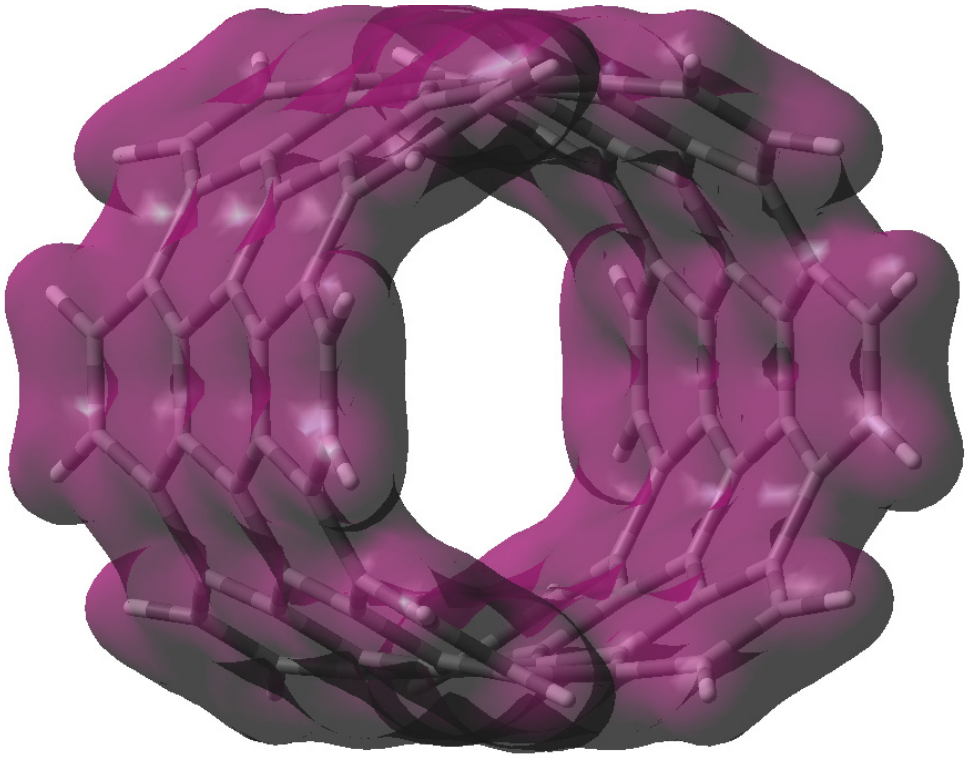

25

Figure 40: The semiempirical (AM1) calculated electron density surface of the [6,6] armchair nanotube (at 0.04 isovalue) that would be formed by dehydrocyclization of the hexamer.

The octamer **26** also has a D_{4d} structure with anthracene units that are twisted with respect to the four-fold axis. A pincer-like movement of the anthracene moieties interconverts the two conformations. Four pincers are always closed and four are opened. Changing the state of one of the pincers reverses the state of the other seven pincers.

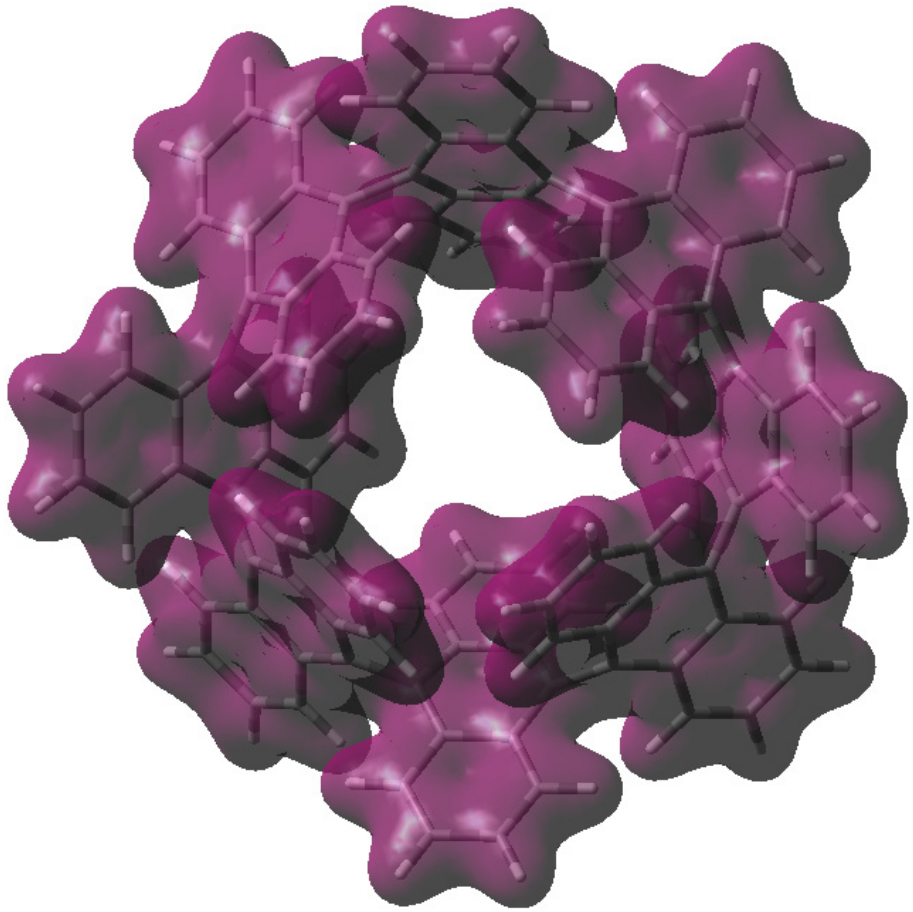

26

Figure 41: The semiempirical (AM1) calculated electron density surface of D_{4d} isomer of octamer at 0.04 isovalue.

The sixteen-fold dehydrocyclization of the octamer would result in a [8,8] armchair carbon nanotube in an exothermic reaction (H°= -62.67 Kcal/mol). This tube has a C_{8h} symmetry and a diameter of 10.80 Å. The diameter of octatube is perfect for encapsulating C_{60} . similar π–complexes are known

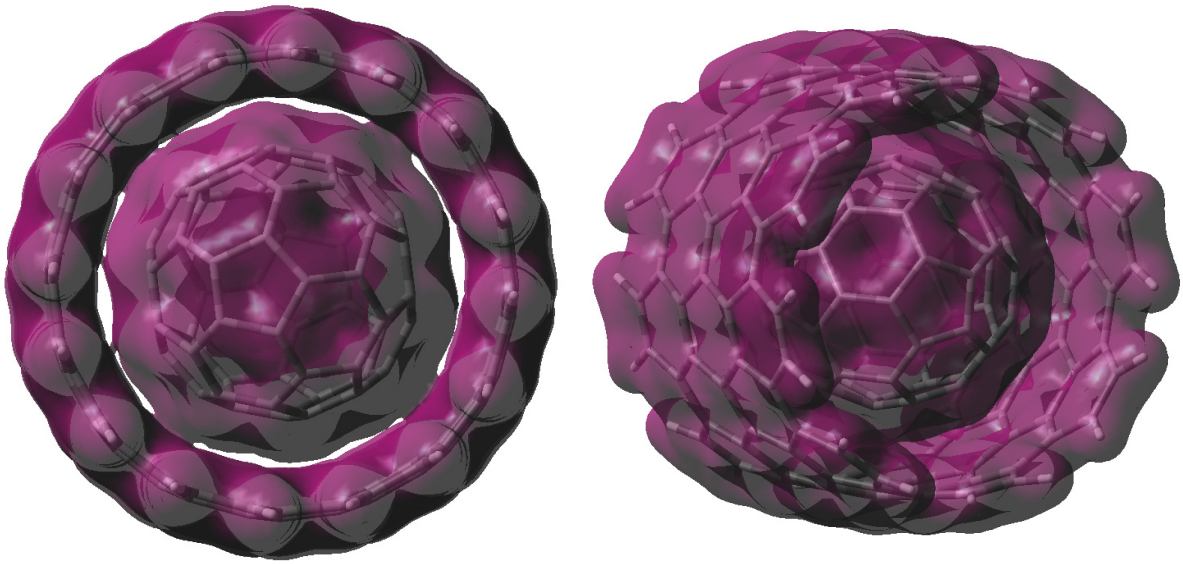

Figure 42: The semiempirical (AM1) calculated electron density surface of encapsulated C_{60} with octatube at 0.04 isovalue.

4.7 Conclusion

The photochemically induced metathetic dimerization of the tetramer was extensively investigated. The expected product of this dimerization is an octamer with D_{4d} symmetry, which is a very important intermediate for the rational synthesis of carbon nanotubes. According to caculation an exothermic dehydrocyclization reaction should form a short piece of a [6,6]armchir nanotube. The sonification of TDDA in benzene during irradiation improved the synthesis of the tetramer but further reaction to give the octamer was not observed. Attempts in micellar systems also failed. The solid phase irradiation of the tetramer in the crystalline state and also as a compressed pill did not yield the octamer. Finally nitrogen laser was used as an energy source for this dimerization reaction. Preliminary experiments with a Bruker FlexIII™ MALDI-TOF MS instrument were positive. Attempt to overcome the technical problems are in progress.

5 Möbius Aromatic compounds

5.1 General

In 1858,J. B. Listing and A. F. Möbius independently discovered and investigated the properties of the one-sided and one-edged surface, which today is famous as the Möbius strip or Möbius band. The mysterious three-dimensional structure is formed physically and mathematically when a ribbon is twisted by 180 degrees and its two ends are joined together (Figure **43**). The Möbius strip has developed a life of its own independent of mathematics—in the realms of magic, science, engineering, literature, music, film, art, and elsewhere. Engineers have been interested in the economical application of the Möbius bands e.g. in using Möbius shaped conveyor belts with increased life time because the one-sided surface would be evenly worn or recording tapes with double the playing time.

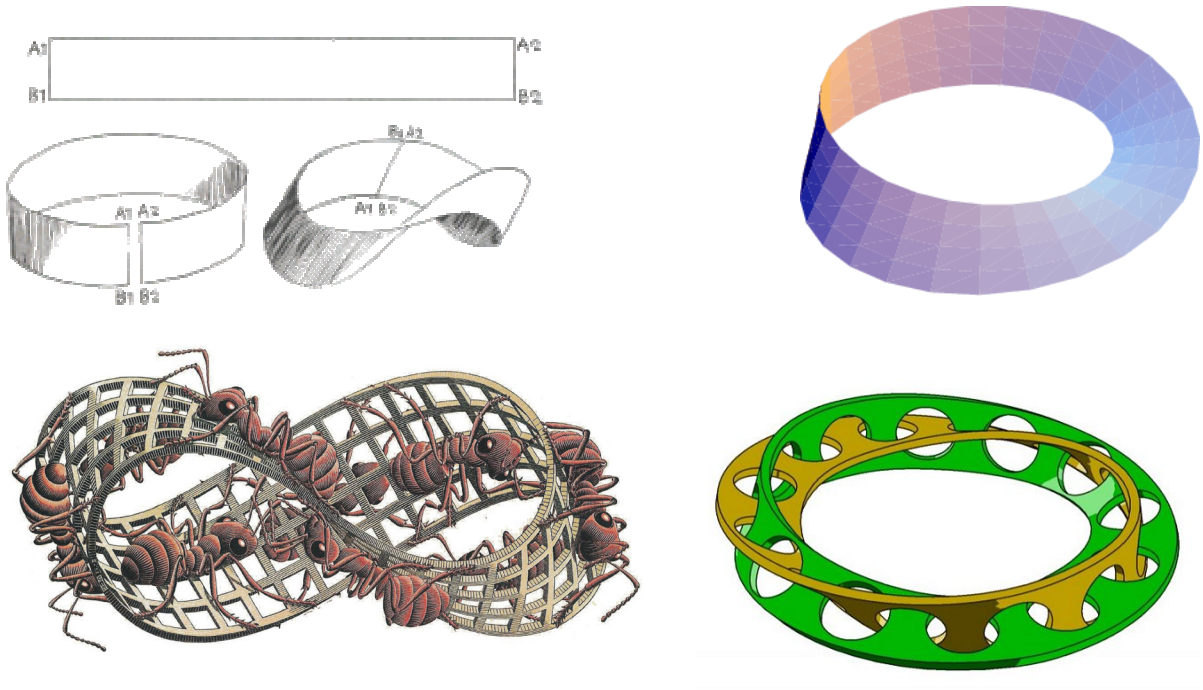

Figure 43: Building a Möbius strip with a 180° twist from a rectangular strip, Escher's artistic picture of a Möbius band with ants.

5.2 Möbius topologies in chemistry

5.2.1 Möbius-type conjugation in annulenes

In 1964, E. Heilbronner[81] based on simple Hückel theory predicted that Möbius-like twisted annulenes would be aromatic with 4n electrons and antiaromatic with 4n+2 electrons, which is reverse to the Hückel rule for "normal" annulenes. In [n]annulenes the p orbitals can be twisted into a Möbius strip when all neighboring p orbitals have an angle of π/n. The resonance integral β^M of a twisted π bond is given by βcosπ/n, where β is the standard integral for parallel p orbitals. The orbital energies E_J^M for Möbius systems according to a simple Hückel equation are:

$$E_J^M = \alpha + 2\beta^M \cos\pi(2J+1)/n$$

J= 0, 1, 2, ……., n-1

In comparison, the corresponding orbital energies for Hückel systems are given by:

$$E_J = \alpha + 2\beta \cos(2\pi J)/n$$

J= 0, 1, 2, ……., n-1

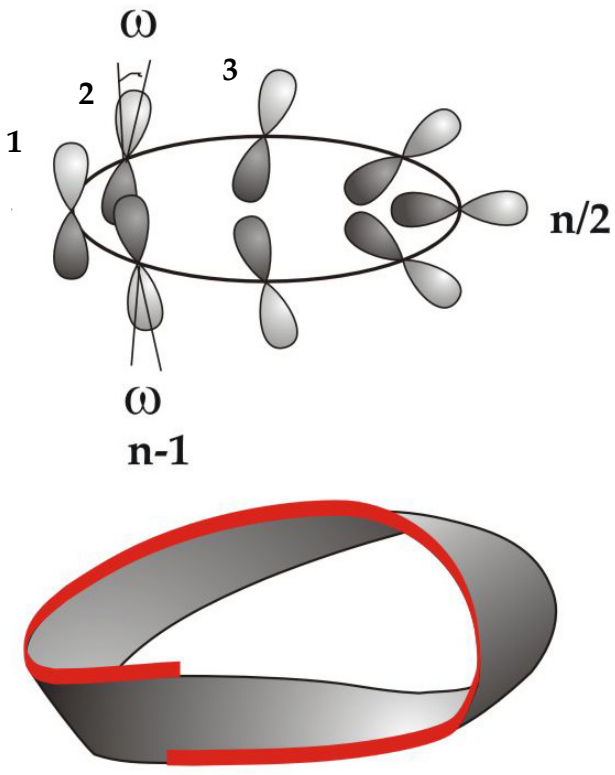

Figure 44: Representation of the Möbius type overlap of p orbitals.

If n is even, the energy levels E_J^M are degenerated in contrast to standard Hückel systems which have a non-degenerate lowest bonding and a non-degenerate highest antibonding level. In a Möbius perimeter with an odd number of electron pairs n the only undegenerated state is the highest antibonding level whereas for Hückel systems, this is true for the lowest bonding level (Figure **45**). Therefore a closed shell configuration is possible with **4n** p electrons in Möbius systems and with **4n+2** p electrons in Hückel systems.

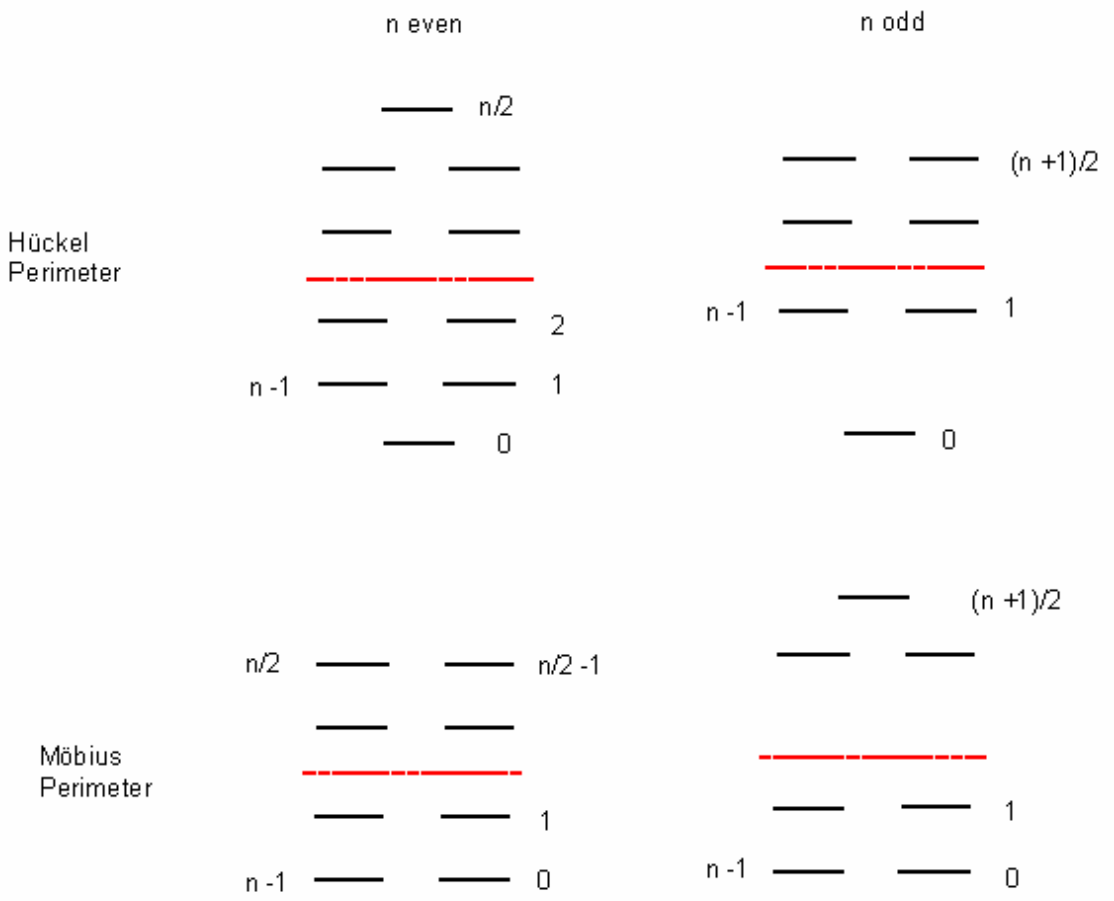

Figure 45: Energy levels of orbitals in Möbius and Hückel systems for even and odd numbers of electron pairs.

5.2.2 Application of the Hückel-Möbius concept in organic chemistry

Frost[82] and Zimmerman[83] described a simple mnemonic to derive the MO energies of Hückel and Möbius systems. This graphical method is useful in quickly obtaining

the energies of orbitals. The circle mnemonics in Figure 52 illustrate the electron counting rules for 3-6 membered Hückel and Möbius rings. The circles have a diameters of 4α and the energies are given in units of β, where α is the coulomb and β the resonance integral as defined inn Hückel theory. The horizontal dashed line separates the bonding from the antibonding levels.

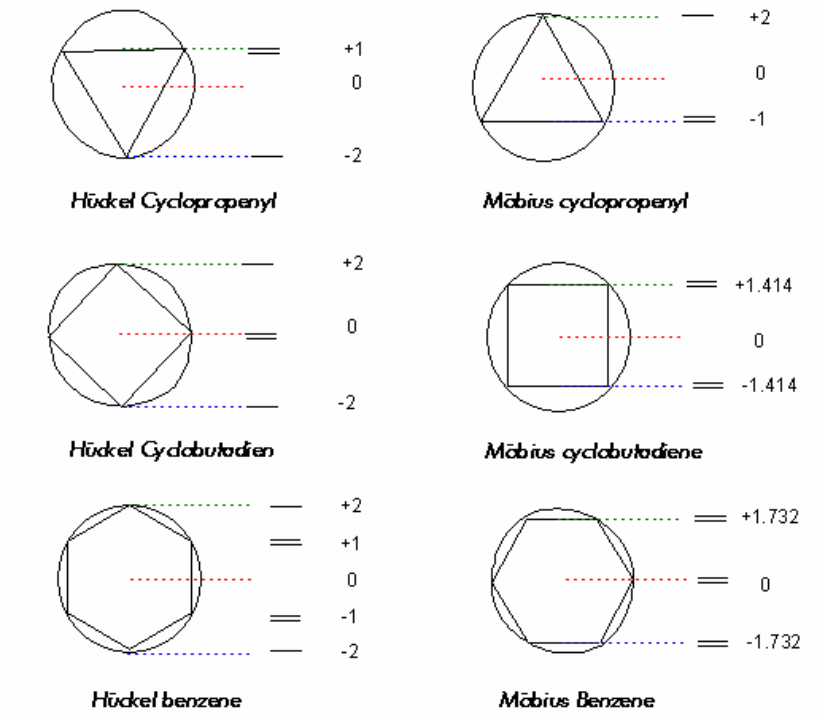

Figure 46: MO energies of the cyclopropenyl, cyclobutadiene and benzene system derived by the Frost (right) and Zimmermann (left) mnemonic.

The differentiation of Hückel-Möbius topologies in electron delocalization has been applied to distinguish between allowed and forbidden with concerted reactions. In electrocyclic reaction, there are two possible ways for closing the ring the terminal p orbitals either rotate in the same direction to make a bond (conrotatory) or they twist in different directions (disrotatory). The conrotatory transition state has one sign inversion in the array of cyclicly overlapping basis orbitals and is a Möbius system while the disrotatory reaction passes a transition state in which the overlapping orbitals don't exhibit a sign inversion and therefore have Hückel topology (Figure **47**). Aromatic transition states are stabilized and the corresponding reactions are allowed, whereas reactions that would pass an antiaromatic transition state are forbidden. Consequently in ground state in 4n electron systems conrotatory

ring closure is allowed and in 4n+2 electron systems the favorable mode is disrotatory[84].

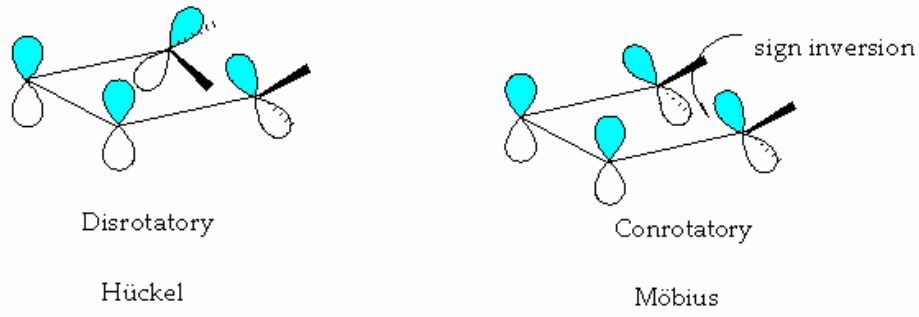

Figure 47: Disrotatory and conrotatory mode in ring closure of cyclobutadiene.

5.2.3 Theoretically calculated Möbius annulenes

Whereas Möbius aromatic transition states are known, so far only theoretical calculation exist for Möbius ground states. In the calculated neutral small *trans*-annulenes, such as *cis, cis, trans*-cyclohexatriene and *cis, cis, cis, trans*-cyclooctatetraene, no indication was found for the existence of a Möbius like p orbital topology.[85] Despite their formal π–conjugated character, both structures are normal but strained cycloalkenes, based on the analysis of their geometries, their highest occupied molecular orbitals and their magnetic properties. Dihedral angles between the double bonds close to 90° result in a poor overlap between the p orbitals and a lack of cyclic conjugation.

***Cis, cis, trans*-cyclohexatriene**

Energy relative to benzene: 107.0 Kcal/

NICS(0)=-1.7

Magnetic susceptibility= -47.8

Non-aromatic

***Cis, cis, cis, trans*-cyclooctatetraene**

Energy relative to all *cis*-COT: 21.3Kcal/mol

NICS(0)=-1.9

Magnetic susceptibility= -74.3

Non-aromatic

Figure 48: Properties of hypothetical Möbius [6]annulene and [8]annulene.

A way out of this dilemma of high ring strain and poor π overlap would be to go to larger ring sizes, the [16]annulene has been synthesized from two different precursors and both of them produced **28**, which in solution is in equilibrium with **29**.[86] Above –50°C conformational mobility occurs, resulting in the magnetic equivalence of all protons, but at –130°C there are 4 protons at δ=10.56 ppm and 12 at δ=5.35 ppm, which clearly shows a the paratopic character of **28**. Calculations showed that **28** is only 2 kcal/mol more stable than **29**. In the solid state, where the compound exists entirely as **28** (probably due to packing effects), X-ray crystallography[87] showed that the molecules are nonplanar with almost complete bond alternation: The single bonds are 1.44-1.47Å long and double bonds are 1.31-1.35Å long. The NICS value of +10.9 ppm and +10.7 ppm for **28** and **29** respectively, are another evidence for paratopic ring currents (antiaromaticity) for these two Hückel structures.[88]

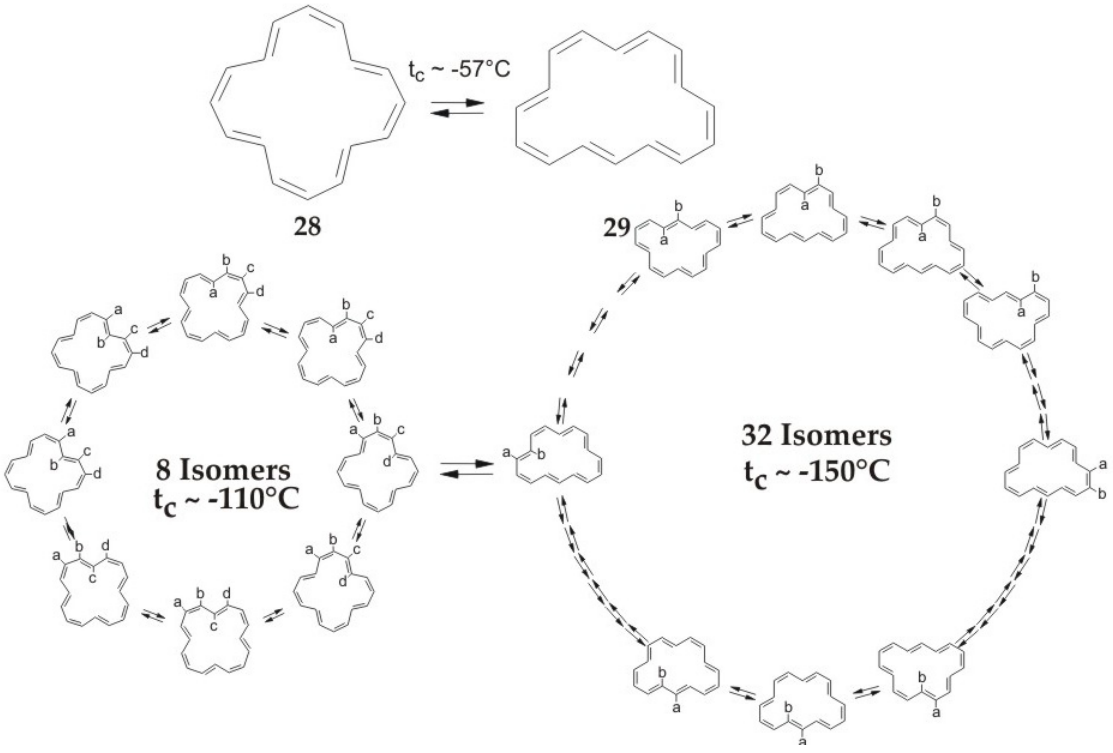

Figure 49: Conformational mobility in [16]annulene Hückel isomers .

The most stable isomer of [16]annulene with Möbius topology **30** is 15.8 kcal/mol higher in energy than the global minimum **28**. Bond length equalization of isomer **30**

is very close to benzene with a HOMA(Harmonic Oscillator Model of Aromaticity) value of 0.997 compared to the HOMA value of 0.979 for benzene. The NICS values of **30** and **31** are –14.5 ppm and –15.6 ppm respectively. Even though **30** is Möbius aromatic according to geometric and magnetic criteria the chances to synthesize it as a stable compound are close to zero. Because of the high configuration and conformation flexibility it will immediately rearrange to the global minimum, which is 15.8 kcal/mol more stable.

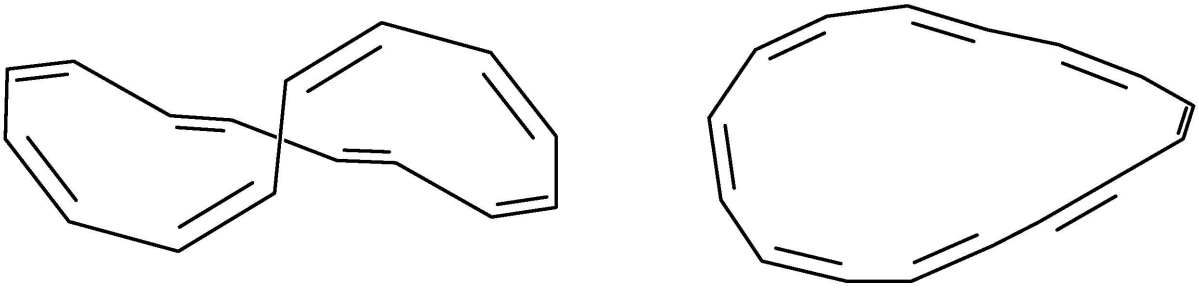

30 **31**

Figure 50: B3LYP/6-31G*optimized geometries of [16]annulene Möbius isomers.

Sondheimer[89] synthesized [20]annulene using all-trans-1,7,13-cycloeicosatriene-4,10,16,18-tetrayne as the starting material. ^{1}H NMR data showed a paramagnetic ring current and a mixture of stereoisomers. The NMR spectrum of [20]annulene was found to be temperature dependent and the coalescence temperature being –60°C. According to the NMR the annulenes has the Hückel structure **32** .

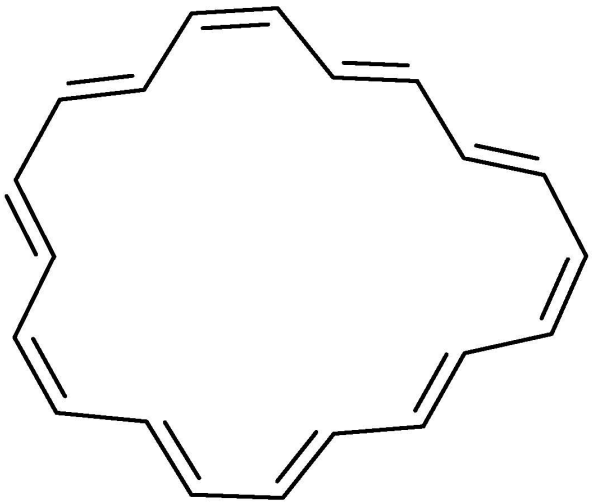

32

Figure 51: B3LYP/6-31G* optimized geometry of [20]annulene Hückel isomer.

The most stable isomer with highest Möbius character **33**, is only 6.2 kcal/mol higher in energy than **32** according to density functional theory calculations.[88]

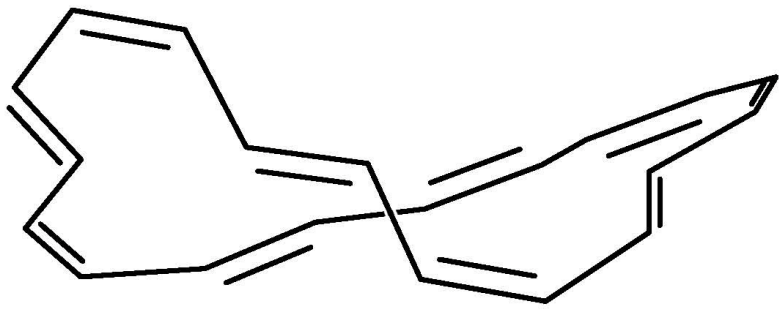

33

Figure 52: B3LYP/6-31G* optimized geometry of [20]annulene Möbius isomer

5.2.4 A double-stranded Möbius strip of carbon and oxygen atoms

The first and according to an extensive literature search the only example of a molecular non-conjugated Möbius strip was synthesized via high-dilution cyclization of the tris-(tetrahydroxymethylethylene) diol ditosylate[90] in a "non-rational" way. A Möbius and a Hückel isomer were formed. The Möbius isomer has neither a mirror plane nor rotational-reflection axis of symmetry nor an inversion centre and therefore is chiral. It was obtained as a racemic mixture.

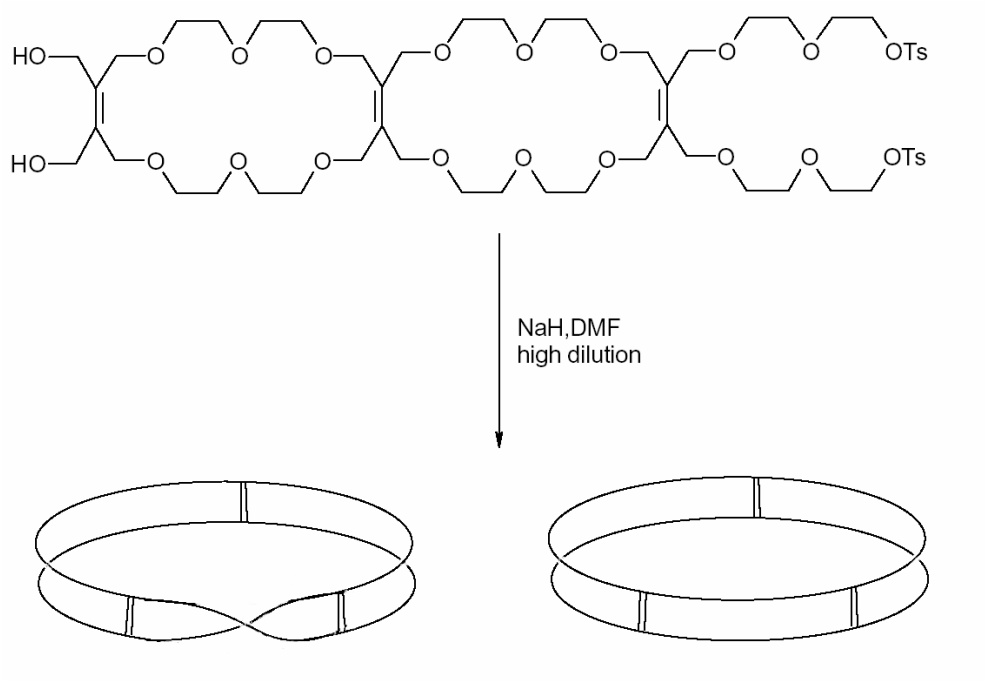

Figure 53: The first synthesized molecular Möbius strip.

5.2.5 Möbius strip of a single crystal

Fibrous crystals of niobium selenide ($NbSe_3$) typically assume ribbon and whisker configurations. Recently niobium selenide in the form of rings has been produced. Among these, Möbius strips, and figure-eights were observed by growing these crystals from selenium and niobium powders.[91] Such closed topologies occur when ribbon-shaped niobium selenide crystals adhere to droplets of liquid selenium, which act as spools around which the crystals are bent by surface tension. Growing along a droplet's equator to minimize bending energy, a crystal eventually meets its tail to form a seamless ring. Apparently, Möbius crystals are produced when twisting

accompanies bending or when the selenium droplet is rotating. The resulting Möbius crystals are about 50 micrometers in diameter and less than 1 micrometer in width.

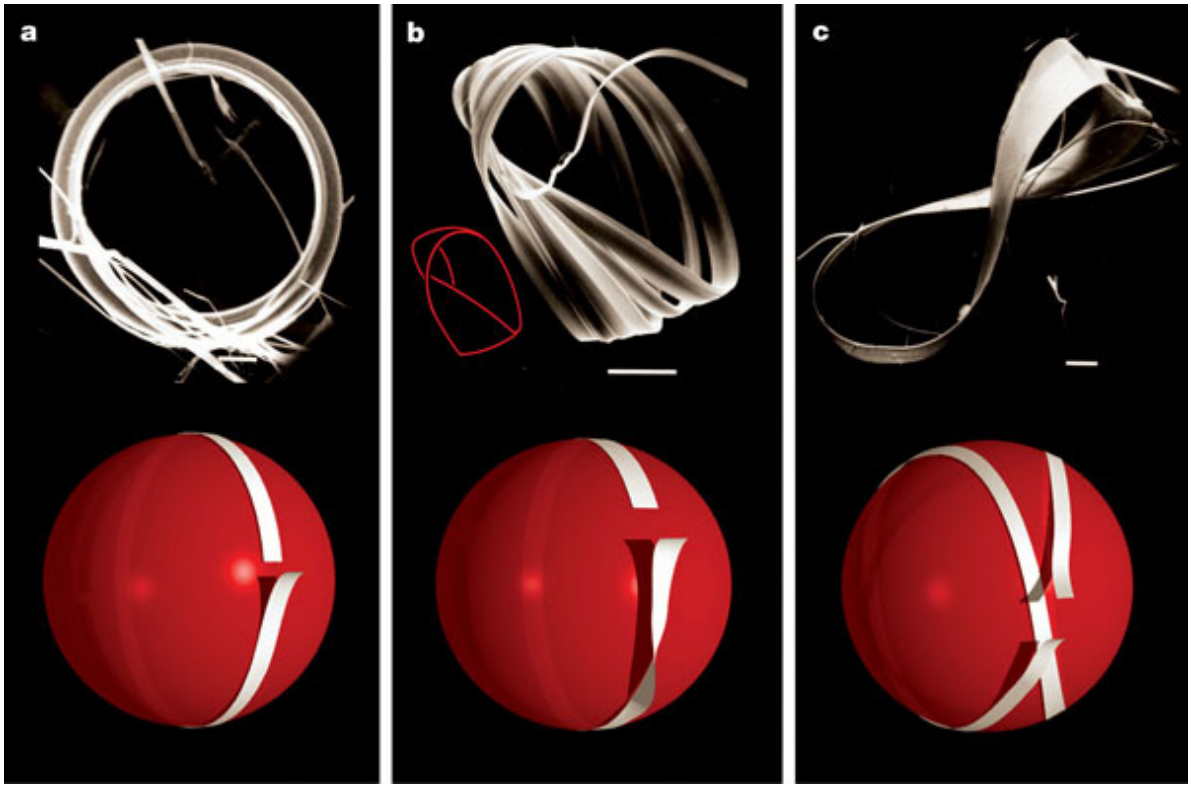

Figure 54: Scanning electron microscopic image of $NbSe_3$ crystal topologies: **a**- Ring structure **b**- Möbius strip **c**- Figure-of-eight strip

5.3 Synthesis of Möbius aromatic compound

Since Heilbronner's prediction of the aromatic character for Möbius [4n]annulenes, several research groups attempted to synthesize such a neutral, fully conjugated annulene with Möbius topology, however, so far unsuccessfully. The crystal structure analysis of synthesized [16]annulene synthesized from two different precursors proved a Hückel structure with S_4 symmetry. According to theoretical calculations the most stable Möbius isomer of [16]annulene is 15.8 Kcal/mol less stable than the global minimum. Sondheimer's synthesis of [20]annulene yielded a

Hückel isomer that according to calculations is 6.2 Kcal/mol more stable than the most stable Möbius [20]annulene isomer.

The strain associated with the twisted geometry of the p orbitals and the poor π overlap of the conjugated π bonds are much higher than the Möbius aromatic stabilization effect especially in smaller rings. The exponential increase of the number of configurations and conformations are another problem that arises in higher membered rings. The low barrier of isomerization between these isomers probably makes the synthesis of a stable Möbius isomer of the parent annulenes impossible.

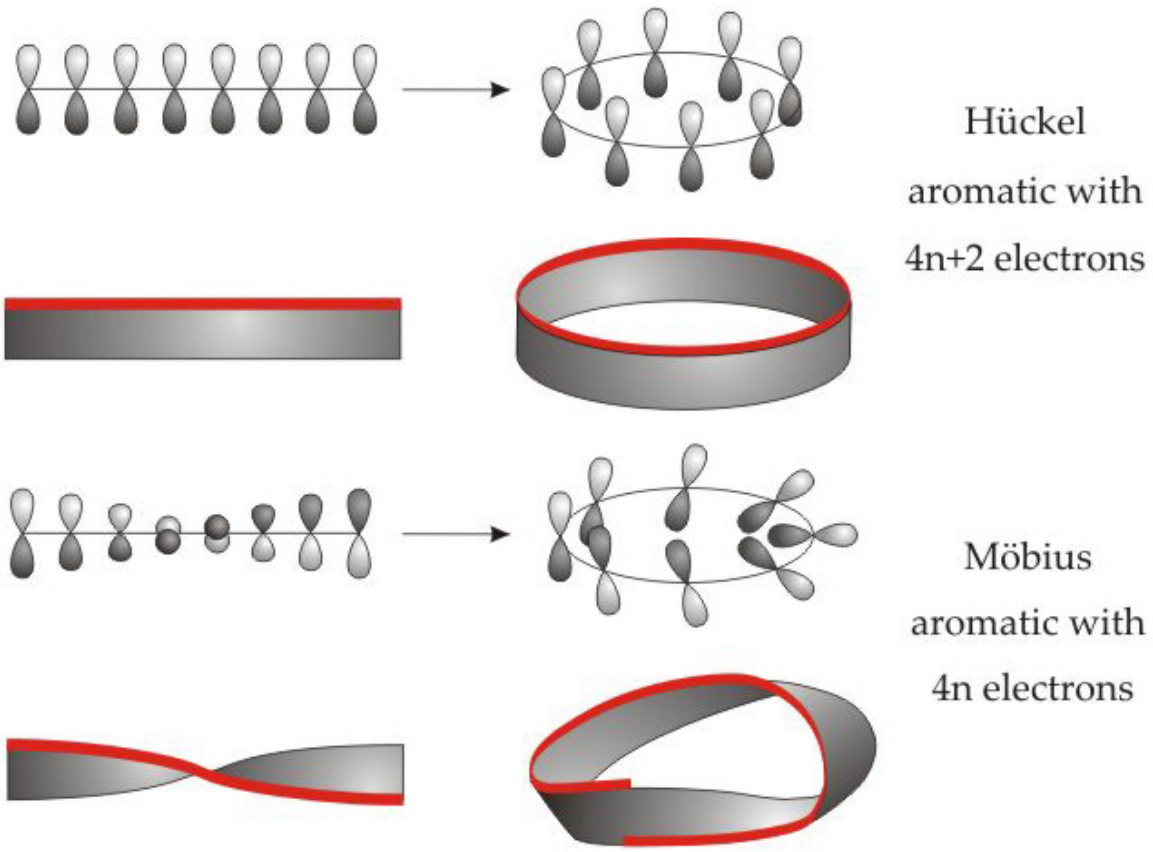

Figure 55: Formal construction of a Hückel and a Möbius π system from linear π systems. The 180° twist in the Möbius system is energetically unfavourable, because the strain increases and the conjugation decrease, leading to a reduced aromatic stabilization.

5.3.1 Proposed strategy for synthesizing Möbius aromatic compounds

Möbius conjugated π systems contain two different types of conjugated p orbitals. In one part the p orbitals are perpendicular with respect to the ring plane and have a

trigonal planar configuration("normal" conjugation) and in the other part p orbital lie in the ring plane and are pyramidalized ("inplane" or "beltlike" conjugation) (Figure**56**). The strain in Möbius system mainly arises from the latter the pyramidalized inplane conjugated part. The basic idea to achieve the synthesis of a Möbius aromatic compound is to introduce a prefabricated pyramidalized inplane conjugated building block into an annulene system. Carefully chosen, this strategy could make the Möbius structure thermodynamically more stable than corresponding Hückel isomers. As the belt-like inplane conjugated building block we chose our frequently used bianthraquinodimethane unit and for combining it with a "normal" π system the ring enlargement metathesis reaction was used.

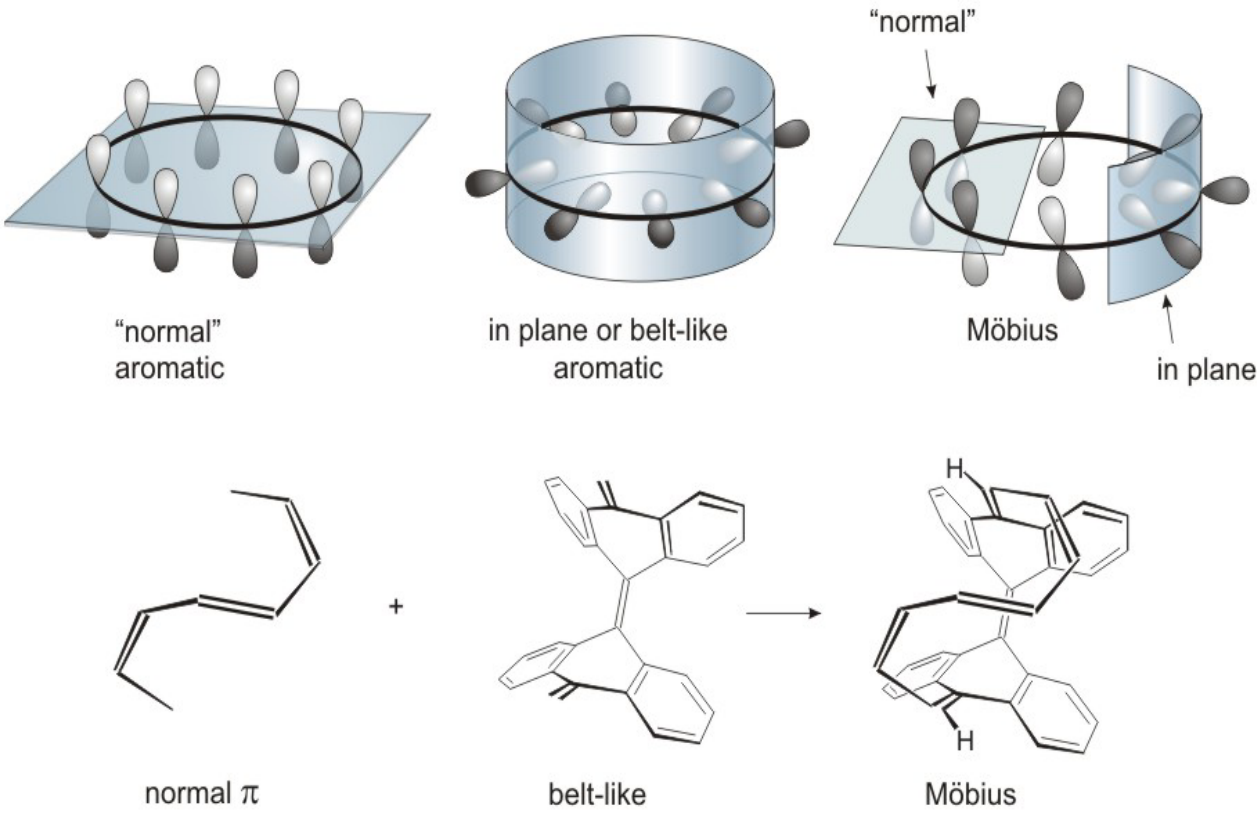

Figure 56: Synthetic strategy to construct Möbius aromatic systems.

5.3.2 Photochemically induced metathesis reactions of TDDA and cyclooctatetraene

Photochemically induced metathesis reactions of TDDA with cycloalkenes are known. TDDA even reacts with cyclic polyenes and [n]annulenes. **7** was formed by the reaction of TDDA with synthetic equivalents of cyclobutadiene (pyridazine or α-pyrone), and **33** was produced by a photochemically induced metathesis reaction of TDDA with benzene ([6]annulene). Both **7** and **33** could be considered as bianthraquinodimethane containing [n]annulenes ([12]annulene and [14]annulene) .

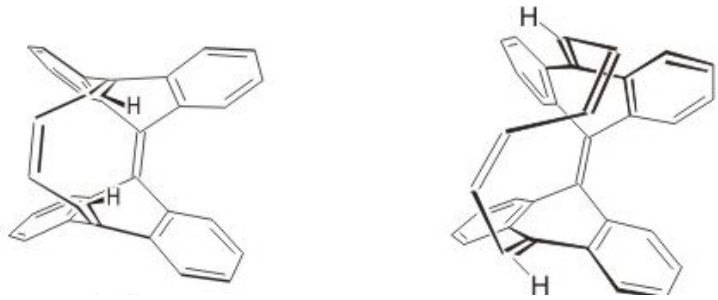

80% **28%**

7 **33**

Figure 57: Ring enlargement metathesis products of TDDA with synthetic equivalents of cyclobutadiene and with benzene.

The photochemically induced metathesis reactions of TDDA with cyclooctatetraene could produce compound **34** (Scheme **32**), which has a cyclic conjugated 16 electron π system in the shortest cyclic periphery and these electrons are as well in conjugation with the rest of the molecule. Compound **34** or isomers thereof might have Möbius aromatic character and due to the stabilization effect of the inplane aromatic part, Möbius isomers should also be more stable than the Hückel ones. Additionally, the geometrically fixed anthraquinodimethane part reduces the number of isomers. Unfortunately, irradiation of TDDA with cyclooctatetraene did not even yield traces of an addition product. The thermal and photochemical isomerization of cyclooctatetraene is one of the disadvantages of this reaction. The mechanistic details of these interconversions are well investigated but not fully understood[92] (Figure **58**). The photochemical reaction of TDDA and cyclooctatetraene was done in benzene using a 150 Watt and 700 Watt high pressure

mercury lamp in a quartz apparatus. Under these conditions, ring opening of TDDA to bianthryl is the major reaction. Most probably, the cyclooctatetraene is excited (instead of TDDA as in the previously performed metathesis reactions with alkenes and benzene). Cyclooctatetraene has a very short singlet excited life time and rapidly undergoes intersystem crossing to the triplet state. The triplet energy is transferred intermolecularly (e.g. via an exciplex) to TDDA. The latter, as known from previous sensitization experiments immediately undergoes ring opening to the 9,10'-bianthryl diradical, which in turn abstracts two hydrogen atoms to give bianthryl..

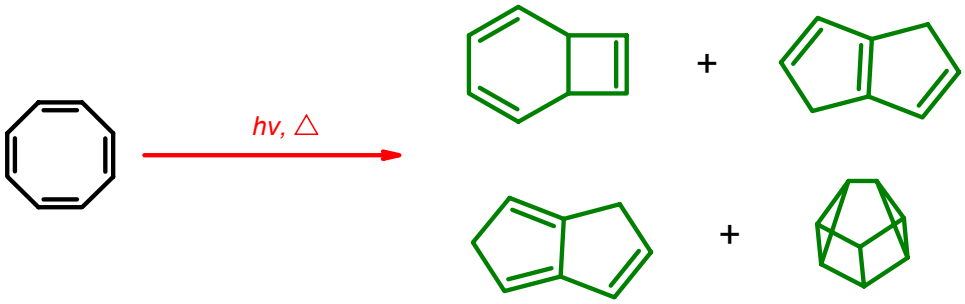

Figure 58: Photoisomerization of cyclooctatetraene.

Triplet state quenchers are compounds with a low energy triplet states. Oxygen and aromatic compounds like naphthalene and anthracene are common examples.

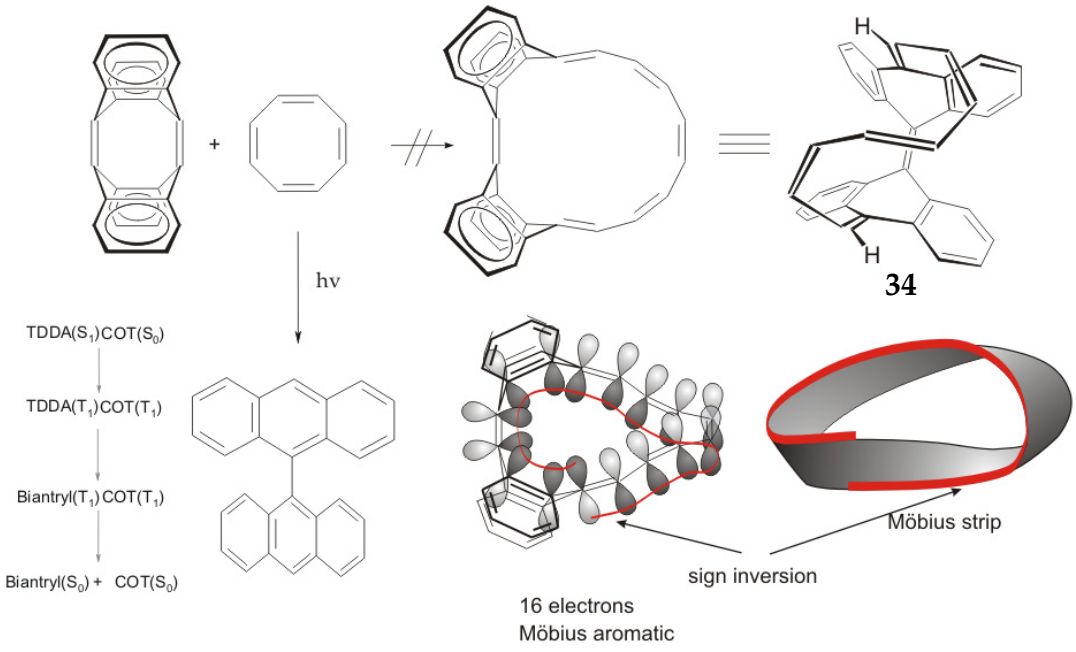

Scheme 32: Photochemical reaction of TDDA and cyclooctatetraene results bianthryl.

They absorb the excited triplet state energy of a substrate via an intermolecular energy transfer process (Scheme**33**). To prevent the formation of bianthryl the photochemical reaction of TDDA and cyclooctatetraene therefore was performed in the presence of naphthalene in benzene with a high-pressure mercury lamp, but again bianthryl was formed.

Also solventless irradiation of TDDA and cyclooctatetraene did not result in the desired cycloaddition product. Thermally TDDA reacts with cyclooctatetraene in a Diels Alder reaction. A mixture of products was generated probably derived from the different dienes from the isomerization of cyclooctatetraene.

To circumvent these problems we used a synthetic equivalent of cyclooctatetraene. *Syn-* or *anti*-tricyclooctadiene are alternatives for cyclooctatetraene because they easily convert to cyclooctatetraene upon heating or in the presence of metal salts. Therefore using *Syn-* or *anti*-tricyclooctadiene instead of cyclooctatetraene in photochemical reactions with TDDA should be a key solution to overcome the problems arising from the triplet sensitization of cyclooctatetraene.

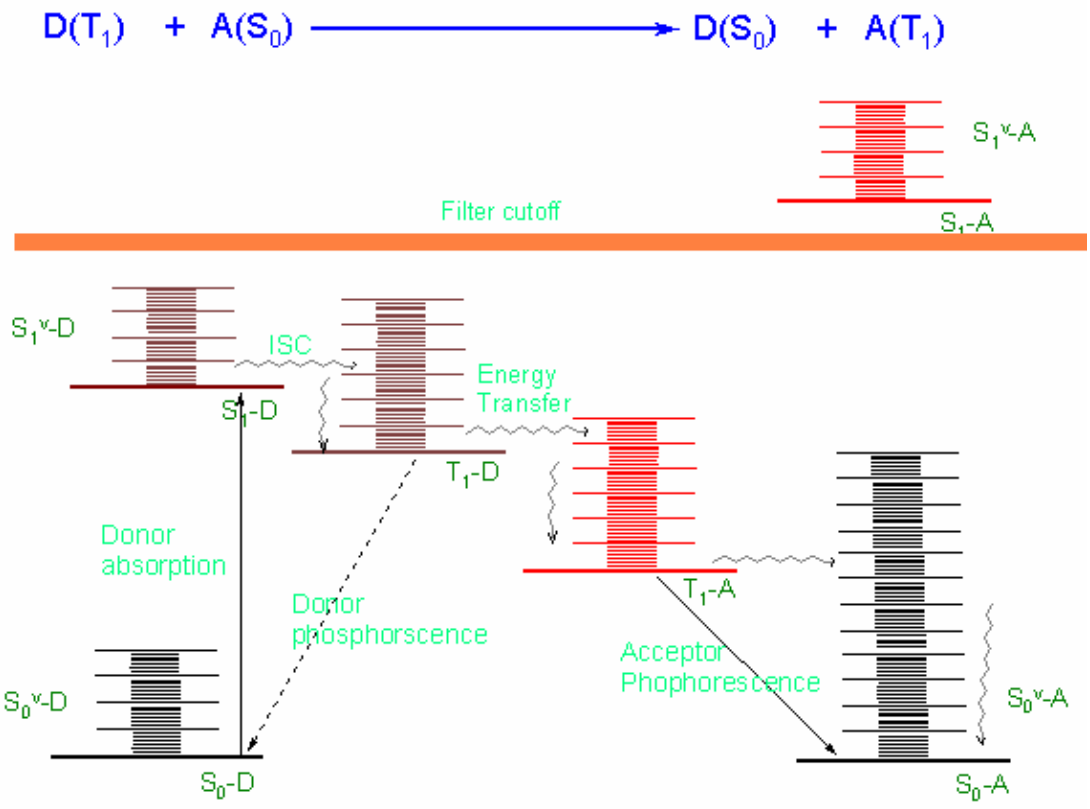

Scheme 33: Mechanism of triplet state quenching of an acceptor.

5.3.3 Synthesis of *cis*- or *trans*-tricyclooctadiene

The only preparative way to synthesize *cis*-tricyclooctadiene[94] is treating *cis*-3,4-dichloro-1-cyclobutene with sodium amalgam in dry ether. Except preparative GC there is no purification method for the separation of the product from the starting material. Therefore the reaction should continue until the quantitative conversion of *cis*-3,4-dichloro-1-cyclobutene is achieved. Unfortunately the conversion is very slow because of the deactivation of the amalgam surface. The crucial point of this reaction is to find an effective way to mix the reaction medium to renew amalgam surface efficiently. Treating the reaction mixture in an ultrasonic bath shortens the reaction time to two months, in which 2 ml pure *cis*-tricyclooctadiene are produced from 5 ml of *cis*-3,4-dichloro-1-cyclobutene, 650 gr. sodium amalgam and 250 ml dry ether.

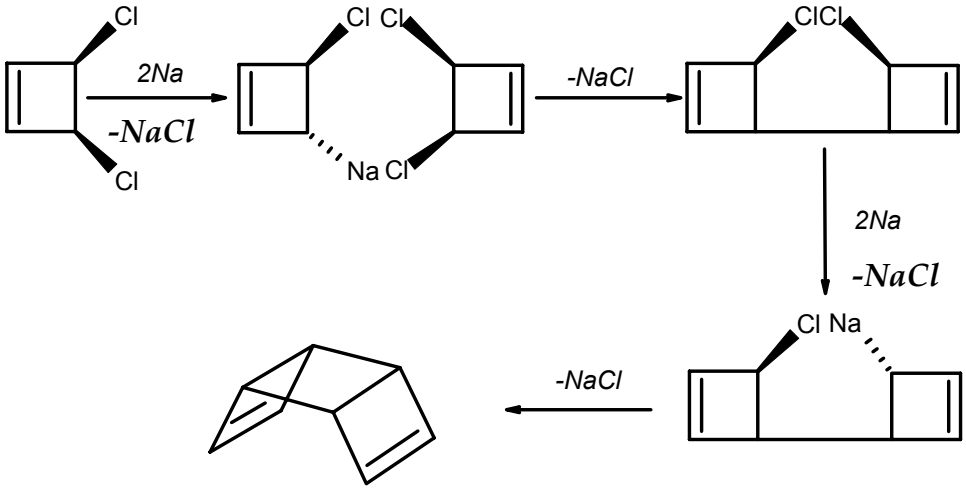

Scheme 34: Proposed mechanism for the reaction of *cis*-3,4-dichloro-1-cyclobutene with sodium amalgam.

Therefore a better way to mix the reaction medium was searched, especially to obtain a suspension of sodium amalgam in the solvent. Ultrasonic probes (cell disruptor) that transfer a high energy of ultrasound to a small area (~500W/cm^2) are good candidates for this kind of application. The above reaction was finished within 2 days when the tip of an ultrasonic probe with 250 Watt output was placed inside the sodium amalgam bulk. Using an elliptical flask instead of a round one further speeds

the reaction. The disadvantage of this method is the corrosion of the ultrasonic probe after two reactions (4days of operation).

Figure 59: The use of an ultrasonic probe in an elliptical flask accelerated the synthesis of tricyclooctadiene.

5.3.4 Photochemically induced metathesis reactions of TDDA with *cis*-tricyclooctadiene

5.3.4.1 Photochemically induced metathesis reactions with using high pressure mercury lamp

TDDA reacts with *cis*-tricyclooctadiene in a photochemically induced metathesis reaction in benzene in a quartz photoreactor with a 150 or 700 Watts high-pressure mercury lamp. The yield of the reaction is much higher in the presence of naphthalene as a triplet quencher. The reaction is very fast and after ten minutes all of the TDDA was consumed. A mixture of products was obtained whose purification was only possible using a preparative HPLC with a silica gel column and a 90/10 heptane/dichloromethane mixture as mobile phase.

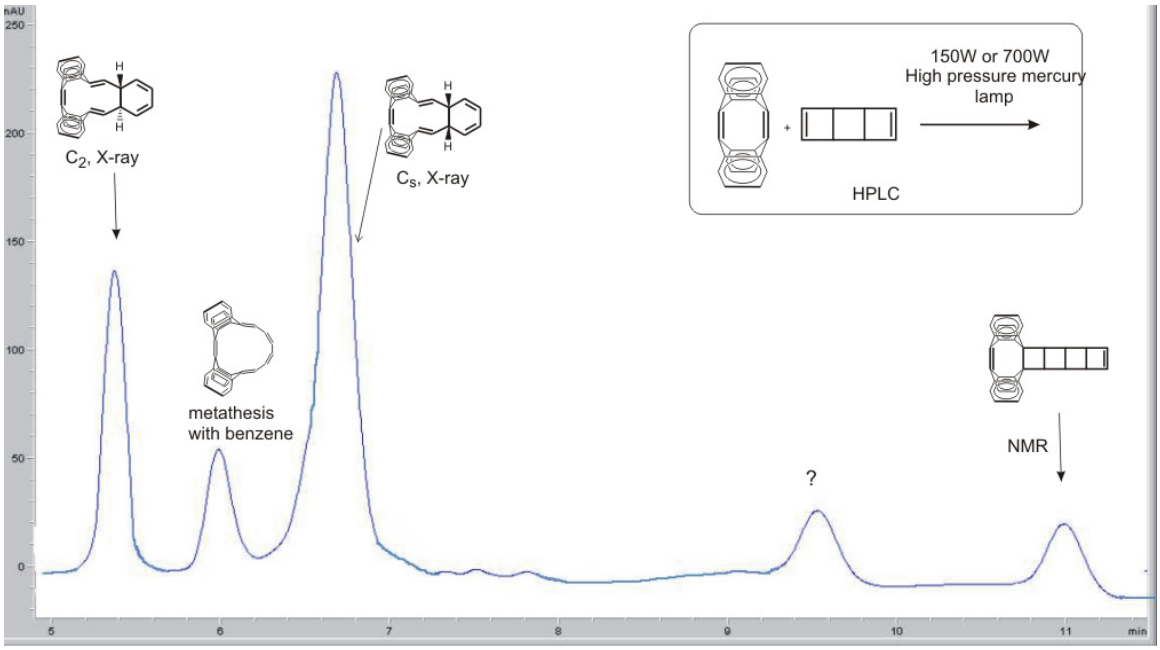

Figure 60: HPLC chromatogram of irradiation of TDDA and TCOD with high pressure mercury lamp.

The combined total yield of the reaction is 35%. Two main products and some minor products are formed. Additionally the photocycloaddition product of TDDA with benzene **33** was detected. NMR spectra of both main products showed two aliphatic hydrogens from which can be followed that the molecules are not fully conjugated. Both of them have symmetry. According to the number of anisochronous proton signals in the NMR spectra this symmetry can either be C_2 or C_s.

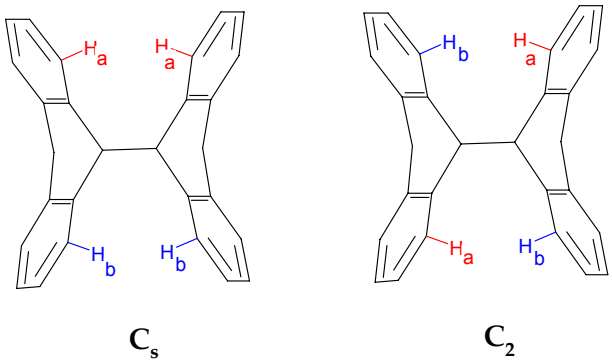

Figure 61: Differentiation of the C_2 and C_s isomer based on NOE signals of the neighbouring ortho protons in the bianthraquinomethane unit.

One way to distinguish between C_2 and C_s symmetry in the metathesis products is based on the NOE spectra. In the isomer with C_2 symmetry, there is a NOE interaction between H_a and H_b, while in the isomer with C_s symmetry, H_a and H_b have no correlation in the NOE spectrum (Figure **61**). The density functional theory calculated (B3LYP/6-31G*) NMR spectra are in good agreement with the experimentally measured values. The theoretical data of the C_2 and the C_s isomer fit slightly better to the structures for which the corresponding symmetry was determined by NOE.

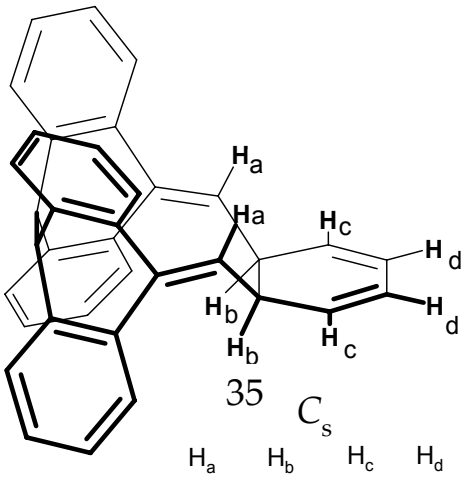

	H_a	H_b	H_c	H_d
Exp.	5.55	3.65	5.67	5.91
Calcd.	5.57	3.94	5.61	5.71

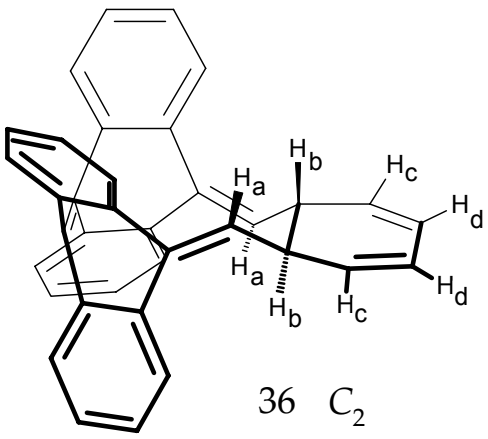

	H_a	H_b	H_c	H_d
Exp.	5.15	3.4	5.67	5.91
Calcd.	5.3	3.94	5.64	5.73

Scheme 35: Measured NMR chemical shifts in comparison with calculated ^{1}H-NMR shifts (B3LYP/6-31G*).

The final structure assignment was achieved by X-ray structure analysis. Single crystals of **35** and **36** were grown by the vapour diffusion method. The compound was dissolved in a small volume of dichloromethane in a small vial. Then this inner vial was placed inside a larger vial that contains a small volume of pentane and large vial was sealed. Vapour from the solvent of the outer vial then diffuses into the solution of the inner vial, causing the compound to precipitate. The vertical surfaces of the inner vial should not touch the outer vial to prevent the outer solution from rising by capillary action and entering the inner vial.

The X-ray structure analysis of **35** confirms the proposed structure with C_s symmetry. The molecule contains a 1,3-cyclohexadiene part fused with a bianthraquinodimethane unit(Figure **62**). The hydrogen atoms of both quinoid CH groups in the bianthraquinodimethane part have *syn* configuration with respect to each other and they are in a *trans* relationship with their neighboring aliphatic hydrogens. The X-ray structure analysis of **36** proved the C_2 symmetry that was determined by NOE. The hydrogen atoms of the CH groups of the bianthraquinodimethane part are *trans* with respect to each other and with the adjacent aliphatic H atoms (Figure **63**). Structure **36** has a C_2 axis as the only symmetry element and therefore is a chiral molecule. The unit cell of **36** contains equal numbers of both enantiomers, which indicates that **36** is a "true racemate" or a racemic compound

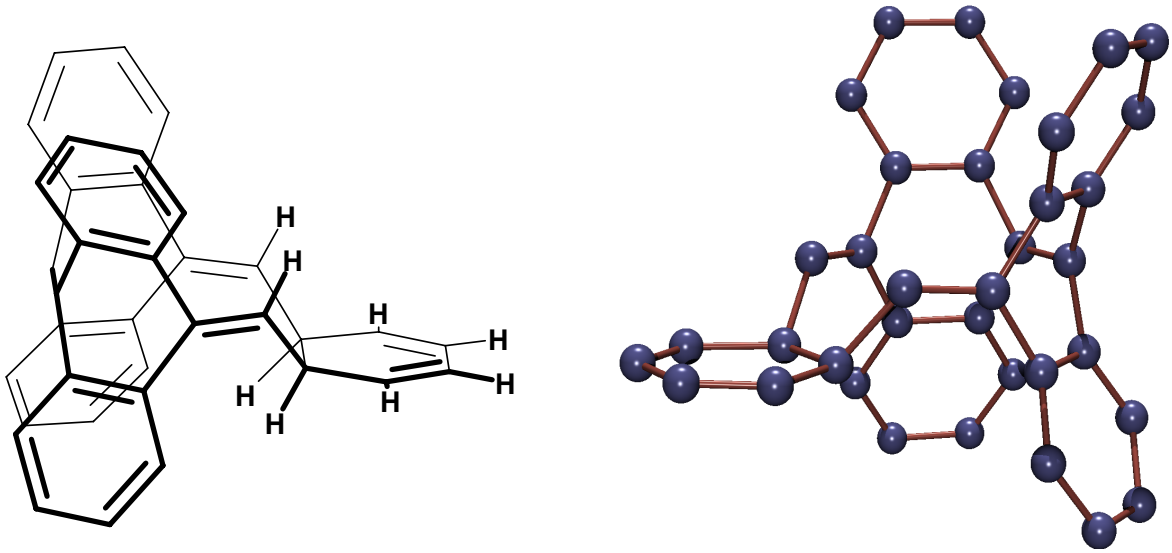

35

Figure 62: X-ray structure of **35**.

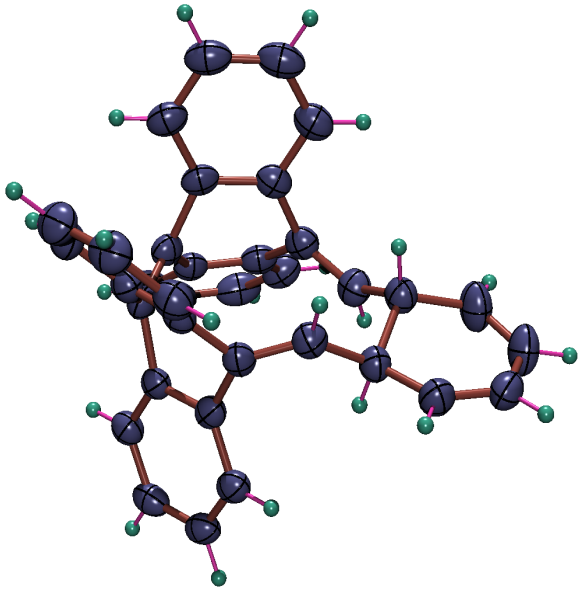

Figure 63: X-ray structure of **36**. **36**

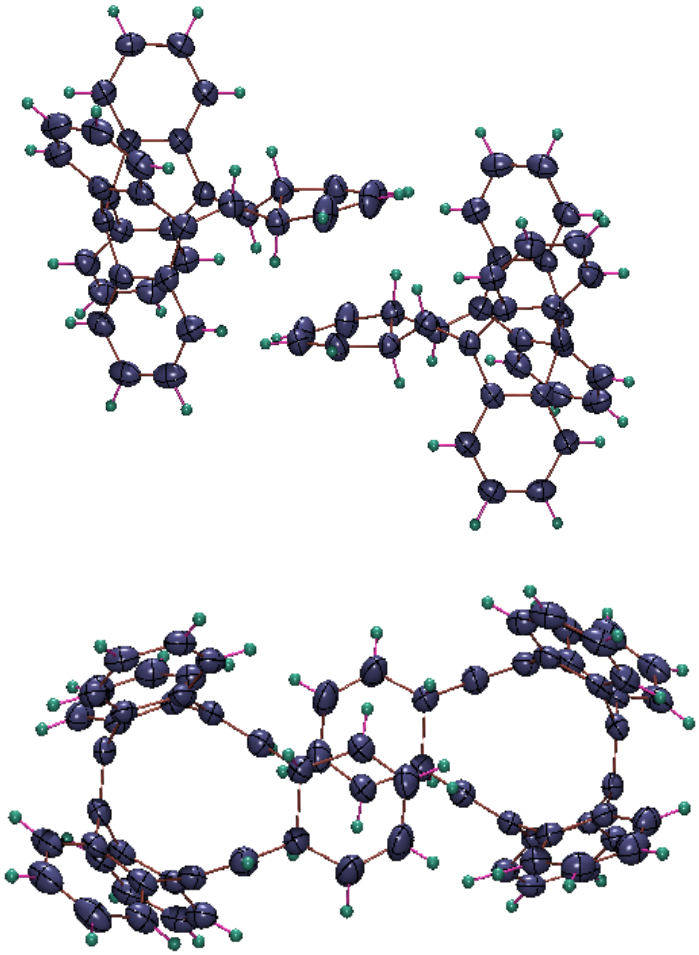

Figure 64: Two views of a small part of the unit cell of **36**, which shows both enantiomers in the crystal structure.

The direct product of the [2+2] photocycloaddition of TDDA and tricyclooctadiene is **37.** All other products were produced through different ring opening pathways thereof. Isomer **37** was isolated and NMR spectra (NOE, HMBC, HSQC) proved the ladder-shape structure (Figure **65**) with C_s symmetry in which four cyclobutane rings are fused. Several attempts were done to get single crystals of this compound, but unfortunately all of them failed.

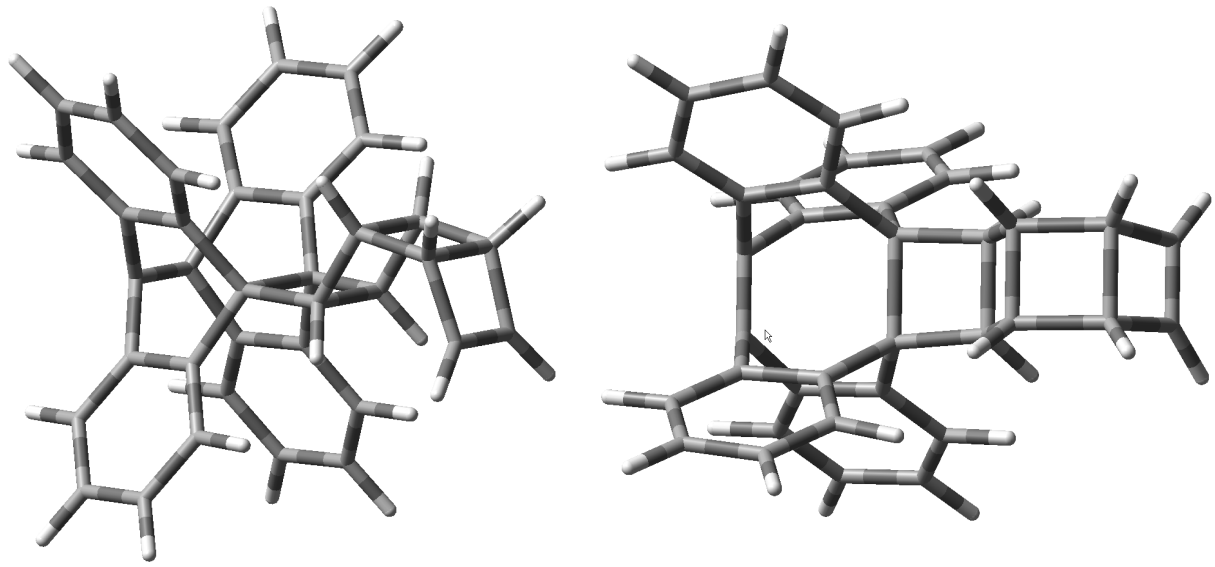

34

Figure 65: Calculated structure of 34 at B3LYP/6-31G* level of theory.

A mixture of other products was obtained in low yields and attempts to separate them with HPLC failed. Mass spectrometry of this mixture indicated that they are isomers of one to one addition products of TDDA and tricyclooctadiene.

The aim of this reaction was to synthesize fully conjugated tubular aromatic compounds and especially Möbius aromatic compounds. All the characterized products of the photochemical reaction of TDDA with tricyclooctadiene using the high-pressure mercury lamp needed another ring-opening step to form fully conjugated annulenes. According to the Woodward-Hoffmann rules, the thermal interconversion of 1,3-cyclohexadiene to hexatriene proceeds by a disrotatory

mechanism and the photochemically it occurs by a conrotatory mechanism (Figure **66**).

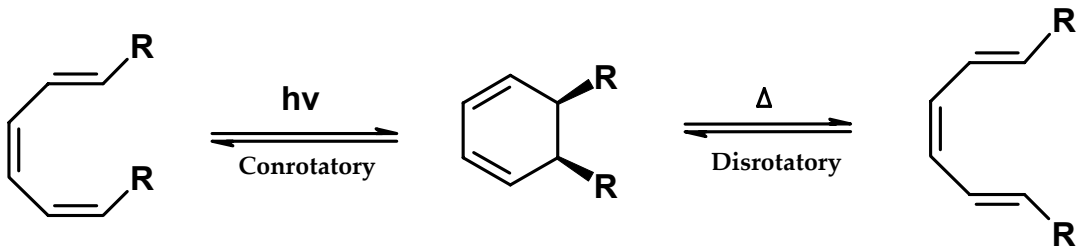

Figure 66: Mechanism of ring opening and ring closure of 1,3-cyclohexadiene and hexatriene based on Woodward-Hoffmann rules.

The conrotatory opening of cyclohexadiene ring in a bicyclic system proceeds efficiently, especially if the resulting ring is sufficiently large to provide stability for the *E* double bond in the triene. Since the triene generally has a higher ε_{max} and broader absorption bands at longer wavelengths, longer wavelength irradiation is required for the reverse reaction[95] (Figure **67**).

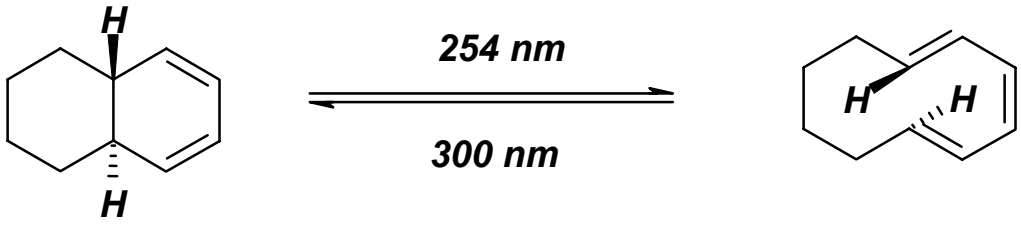

Figure 67: The equilibrium of the electrocyclic ring opening and ring closure of a bridged system depends on the wavelength of irradiation.

Isomers **35** and **36** were heated in toluene and xylene to open the cyclohexadiene part of the molecules. However, there was no change of the isomers ratio. Thus, the thermal ring-opening failed. Irradiation of pure **35** or **36** with a high-pressure mercury lamp in benzene resulted in a mixture of closed isomers (**35**, **36** and **37** in low yield). It was assumed that the ring opening of the closed isomers would result in fully conjugated polyenes that have higher ε_{max} and broader absorption bands at longer wavelengths. Therefore the ring opening reaction is less effective under irradiation with a high-pressure mercury lamp with an output in both the UV and

visible light. Using cut-off filters or the use of a low-pressure mercury lamp is promising methods in order to overcome this problem.

5.3.4.2 Photochemically induced metathesis reactions using a low-pressure mercury lamp

Low-pressure mercury lamps are miniature U-shape or straight tube fluorescent lamps. A discharge of mercury vapour (10^{-5} atm) converts the electrical energy into UV radiative energy with an efficiency of about 60% in which 95% of this energy is emitted at 253.7 nm. The remaining energy is converted into visible radiation and heat. The arc length of the lamp is a function of the power rating. A typical low-pressure lamp has about 35 cm arc lengths with power consumption of 15 W.

The irradiation of TDDA and *cis*-tricyclooctadiene in benzene in the presence of naphthalene with a low-pressure mercury lamp was monitored. All TDDA was consumed after 2 hours of irradiation and a mixture of closed and opened (fully conjugated polyene) isomers was obtained. The total combined yield of the reaction based on TDDA was 50%. Continuing irradiation up to 24 h improved the yield of obviously opened isomers with longer wavelength absorption (in the UV detector of the analytical HPLC). The separation of the mixture (on a preparative scale of products) was more difficult than the separation of the closed isomers in the reaction using the high pressure lamp. The separation was achieved with HPLC on a silica gel column with a mobile phase of heptane/dichloromethane (95/5). Six fully conjugated isomers and three closed isomers were observed in HPLC. The closed isomers are the same that were separated and identified in the photoreaction of TDDA and *cis*-tricyclooctadiene with the 700 and 150 watts lamps.

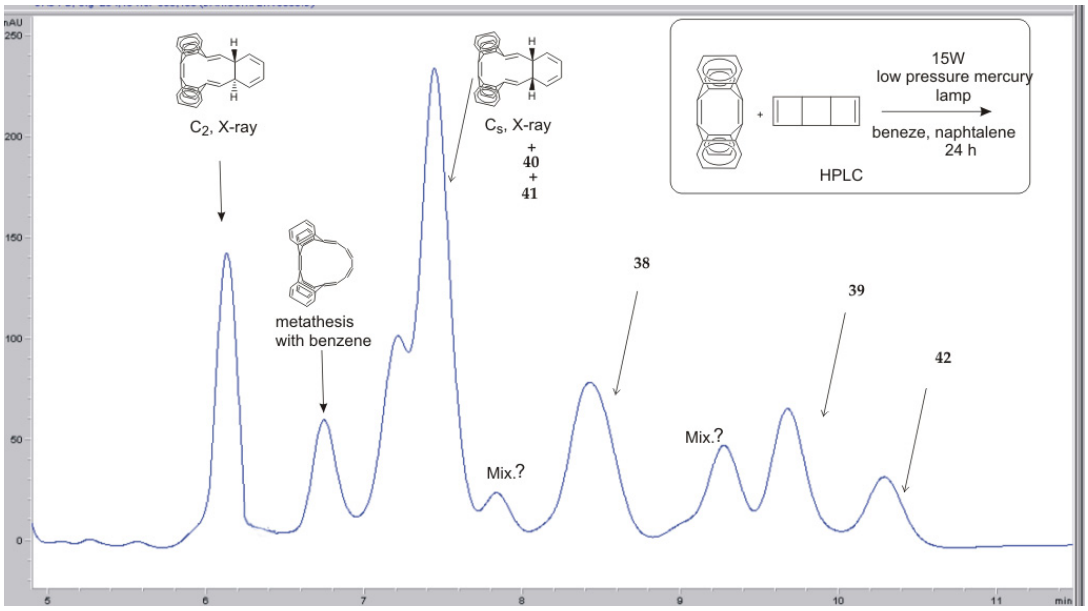

Figure 68: Chromatogram of the mixture of products, (silica gel, 95/5 heptane/dichloromethane) upon irradiation of TDDA with tricyclooctadiene with a low pressure mercury lamp for 24h.

Three fully conjugated isomers were purified with the first run of the HPLC and two opened isomers come together with the C_s closed isomer. In order to remove of the C_s closed isomer **32** from this mixture, a Diels-Alder reaction with tetracyanoethylene (TCNE) was applied because **35** can act as a more reactive diene as the fully opened structures. TCNE is a polar compound and with a simple silica gel column chromatography with an unpolar solvent, unreacted TCNE and the Diels Alder product of TCNE and **35** remained at the top of column and the opened isomers passed through the column. Two opened isomers were separated with further HPLC chromatography of this simplified mixture.

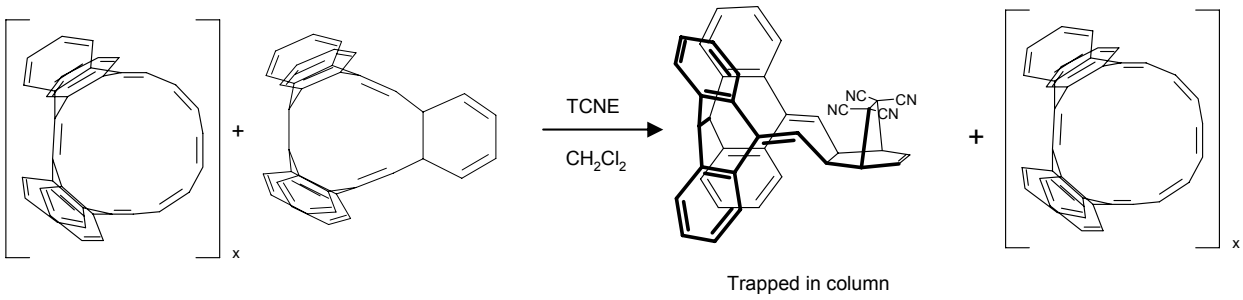

Scheme 36: Chemical separation method of closed and opened isomers.

In the fully conjugated products, 12 E/Z isomers are conceivable, each of which can have 9 *s-cis*, *s-trans* conformations. This sums up to 108 configurational and conformational isomers of which most are chiral and have two enantiomeric isomers. Since the anthraquinodimethane part is fixed, the following simplification considered in order to name each isomer (Scheme **37**). The isomers were first divided into a *syn* and *trans* group based on the relative stereochemistry of the hydrogen atoms at position 1 and 8. In each group the remaining three double bonds can generate six different configurational combinations and each of these isomers has nine different conformational isomers.

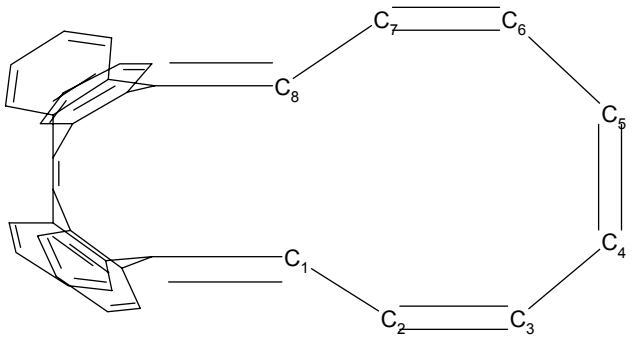

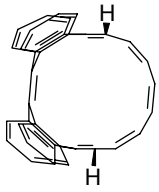

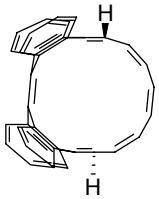

Configuration isomers **Conformation isomers**

SYN

EEE → cEcEcEc, cEcEcEt, cEcEcTc, cEcEtEt, cEtEtEc, cEtEcEt, cEtEtEt, tEcEtEt, tEtEtEt

EEZ
EZE
EZZ
ZEZ
ZZZ

ANTI

EEE
EEZ
EZE
EZZ
ZEZ
ZZZ

Scheme 37: Theoretically possible isomers of the fully conjugated products of TDDA with TCOD.

For the identification and characterization of the purified isomers all compounds were investigated by MS, NMR (COSY, NOESY, HMBC, HSQC) and UV spectroscopy. These spectra were also compared with theoretical calculated spectra of the possible isomers. Additionally, numerous attempts were done to obtain single crystals of the purified isomers because X-ray structure analysis is the most reliable way to determine the exact structure of isomers. Single crystals of **38** were obtained from a mixture of dichloromethane and pentane. The X-ray structure analysis proved a *syn*-tZtZtZt structure with Hückel topological p orbital conjugation. The molecule has C_s symmetry and therefore it is achiral.

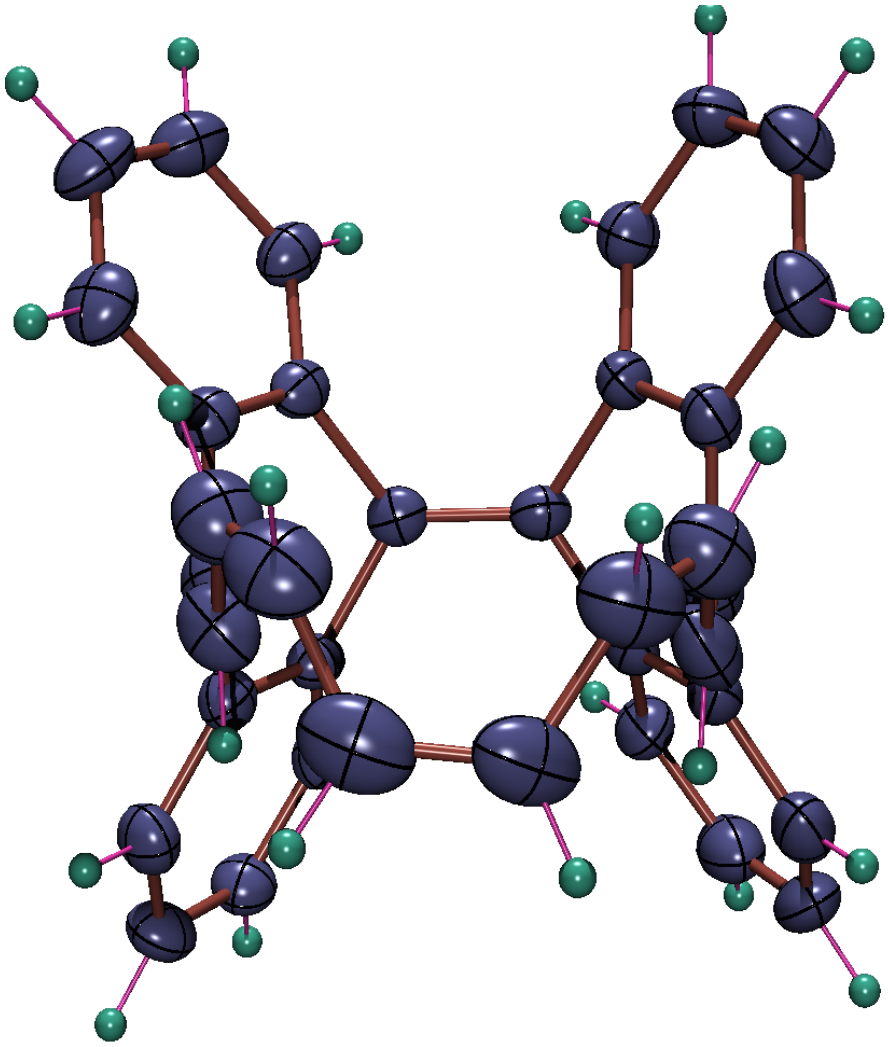

38

Figure 69: Ortep plot of the X-ray structure of **38** an *syn*-tZtZtZt.

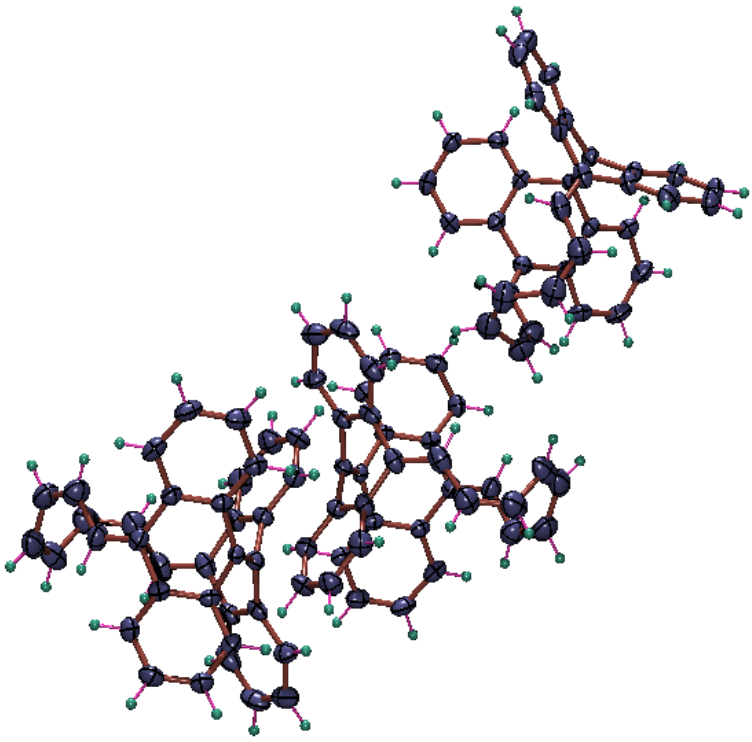

Figure 70: Unit cell structure of the isomer **38**.

Single crystals of **39** were obtained from slow evaporation of its heptane solution. The X-ray structure analysis revealed an *anti*-tZtEcZt structure for this isomer. The arrangement of conjugated p orbitals takes the shape of a Möbius strip. The molecule has no element of symmetry and it is a chiral compound. Both enantiomers were found in the unit cell of the crystal structure thus **39** is a racemic mixture. E compound is stable in daylight at room temperature and its solution in dichloromethane can be stored for several months. Epoxidation in the presence of oxygen and isomerization by UV irradiation are the two modes of destruction for this kind of compounds.

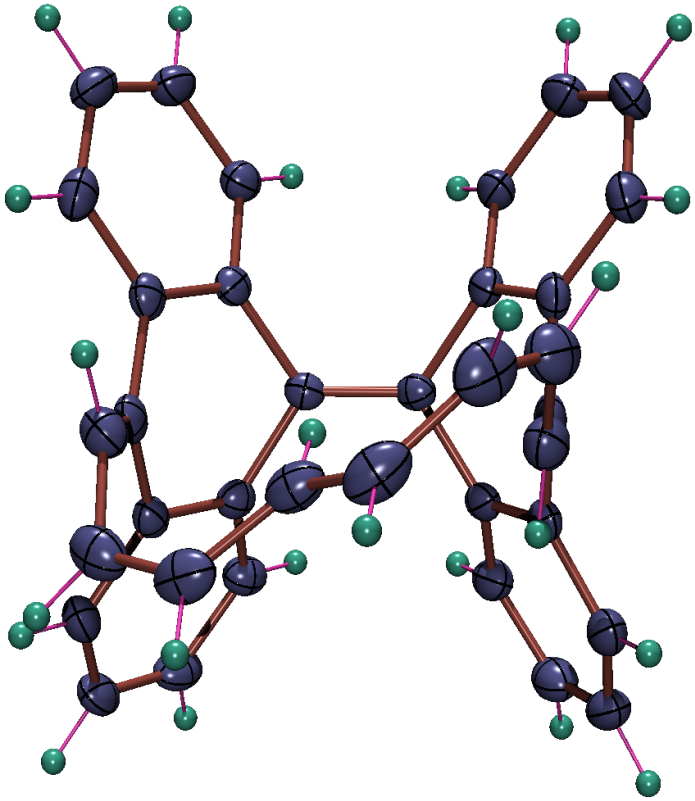

39

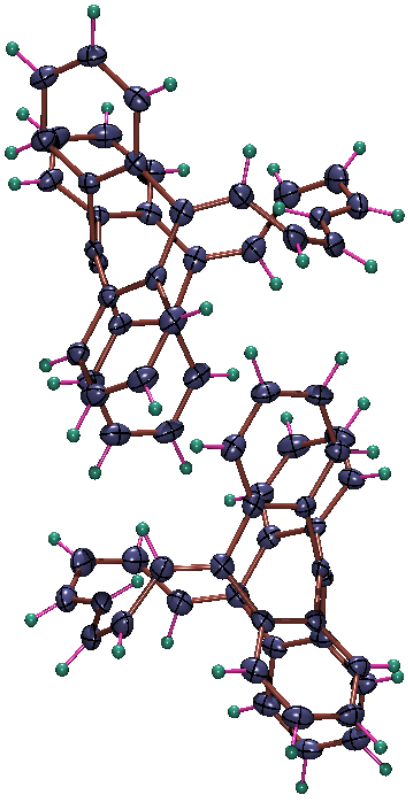

Figure 71: Ortep plot of the X-ray structure of *anti*-tZtEcZt **39** and its racemic unit cell.

Single crystals of **40** were formed by slow addition of micro drops of pentane to the concentrated solution of **40** in dichloromethane. The X-ray structure analysis has determined an *anti*-tZcZcZt structure. The molecule has C_2 symmetry and is chiral. Both enantiomers were observed in the unit cell of the crystal structure. The molecule has a perfect Möbius topology and it is stable at room temperature and daylight. Isomer **40** has an additional absorption band at 400 nm than isomer **38** and **39** and its crystals are red in contrast to the colourless crystals of **38** and **39**.

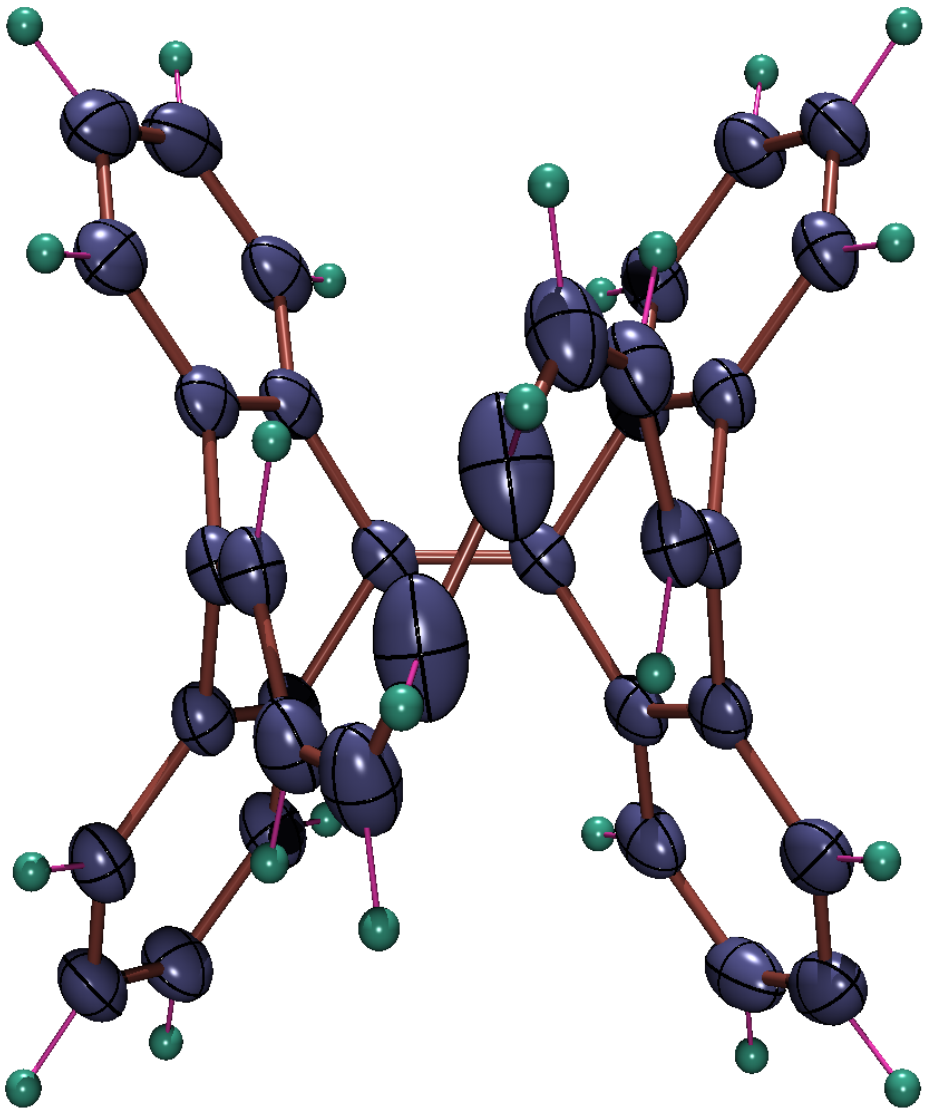

40

Figure 72: Ortep plot of x-ray structure of **40** an *anti*-tZcZcZt structure.

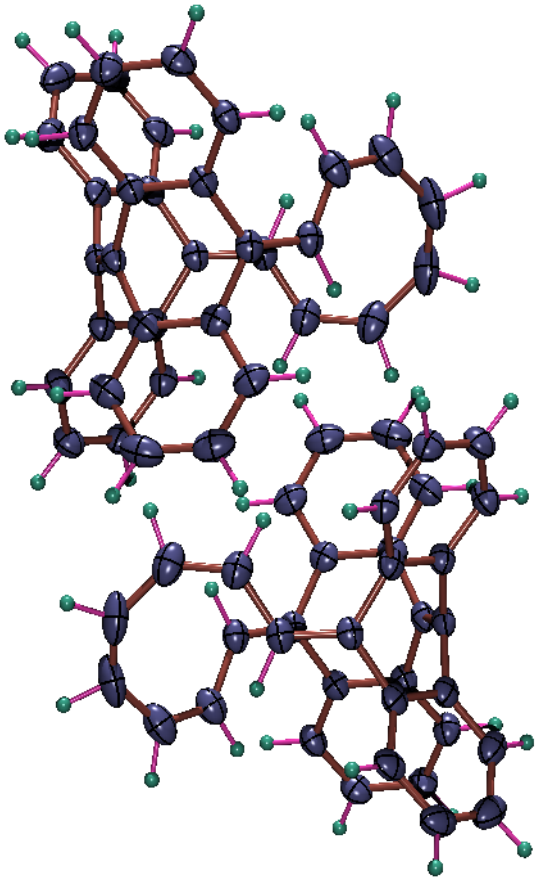

Figure 73: Part of the unit cell of **40**.

Attempts to crystallize **41** and **42** failed. The NMR spectrum of isomer **41** predicts an asymmetric structure. The compound has broader absorption bands than **40** and it is unstable and easily undergoes ring closure form **35**. The interpretation of NMR data and the comparison with NMR shifts calculated at the GIAO B3LYP/6-31G* level of DFT proposed *syn*-tZcZcEt structure for this isomer (Figure **73**). The arrangement of the conjugated p orbital represents a Möbius structure and therefore the molecule is chiral. Ring closure of *syn*-tZcZcEt easily gives the closed isomer **35**.

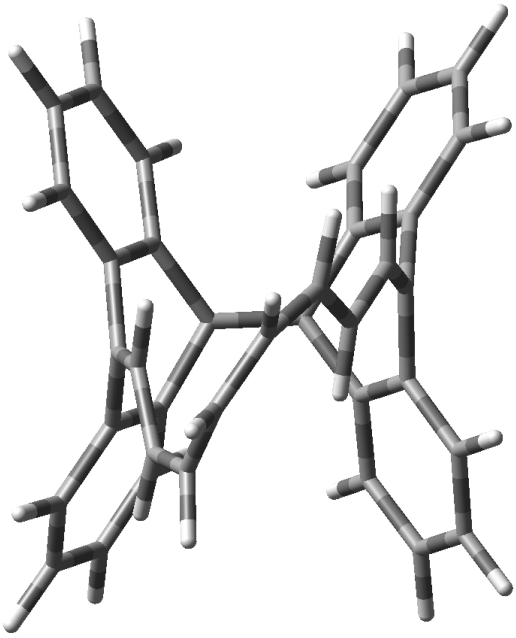

41

Figure 74: Proposed structure for **41**.

The NMR data predict a C_2 symmetry for isomer **42** and the structure of the molecule probably is *anti*-tEcZcEt according to a comparison of the properties of **42** with calculated *anti*-tEcZcEt (Figure **75**). The molecule has Möbius topology and it is chiral. However, unlike the other Möbius structures which have broader absorption bands at ~400-480 nm, the *anti*-tEcZcEt molecule **42** has only short absorption bands at ~300-350 nm like closed **35** and **36** isomers.

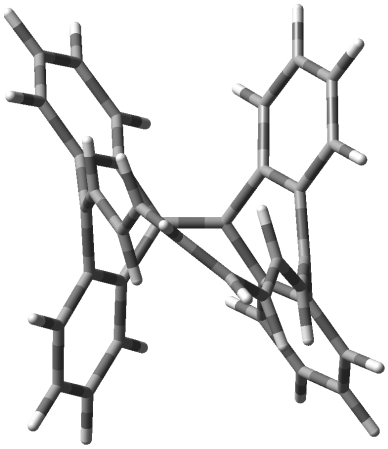

Figure 75: Proposed structure of **42**.

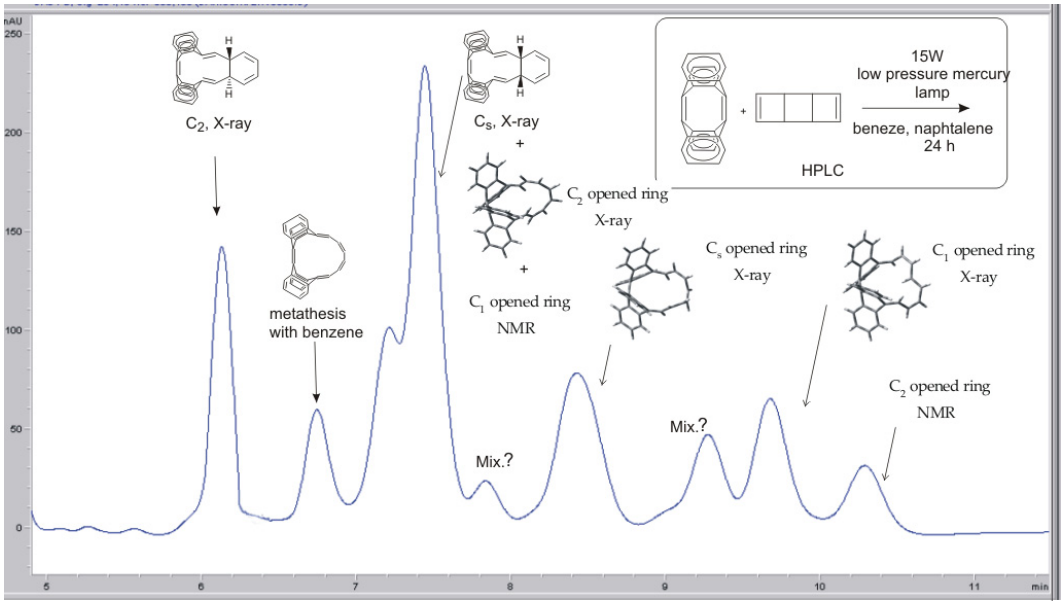

Figure 76: HPLC chromatogram of the irradiation of TDDA and TCOD with the characterized structures of the isomers

5.3.5 Quantitative Measures of Aromaticity

Several criteria were considered in the attempt to rationalize and to quantify the aromaticity of the TDDA/TCOD addition products. These can be roughly divided into four categories: energetic, structural and geometrical, magnetic, and reactivity based measures.

5.3.5.1 Calculated energy of isomers

All 108 isomers of the fully conjugated addition products of TDDA to tricyclooctadiene were optimised using semiempirical PM3 method. The most stable conformational of each of the twelve configurational isomers was submitted to density functional theory calculations at the B3LYP/6-31G* level of theory. As shown in Scheme **41** and **42**, there are configurations with Möbius topology are more stable than the Hückel structures. The isomer **42** a *syn*-tZcZcEt structure, is the global minimum and has a Möbius topology with C_1 symmetry. The most stable Hückel isomer is 6.9 Kcal/mol higher in energy than most stable Möbius structure and between these two isomers there are several Möbius conformation isomers.

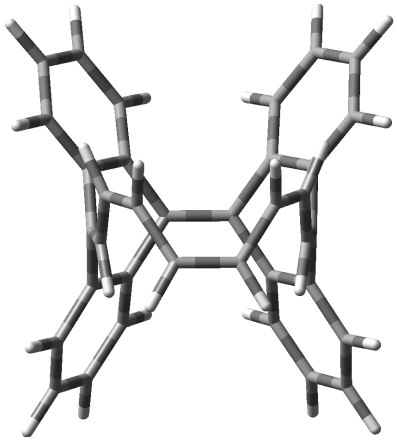

38

syn-tZtZtZt(H)-C_s E_{rel} : 6.9 kcal/mol

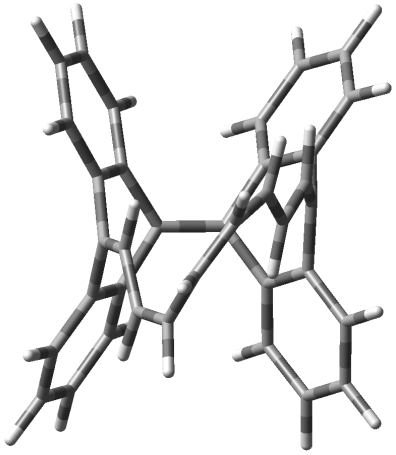

41

syn-tZcZcEt(M)-C_1 E_{rel} : 0 kcal/mol

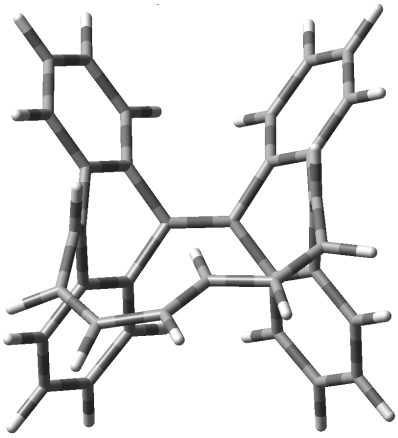

43

syn-tZcEtZc(M)-C_1 E_{rel} : 13.4 kcal/mol

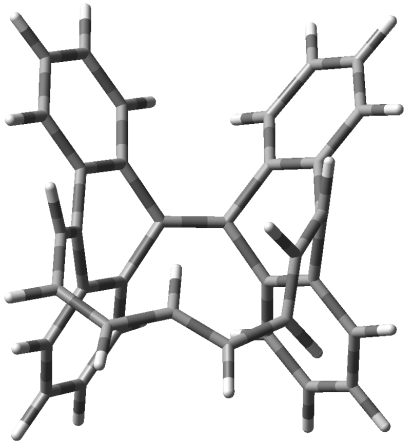

44

syn-cZtEcEc(M)-C_1 E_{rel} : 14. kcal/mol

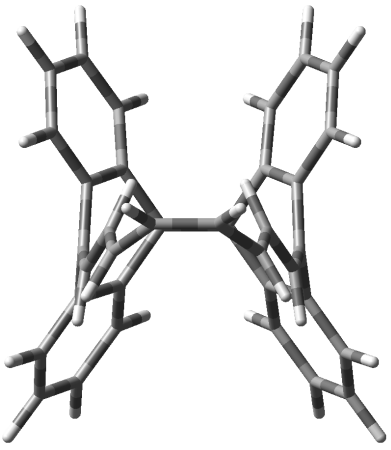

45

syn-tEcZcEt(H)-C_s E_{rel} : 4.2 kcal/mol

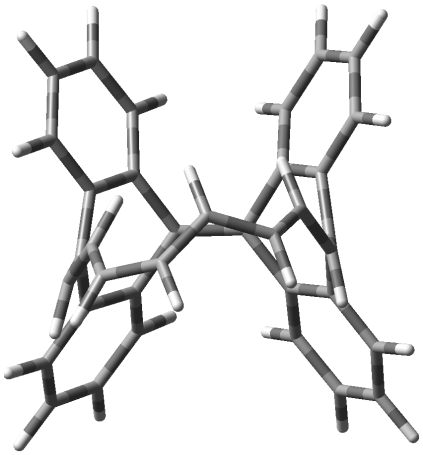

46

syn-tEcEtEt(H)-C_1 E_{rel} : 27.1 kcal/mol

Scheme 38: Optimised structures of *syn* configuration isomers and energies relative to the *syn*-tZcZcEt isomer at B3Lyp/6-31G* of (H= Hückel, M= Möbius).

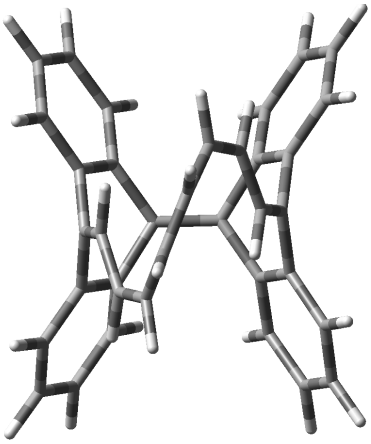

40

anti-tZcZcZt(M)-C_2 E_{rel} : 2.8 kcal/mol

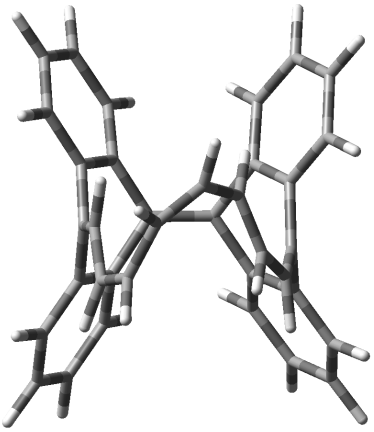

47

anti-cEcZcZt(M)-C_1 E_{rel} : 6.7 kcal/mol

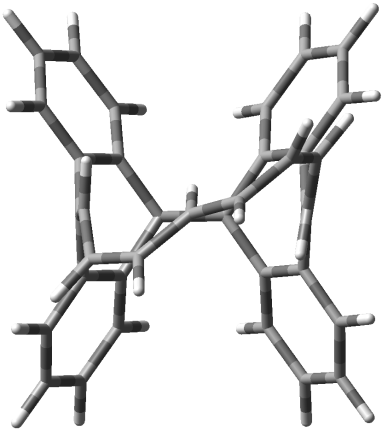

39

anti-tZcEtZt(M)-C_1 E_{rel} : 2.8 kcal/mol

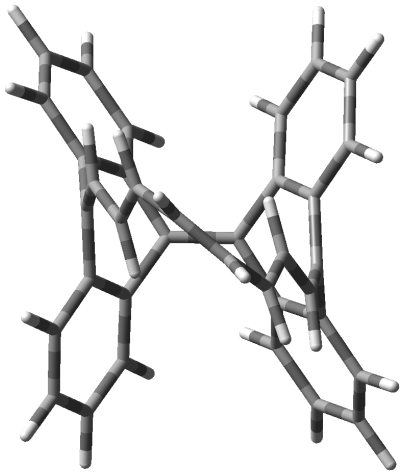

42

anti-tEcZcEt(M)-C_2 E_{rel} : 2.4 kcal/mol

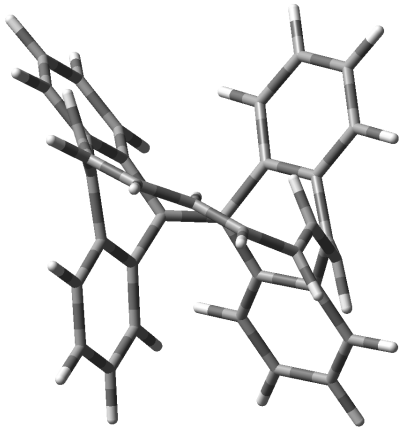

48

anti-cZtEcEt(M)-C_1 E_{rel} : 8.4 kcal/mol

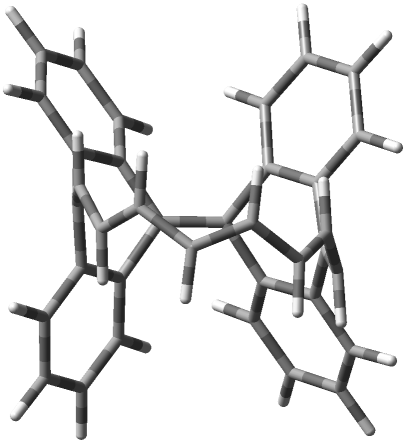

49

anti-tEtEtEt(H)-C_2 E_{rel} : 23.8 kcal/mol

Scheme 39: Optimised structures and energies relative to the *syn*-tZcZcEt isomer at B3Lyp/6-31G* of anti configuration isomers (H= Hückel, M= Möbius).

5.3.5.2 Harmonic oscillator model of aromaticity (HOMA)

On the basis of geometrical considerations, molecules should show a decrease in aromatic character when they possess a high degree of bond alternation (difference of bond lengths in a conjugated ring). Several quantitative measures of this bond alternation have been proposed.[96] Among them, the harmonic oscillator model of aromaticity index for hydrocarbons probably is most frequently used. It is defined as follows:

$$HOMA=1-\alpha/n\sum (R_{opt}- R_i)^2$$

where n is the number of bonds taken into the summation and α is an empirical constant chosen to give HOMA=0 for the hypothetical Kekulé structures of the aromatic systems and 1 for the system with all bonds equal to the optimal value R_{opt}, which this value is 1.88 for carbon-carbon bonds. R_i are the individual bond lengths. The model allows separating two terms describing different contributions to a decrease in aromaticity: (i) the bond elongation (the term called EN) and (ii) the bond length alternation (the term called GEO).

$$HOMA=1-\alpha/n\sum (R_{opt}- R_i)^2 =$$

$$=1-[\ \alpha(R_{opt}-R_{av})^2 + \alpha/n\sum (R_{av}- R_i)^2]$$

$$=1-EN-GEO$$

Where R_{av} is an averaged bond length.

HOMA, EN and GEO have calculated for isomers **38**-**42**. Bond length alternation parameters we calculated for (a) only polyene bridge, (b) [16]annulene part of molecule and (c) the whole molecule. As shown in Scheme **40**, bond alternation in *syn*-tZtZtZt **38** with Hückel structure is much higher than in the isomer with Möbius character and this value is a minimum for *anti*-tZcZcZt **40** that is a Möbius isomer with C_2 symmetry.

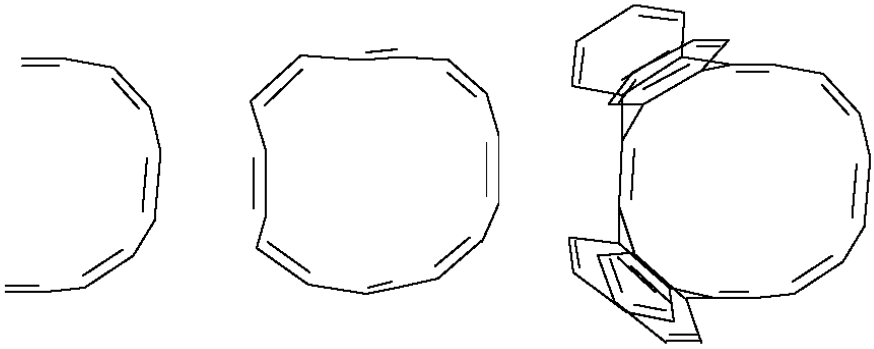

		EN	GEO	HOMA
Benzene		0.021	0.000	0.979
	a	0.024	0.919	0.056
38	b	0.358	0.922	-0.028
	c	0.256	0.572	0.171
	a	0.045	0.6235	0.3317
39	b	0.342	0.771	-0.113
	c	0.216	0.479	0.305
	a	0.021	0.478	0.502
40	b	0.297	0.681	0.022
	c	0.207	0.446	0.347
	a	0.039	0.492	0.469
41	b	0.321	0.692	-0.013
	c	0.210	0.441	0.349
	a	0.036	0.453	0.510
42	b	0.320	0.644	0.036
	c	0.199	0.398	0.403

Scheme 40: HOMA, GEO and EN index for isomers 38-42 in comparison with benzene. a: only the polyene bridge is included; b: the average of the four [16]annulene periphery is included; c: all bonds are included.

5.3.5.3 Nucleus independent chemical shift (NICS)

The nucleus independent chemical shift (NICS)[17] value is the absolute magnetic shielding, computed at the ring centre of the molecule. Negative NICS's indicate to aromaticity and this value has been calculated for benzene as about –10 ppm (small variations depending on the theoretical level). In nonplanar molecules like the TDDA/TCOD addition, several points can be defined as the centre of the ring. Therefore, unambiguous NICS values cannot be given for **38**-**45**. The lowest NICS value along the C_s axis of the Hückel isomer **38** is found to be –1.2 ppm and this value for Möbius isomers are between –3.2(for **39**) and –3.5(for **40**) ppm that indicate a weak aromaticity for Möbius isomers.

5.3.5.4 Magnetic susceptibility

The magnetic susceptibility of the isomers is dominated by the four benzene rings in the bianthraquinodimethane part of the structures. As expected, there is no big difference between the calculated values of the magnetic susceptibility for the different isomers and surprisingly these values are positive.

	38	**39**	**40**	**41**	**42**
χ	228.9191	230.0252	229.0684	230.9177	239.3348

Scheme 41: CSGT magnetic susceptibilities (cgs-ppm) at B3LYP/6-31G* level of theory.

5.3.5.5 Anisotropy of current induced density

The ACID (anisotropy of the current induced density) is a powerful method to visualize the density of delocalized electrons (both π-electrons and σ-electrons) and to quantify conjugation effects. In order to quantify aromaticity with this method one should separate π-electrons from σ-electrons. The CIV (critical isosurface value) of

each bond for **38** and **40** was calculated but as these densities consist both of π bonds electrons and σ bonds electrons, it isn't possible to decide about aromaticity.

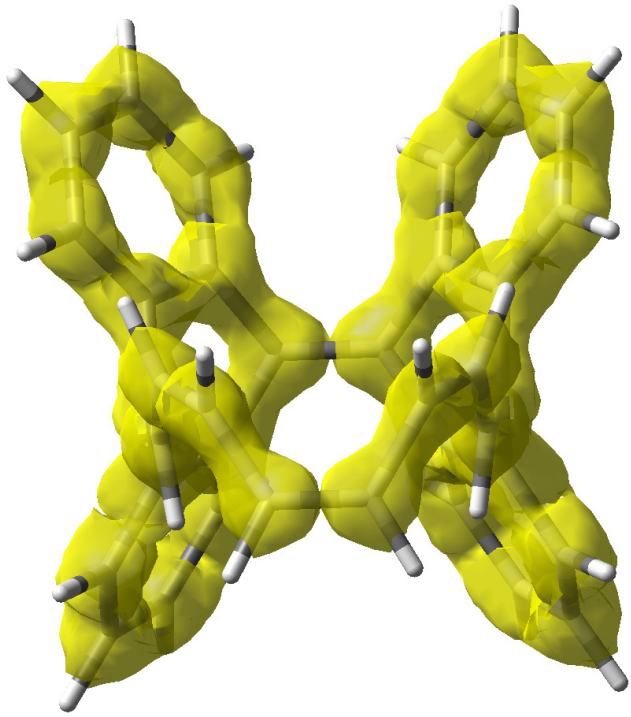

Figure 77: ACID plot of **38** (*syn*-tZtZtZt) at an isosurface value of 0.063.

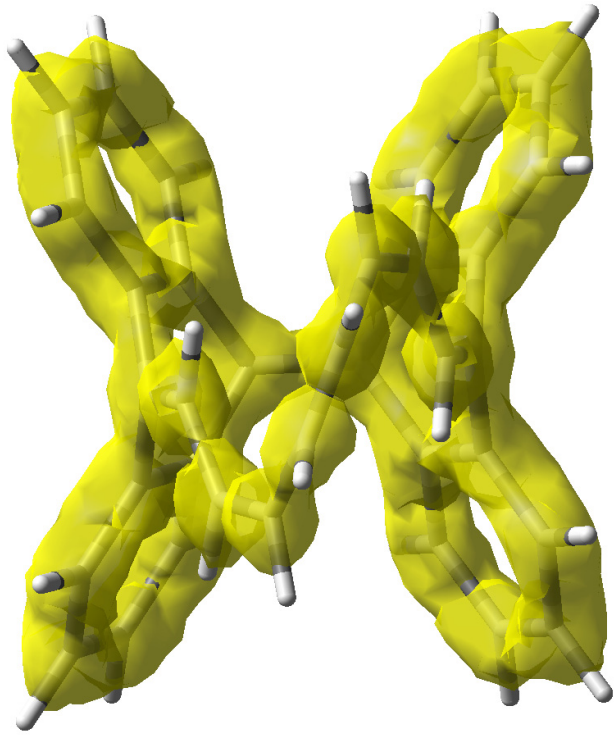

Figure 78: ACID plot of **40** (*anti*-tZcZcZt) at an isosurface value of 0.059.

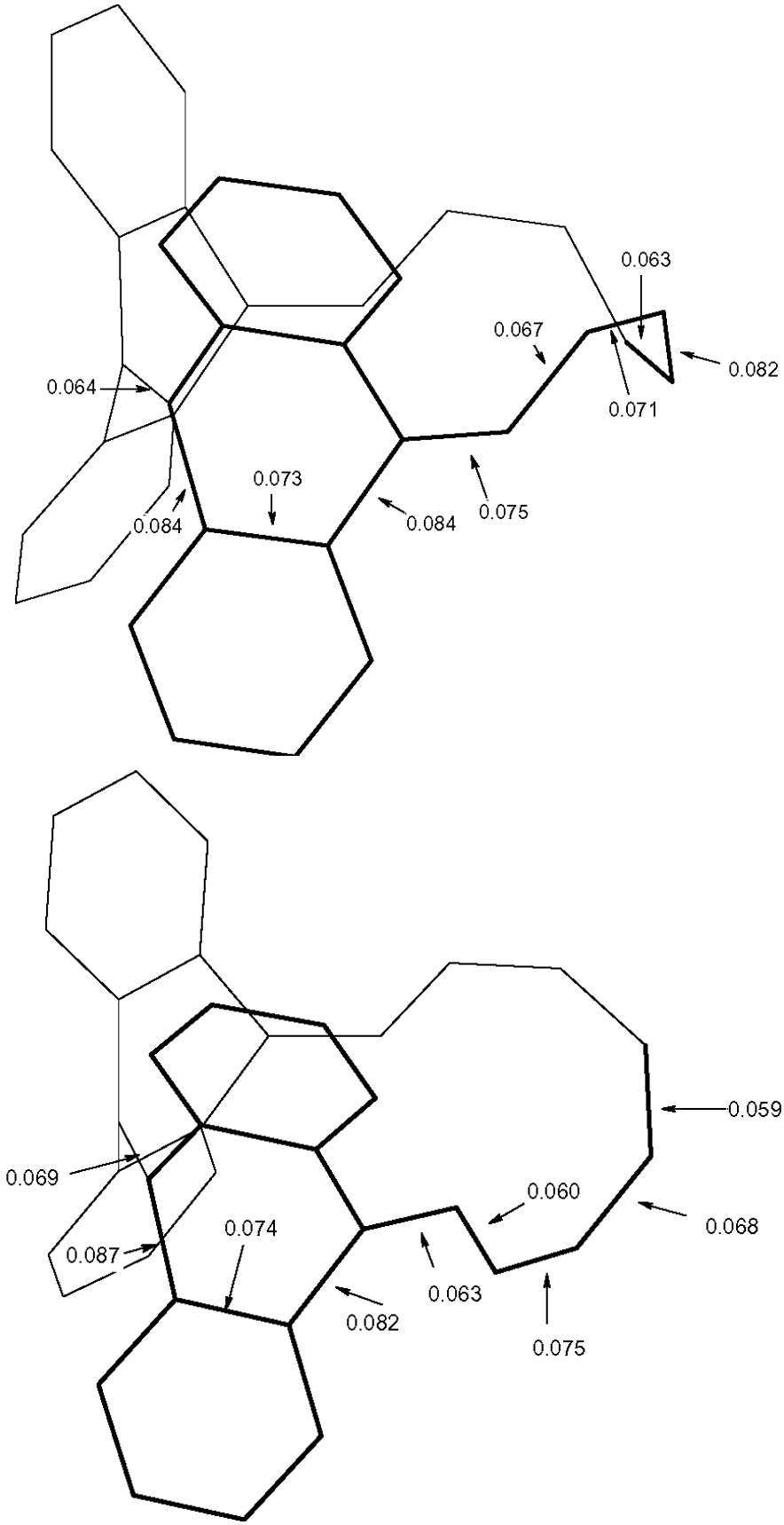

Figure 79: CIV value for each bond in the [16]annulene periphery of **38** and **40**.

5.3.5.6 UV absorption spectra

The UV spectra of the purified isomers differ in the wavelength and intensity of absorption. Crystals of the Möbius isomer **40** are red (λ_{max}=400nm ε=3301.81), whereas crystals of the Hückel isomer **38** are colorless ((λ_{max}=299.2nm ε=16334.50). A comparison of the UV/Vis spectra of isomers **38**, **39** and **40** has shown that the Möbius isomers absorb at longer wavelengths with higher extinction coefficients that means Möbius isomers are better conjugated. Calculated electronic structures of isomers confirm that HOMO-LUMO gap for Möbius isomers is smaller than in Hückel isomers. The gap between HOMO and LUMO is 0.115 eV for the Möbius isomer **40** and 0.148 eV for Hückel isomer **38** (Figure **80**).

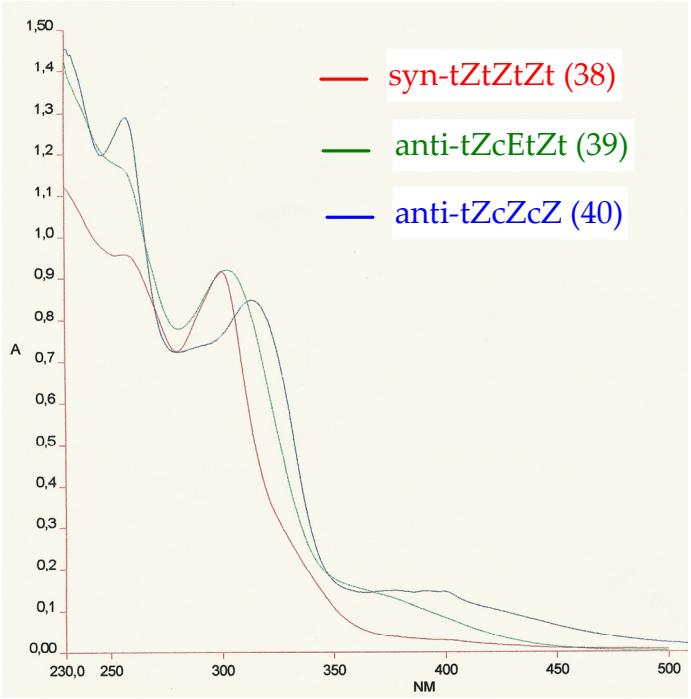

38		**39**		**40**	
λ	**ε**	**λ**	**ε**	**λ**	**ε**
298.8	16334.5	300	15558.56	400	3301.81
259.54	17026.94	250	19649.66	311.8	17498.57
				252.6	26296.62

Figure 80: Comparison of UV spectra of isomers **38**,**39**,**40**.

5.4 Conclusion

In 1964, Heilbronner propounded his theory about Möbius aromatic [4n]annulenes. He suggested that large cyclic [4n]annulenes might be stabilized if the π orbitals were twisted gradually around a Möbius strip. Numerous attempts have been done in order to synthesize Möbius aromatic compounds, especially Möbius [4n]annulenes, but all of them have failed. Twisted small annulenes are unstable because of the high strain in the molecules and increasing the ring size causes an exponentially increasing number of isomers, whose separation is almost impossible. The combination of inplane aromaticity and normal aromaticity was considered to stabilize the Möbius structures and to facilitate their synthesis. Irradiation of TDDA and *syn*-tricyclooctadiene with a low pressure mercury lamp in a quartz apparatus in benzene resulted in a mixture of seven isomers. Five of them were characterized by X-ray structure analysis including, two closed (1,3-cyclohexadiene) isomers and three ring opened isomers (Möbius C_2, C_1 and Hückel C_s). A comparison of energetic, structural and geometrical and magnetic properties of the Möbius and Hückel isomers predicted a weakly aromatic character for Möbius C_2 isomer **40** and a nonaromatic character for Hückel C_s isomers **38.**

6 Summary

This study was aimed at the synthesis of tubular, belt-like and Möbius aromatic compounds using the ring enlargement metathesis reaction with tetradehydrodianthracene. The high reactivity of TDDA is due to its extraordinary structure. Both bridgehead double bonds are fixed exactly in a parallel orientation at a distance of only 2.4 Å that is far below the van der Waals distance. Even though TDDA is extremely strained it is stable under ambient conditions. TDDA reacts with electrophiles, nucleophiles and as an electron deficient olefin in cycloaddition reactions like the Diels-Alder reaction and [2+2] photocycloadditions.

One of the synthetic goals was the synthesis of 9,9′,9′′,10,10′,10′′-hexadehydrotrianthracene (trimer) **9**. Two different strategies were considered. The first one comprises a Diels-Alder reaction of TDDA with anthracene and an oxidative dehydration and ring opening. This strategy failed in the first step because of the sterical hindrance between anthracene and TDDA. In the second approach the trimer synthesis started from TDDA by subsequently building up the phenyl rings. The semitrimer **14** was prepared by a Diels-Alder reaction of TDDA with α,α,α′,α′-tetrabromo-*o*-xylene. The conversion of the semitrimer to the trimer was not yet achieved, but might be possible by a bromination, dehydrobromination and Friedel-Crafts alkylation sequence (Scheme **42**).

In the presence of Montmorillonite K10, TDDA reacts with toluene and anthracene in a transannular fashion. The mechanism of the reaction might be explained by generation of radical cation of TDDA by Montmorillonite K10 and subsequent rearrangement to form a transannular 1,4-radical cation. Finally an electrophilic aromatic substitution reaction forms the products (Scheme **43**).

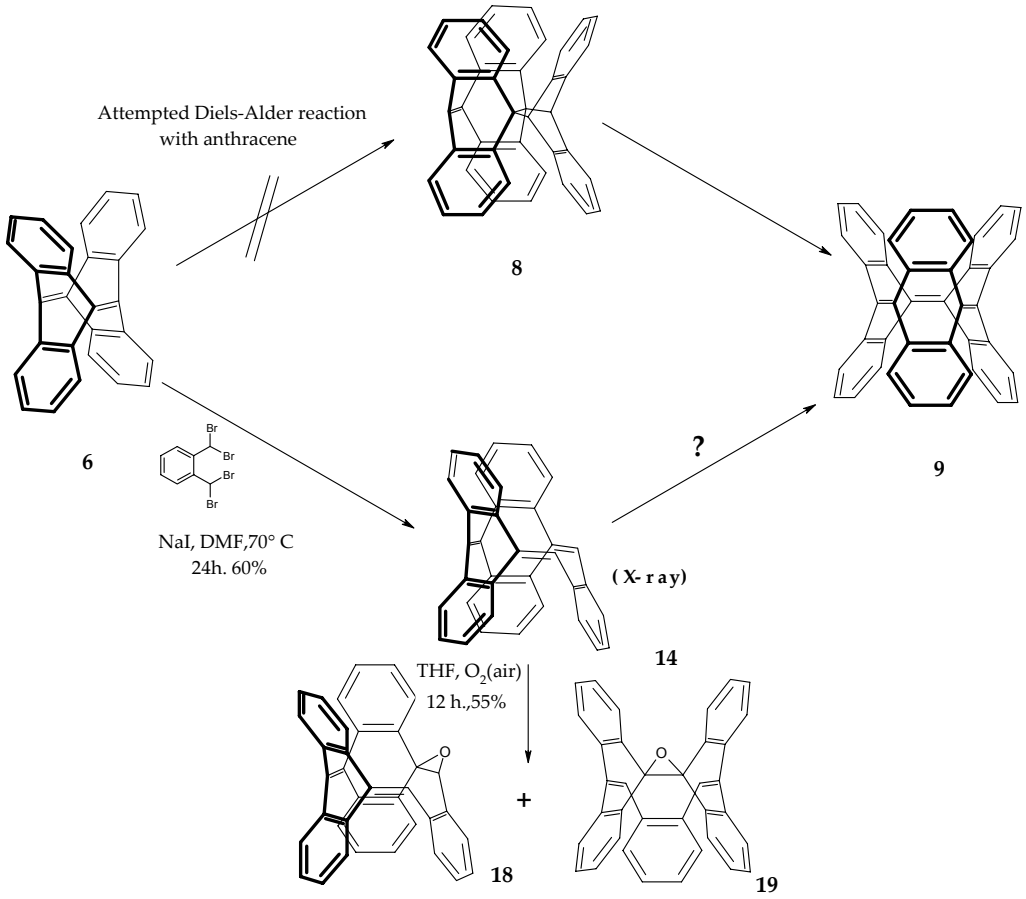

Scheme 42: Synthesis of the semitrimer and the proposed strategy to synthesize the trimer.

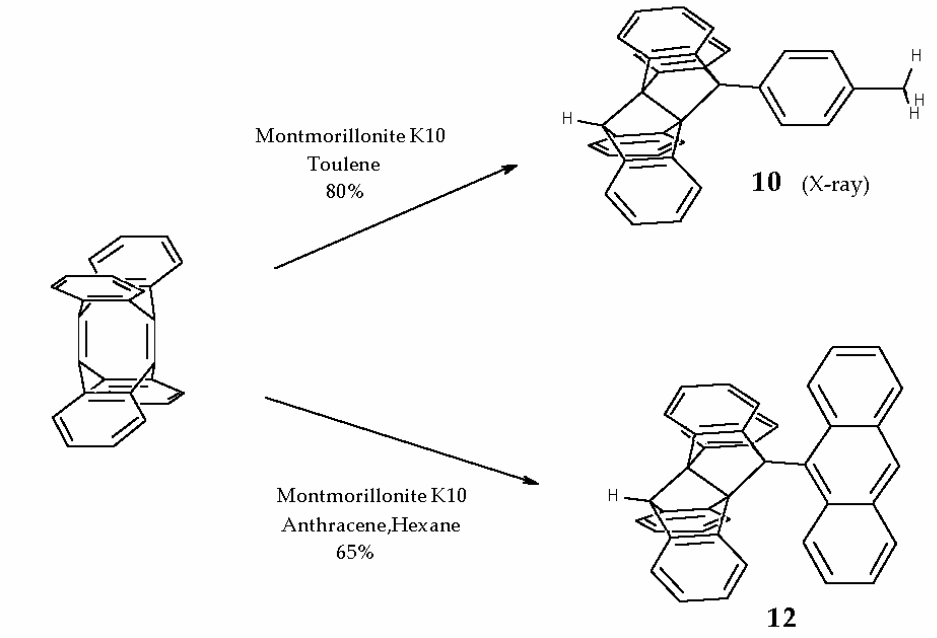

Scheme 43: Transannular addition to TDDA.

The photochemically induced metathesis reaction of TDDA was extensively investigated. Dimerization metathesis of TDDA to the tetramer **4** was achieved by irradiation of a suspension of TDDA in benzene with a 700 W high-pressure lamp in a quartz apparatus for 40 hours. Using ultrasound (cell disruptor) during the irradiation accelerated the reaction so that TDDA was completely converted to the tetramer after 3 hours in 45% yield. The conversions of the tetramer to the hexamer **24** or octamer **26** were carefully investigated. All conventional irradiation methods for this reaction failed probably because of the sterical hindrance at the quinoid double bonds in the tetramer. However, upon irradiation of the tetramer with a nitrogen laser in a MALDI TOF mass spectrometer, a large signal was detected which is most probably the molecular peak of the octamer **26**. Experiments to produce **26** on a preparative scale using a strong laser are under way.

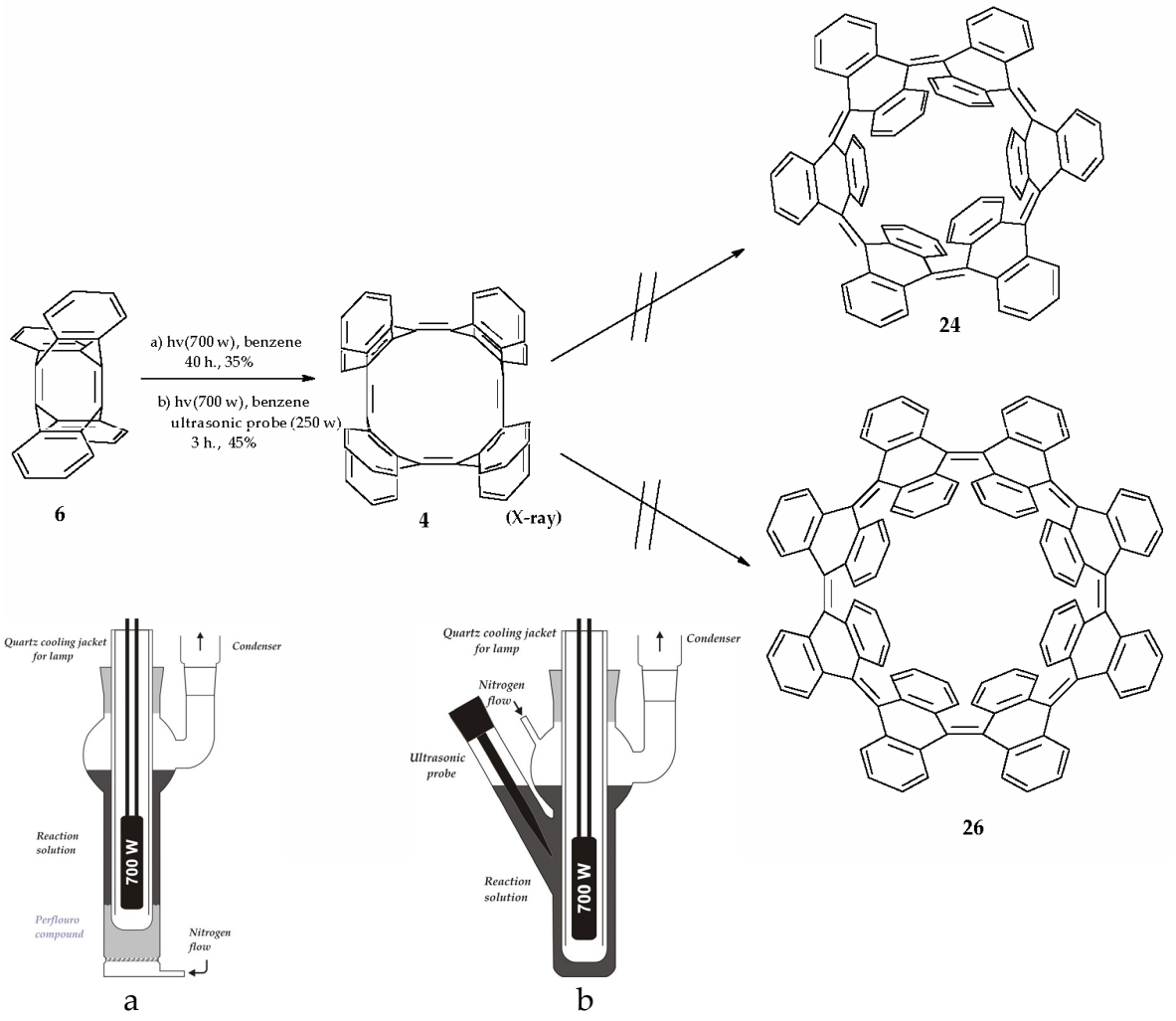

Scheme 44: Improvement of the tetramer synthesis using an ultrasonic probe.

Since Heillbornner's prediction of the aromaticity of Möbius [4n]annulenes, a large amount of research has been dedicated to their synthesis but all attempts so far failed. There are three problems associated with the synthesis of Möbius system:

1. High strain energy is induced by the twist, which are mainly due to the pyramidalization of the sp2 hybridized carbon atoms.
2. The overlap is reduced by twisting the p orbitals with respect to each other.
3. Large annulenes have numerous configurational and conformational isomers that rapidly interconvert, which makes the synthesis of a specific (Möbius) isomer difficult.

A Möbius system includes a "normal" part with trigonal planar sp^2 atoms and a belt-like system with pyramidalized sp^2 atoms. The strain arises from pyramidalization. Thus, introducing a "prefabricated" pyramidalized building block in a ring should stabilize the Möbius versus Hückel type isomers.

We chose tetradehydrodianthracene as the in-plane pyramidalized part, cyclooctatetraene as the "normal" π system and the ring enlargement metathesis as the synthetic method to combine both parts.

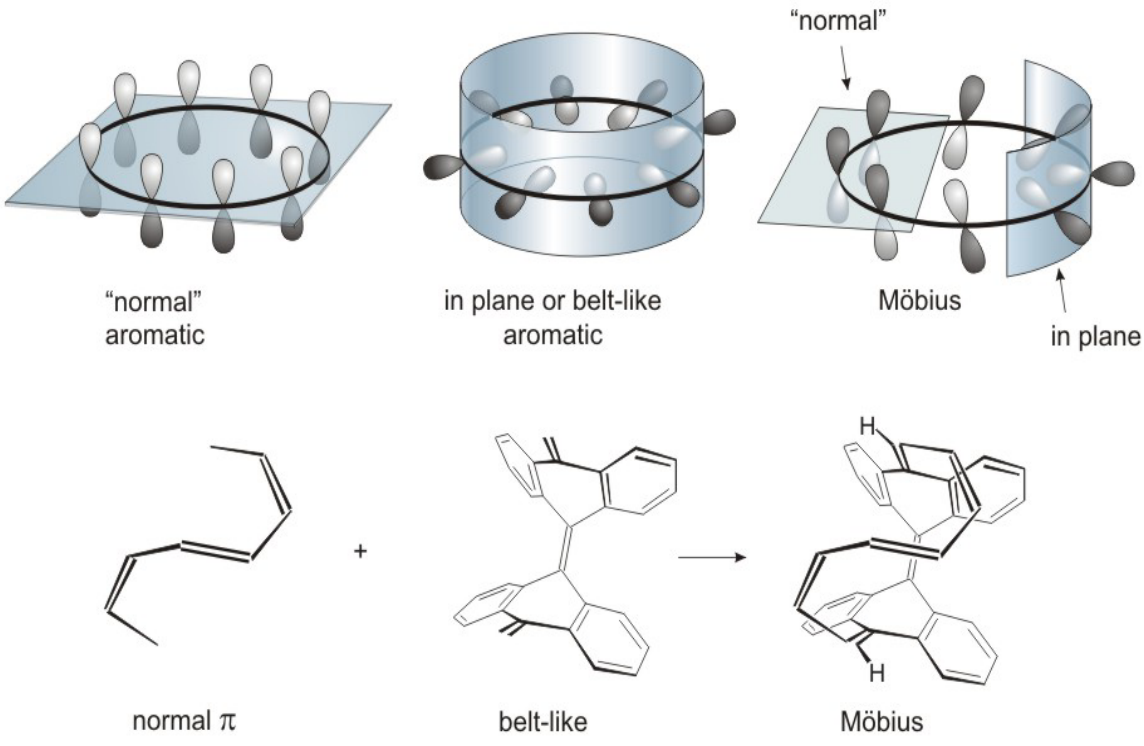

Scheme 45: Strategy to synthesize Möbius aromatic compounds.

Irradiation of TDDA and *syn*-tricylooctadiene (TCOD) with a 700 W high-pressure mercury lamp in a quartz apparatus in benzene gave as the main products two isomers containing a 1,3-cyclohexadiene ring and a ladder-shaped isomer. The yield of the reaction was higher when naphthalene was used as a triplet quencher during irradiation.

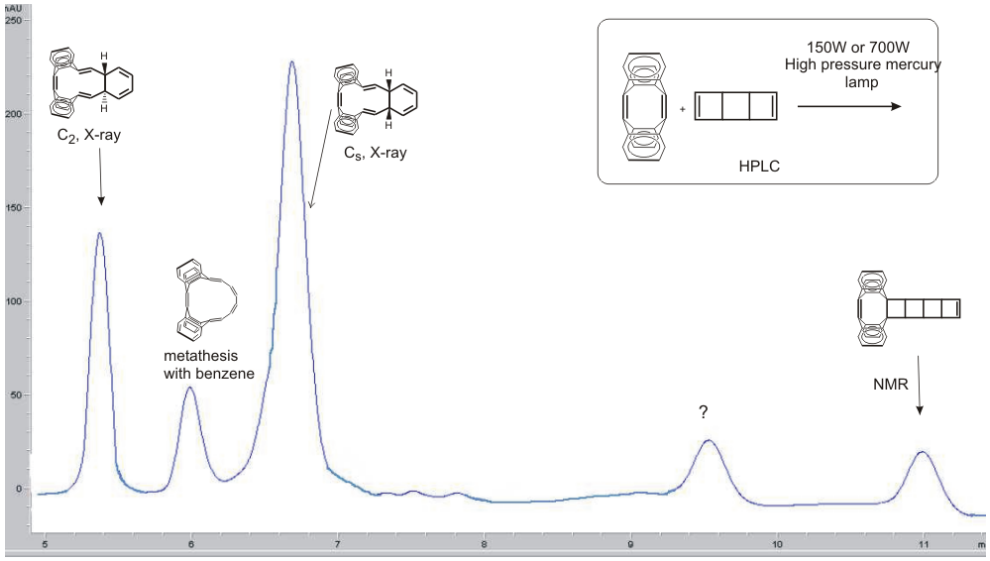

Scheme 46: HPLC Chromatogram after irradiation of TDDA and TCOD with a high-pressure mercury lamp.

Changing the high-pressure mercury lamp to a 15 W low-pressure mercury lamp under the same reaction conditions gave five ring opened products alongside with two 1,3-hexadiene structures.

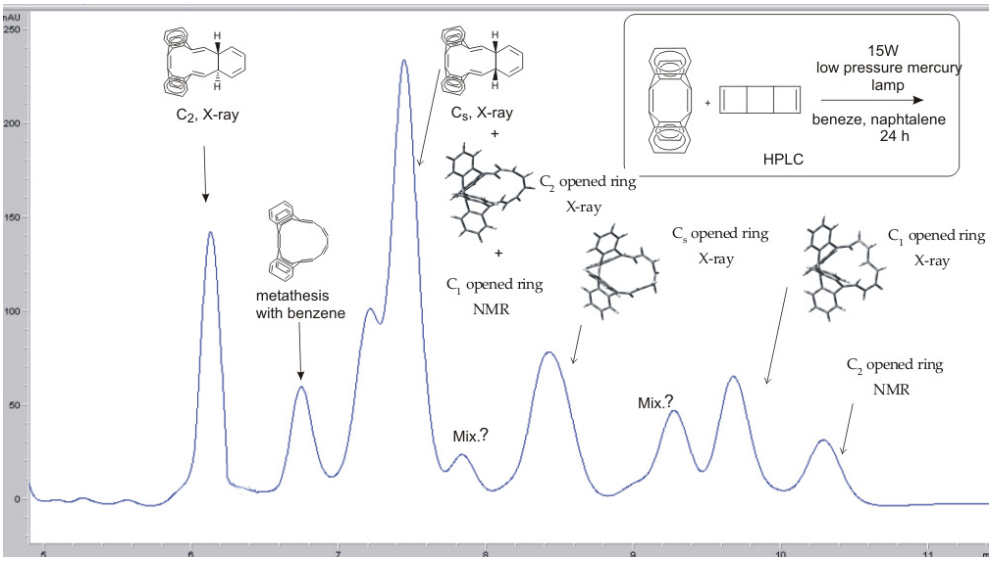

Scheme 47: Chromatogram after irradiation of TDDA and TCOD with a low-pressure mercury lamp.

Three ring-opened isomers were characterized based on x-ray structure analyses. Two of them have Möbius (C_1 and C_2 symmetric) topology and another one is a Hückel isomer with C_s symmetry. The C_2 symmetric Möbius compound formed red crystals and has an additional absorption bond at 400nm whereas the C_s symmetric Hückel compound is colorless and is 4.1 kcal/mol higher in energy than the C_2 symmetric Möbius compound according to a density functional calculation (B3LYP/6-31G*). Unfortunately magnetic criteria as aromaticity probes (magnetic susceptibility, exaltation or anisotropy of the magnetic susceptibility) are difficult to apply because the four benzene rings dominate the magnetic properties.

The HOMA value, which is used to quantify aromaticity effects, is 0.50 in the polyene bridge (9 bonds) of the Möbius and 0.05 in the Hückel isomer. The total HOMA is 0.35 in the Möbius and 0.17 in the Hückel structure. Thus, the Möbius structure can be called weakly aromatic, whereas Hückel isomer is non-aromatic.

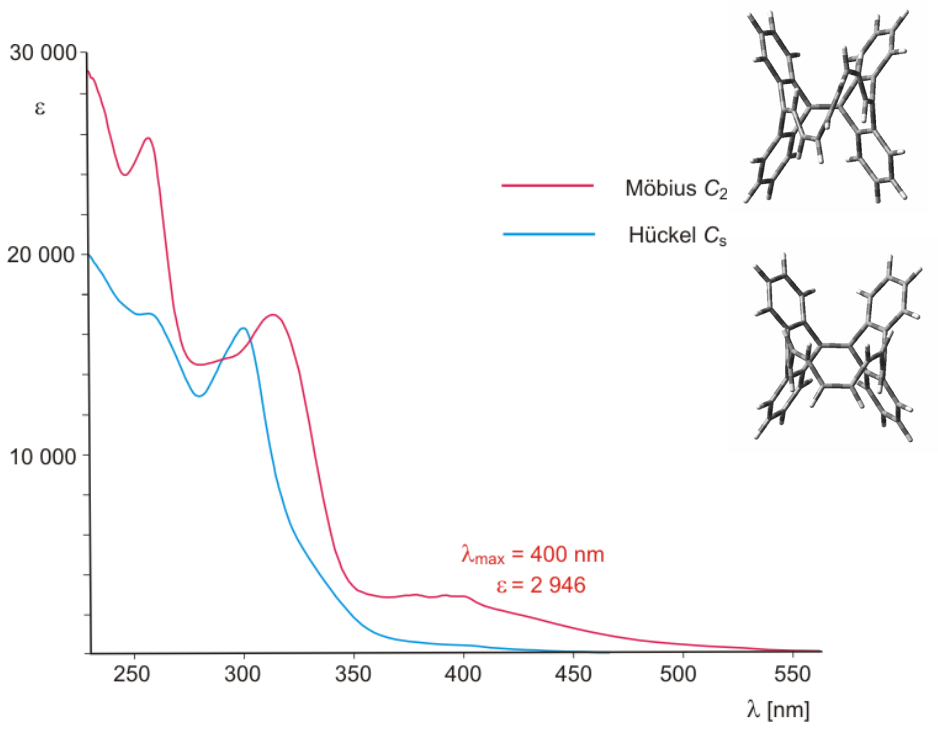

Scheme 48: Comparison of the UV spectra of Möbius C_2 (**40**) and Hückel C_s (**38**).

7 Experimental part

7.1 Apparatus

NMR:

BRUKER AC 200	^{1}H-NMR (200.1 MHz)	^{13}C-NMR(50.3MHz)
BRUKER AC 300	^{1}H-NMR (300.1 MHz)	^{13}C-NMR(75.5MHz)
BRUKER AC 400	^{1}H-NMR (400.1 MHz)	^{13}C-NMR(100.6MHz)
BRUKER AC 500	^{1}H-NMR (500.1 MHz)	^{13}C-NMR(125.8MHz)

Samples have solved in deuterochloroform ($CDCl_3$) and tetramethylsilane used as internal standard.

IR: FT-IR_Spectrometer Nicolet 320

MS: Varian MAT 311 A
Finnigan MAT 8430
Finnigan MAT 8200/8239
Bruker FlexIII™ MALDI TOF

UV/Vis: Hewlett-Packard Diode Array Spectrometer 8542A
Beckmann UV 5230

X-Ray: Siemens P4-Diffractometer and STOE Imaging Plate Diffraction System (IPDS) with $Mo_{K\alpha}$ irradiation. Diffraction information have solved with SHELXL-97, G.M. Sheldrick, Univ. Göttingen.

HPLC: Hewlett-Packard/Agilent Serie 1100
Gilson M305, M306, UV-detector 117

7.2 Common procedure

Solvents were purified and dried with usual methods. Starting materials were ordered from Aldrich, Acros-Chimica, Fluka, Merck, Roth and Riedel-de Haën companies.

The reaction progresses were monitored by thin layer chromatography with silica gel 60 F_{254} and aluminiumoxid 60 F_{254} plates of Macherey-Nagel. New products were separated using of Flash chromatography and HPLC. Special glass columns of Aldrich and silica gel (mesh: 0.04-0.063 μm) were applied in flash chromatography. The configuration of preparative HPLC of Gilson company are: M305 major pump, M306 mixing pump, 50 SC head pump, Gilson 117 UV detector and columns:

Dynamax Si 60(8 μm)	250.41.4 mm (Rainen Co.)
Silicagel Si 100 (12μm)	250.20 mm(Mz-Analysentechnik)
PSS-SDV-Gel 100 Å (13μm)	250.20 mm(Mz-Analysentechnik)

All photochemical reactions were performed in a quartz apparatus with extra cooling jacket with the following lamps:

High pressure mercury lamps:	150 W	Heraeus TQ 150
	700 W	Heraeus TQ 718
Low pressure mercury lamp:	15 W	Heraeus TNN 15/32

7.3 Synthesis

7.3.1 Synthesis of TDDA

7.3.1.1 Synthesis of 9-bromoanthracene

To a stirred solution of anthracene (126.0 g., 0.706 mol) in carbon tetrachloride (1000 mL) at –6°C was added dropwise a solution of bromine (35 mL, 0.679 mol) in carbon tetrachloride (200 mL). After 1 hour the yellowish precipitate was washed with tetrachlorocarbon and dried over night in air and stirred in toluene (900 mL) and phenol (1.8 g) at room temperature for 5 d. The dark mixture was warmed up to 60°C for 4 h and washed with 1M sodium hydrogen carbonate (300 mL) and toluene evaporated off. Remaining yellowish solid was washed with water several times and crystallization in ethanol provided the title compound, (145.0 g, 80%) as green crystals.

M.p. 98-100°C.

^{1}H-NMR (400 MHz, $CDCl_3$/TMS): δ=8.49 (dd, ^{3}J=9.1 Hz, ^{5}J=1.2 Hz, 2H, H-1,8), 8.39 (s, 2H, H-10), 7.96 (dd, ^{3}J=8.5 Hz, ^{5}J=1.2 Hz, 2H, H-4,5), 7.58 (ddd, ^{3}J=9.1 Hz, ^{3}J=6.8 Hz, ^{5}J=1.2 Hz 2H, H-2,7), 7.47 (ddd, ^{3}J=8.5 Hz, ^{3}J=6.8 Hz, ^{5}J=1.2 Hz 2H, H-3,6).

^{13}C-NMR (100.6 MHz, $CDCl_3$/TMS): δ=132.12 (s, C-8a,9a), 130.52 (s, C-4a,10a), 128.52 (d, C-4,5), 127.11 (d,C-2,7), 126.97 (d, C-10), 125.63 (d, C-3,6), 122.29 (s, C-9).

7.3.1.2 Synthesis of 9,10′-dibromoanthracene

A solution of 9-bromoanthrance (80.0 g , 0.311 mol) in toluene (1000 mL) was irradiated with a usual garden lamp (Osram HQL-R de luxe, 80 W) for one month. The green crystals (40g) that precipitated were crystallized from toluene several times till colorless crystal were obtained (37.3 g ,47%)

M.p. 250°C.

^{1}H-NMR (400 MHz, $CDCl_3$/TMS): δ=7.74(d, ^{3}J=7.6 Hz, ^{5}J=1.5 Hz, 4H, CH arom.), 6.86-6.97 (m, 12H, CH arom.), 5.33 (s, 2H, CH aliph.).

^{13}C-NMR (100.6 MHz, $CDCl_3$/TMS): δ=142.54 (s), 130.52 (s), 128.52 (d), 127.11 (d), 126.97 (d), 125.63 (d), 122.29 (s, C-Br).

7.3.1.3 Synthesis of bistriazolindianthracene

9,10′-dibromoanthracene(14.06 g, 0.027 mol) and sodium azide (48.9 g, 0.752 mol) were suspended in dimethylsulphoxide (700 mL). After 1 h potassium *tert*-butoxide (24.4g, 0.218 mol) in dimethylsulphoxide (300 mL) was added dropwise. The reaction mixture was stirred for 14 d. at 30-35°C and then poured into cold water. The light green crystals were filtrated and dried under high vacuum for 12 h. the product (12.93 g, some water stays in the crystals) used into next step without further purification.

^{1}H-NMR (400 MHz, DMSO-d_6): δ=11.89 (s, 2H, N-H), 7.02 (d, ^{3}J=6.0 Hz, 4H, CH arom.), 6.95-6.85(m, 12H, CH arom.).

IR (KBr, cm^{-1}): $\tilde{\upsilon}$= 3300, 3080 (m, C-H arom.), 1460,1400 (m, C=C arom.), 1030(s, C-N), 740 (s, C-H arom.).

7.3.1.4 Synthesis of N-aminobistriazolindianthracene

To a mechanically stirred and sonificated(with ultrasonic bath) solution of sodium hydride (7.58g , 0.158 mol) in dimethylethane (100mL) was added portionwise bistriazolinanthracene (12.93g , 0.027 mol) and after 1 h further sonification a cold solution of o-mesitylesulfounylhydroxylamine(carpinos reagent) (16.7g , 83.8 mmol)

in demethylethane (100 mL) was added dropwise. After further 30 min stirring, it kept in the refrigerator over night. The filtrated solid was washed with diethyether till it became colorless and it suspended in water (500 mL) and again filtrated and dried in high vacuum (9.87g , 77%)

^{1}H-NMR (400 MHz, DMSO-d_6): δ= 7.02 (br, 4H, CH arom.), 6.90(br, 8H, CH arom.), 6.82 (br, 4H, CH arom.), 6.30 (br, 4H, NH_2).
IR (KBr, cm^{-1}): ῡ= 3260,3240 (s, N-H), 3080(s, C-H aro.),1480,1460 (m, C=C arom.), 1030(s, C-N).

7.3.1.5 Synthesis of tetradehydrodianthracene

To a sonificated solution of N-aminobistriazolindianthracene (9.87g , 21.1 mmol) in benzotriflouride (150mL) was added portionwise lead tetraacetate (18.7g , 42.2 mmol). The excess of lead tetraacetate was destroyed with ethylene glycol. The filtrated solid was washed with dichloromethane and dried and then stirred for 30 min in sat. aq. sodium bicarbonate (500 mL). The filtrate was washed with water and dired over night and stirred for 3h in dichloromethane (300mL) and filtrated and dried. Crystallization in toluene provided light yellow crystals of TDDA (2.5g , 33%).

M.p. 388°C.
^{1}H-NMR (400 MHz, $CDCl_3$/TMS): δ=7.15 (dd, ^3J=5.7 Hz, ^4J=3.4 Hz, 8H, CH arom.), 6.89 (dd, ^3J=5.7 Hz, ^4J=3.4 Hz, 8H, CH arom.).
^{13}C-NMR (100.6 MHz, $CDCl_3$/TMS): δ=152.2 (s, C=C), 140.0 (s), 125.8(d), 124.1(d).
IR (KBr, cm^{-1}): ῡ= 3064,3037 (m, C-H arom.), 1566(m), 1449 (s, C=C arom.), 740(s, C-H arom.), 614 (s) cm^{-1}.
UV/Vis.($CHCl_2$): λ_{max} (ε)=233(10700), 270(2500), 282(1270) nm.
MS(70 eV) : *m*/*z*(%) : 352(100)[M^+].

7.3.2 Synthesis of o-mesitylensulfonylhydroxylamin (Carpino's reagent)

7.3.2.1 Synthesis of *tert*-butyl phenyl carbonate

A solution of *tert*-butyl alcohol (296.5g , 4.00 mol) and quinoline (519.2g , 4.02 mol) in methylene dichloride (600mL) was stirred and cooled by a slow stream of running tap water while phenyl chloroformate (500mL, 3.97mol) was added dropwise during about four hours while maintaining the temperature at 30°C. The solution was allowed to stand overnight, sufficient water was added to dissolve the precipitated salt and the organic layer was washed two times with 250 mL of 5% hydrochloric acid. The solvent was removed from the dried ($MgSO_4$) solution and the product distilled through a Claisen flask, (499.7g , 66%).

B.p. 105°C/1mbar

^{1}H-NMR (200 MHz, $CDCl_3$/TMS): δ=7.40-7.14 (m, 5H, phenyl), 1.31 (s, 9H, *tert*-butyl).

^{13}C-NMR (50.3 MHz, $CDCl_3$/TMS): δ=151.9(s, C=O), 151.0(s, C-O), 129.3(d, phenyl), 125.7(d, phenyl), 121.1(d, phenyl), 83.4(s, *tert*-butyl), 27.6(q, *tert*-butyl).

7.3.2.2 Synthesis of *tert*-butyl carbazate

A mixture of *tert*-butyl phenyl carbonate (499.7g, 2.58mol) and 85% hydrazine (267.5 mL, 7.31 mol) was warmed on a hot-plate. When the temperature reached 75°C instantaneous solution occurred and the temperature rose spontaneously to 103°C. After standing for 12 hours the solution was diluted to one liter with ether and shaken well with an aqueous solution containing 150g of sodium hydroxides. The mixture was extracted with ether for 24 hours in a continuous extractor, the solvent removed on a steam-bath and the carbazate distilled through a Claisen flask (328.9g, 85%).

B.p. 85°C/1.33 mbar.

^{1}H-NMR (200MHz, $CDCl_3$/TMS): δ=6.48 (s, 1H, NH), 3.80 (s, 2H, NH_2), 1.45 (s, 9H, *tert*-butyl).

^{13}C-NMR (50.3 MHz, $CDCl_3$/TMS): δ=158.0(s, C=O), 80.4(s, *tert*-butyl), 28.2(q, *tert*-butyl).

7.3.2.3 Synthesis of *tert*-butyl azidoformate

A solution of *tert*-butyl carbazate (264.3g, 2.00 mol), glacial acetic acid (211mL) in water (315 mL) was cooled in an ice-bath and with vigorous stirring and a solution of sodium nitrite (144.0g, 2.08 mol) in water (200 mL) was added dropwise. As soon as yellowish phase start to become dark, the addition was stopped and the phase was separated and the aqueous layer extracted with four 100 mL portions of ether. The combined organic layers were washed three times with 150 mL portions of water and three times with 150 mL portions of 1 *M* sodium bicarbonate solution. The light yellow solution was dried over magnesium sulfate and the solvent removed and remained mixture distillated (154.1g, 56%).

B.p. 71°C/93 mbar.

^{1}H-NMR (200 MHz, $CDCl_3$/TMS): 1.50 (s, 9H, *tert*-butyl).

^{13}C-NMR (50.3 MHz, $CDCl_3$/TMS): δ=156.0(s, C=O), 84.3(s, *tert*-butyl), 28.0(q, *tert*-butyl).

7.3.2.4 Synthesis of *tert*-butyl N-hydroxycarbamate

A solution of hydroxylamine hydrochloride (100.2g, 1.44 mol) in water (200 mL) was cooled in an ice-bath and tert-butyl azidoformate (154.1g, 1.08 mol) added. While stirring vigorously, a cold solution of sodium hydroxide (194.3g, 4.31 mol) in water (400mL) was dropped in during 40 min. the mixture was allowed to stir in the ice-bath for one hour and water (800 mL) was added to dissolve a precipitated solid. The solution was extracted twice with 500 mL portions of ether and extracts discarded. The aqueous solution was cooled in an ice-bath and acidified to pH 5-6 with 6 *N* hydrochloric acid (700 mL). The resulting mixture was extracted with five 400 mL portions of ether, the solution dried (magnesium sulfate) and the solvent removed. The thick oil solidified within several hours after placing in a vacuum desiccator giving white crystals (77.9g, 55%).

M.p. 50°C

^{1}H-NMR (200 MHz, $CDCl_3$/TMS): δ=7.33 (s, 1H, NH), 7.14 (s, 1H, OH), 1.47 (s, 9H, *tert*-butyl).

^{13}C-NMR (50.3 MHz, $CDCl_3$/TMS): δ=159.0(s, C=O), 82.0(s, *tert*-butyl), 28.2(q, *tert*-butyl).

7.3.2.5 Synthesis of *tert*-butyl N-*p*-toluenesulfonoxycarbamate

To a solution of *tert*-butyl N-hydroxycarbamate (33.2g, 0.250 mol) and *p*-toluenesulfonyl chloride (54.5g, 0.249 mol) in ether (800 mL) at 0°C was added dropwise triethylamine (35mL, 0.250 mol). After standing 30 min. in the ice-bath the solution filtrated and washed with ether. The ether phases combined and half of the ether was removed and washed with water and dried (magnesium sulfate) and the solvent evaporated. Collected colorless oil will convert to colorless solid (65g, 83%).

M.p. 95-100°C

^{1}H-NMR (400 MHz, $CDCl_3$/TMS): δ=8.05 (s, 1H, NH), 6.95 (s, 2H, phenyl), 2.67 (s, 6H, $PhCH_3$),2.32(s, H, $PhCH_3$), 1.31 (s, 9H, *tert*-butyl).

^{13}C-NMR (100.6 MHz, $CDCl_3$/TMS): δ=154.3 (s, C=O),144.2 (s, phenyl), 141.8 (s, phenyl), 131.5 (d, phenyl), 128.4 (s, phenyl), 45.8 (s, *tert*-butyl), 27.6 (q, *tert*-butyl), 22.9(q, $PhCH_3$), 20.9 (q, $PhCH_3$).

7.3.2.5 Synthesis of hydroxylamine *o*-mesitylene sulfonate (Carpino's reagent)

To *tert*-butyl N-*p*-toluenesulfonoxycarbamate (30.3g, 0.102 mol) was added trifluoroacetic acid (110 g) at 5° C. Vigorous gas evolution occurred and was allowed to subside between addition and then cold water (400 mL, 5° C) was added. The mixture was filtrated and the filtrate solid washed with water and dried. The solid was dissolved in minimum ether (20 mL) and the water phase was separated. Pentane (100 ml) added to the ether phase and the resulted white crystals were filtrated and dried (16.7 g, 76%).

^{1}H-NMR (400 MHz, $CDCl_3$/TMS): δ=7.00 (s, 2H, phenyl), 4.98 (s, 2H, NH), 2.65 (s, 6H, $PhCH_3$), 2.32(s, 3H, $PhCH_3$).

7.3.3 Attempted Diels-Alder reaction

7.3.3.1 Typical reaction

To a solution of TDDA (100mg, 0.28 mmol) in xylene (20 mL) was added anthracene (149.5 mg, 0.84 mmol). After 50 min at room temperature the mixture was refluxed for 24 h. After chromatography of the reaction mixture unreacted anthracene and bianthryl were isolated.

Data for bianthryl:

^{1}H-NMR (400 MHz, $CDCl_3$/TMS): δ=8.67 (s, 2H, 9,9′-H), 8.13 (d, *J*=8.3 Hz, 4H, 1,1′,8,8′-H), 7.42 (m, 4H, 2,2′,7,7′-H), 7.10 (m, 8H, 3,3′,4,4′,5,5′,6,6′-H).

^{13}C-NMR (100.6 MHz, $CDCl_3$/TMS): δ=133.06 (C_q), 131.60 (C_q), 128.51(C_q), 127.20 (C_q), 126.81 (CH, arom.), 125.79 (CH, arom.), 125.28 (CH, arom.).

IR (KBr, cm^{-1}): $\tilde{\upsilon}$= 3049,3029 (m, C-H arom., olef.), 1623(m, C=C, arom.), 1441, 1317 (s, C=C arom.), 736(s, C-H arom.).

UV/Vis.($CHCl_2$): $_{max}$ (ε)=228 (36000), 258 (17000), 372 (16000), 392 nm(20300).

MS(70 eV) : *m*/*z*(%) : 354(100)[M^+].

7.3.3.2 Attempted Diels-Alder using ultrasound

To a solution of TDDA (100mg, 0.28 mmol) in toluene (20 mL) was added anthracene (149.5 mg, 0.84 mmol). The flask was placed in ultrasonic bath and sonificated for 10 hours. Unreacted anthracene and bianthryl are the only species in the reaction mixture.

7.3.3.3 Solid phase reaction under microwave irradiation

The solid mixture of TDDA (100mg, 0.28 mmol) and anthracene (149.5 mg, 0.84 mmol) was irradiated with 700 W microwave power for 5 min. Unreacted anthracene and bianthryl are the only species in the reaction mixture.

7.3.3.4 Attempted high-pressure Diels-Alder reaction

To a solution of TDDA (100mg, 0.28 mmol) in xylene (20 mL), anthracene (149.5 mg, 0.84 mmol) was added and the mixture was kept, under 12 Kbar at 120° C for 3d. Again there was no addition product monitored.

7.3.3.5 Attempted solid phase Diels-Alder reaction

The solid mixture of TDDA (100mg, 0.28 mmol) and anthracene (149.5 mg, 0.84 mmol) was heated at 240° C for 30 min. the dark solid was dissolved in dichloromethane and passed through a silica gel column. A mixture of products was observed.

MS(70 eV) : *m*/*z* : 354, 530, 706, 882, 1058, 1232, 1410.

7.3.4 Solid support reactions

7.3.4.1 Addition of toluene to TDDA in the presence of Montmorillonite k10

To a solution of TDDA (100mg, 0.28 mmol) in toluene (70 mL) was added Montmorillonite K10 (1.2g) at room temperature. Silica gel flash chromatography with 90/10 hexane/dichloromethane as the mobile phase resulted in compound **10** (99.4 mg, 80%). A single crystal was obtained in acetonitrile/CS_2 solution.

^{1}H-NMR (500 MHz, $CDCl_3$/TMS): δ=7.9 (d, 2H, added toluene ring), 7.55 (d, 2H, added toluene ring), 7.3 (d, 2H, CH, arom.), 7.17 (d, 2H, CH, arom.), 7.05 (d, 2H, CH, arom.), 7.0 (d, 2H, CH, arom.) , 6.8 (m, 6H, CH, arom.), 6.70 (dd, 2H, CH, arom.), 5.05 (s, 1H, CH aliph.), 2.6 (s, 1H, CH_3), 2.56 (s, 1H, CH_3).

^{13}C-NMR (125.8 MHz, $CDCl_3$/TMS): δ=155.12 (C_q), 153.86 (C_q), 147.12(C_q), 146.92 (C_q), 138.41 (C_q), 137.02 (C_q), 130.47 (CH, arom.), 129.70 (CH, arom.),.129.62 (CH, arom.), 128.79 (CH, arom.), 128.11 (CH, arom.), 126.93 (CH, arom.), 125.51 (CH, arom.), 125.47 (CH, arom.), 125.39 (CH, arom.), 125.35 (CH, arom.), 12.98 (CH, arom.), 124.39 (CH, arom.), 124.08 (CH, arom.), 122.46 (CH, arom.), 122.05 (CH, arom.), 121.26 (CH, arom.), 98.12 (C_q), 96.10 (C_q), 66.13 (C_q), 50.28 (CH, aliph.), 21.80 (CH, aliph.), 21.30 (CH, aliph.).

MS(70 eV) : *m*/*z*(%) : 444(100)[M^+].

7.3.4.2 Addition of anthracene to TDDA in the presence of Montmorillonite k10

To a solution of TDDA (100mg, 0.28 mmol) in hexane (80 mL) was added anthracene (149.5 mg, 0.84 mmol) and Montmorillonite K10 (1.2g) at room temperature. After 4 h the silica gel flash chromatography with 90/10 hexane/dichloromethane as the mobile phase furnished compound **12** (96.5 mg, 65%).

^{1}H-NMR (500MHz, $CDCl_3$/TMS): δ=8.65 (s, 1H, added anthracene ring[AAR]), 8.62 (d, 2H,AAR), 8.20 (dd, 2H, AAR), 8.07 (dd, 4H, AAR), 7.53 (dd, 2H, AAR), 7.27 (dd, 2H) , 7.07 (dd, 4H), 6.80 (m, 6H), 6.73 (t, 2H), 5.07 (s, 1H, CH aliph).

^{13}C-NMR (125.8 MHz, $CDCl_3$/TMS): δ=154.61 (C_q), 153.39 (C_q), 146.82(C_q), 146.50 (C_q), 133.60 (C_q), 132.02 (C_q),.128.61 (CH, arom), 128.50 (CH, arom), 128.30 (CH, arom.), 128.21 (CH, arom.), 127.57 (CH, arom.), 126.37 (CH, arom.), 126.33 (CH, arom.),

125.72 (CH, arom.), 125.58 (CH, arom.), 125.51 (CH, arom.), 125.11 (CH, arom.), 124.539 (CH, arom.), 124.16 (CH, arom.), 122.59 (CH, arom.), 122.16 (CH, arom.), 121.52 (CH, arom.), 98.12 (C_q), 96.10 (C_q), 66.13 (C_q), 50.40 (CH, aliph.).

MS(70 eV) : *m*/*z*(%) : 530(100)[M^+].

7.3.4 Step by step synthesis of the trimer

7.3.4.1 Synthesis of the semitrimer 14

A mixture of tetrabromide **13** (422mg, 1 mmol), sodium iodide (2g), TDDA (200mg, 0.57mmol) and dry dimethylformamide (10 mL) was stirred at 60-70° C for 24 hours. The reaction mixture was poured into water (150 mL) containing sodium bisulfite (2g). The brown precipitate was separated by silica gel flash chromatography with 80/20 hexane/dichloromethane as the mobile phase. The semitrimer was obtained as a white powder (155mg, 60%). Colourless single crystals of the semitrimer were obtained mixture of acteonitrille/CS_2.

^{1}H-NMR (500 MHz, $CDCl_3$/TMS): δ=7.35 (dd, 4H, CH arom.), 7.45 (dd, 2H, CH arom.), 7.18 (dd, 4H, CH arom.), 7.06 (m, 6H,CH arom.), 6.8(dd, 4H, CH arom.), 6.35 (s, 2H, CH olefinic).

^{13}C-NMR (125.8 MHz, $CDCl_3$/TMS): δ=141.80 (C_q, C=C bridgehead), 141.04 (C_q, CR_2=CHR), 140.40 (C_q), 139.90 (C_q), 137.46 (C_q), 137.03 (C_q),.135.25 (C_q), 129.20 (CH, olefinic), 129.02 (CH, arom.), 126.67 (CH, arom.), 126.54 (CH, arom.), 126.40 (CH, arom.), 126.08 (CH, arom.), 125.49 (CH, arom.), 125.32 (CH, arom.), 125.13 (CH, arom.), 124.90 (CH, arom.), 121.90 (CH, arom.)

MS(70 eV) : *m*/*z*(%) : 454(100)[M^+].

7.3.4.2 Complexation of the semitrimer

To a solution of the semitrimer (100mg, 0.22 mmol) in THF (20mL) was added silver(I)triflate (56 mg, 0.22 mmol) at room temperature under a flow of nitrogen. After 2 hours, half of the THF was evaporated and the solution was allowed to stand for crystallization. A silica gel column used for separation of the products because crystallization was not successful. Compound **17** (9.4 mg, 10%) and unreacted semitrimer and some unseparated minor product mixture was obtained.

Data for **17**:

^{1}H-NMR (500 MHz, $CDCl_3$/TMS): δ=8.00 (d, 2H, CH arom.), 7.83 (dd, 2H, CH arom.), 7.63 (dd, 2H, CH arom.), 7.46 (dd, 2H,CH arom.), 7.42 (dd, 2H,CH arom.), 7.20 (dd, 2H, CH arom.), 7.17 (dd, 2H, CH arom.), 7.01 (dd, 2H,CH arom.), 6.92 (dd, 2H,CH arom.), 6.8 (dd, 1H,CH arom.), 6.74 (dd, 2H,CH arom.), 6.6 (dd, 2H,olefinic.), 4.40 (s, 1H,CH aliphatic.), 3.98 (dd, 2H,CH aliphatic.).

^{13}C-NMR (125.8 MHz, $CDCl_3$/TMS): δ=150.93, 148.72, 146.72, 146.47, 141.19, 139.28, 138.43 (C_q), 132.13, 131.56, (CH, olefinic), 126.72, 126.53, 125.14, 124.8, 124.22, 124.14, 123.97, 123.814, 123.746, 123.70, 123.59, 123.47, 123.08, 122.72, 121.38, 120,95, 118,43 (CH, arom.), 63,80(C_q, aliphatic), 58.17(CH, aliphatic.), 55.75 (CH_2, aliphatic.)

MS (70 eV) : *m*/*z*(%) : 470(100)[M^+].

7.3.4.3 Epoxidation of the semitrimer

A solution of the semitrimer (100 mg, 0.22 mmol) in THF was stirred for 12 hours under air. After a silica gel flash chromatography with 80/20 hexane/dichloromethane as a mobile phase the compounds **18** (41.4 mg, 40%) and **19** (15.51mg, 15%) was separated.

Data for **18**:

^{1}H-NMR (500 MHz, $CDCl_3$/TMS): δ=7.72 (d, 1H, CH arom.), 7.68 (dd, 2H, CH arom.), 7.58 (dd, 2H, CH arom.), 7.43 (m, 4H,CH arom.), 7.32 (dd, 1H,CH arom.), 7.26 (dd, 2H, CH arom.), 7.17 (m, 4H, CH arom.), 6.98 (m, 2H,CH arom.), 6.85 (m, 2H,CH arom.), 6.6 (s, 1H,CH olefinic.), 4 (s, 1H,CH epoxid.).

^{13}C-NMR (125.8 MHz, $CDCl_3$/TMS): δ=143.66, 143.50 (C_q, C=C bridgehead), 141.15, 141.05 (C_q, CR_2=CHR), 141.01 (C_q), 139.93,139.44 (C_q), 138.10,137.81 (C_q), 137.66,137.32 (C_q), 136.13,136.08 (C_q),.135.63,135.28 (C_q), 129.54(CH, olefinic), 127.62,127.60 (CH, arom.), 127.51,127.48 (CH, arom.), 127.29,127.22 (CH, arom.), 127.14,126.94 (CH, arom.), 126.82,126.77 (CH, arom.), 126.16,126.12 (CH, arom.), 125.99, 125.88 (CH, arom.), 125.67,125.63 (CH, arom.), 124.58,124.37 (CH, arom.) 73.79 (C_q, epoxid.), 70.06 (CH, epoxid)

MS(70 eV) : *m*/*z*(%) : 470(100)[M^+].

Data for **19**:

^{1}H-NMR (500 MHz, $CDCl_3$/TMS): δ=7.55 (dd, 4H, CH arom.), 7.33 (m, 6H, CH arom.), 7.15 (m, 6H, CH arom.), 6.85 (dt, 4H, CH arom.), 6.55 (s, 2H, CH olefinic).

^{13}C-NMR (125.8 MHz, $CDCl_3$/TMS): δ=141.39 (C_q, CR_2=CHR), 139.56 (C_q), 137.74 (C_q), 135.58 (C_q), 134.74 (C_q),.131.56 (C_q), 130.06 (CH, olefinic), 129.54 (CH, arom.), 129.22 (CH, arom.), 126.68 (CH, arom.), 126.56 (CH, arom.), 126.41 (CH, arom.), 125.49 (CH, arom.), 125.32 (CH, arom.), 123.83 (CH, arom.), 123.54 (CH, arom.), 122.22 (CH, arom.) 73.79 (C_q, epoxid.), 72.50 (C_q, epoxid.) .

MS(70 eV) : *m*/*z*(%) : 470(100)[M^+].

7.3.4.4 Attempted conversion of the semitrimer to the trimer by Heck reaction

To a suspension of n-butylammonium chloride (122.1 mg, 0.44 mmol), sodium hydrogen carbonate (92.4 mg, 1.1 mmol) and crushed 4Å molecular sieve (200 mg) in acetonitrille (10 mL) was added 1,2-diiodobenzene (73 mg, 0.22 mmol) and the semitrimer (100mg, 0.22 mmol) and was stirred for 30 min before addition of $Pd(OAc)_2$ (4.5 mg, 0.02 mmol). After 4 hours stirring at 50° C, the reaction mixture was diluted with water and ether and ether layer was separated and dried. There was no any indication of an addition product after chromatography analysis.

7.3.4.4 Attempted bromination of the semitrimer

To a solution of the semitrimer (50mg, 0.11 mmol) in dichloromethane (20 mL) under nitrogen gas flow a solution of bromine (100mg, 0.62 mmol) in dichloromethane (5 mL) was added dropwise. After 1 h at room temperature the solution was diluted with a solution of sodium bicarbonate. The organic layer was separated and dried. There was no evidence of a bromination product after chromatography analysis.

7.3.4.5 Irradiation of the semitrimer and TDDA

A solution of the semitrimer (300 mg, 0.66 mmol) and TDDA (233 mg, 0.66 mmol) in benzene (80 mL) was irradiated with a 700 W high-pressure mercury lamp in a quartz photoreactor with FC-40 [perfluoro compound](40 mL) and a nitrogen gas flow for 10 hours. The two phases were separated and the benzene phase was evaporated and the residue was separated by a column chromatography which furnished tetramer , bianthryl and unreacted semitrimer.

7.3.5 Photochemically induced metathesis reaction of tetramer

7.3.5.1 Synthesis of the tetramer

Method A: A suspension of TDDA (600 mg, 1.7 mmol) in benzene (60 mL) in a quartz photoreactor and FC-40 compound (40ml) with nitrogen flow was irradiated with a 700 W high-pressure mercury lamp for 40 hours. The benzene phase was separated and evaporated. After chromatography on a flash column filled with silica gel 2/1 hexane/dichloromethane, the tetramer crystallized in (1:1) pentane/dichloromethane (210 mg, 35%)

Method B: A suspension of TDDA (1g, 2.84 mmol) in benzene (120 ml) under nitrogen gas flow and a 250 W ultrasonic probe (50 % output) was irradiated with a 700 W high-pressure mercury lamp for 3 hours. The work up procedure was the same as in method A (410 mg, 41%).

^{1}H-NMR (400 MHz, $AsCl_3$: CD_2Cl_2=2:1): δ=7.93 (dd, ^{3}J=5.7 Hz, ^{4}J=3.4 Hz, 16H, CH arom.), 7.15 (dd, ^{3}J=5.7 Hz, ^{4}J=3.4 Hz, 16H, CH arom.).

^{13}C-NMR (100.6 MHz, $AsCl_3$: CD_2Cl_2=2:1): δ=139.0 (s, C=C), 134.2 (s), 129.3(d), 125.8(d).

IR (KBr, cm^{-1}): $\tilde{\upsilon}$= 3058,3023 (m, C-H arom.), 1632(m), 1447 (s, C=C arom.), 764(s, C-H arom.), 750 (s), 632 (s) cm^{-1}.

UV/Vis.($CHCl_2$): λ_{max} (ε)=231 (21000), 275 (27000), 300 (15000) nm.

MS(70 eV) : *m*/*z*(%) : 704 (100)[M^+].

7.3.5.2 Irradiation of the tetramer in micelles

A colloidal solution of tetramer (20 mg, 0.03 mmol) in 5% aq. sodium dodecyl sulfate (100 mL) was irradiated in a quartz photoreactor under a nitrogen flow with a 700 W

high-pressure mercury lamp for 48 hours. There was no evidence of a reaction of the tetramer after analysis of reaction mixture.

7.3.5.3 Irradiation of tetramer in dodecane

A suspension of the tetramer (200 mg, 0.28 mmol) in dodecane (50 ml) under nitrogen gas flow and a 250 W ultrasonic probe (50 % output) was irradiated with a 700 W high-pressure mercury lamp for 10 hours. The solvent was evaporated and the residue separated on a silica gel column with hexane as a mobile phase and then the column was washed with dichloromethane. Gel permeation chromatography with dichloromethane resulted in a separated mixture with lower R_f. The compounds could not be identified by spectroscopy.

7.3.5.4 Solid phase irradiation of the tetramer with a laser

A compressed pill of tetramer (100 mg, 0.14 mmol) was produced with a conventional IR press and then irradiated with a laser (254 nm, 3 mJ) in a normal atmosphere. The pill was dissolved in dichloromethane and monitored. There was not any evidence of addition product.

7.3.6 Synthesis of Möbius aromatic compounds

7.3.6.1 Irradiation of TDDA and cyclooctatetraene

A suspension of TDDA (300 mg, 0.82 mmol) and cyclooctatetraene (426 mg, 4.1 mmol) and naphthalene (30 mg, 0.23 mmol) in benzene (100 mL) in a quartz photoreactor was irradiated with a with a 700 W high-pressure mercury lamp for 10 hours. The solvent was evaporated. According to a HPLC analysis the only new product was bianthryl.

7.3.6.2 Thermal reaction of TDDA and cyclooctatetraene

A solution of TDDA (100 mg, 0.28 mmol) and cyclooctatetraene (426 mg, 4.1 mmol) in toluene (100 mL) was stirred at 50° C for 50 min. A mixture of products was obtained. Further separation was not successful.

MS of mixture (70 eV) : *m*/*z* : 456.

7.3.6.3 Synthesis of the *syn*-tricyclooctadiene

To the mercury (650 g) was added sodium (6.5 g) in small portions under argon atmosphere at room temperature. The sodium amalgam was cooled and ether (250 mL) was added. The mixture was sonified with ultrasonic probe (250 W, 50% output) and ultrasonic bath for 30 min at 5° C under argon flow and 3,4-*cis*-dichlorocyclobutene (5mL, Fluka) was added. The mixture was sonified at 5-10° C for 2-7 d. (the reaction was monitored with GC at 30° C, the reaction was allowed to run till all 3,4-*cis*-dichlorocyclobutene was converted to the tricyclooctadiene). The mixture was filtrated with celite and the ether evaporated carefully first at 30° C (800 mbar) and then 0° C (200 mbar). A flow of argon was passed through the yellowish liquid if ether was detected in the NMR spectrum. The *syn*-tricyclooctadiene (1.5 g, 68%) was stored in benzene (10 mL).

^{1}H-NMR (500 MHz, $CDCl_3$/TMS): δ=6.03 (s, 4H), 3.13 (s, 4H)

7.3.6.4 Irradiation of TDDA and TCOD with 700 W high-pressure mercury lamp

A suspension of TDDA (100 mg, 0.28 mmol), TCOD (300 mg, 2.88 mmol) and naphthalene (20 mg, 0.15 mmol) was irradiated with 700 w high-pressure mercury lamp in a quartz photoreactor with argon gas flow. After 10-20 min irradiation, the solvent was evaporated and the residue was dissolved in dichloromethane and passed through a short column of silica gel and then preparative HPLC was used (90/10 heptane/dichloromethane). Three isomers were successfully separated, C_s

closed (12mg, 9.4%), C_2 closed (8 mg, 6.3%), ladder-shaped isomer (2mg, 1.6%). the single crystal of and have obtained in heptane/dichloromethane mixture.

Data for C_s closed **35**:

^{1}H-NMR (500MHz, $CDCl_3$/TMS): δ=7.61 (d, 2H), 7.26 (d, 2H), 7.21 (dd, 2H), 7.16 (d, 2H), 7.13 (dd, 2H), 7.01 (d, 2H), 6.91 (dd, 2H), 6.86 (dd, 2H), 5.92 (dd, 2H), 5.67 (dd, 2H), 5.14 (dd, 2H), 3.40 (dd, 2H)

^{13}C-NMR (125.8 MHz, $CDCl_3$/TMS): δ=141.40 (C_q, C=C bridgehead), 141.08 (C_q, CR_2=CHR), 140.27 (C_q), 138.58 (C_q), 137.6 (C_q), 134.47 (C_q),.131.13 (CH, olefinic), 127.42 (CH, arom.), 127.33 (CH, cyclohexadiene), 127.28 (CH, arom.), 125.21 (CH, arom.), 125.16 (CH, arom.), 125.12 (CH, arom.), 124.90 (CH, arom.), 124.86 (CH, arom.), 124.68 (CH, arom.), 123.15 (CH, cyclohexadiene), 40.75 (CH, aliphatic.)

MS(70 eV): *m*/*z*(%) : 456 (100)[M^+].

Data for C_2 closed **36**:

^{1}H-NMR (500MHz, $CDCl_3$/TMS): δ=7.53 (m, 4H), 7.26 (d, 2H), 7.15 (d, 2H), 7.11 (d, 2H), 7.06 (dd, 2H), 7.02 (dd, 2H), 6.99 (dd, 2H), 5.92 (dd, 2H), 5.66 (dd, 2H), 5.54 (dd, 2H), 3.67 (dd, 2H).

^{13}C-NMR (125.8 MHz, $CDCl_3$/TMS): δ=140.68 (C_q, C=C bridgehead), 140.48 (C_q, CR_2=CHR), 140.40 (C_q), 140.05 (C_q), 137.17 (C_q), 134.88 (C_q),.129.28 (CH, olefinic), 127.96 (CH, cyclohexadiene), 127.18 (CH, arom.), 126.52 (CH, arom.), 126.36 (CH, arom.), 125.89 (CH, arom.), 125.50 (CH, arom.), 125.03 (CH, arom.), 124.48 (CH, arom.), 122.38 (CH, arom.), 121.86 (CH, cyclohexadiene), 36.99 (CH, aliphatic.)

MS(70 eV) : *m*/*z*(%) : 456 (100)[M^+].

Data for ladder-shaped isomer **37**:

^{1}H-NMR (500MHz, $CDCl_3$/TMS): δ=7.85 (dd, 2H), 7.45 (dd, 2H), 7.40 (dd, 2H), 7.33 (dd, 2H), 7.22 (dd, 2H), 6.10 (dd, 2H), 7.02 (dd, 2H), 6.67 (dd, 2H), 6.50 (s, 2H, olefinic), 4.31 (dd, 2H), 3.27 (dd, 2H), 2.86 (dd, 2H).

^{13}C-NMR (125.8 MHz, $CDCl_3$/TMS): δ=144.20 (C_q, C=C bridgehead), 143.38 (C_q, CR_2=CHR), 138.11 (C_q), 137.78 (C_q), 137.56 (C_q), 134.47 (C_q),.129.27 (CH, olefinic), 129.12 (CH, arom.), 128.78 (CH, arom), 128.45 (CH, arom.), 128.31 (CH, arom.), 128.08 (CH, arom.), 126.90 (CH, arom.), 126.7 (CH, arom.), 125.37 (CH, arom.), 125.12 (CH, arom.), 124.12 (CH, arom), 121.60 (CH, arom), 46.76 (CH, aliphatic.), 39.10 (CH, aliphatic.), 29.71 (CH, aliphatic.).

MS(70 eV) : *m*/*z*(%) : 456 (100)[M^+].

7.3.6.5 Irradiation of TDDA and TCOD with 15 W low-pressure mercury lamp

The solution of TDDA (100mg, 0.28 mmol), TCOD (300mg, 2.88 mmol) and naphthalene (20 mg, 0.15 mmol) was irradiated with 15 w high-pressure mercury lamp in a quartz photoreactor with argon gas flow. After 24 hours irradiation, the solvent evaporated and the residue solid solved in dichloromethane and passed through short column of silica gel and then preparative HPLC was used (95/ 5 heptane/dichloromethane). Closed ring compound and two compound separated .a mixture of cs closed one and two opened ring isomer have very close R_f which separation are not possible. Diels-Alder reaction of this mixture

The single crystal of and have obtained in heptane/dichloromethane mixture.

Data for C_s hückel opened **38**

^{1}H NMR (500 MHz, $CDCl_3$/TMS): δ = 7.733 (ddd, $^3J_{8\text{-H, }7\text{-H}}$ = 7.5 Hz, $^4J_{8\text{-H, }6\text{-H}}$ = 1.3, $^5J_{8\text{-H, }5\text{-H}}$ = 0.6, 2H, 8-H); 7.609 (ddd, $^3J_{1\text{-H, }2\text{-H}}$ = 7.3 Hz, $^4J_{1\text{-H, }3\text{-H}}$ = 1.5, $^5J_{1\text{-H, }4\text{-H}}$ = 0.6, 2H, 1-H); 7.332 (ddd, $^3J_{5\text{-H, }6\text{-H}}$ = 7.3 Hz, $^4J_{5\text{-H, }7\text{-H}}$ = 1.5 Hz, 2H, 5-H); 7.114 (m, 2H, 4-H); 7.087 (ddd, $^3J_{7\text{-H, }8\text{-H}}$ = 7.5 Hz, $^3J_{7\text{-H, }6\text{-H}}$ = 7.3, $^4J_{7\text{-H, }5\text{H}}$ = 1.5, 2H, 7-H); 7.043 (ddd, $^3J_{6\text{-H, }7\text{-H}}$ = 7.3 Hz, $^3J_{6\text{-H, }5\text{-H}}$ = 7.5, $^4J_{6\text{-H, }8\text{-H}}$ = 1.3, 2H, 6-H); 7.005 (ddd, $^3J_{2\text{-H, }1\text{-H}}$ = 7.3 Hz, $^3J_{2\text{-H, }3\text{-H}}$ = 7.3, $^4J_{2\text{-H, }4\text{-H}}$ = 1.5, 2H, 2-H); 6.978 (ddd, $^3J_{3\text{-H, }2\text{-H}}$ = 7.3 Hz, $^3J_{3\text{-H, }4\text{-H}}$ = 7.5, $^4J_{3\text{-H, }1\text{-H,}}$ = 1.5, 2H, 3-H); 6.624 (dd, $^3J_{12\text{-H, }11\text{-H}}$ = 11.0 Hz, $^3J_{12\text{-H, }13\text{-H}}$ = 10.8, 2H, 12-H); 6.260 (dd, $^3J_{11\text{-H, }12\text{-H}}$ = 11.0 Hz, $^4J_{11\text{-H, }13\text{-H}}$ = 1.3, 2H, 11-H); 6.238 (ddd, $^3J_{14\text{-H, }14'\text{-H}}$ = 11.0 Hz, $^3J_{14\text{-H, }13\text{-H}}$ = 2.4, $^4J_{14\text{-H, }13'\text{-H}}$ = 1.1, 2H, 14-H); 5.875 (dddd, $^3J_{13\text{-H, }12\text{-H}}$ = 10.8 Hz, $^3J_{13\text{-H, }14\text{-H}}$ = 2.4, $^4J_{13\text{-H, }14'\text{-H}}$ = 1.1, $^4J_{13\text{-H, }11\text{-H}}$ = 0.9, 2H, 13-H).

^{13}C NMR (125.8 MHz, $CDCl_3$/TMS): δ = 139.76 (9-C)*, 138.19 (10-C)*, 137.93 (10a-C)*, 137.65 (9b-C)*, 137.47 (9a-C)*, 136.31 (10b-C)*, 131.52 (13-C), 129.83 (14-C), 128.45 (8-C), 128.02 (12-C), 127.94 (1-C), 126.44 (3-C), 126.06 (6-C), 125.41 (5-C), 125.23 (7-C), 124.60 (2-C), 123.29 (4-C), 122.00 (11). *assignement according to a CSGT B3LYP/6-31G* calculation.

UV/Vis (CH_2Cl_2): λ_{max} (ε) = 259 (17027), 299 (16334) nm.

MS (70 eV): *m*/*z* (%): 456 (100) [M^+].

Data for C_1 Möbius opened **39**

^{1}H-NMR (500MHz, $CDCl_3$/TMS): δ=7.83 (dd, 4H), 7.44 (dd, 2H), 7.20 (dd, 4H), 7.09 (dd, 4H), 6.72 (dd, 2H, olefinic), 6.41 (dd, 2H, olefinic), 6.22 (dd, 4H, olefinic).

^{13}C-NMR (125.8 MHz, $CDCl_3$/TMS): δ=139.81 (C_q, C=C bridgehead), 138.09 (C_q, CR_2=CHR), 136.98 (C_q), 136.52 (C_q), 135.90 (C_q), 135.5 (C_q), 132.97 (CH, olefinic), 132.72 (CH, olefinic), 128.72 (CH, arom.), 128.65 (CH, arom.), 127.75 (CH, olefinic), 126.78 (CH, arom.), 126.14 (CH, arom.), 125.01 (CH, arom.), 124.81 (CH, arom.), 124.77 (CH, arom), 123.97 (CH, arom) 123.84 (CH, olefinic).

UV/Vis.($CHCl_2$): $_{max}$ (ε)=250 (19528), 300 (15199) nm.

MS(70 eV) : *m*/*z*(%) : 456 (100)[M^+].

Data for C_2 Möbius **40**

^{1}H NMR (500 MHz, $CDCl_3$/TMS): δ = 7.709 (ddd, $^3J_{1\text{-H, }2\text{-H}}$ = 7.5 Hz, $^4J_{1\text{-H, }3\text{-H}}$ = 1.3, $^5J_{1\text{-H, }4\text{-H}}$ = 0.5, 2H, 1-H); 7.516* (m, 2H, 8-H); 7.209* (m, 2H, 4-H); 7.201* (m, 2H, 5-H); 7.184 (ddd, $^3J_{2\text{-H, }1\text{-H}}$ = 7.5 Hz, $^4J_{2\text{-H, }4\text{-H}}$ = 1.3, 2H, 2-H); 7.098 (ddd, $^3J_{3\text{-H, }2\text{-H}}$ = 7.5 Hz, $^3J_{3\text{-H, }4\text{-H}}$ = 7.5, $^4J_{3\text{-H, }1\text{-H}}$ = 1.3, 2H, 3-H); 7.009 (ddd, $^3J_{7\text{-H, }6\text{-H}}$ = 7.4 Hz, $^3J_{7\text{-H, }8\text{-H}}$ = 7.4, $^4J_{7\text{-H, }5\text{-H}}$ = 2.0, 2H, 7-H_A); 7.003 (ddd, $^3J_{6\text{-H, }7\text{-H}}$ = 7.4 Hz, $^3J_{6\text{-H, }7\text{-H}}$ = 7.4, $^4J_{6\text{-H, }8\text{-H,}}$ = 2.0, 2H, 6-H_B); 6.486 (dd, $^3J_{11\text{-H, }12\text{-H}}$ = 12.5 Hz, $^4J_{11\text{-H, }13\text{-H}}$ = 1.5, 2H, 11-H); 6.118 (dd, $^3J_{12\text{-H, }11\text{-H}}$ = 12.5 Hz, $^3J_{12\text{-H, }13\text{-H}}$ = 11.9, 2H, 12-H); 5.940 (dd, $^3J_{14\text{-H, }13\text{-H}}$ = 4.7 Hz, $^4J_{14\text{-H, }14'\text{-H}}$ = 1.9, 2H, 14-H); 5.690 (dddd, $^3J_{13\text{-H, }12\text{-H}}$ = 11.9 Hz, $^3J_{13\text{-H, }14\text{-H}}$ = 4.7, $^4J_{13\text{-H, }14'\text{-H}}$ = 1.9, ^nJ = 0.9, 2H, 13-H). *chemical shifts were calculated from HSQC spectra.

^{13}C NMR (125.8 MHz, $CDCl_3$/TMS): δ = 140.67 (10-C), 139.92 (9-C), 139.36 (10b-C), 138.93 (9a-C), 138.34 (9b-C), 135.91 (10a-C), 128.09 (1-C), 127.79 (12-C), 127.04 (14-C), 126.42 (6-C), 126.27 (8-C), 126.15 (4-C), 125.97 (3-C), 125.41 (2-C), 125.24 (7-C), 124.89 (11-C), 122.05 (5-C).

UV/Vis (CH_2Cl_2): λ_{max} (ε) = 253 (26231), 312 (17251), 400 (broad, 2946) nm.

MS (70 eV): *m*/*z* (%): 456 (100) [M^+].

Data for C_1 **41**

^{1}H-NMR (500MHz, $CDCl_3$/TMS): δ=7.75 (dd, 2H), 7.37 (dd, 2H), 7.20 (dd, 2H), 7.15 (m, 2H), 7.12 (m, 2H), 6.94 (dd, 2H), 6.80 (t, 2H), 6.72 (dd, 1H, olefinic), 6.25 (d, 1H, olefinic), 6.15 (t, 1H, olefinic), 5.97 (d, 1H, olefinic), 5.90 (dd, 1H, olefinic), 5.85 (dd, 1H, olefinic), 5.78 (dd, 1H, olefinic), 5.72 (dd, 1H, olefinic).

MS(70 eV) : *m*/*z*(%) : 456 (100)[M^+].

Data for C_2 **42**

^{1}H-NMR (500MHz, $CDCl_3$/TMS): δ=7.75 (dd, 2H), 7.62 (dd, 2H), 7.42 (dd, 2H), 7.22 (m, 2H), 7.10 (m, 2H), 6.94 (dd, 2H), 6.80 (t, 2H), 6.65 (s, 2H, olefinic), 6.35 (d, 2H, olefinic), 6.20 (d, 2H, olefinic), 5.98 (dd, 2H, olefinic).

MS(70 eV) : *m*/*z*(%) : 456 (100)[M^+].

7.4 X-ray structure data

7.4.1 X-ray structure of compound 10

Crystal data:

Formula sum $C_{35}H_{24}$

Formula weight 444.19

Crystal system triclinic

Space group *P* -1 (no. 2)

Unit cell dimensions *a* = 8.053(2) Å

b = 8.793(2) Å

c = 20.608(4) Å

α = 89.68(3) °

β = 79.39(3) °

γ = 65.28(3) °

Cell volume 1298.69(2091) Å^3

Density, calculated 1.242 g/cm^3

Pearson code aP130

Formula typeNO27P37

Wyckoff sequence i^{65}

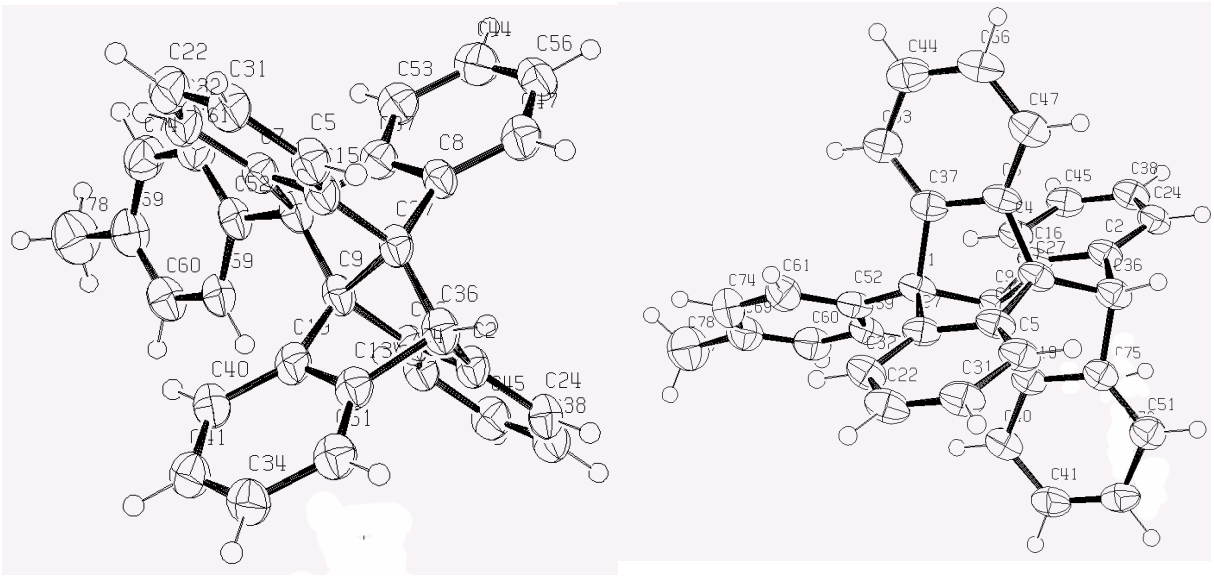

Bond distances (Angstroms)

Atom	A	B	Dist						
C1	C52	1.505		C1	C9	1.554		C1	C37	1.561
C1	C7	1.565		C2	C24	1.393		C2	C16	1.405
C2	C36	1.545		C4	H4	0.950		C4	C16	1.382
C4	C45	1.402		C5	H5	0.950		C5	C15	1.381
C5	C31	1.413		C7	C32	1.387		C7	C15	1.398
C7	C1	1.565		C8	C47	1.395		C8	C37	1.404
C8	C27	1.516		C9	C16	1.532		C9	C19	1.537
C9	C1	1.554		C9	C27	1.575		C13	C51	1.374
C13	C19	1.398		C13	C36	1.550		C15	C5	1.381
C15	C7	1.398		C15	C27	1.527		C16	C4	1.382
C16	C2	1.405		C16	C9	1.532		C19	C40	1.387
C19	C13	1.398		C19	C9	1.537		C22	H22	0.950
C22	C31	1.355		C22	C32	1.409		C24	H24	0.950
C24	C2	1.393		C24	C38	1.398		C27	C8	1.516
C27	C15	1.527		C27	C36	1.536		C27	C9	1.575
C31	H31	0.950		C31	C22	1.355		C31	C5	1.413

C32	H32	0.950	C32	C7	1.387	C32	C22	1.409
C34	H34	0.950	C34	C41	1.365	C34	C51	1.416
C36	H36	1.000	C36	C27	1.536	C36	C2	1.545
C36	C13	1.550	C37	C53	1.379	C37	C8	1.404
C37	C1	1.561	C38	H38	0.950	C38	C45	1.376
C38	C24	1.398	C40	H40	0.950	C40	C19	1.387
C40	C41	1.402	C41	H41	0.950	C41	C34	1.365
C41	C40	1.402	C44	H44	0.950	C44	C56	1.388
C44	C53	1.405	C45	H45	0.950	C45	C38	1.376
C45	C4	1.402	C47	H47	0.950	C47	C56	1.394
C47	C8	1.395	C51	H51	0.950	C51	C13	1.374
C51	C34	1.416	C52	C61	1.384	C52	C59	1.405
C52	C1	1.505	C53	H53	0.950	C53	C37	1.379
C53	C44	1.405	C56	H56	0.950	C56	C44	1.388
C56	C47	1.394	C59	H59	0.950	C59	C60	1.381
C59	C52	1.405	C60	H60	0.950	C60	C69	1.365
C60	C59	1.381	C61	H61	0.950	C61	C52	1.384
C61	C74	1.394	C69	C60	1.365	C69	C74	1.382
C69	C78	1.508	C72	N68	1.135	C72	C75	1.443
C74	H74	0.950	C74	C69	1.382	C74	C61	1.394
C75	H75a	0.980	C75	H75b	0.980	C75	H75c	0.980
C75	C72	1.443	C78	H78a	0.980	C78	H78b	0.980
C78	H78c	0.980	C78	C69	1.508	H4	C4	0.950
H5	C5	0.950	H22	C22	0.950	H24	C24	0.950
H31	C31	0.950	H32	C32	0.950	H34	C34	0.950
H36	C36	1.000	H38	C38	0.950	H40	C40	0.950
H41	C41	0.950	H44	C44	0.950	H45	C45	0.950
H47	C47	0.950	H51	C51	0.950	H53	C53	0.950
H56	C56	0.950	H59	C59	0.950	H60	C60	0.950
H61	C61	0.950	H74	C74	0.950	H75a	C75	0.980
H75b	C75	0.980	H75c	C75	0.980	H78a	C78	0.980
H78b	C78	0.980	H78c	C78	0.980			

Bond angles (degrees)

C52	C1	C9	120.74	C52	C1	C37	117.56	C52	C1	C7	116.72
C9	C1	C37	97.99	C9	C1	C7	97.46	C37	C1	C7	102.58
C24	C2	C16	120.91	C24	C2	C36	130.85	C16	C2	C36	108.17
H4	C4	C16	120.83	H4	C4	C45	120.84	C16	C4	C45	118.33
H5	C5	C15	121.36	H5	C5	C31	121.36	C15	C5	C31	117.27
C32	C7	C15	120.87	C32	C7	C1	131.29	C15	C7	C1	107.84

C47	C8	C37	120.55	C47	C8	C27	132.57	C37	C8	C27	106.84
C16	C9	C19	104.66	C16	C9	C1	125.37	C16	C9	C27	98.83
C19	C9	C1	124.84	C19	C9	C27	98.83	C1	C9	C27	95.22
C51	C13	C19	121.70	C51	C13	C36	130.72	C19	C13	C36	107.51
C5	C15	C7	121.61	C5	C15	C27	131.84	C7	C15	C27	106.47
C4	C16	C2	120.63	C4	C16	C9	133.57	C2	C16	C9	105.72
C40	C19	C13	120.61	C40	C19	C9	132.74	C13	C19	C9	106.52
H22	C22	C31	118.88	H22	C22	C32	118.89	C31	C22	C32	122.23
H24	C24	C2	121.10	H24	C24	C38	121.11	C2	C24	C38	117.79
C8	C27	C15	104.24	C8	C27	C36	126.02	C8	C27	C9	99.74
C15	C27	C36	123.91	C15	C27	C9	99.25	C36	C27	C9	95.44
H31	C31	C22	119.50	H31	C31	C5	119.50	C22	C31	C5	121.00
H32	C32	C7	121.51	H32	C32	C22	121.52	C7	C32	C22	116.97
H34	C34	C41	119.57	H34	C34	C51	119.58	C41	C34	C51	120.85
H36	C36	C27	117.85	H36	C36	C2	117.83	H36	C36	C13	117.84
C27	C36	C2	97.81	C27	C36	C13	98.80	C2	C36	C13	103.15
C53	C37	C8	121.47	C53	C37	C1	131.12	C8	C37	C1	107.41
H38	C38	C45	119.32	H38	C38	C24	119.31	C45	C38	C24	121.37
H40	C40	C19	121.15	H40	C40	C41	121.15	C19	C40	C41	117.70
H41	C41	C34	119.19	H41	C41	C40	119.20	C34	C41	C40	121.61
H44	C44	C56	119.41	H44	C44	C53	119.40	C56	C44	C53	121.20
H45	C45	C38	119.52	H45	C45	C4	119.52	C38	C45	C4	120.97
H47	C47	C56	120.96	H47	C47	C8	120.97	C56	C47	C8	118.07
H51	C51	C13	121.24	H51	C51	C34	121.24	C13	C51	C34	117.53
C61	C52	C59	116.97	C61	C52	C1	122.53	C59	C52	C1	120.49
H53	C53	C37	121.15	H53	C53	C44	121.16	C37	C53	C44	117.69
H56	C56	C44	119.50	H56	C56	C47	119.51	C44	C56	C47	120.99
H59	C59	C60	119.76	H59	C59	C52	119.77	C60	C59	C52	120.47
H60	C60	C69	118.88	H60	C60	C59	118.87	C69	C60	C59	122.24
H61	C61	C52	119.15	H61	C61	C74	119.17	C52	C61	C74	121.68
C60	C69	C74	118.17	C60	C69	C78	122.79	C74	C69	C78	119.04
H74	C74	C69	119.77	H74	C74	C61	119.77	C69	C74	C61	120.46
H75a	C75	H75b	109.47	H75a	C75	H75c	109.47	H75a	C75	C72	109.47
H75b	C75	H75c	109.48	H75b	C75	C72	109.47	H75c	C75	C72	109.47
H78a	C78	H78b	109.47	H78a	C78	H78c	109.47	H78a	C78	C69	109.47
H78b	C78	H78c	109.47	H78b	C78	C69	109.47	H78c	C78	C69	109.47

7.4.2 X-ray structure of the semitrimer 14

Formula sum C_{36} H_{22}

Formula weight 454.55

Crystal system monoclinic

Space group *P* 1 21/c 1 (no. 14)

Unit cell dimensions *a* = 16.037(1) Å

b = 21.287(2) Å

c = 16.531(1) Å

β = 148.86(2) °

Cell volume 2918.35(9660) Å^3

Density, calculated 1.301 g/cm^3

Pearson code mP268

Formula type NO2P25Q39

Wyckoff sequence e^{67}

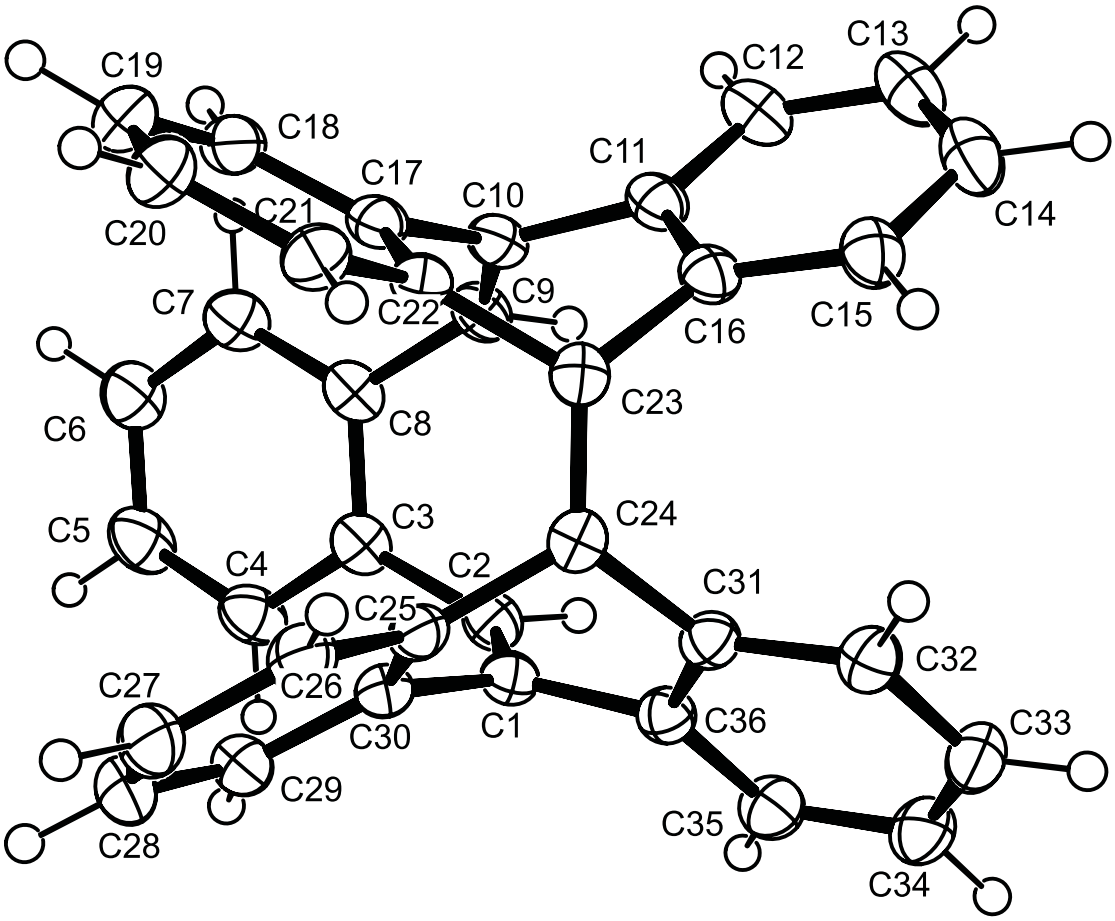

Bond distances (Angstroms)

Atom	A	B	Dist						
C1	C2	1.340		C1	C30	1.484		C1	C36	1.490
C2	H2	0.997		C2	C1	1.340		C2	C3	1.492
C3	C4	1.394		C3	C8	1.413		C3	C2	1.492
C4	H4	0.978		C4	C5	1.386		C4	C3	1.394
C5	H5	0.974		C5	C4	1.386		C5	C6	1.387
C6	H6	1.014		C6	C5	1.387		C6	C7	1.390
C7	H7	0.984		C7	C6	1.390		C7	C8	1.391
C8	C7	1.391		C8	C3	1.413		C8	C9	1.485
C9	H9	0.967		C9	C10	1.337		C9	C8	1.485
C10	C9	1.337		C10	C17	1.486		C10	C11	1.492
C11	C12	1.390		C11	C16	1.411		C11	C10	1.492
C12	H12	0.977		C12	C13	1.390		C12	C11	1.390
C13	H13	0.981		C13	C14	1.384		C13	C12	1.390
C14	H14	1.008		C14	C13	1.384		C14	C15	1.396
C15	H15	0.986		C15	C16	1.390		C15	C14	1.396
C16	C15	1.390		C16	C11	1.411		C16	C23	1.492
C17	C18	1.392		C17	C22	1.409		C17	C10	1.486
C18	H18	0.999		C18	C19	1.391		C18	C17	1.392
C19	H19	0.960		C19	C20	1.384		C19	C18	1.391
C20	H20	0.979		C20	C19	1.384		C20	C21	1.393
C21	H21	0.973		C21	C22	1.388		C21	C20	1.393
C22	C21	1.388		C22	C17	1.409		C22	C23	1.492
C23	C24	1.350		C23	C16	1.492		C23	C22	1.492
C24	C23	1.350		C24	C31	1.487		C24	C25	1.494
C25	C26	1.392		C25	C30	1.409		C25	C24	1.494
C26	H26	0.970		C26	C25	1.392		C26	C27	1.394

C27	H27	0.975	C27	C28	1.378	C27	C26	1.394
C28	H28	0.972	C28	C27	1.378	C28	C29	1.390
C29	H29	1.002	C29	C28	1.390	C29	C30	1.393
C30	C29	1.393	C30	C25	1.409	C30	C1	1.484
C31	C32	1.392	C31	C36	1.412	C31	C24	1.487
C32	H32	1.000	C32	C33	1.390	C32	C31	1.392
C33	H33	0.944	C33	C34	1.383	C33	C32	1.390
C34	H34	0.991	C34	C33	1.383	C34	C35	1.392
C35	H35	0.961	C35	C36	1.388	C35	C34	1.392
C36	C35	1.388	C36	C31	1.412	C36	C1	1.490
C37	S1	1.534	C37	S2	1.546	C38	H38c	0.940
C38	H38a	0.944	C38	H38b	0.969	C38	C39	1.422
C39	C38	1.422	H2	C2	0.997	H4	C4	0.978
H5	C5	0.974	H6	C6	1.014	H7	C7	0.984
H9	C9	0.967	H12	C12	0.977	H13	C13	0.981
H14	C14	1.008	H15	C15	0.986	H18	C18	0.999
H19	C19	0.960	H20	C20	0.979	H21	C21	0.973
H26	C26	0.970	H27	C27	0.975	H28	C28	0.972
H29	C29	1.002	H32	C32	1.000	H33	C33	0.944
H34	C34	0.991	H35	C35	0.961	H38a	C38	0.944
H38b	C38	0.969	H38c	C38	0.940			

Bond angles (degrees)

Atom	A	B	C	Angle	ADC(A)	ADC(B)	ADC(C)
C2	C1	C30	125.43	C2	C1	C36	121.93	C30	C1	C36	111.88
H2	C2	C1	118.44	H2	C2	C3	115.54	C1	C2	C3	125.25
C4	C3	C8	119.11	C4	C3	C2	122.91	C8	C3	C2	117.95
H4	C4	C5	119.97	H4	C4	C3	119.36	C5	C4	C3	120.66

H5	C5	C4	119.90	H5	C5	C6	119.77	C4	C5	C6	120.26
H6	C6	C5	120.37	H6	C6	C7	119.83	C5	C6	C7	119.80
H7	C7	C6	119.60	H7	C7	C8	119.72	C6	C7	C8	120.66
C7	C8	C3	119.50	C7	C8	C9	122.45	C3	C8	C9	117.90
H9	C9	C10	116.04	H9	C9	C8	114.26	C10	C9	C8	128.89
C9	C10	C17	127.55	C9	C10	C11	119.10	C17	C10	C11	111.80
C12	C11	C16	120.17	C12	C11	C10	124.49	C16	C11	C10	115.22
H12	C12	C13	121.29	H12	C12	C11	118.77	C13	C12	C11	119.94
H13	C13	C14	119.33	H13	C13	C12	120.57	C14	C13	C12	120.08
H14	C14	C13	121.23	H14	C14	C15	118.20	C13	C14	C15	120.57
H15	C15	C16	119.51	H15	C15	C14	120.58	C16	C15	C14	119.91
C15	C16	C11	119.31	C15	C16	C23	127.46	C11	C16	C23	113.22
C18	C17	C22	119.37	C18	C17	C10	125.82	C22	C17	C10	114.67
H18	C18	C19	119.31	H18	C18	C17	121.03	C19	C18	C17	119.64
H19	C19	C20	121.17	H19	C19	C18	117.96	C20	C19	C18	120.82
H20	C20	C19	120.28	H20	C20	C21	119.49	C19	C20	C21	120.21
H21	C21	C22	120.51	H21	C21	C20	120.07	C22	C21	C20	119.42
C21	C22	C17	120.52	C21	C22	C23	125.70	C17	C22	C23	113.74
C24	C23	C16	124.46	C24	C23	C22	119.72	C16	C23	C22	111.10
C23	C24	C31	124.14	C23	C24	C25	120.78	C31	C24	C25	111.21
C26	C25	C30	119.64	C26	C25	C24	127.04	C30	C25	C24	113.28
H26	C26	C25	118.92	H26	C26	C27	121.54	C25	C26	C27	119.53
H27	C27	C28	120.10	H27	C27	C26	119.15	C28	C27	C26	120.73
H28	C28	C27	119.94	H28	C28	C29	119.63	C27	C28	C29	120.42
H29	C29	C28	120.80	H29	C29	C30	119.50	C28	C29	C30	119.58
C29	C30	C25	120.05	C29	C30	C1	123.27	C25	C30	C1	116.48
C32	C31	C36	119.69	C32	C31	C24	125.58	C36	C31	C24	114.73
H32	C32	C33	120.12	H32	C32	C31	119.98	C33	C32	C31	119.89
H33	C33	C34	120.18	H33	C33	C32	119.32	C34	C33	C32	120.50

H34	C34	C33	121.39	H34	C34	C35	118.55	C33	C34	C35	120.05
H35	C35	C36	119.77	H35	C35	C34	119.95	C36	C35	C34	120.27
C35	C36	C31	119.56	C35	C36	C1	125.20	C31	C36	C1	115.21
H38c	C38	H38a	108.12	H38c	C38	H38b	110.75	H38c	C38	C39	107.44
H38a	C38	H38b	110.85	H38a	C38	C39	108.36	H38b	C38	C39	111.20

7.4.3 X-ray structure of tetramer 4

Formula sum C_{64} H_{32}

Formula weight 704

Crystal system monoclinic

Space group *P* 1 21/c 1 (no. 14)

Unit cell dimensions *a* = 12.4700(25) Å

b = 16.0300(32) Å

c = 20.9500(42) Å

β = 98.13(3) °

Cell volume 4145.69(1783) $Å^3$

Density, calculated 1.317 g/cm^3

Pearson code mP388

Formula type NO2P35Q59

Wyckoff sequence e^{97}

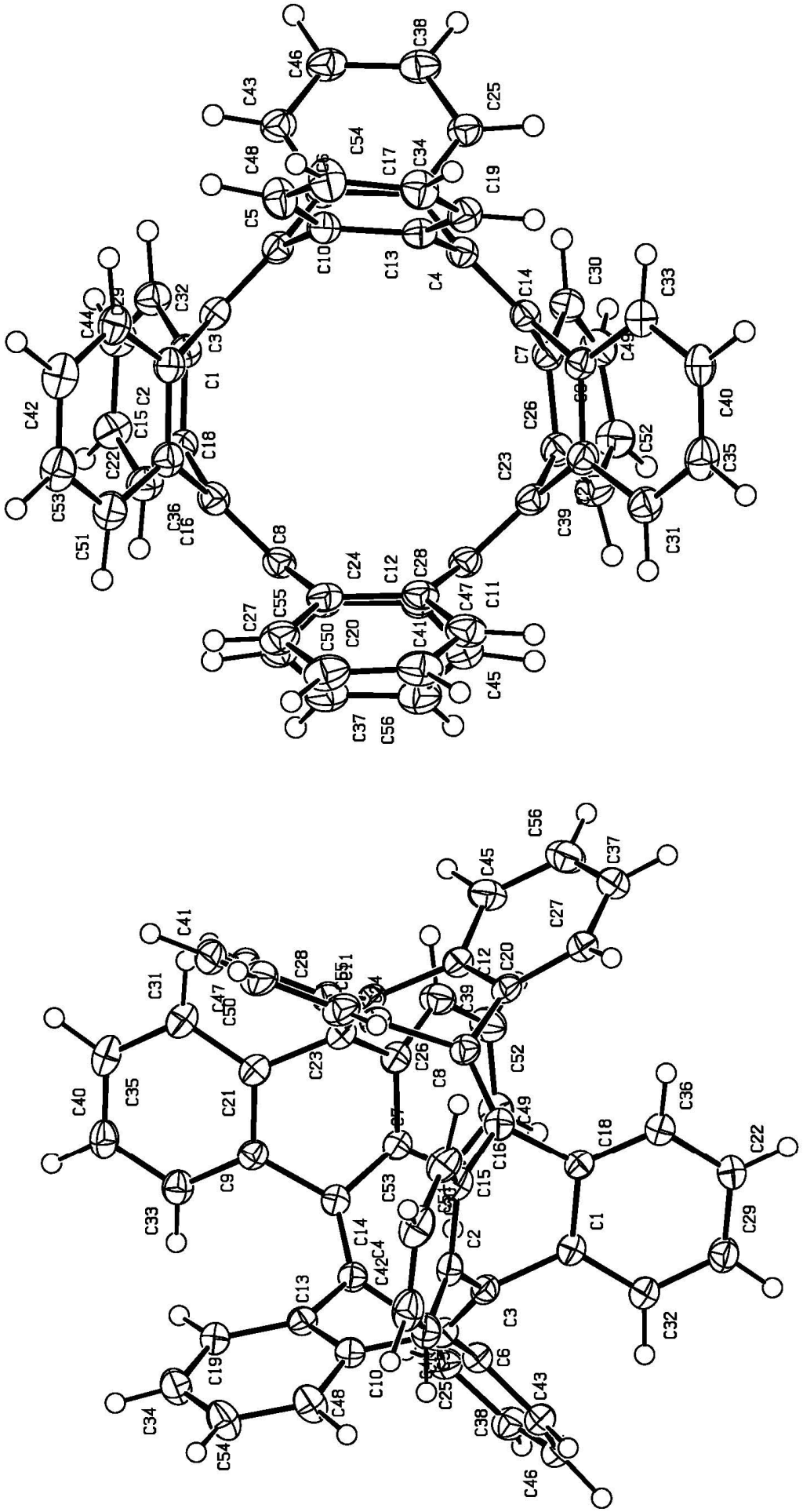
C38
C46
C43
C25
C54
C48
C17
C34
C19
C5
C10
C13
C4
C14
C30
C33
C44
C32
C3
C1
C7
C49
C42
C15
C2
C18
C26
C40
C22
C52
C23
C53
C36
C16
C8
C39
C35
C51
C31
C24
C12
C28
C27
C55
C50
C20
C47
C11
C41
C45
C37
C56

Bond distances (Angstroms)

Atom	A	B	Dist							
C1	C32	1.394	C1	C18	1.423	C1	C3	1.500
C2	C44	1.391	C2	C15	1.408	C2	C3	1.498
C3	C5	1.355	C3	C2	1.498	C3	C1	1.500
C4	C14	1.353	C4	C17	1.493	C4	C13	1.504
C5	C3	1.355	C5	C10	1.498	C5	C6	1.499
C6	C43	1.397	C6	C17	1.401	C6	C5	1.499
C7	C30	1.402	C7	C26	1.425	C7	C14	1.507
C8	C16	1.362	C8	C20	1.481	C8	C24	1.502
C9	C33	1.396	C9	C21	1.404	C9	C14	1.492
C10	C48	1.389	C10	C13	1.424	C10	C5	1.498
C11	C23	1.356	C11	C12	1.489	C11	C28	1.495
C12	C45	1.386	C12	C20	1.413	C12	C11	1.489
C13	C19	1.402	C13	C10	1.424	C13	C4	1.504
C14	C4	1.353	C14	C9	1.492	C14	C7	1.507
C15	C51	1.396	C15	C2	1.408	C15	C16	1.488
C16	C8	1.362	C16	C15	1.488	C16	C18	1.501
C17	C25	1.397	C17	C6	1.401	C17	C4	1.493
C18	C36	1.391	C18	C1	1.423	C18	C16	1.501
C19	H6	1.010	C19	C34	1.383	C19	C13	1.402
C20	C27	1.397	C20	C12	1.413	C20	C8	1.481
C21	C31	1.396	C21	C9	1.404	C21	C23	1.488
C22	H27	0.955	C22	C29	1.380	C22	C36	1.386
C23	C11	1.356	C23	C21	1.488	C23	C26	1.500
C24	C55	1.392	C24	C28	1.421	C24	C8	1.502
C25	H7	1.034	C25	C38	1.393	C25	C17	1.397
C26	C39	1.386	C26	C7	1.425	C26	C23	1.500
C27	H29	0.975	C27	C37	1.385	C27	C20	1.397
C28	C47	1.397	C28	C24	1.421	C28	C11	1.495
C29	H23	0.937	C29	C22	1.380	C29	C32	1.385
C30	H8	0.973	C30	C49	1.391	C30	C7	1.402
C31	H12	0.983	C31	C35	1.391	C31	C21	1.396
C32	H2	0.989	C32	C29	1.385	C32	C1	1.394
C33	H5	0.947	C33	C40	1.391	C33	C9	1.396
C34	H30	0.946	C34	C54	1.377	C34	C19	1.383
C35	H13	1.012	C35	C40	1.387	C35	C31	1.391
C36	H20	0.935	C36	C22	1.386	C36	C18	1.391
C37	H21	0.990	C37	C56	1.384	C37	C27	1.385
C38	H18	1.046	C38	C46	1.385	C38	C25	1.393
C39	H11	1.021	C39	C26	1.386	C39	C52	1.394

C40	H22	0.982	C40	C35	1.387	C40	C33	1.391
C41	H24	1.000	C41	C50	1.376	C41	C47	1.388
C42	H16	1.088	C42	C53	1.386	C42	C44	1.391
C43	H1	0.978	C43	C46	1.388	C43	C6	1.397
C44	H3	0.969	C44	C2	1.391	C44	C42	1.391
C45	H10	1.035	C45	C12	1.386	C45	C56	1.387
C46	H14	1.013	C46	C38	1.385	C46	C43	1.388
C47	H9	1.010	C47	C41	1.388	C47	C28	1.397
C48	H4	1.008	C48	C10	1.389	C48	C54	1.392
C49	H17	1.017	C49	C52	1.381	C49	C30	1.391
C50	H28	0.976	C50	C41	1.376	C50	C55	1.396
C51	H15	1.019	C51	C53	1.388	C51	C15	1.396
C52	H19	1.026	C52	C49	1.381	C52	C39	1.394
C53	H32	0.988	C53	C42	1.386	C53	C51	1.388
C54	H25	0.951	C54	C34	1.377	C54	C48	1.392
C55	H26	0.937	C55	C24	1.392	C55	C50	1.396
C56	H31	0.945	C56	C37	1.384	C56	C45	1.387
H1	C43	0.978	H2	C32	0.989	H3	C44	0.969
H4	C48	1.008	H5	C33	0.947	H6	C19	1.010
H7	C25	1.034	H8	C30	0.973	H9	C47	1.010
H10	C45	1.035	H11	C39	1.021	H12	C31	0.983
H13	C35	1.012	H14	C46	1.013	H15	C51	1.019
H16	C42	1.088	H17	C49	1.017	H18	C38	1.046
H19	C52	1.026	H20	C36	0.935	H20a	C202	0.980
H20b	C202	0.980	H20c	C202	0.980	H21	C37	0.990
H22	C40	0.982	H23	C29	0.937	H24	C41	1.000
H25	C54	0.951	H26	C55	0.937	H27	C22	0.955
H28	C50	0.976	H29	C27	0.975	H30	C34	0.946
H31	C56	0.945	H32	C53	0.988			

Bond angles (degrees)

Atom	**A**	**B**	**C**	**Angle**							
C32	C1	C18	118.77	C32	C1	C3	124.36	C18	C1	C3	116.54
C44	C2	C15	118.91	C44	C2	C3	123.01	C15	C2	C3	116.77
C5	C3	C2	125.59	C5	C3	C1	125.70	C2	C3	C1	108.57
C14	C4	C17	124.96	C14	C4	C13	126.97	C17	C4	C13	107.89
C3	C5	C10	124.78	C3	C5	C6	127.19	C10	C5	C6	107.51
C43	C6	C17	119.13	C43	C6	C5	123.86	C17	C6	C5	115.56
C30	C7	C26	117.78	C30	C7	C14	126.33	C26	C7	C14	115.64

C16	C8	C20	125.56	C16	C8	C24	125.00	C20	C8	C24	109.11
C33	C9	C21	119.26	C33	C9	C14	121.95	C21	C9	C14	117.63
C48	C10	C13	119.40	C48	C10	C5	124.39	C13	C10	C5	116.02
C23	C11	C12	124.12	C23	C11	C28	126.46	C12	C11	C28	109.22
C45	C12	C20	119.01	C45	C12	C11	122.78	C20	C12	C11	117.48
C19	C13	C10	117.65	C19	C13	C4	126.27	C10	C13	C4	115.91
C4	C14	C9	124.73	C4	C14	C7	126.56	C9	C14	C7	108.56
C51	C15	C2	119.35	C51	C15	C16	122.63	C2	C15	C16	116.81
C8	C16	C15	125.62	C8	C16	C18	126.38	C15	C16	C18	107.62
C25	C17	C6	119.70	C25	C17	C4	121.43	C6	C17	C4	117.58
C36	C18	C1	118.57	C36	C18	C16	125.12	C1	C18	C16	116.05
H6	C19	C34	120.05	H6	C19	C13	117.99	C34	C19	C13	121.95
C27	C20	C12	118.48	C27	C20	C8	124.18	C12	C20	C8	116.44
C31	C21	C9	119.58	C31	C21	C23	123.42	C9	C21	C23	115.55
H27	C22	C29	119.21	H27	C22	C36	120.97	C29	C22	C36	119.77
C11	C23	C21	127.39	C11	C23	C26	124.32	C21	C23	C26	107.58
C55	C24	C28	119.05	C55	C24	C8	124.09	C28	C24	C8	116.62
H7	C25	C38	118.79	H7	C25	C17	120.34	C38	C25	C17	120.46
C39	C26	C7	119.29	C39	C26	C23	124.61	C7	C26	C23	115.88
H29	C27	C37	119.61	H29	C27	C20	118.72	C37	C27	C20	121.26
C47	C28	C24	118.86	C47	C28	C11	124.42	C24	C28	C11	116.45
H23	C29	C22	119.80	H23	C29	C32	120.22	C22	C29	C32	119.95
H8	C30	C49	118.53	H8	C30	C7	120.04	C49	C30	C7	121.41
H12	C31	C35	120.94	H12	C31	C21	118.72	C35	C31	C21	120.30
H2	C32	C29	115.06	H2	C32	C1	123.48	C29	C32	C1	121.30
H5	C33	C40	119.37	H5	C33	C9	119.67	C40	C33	C9	120.86
H30	C34	C54	118.73	H30	C34	C19	121.21	C54	C34	C19	119.84
H13	C35	C40	121.27	H13	C35	C31	118.38	C40	C35	C31	120.32
H20	C36	C22	117.88	H20	C36	C18	120.51	C22	C36	C18	121.59
H21	C37	C56	118.48	H21	C37	C27	121.32	C56	C37	C27	120.10
H18	C38	C46	119.49	H18	C38	C25	120.83	C46	C38	C25	119.68
H11	C39	C26	120.78	H11	C39	C52	117.34	C26	C39	C52	121.71
H22	C40	C35	122.50	H22	C40	C33	117.76	C35	C40	C33	119.54
H24	C41	C50	124.47	H24	C41	C47	115.71	C50	C41	C47	119.79
H16	C42	C53	123.47	H16	C42	C44	116.81	C53	C42	C44	119.57
H1	C43	C46	116.38	H1	C43	C6	122.56	C46	C43	C6	120.68
H3	C44	C2	120.96	H3	C44	C42	117.54	C2	C44	C42	121.33
H10	C45	C12	118.19	H10	C45	C56	119.65	C12	C45	C56	121.87
H14	C46	C38	120.57	H14	C46	C43	119.00	C38	C46	C43	120.27
H9	C47	C41	119.18	H9	C47	C28	119.31	C41	C47	C28	121.19
H4	C48	C10	118.92	H4	C48	C54	119.78	C10	C48	C54	121.15
H17	C49	C52	121.41	H17	C49	C30	118.25	C52	C49	C30	120.32
H28	C50	C41	121.81	H28	C50	C55	117.84	C41	C50	C55	120.35
H15	C51	C53	119.43	H15	C51	C15	119.71	C53	C51	C15	120.80

H19	C52	C49	118.46	H19	C52	C39	122.42	C49	C52	C39	119.04
H32	C53	C42	120.03	H32	C53	C51	119.97	C42	C53	C51	119.92
H25	C54	C34	118.59	H25	C54	C48	121.55	C34	C54	C48	119.82
H26	C55	C24	118.93	H26	C55	C50	120.33	C24	C55	C50	120.71
H31	C56	C37	120.34	H31	C56	C45	120.64	C37	C56	C45	119.03

7.4.4 X-ray structure of the C_2 closed isomer 36

Messprotokoll

Kristall Daten:

Verbindung: $C_{36}H_{24}$

Formel: $C_{36}H_{24}$

Kristall-Farbe, -Habitus: Transparenter, farbloser Block

Kristallformat: 0.5 mm · 0.3 mm · 0.3 mm

Molekulargewicht: 456.55 g/mol

Raumgruppe: monoklin $P2_1/c$; IT – Nr.: 14

Berechnete Dichte: 1.239 g · cm^3

F(000): 960

Gitterparameter: Least-Squares-Verfeinerung von 8000 Reflexlagen im Winkelbereich zwischen $29° \leq 2\theta \leq 40°$

a =10.1574(8) Å α = 90.00
b = 8.7109 (6) Å β = 100.066 (8) °
c =28.100 (2) Å γ = 90.0
V = 2448.0 (3) Å^3
Z = 4

Datensammlung

Gerät: STOE Imaging Plate Diffraction System (IPDS)

Strahlung: Mo-Kα; 71.073 pm; Graphit-Monochromator

Messtemperatur: 170 K

Messbereich: $3° \leq 2\theta \leq 48°$
$-11 \leq h \leq 11$
$-9 \leq k \leq 9$
$-31 \leq l \leq 31$

Messbereich in Phi: 0-199.8° (333 Bilder a 0.6°)

Belichtungszeit/Bild 4 min.

Phi-Messmodus: Oszillierend

Detektor-Abstand: 80 mm

Indizierung: 865 Reflexe

Mosaikbreite: 0.016

Integration: Dynamische Profile

Orientierungskontrolle: min.: 80/ max.: 300

Strukturlösung und Verfeinerung:

Reflexe: 14496 gemessene Reflexe
410 systematische ausgelöschte Reflexe
3651 unabhängige Reflexe
0 unterdrückte Reflexe
3651 unabhängige Reflexe zu Verfeinerung verwendet
3064 unabhängige Reflexe mit Fo>4σ(Fo)

Durchschnittliches I/σ(I) 22.70

$R_{int.}$: $\Sigma |F_o^2-(F_o^2)mean| / [\Sigma F_o^2] = 0.0535$

Absorptionskorrektur: keine; $\mu = 0.07\ mm^{-1}$

Strukturlösung: Direkte Methoden (SHELXS-97)

Strukturverfeinerung: Full-Matrix Least-Squares gegen F^2 (SHELXL-97)

Parameter: In der asymmetrischen Einheit:
36 C-Atome anisotrope Auslenkungsparameter
24 H-Atome isotrope Auslenkungsparameter
326 Parameter full matrix verfeinert

Reflexe pro Parameter: 11.2

Wasserstoffatome: Die Wasserstoffatome wurden geometrisch ideal positioniert (d_{C-H}(aromatisch) = 0.95; d_{C-H}(methin) = 1.00) und mit festen isotropen Auslenkungsparametern [U_{iso} = 1.2× $U_{eq}(C_{aromatisch/methin})$] nach dem Reitermodell verfeinert.

Atomformfaktoren: Für Neutralatome

LP-Korrektur: *J*a

Extinktionskorrektur: $F^* = F_c (k[1 + 0.001 \cdot x \cdot F_c^2 \cdot \lambda^3 / \sin(2\theta)]^{-0.25})$ x = 0.012 (2)

Gewichtung: $w = 1/[\sigma^2(F_o^2) + (0.0655 \cdot P)^2 + 0.93 \cdot P]$; $P = (Max(F_o^2,0) + 2 \cdot F_c^2) / 3$

Shift/Error: ≤ 0.001 im letzten Verfeinerungszyklus

Restelektronendichte: Max.: 0.26 / Min.: -0.19 e/Å^3

R1 für 3064 Fo>4σ(Fo) $R1 = \Sigma ||Fo| - |Fc|| / \Sigma |Fo|$ = 0.0495

R1 für alle 3651 Reflexe = 0.0593

wR2 für 3064 Fo>4σ(Fo) $wR2 = [\Sigma[w(F_o^2-F_c^2)^2] / \Sigma[w(F_o^2)^2]]^{1/2}$ = 0.1264

wR2 für alle 3651 Reflexe = 0.1341

Goodness of fit (Alle R.) $S = [\Sigma[w(F_o^2-F_c^2)^2] / (n-p)]^{1/2}$ = 1.070

Restrained GoF (Alle R.) = 1.070

Restraints 0

Bemerkungen:

Datensammlung und Datenreduktion: STOE IPDS-Programmpaket; Graphik: SHELXTL PC XP;

Graphik: SHELXTL PC XP; Erstellung von Tabellen: SHELXL-97 CIFTAB

Es wurde eine zusätzliche Messung bis Phi = 74° mit 9.5 min. pro Bild durchgeführt und beide Datensätze aufeinander skaliert.

Atomkoordinaten [$\cdot 10^4$] und äquivalente isotrope Auslenkungsparameter [$Å^2 \cdot 10^3$]

	X		Y		Z		U_{eq}	
C(1)	7311	(2)	6622	(2)	5090	(1)	44	(1)
C(2)	6685	(3)	6412	(3)	4566	(1)	61	(1)
C(3)	6915	(3)	5200	(3)	4310	(1)	62	(1)
C(4)	7804	(2)	4015	(3)	4523	(1)	52	(1)
C(5)	8187	(2)	3937	(3)	4995	(1)	51	(1)
C(6)	7704	(2)	5042	(2)	5338	(1)	43	(1)
C(7)	6367	(2)	7430	(3)	5353	(1)	47	(1)
C(8)	8721	(2)	5288	(2)	5783	(1)	43	(1)
C(11)	4184	(2)	9208	(3)	5775	(1)	53	(1)
C(12)	3279	(2)	9409	(3)	6084	(1)	61	(1)
C(13)	3660	(2)	9288	(3)	6574	(1)	59	(1)
C(14)	4968	(2)	8961	(2)	6766	(1)	52	(1)
C(15)	5912	(2)	8766	(2)	6470	(1)	40	(1)
C(16)	7351	(2)	8468	(2)	6644	(1)	38	(1)
C(17)	8216	(2)	9443	(2)	6385	(1)	41	(1)
C(18)	9330	(2)	10277	(2)	6587	(1)	49	(1)
C(19)	10101	(2)	11010	(3)	6290	(1)	55	(1)
C(20)	9760	(2)	10886	(3)	5800	(1)	56	(1)
C(21)	8635	(2)	10076	(3)	5589	(1)	50	(1)
C(22)	7845	(2)	9345	(2)	5876	(1)	41	(1)
C(23)	6576	(2)	8537	(2)	5685	(1)	42	(1)
C(24)	5520	(2)	8879	(2)	5970	(1)	45	(1)
C(31)	6722	(2)	3347	(2)	6329	(1)	44	(1)
C(32)	5650	(2)	2971	(2)	6546	(1)	46	(1)
C(33)	5251	(2)	3927	(2)	6884	(1)	48	(1)
C(34)	5926	(2)	5307	(2)	7012	(1)	43	(1)
C(35)	6997	(2)	5702	(2)	6794	(1)	37	(1)
C(36)	7819	(2)	7134	(2)	6853	(1)	38	(1)
C(37)	9274	(2)	6797	(2)	6948	(1)	40	(1)
C(38)	10198	(2)	7469	(3)	7313	(1)	50	(1)
C(39)	11535	(2)	7101	(3)	7355	(1)	56	(1)
C(40)	11951	(2)	6095	(3)	7038	(1)	55	(1)
C(41)	11055	(2)	5411	(3)	6673	(1)	49	(1)
C(42)	9690	(2)	5762	(2)	6628	(1)	40	(1)
C(43)	8615	(2)	5174	(2)	6250	(1)	39	(1)
C(44)	7403	(2)	4712	(2)	6448	(1)	39	(1)

Äquivalente isotrope U berechnet als ein Drittel der Spur des orthogonalen U_{ij} Tensors

Anisotrope Auslenkungsparameter [$Å^2 \cdot 10^3$]

	U_{11}	U_{22}	U_{33}	U_{23}	U_{13}	U_{12}
C(1)	48 (1)	43 (1)	40 (1)	2 (1)	5 (1)	3 (1)
C(2)	70 (2)	72 (2)	39 (1)	4 (1)	2 (1)	21 (1)
C(3)	66 (2)	81 (2)	36 (1)	-6 (1)	1 (1)	9 (1)
C(4)	61 (1)	51 (1)	46 (2)	-12 (1)	13 (1)	-8 (1)
C(5)	65 (1)	40 (1)	47 (2)	-3 (1)	9 (1)	2 (1)
C(6)	48 (1)	43 (1)	37 (1)	1 (1)	5 (1)	0 (1)
C(7)	44 (1)	49 (1)	45 (1)	1 (1)	3 (1)	3 (1)
C(8)	43 (1)	41 (1)	46 (1)	0 (1)	8 (1)	3 (1)
C(11)	48 (1)	42 (1)	66 (2)	-3 (1)	0 (1)	5 (1)
C(12)	41 (1)	44 (1)	99 (2)	-7 (1)	17 (1)	2 (1)
C(13)	55 (1)	41 (1)	87 (2)	3 (1)	30 (1)	3 (1)
C(14)	53 (1)	36 (1)	70 (2)	3 (1)	23 (1)	5 (1)
C(15)	46 (1)	25 (1)	50 (1)	-1 (1)	10 (1)	1 (1)
C(16)	42 (1)	33 (1)	41 (1)	-6 (1)	10 (1)	0 (1)
C(17)	42 (1)	26 (1)	56 (1)	-3 (1)	8 (1)	4 (1)
C(18)	48 (1)	34 (1)	64 (2)	-4 (1)	5 (1)	1 (1)
C(19)	45 (1)	38 (1)	81 (2)	4 (1)	7 (1)	1 (1)
C(20)	45 (1)	43 (1)	81 (2)	15 (1)	14 (1)	5 (1)
C(21)	48 (1)	44 (1)	58 (2)	11 (1)	12 (1)	7 (1)
C(22)	42 (1)	32 (1)	50 (1)	5 (1)	11 (1)	10 (1)
C(23)	44 (1)	37 (1)	46 (1)	6 (1)	3 (1)	5 (1)
C(24)	46 (1)	28 (1)	60 (2)	-1 (1)	9 (1)	2 (1)
C(31)	49 (1)	35 (1)	43 (1)	4 (1)	-1 (1)	2 (1)
C(32)	49 (1)	35 (1)	50 (1)	7 (1)	-2 (1)	-1 (1)
C(33)	41 (1)	47 (1)	54 (1)	16 (1)	4 (1)	-2 (1)
C(34)	45 (1)	42 (1)	43 (1)	7 (1)	5 (1)	4 (1)
C(35)	41 (1)	33 (1)	35 (1)	6 (1)	1 (1)	2 (1)
C(36)	45 (1)	37 (1)	33 (1)	-5 (1)	5 (1)	-1 (1)
C(37)	43 (1)	39 (1)	37 (1)	6 (1)	3 (1)	1 (1)
C(38)	55 (1)	49 (1)	43 (1)	1 (1)	-1 (1)	-6 (1)
C(39)	48 (1)	61 (1)	54 (2)	4 (1)	-6 (1)	-9 (1)
C(40)	42 (1)	57 (1)	62 (2)	9 (1)	-1 (1)	0 (1)
C(41)	47 (1)	47 (1)	52 (1)	8 (1)	7 (1)	3 (1)
C(42)	43 (1)	38 (1)	38 (1)	8 (1)	5 (1)	3 (1)
C(43)	47 (1)	31 (1)	40 (1)	2 (1)	8 (1)	7 (1)
C(44)	44 (1)	32 (1)	37 (1)	4 (1)	-4 (1)	4 (1)

Der Temperaturfaktorexponent hat die Form: $-2\pi^2(h^2 \cdot a^{*2} U_{11}+...+2hka^*b^*U_{12})$

H-Atomkoordinaten [· 10^4] und isotrope Auslenkungsparameter [$Å^2$· 10^3]

	X	Y	Z	U_{eq}
H(1)	8136	7260	5107	53
H(2)	6100	7187	4413	73
H(3)	6487	5113	3983	74
H(4)	8121	3276	4322	63
H(5)	8792	3149	5124	61
H(6)	6887	4594	5437	52
H(7)	5464	7103	5270	56
H(8)	9583	5571	5726	52
H(11)	3904	9291	5435	64
H(12)	2373	9635	5954	73
H(13)	3023	9431	6781	71
H(14)	5228	8867	7106	62
H(18)	9572	10352	6929	59
H(19)	10862	11595	6429	66
H(20)	10303	11364	5600	67
H(21)	8404	10019	5247	60
H(31)	6994	2673	6099	52
H(32)	5180	2040	6462	55
H(33)	4513	3649	7032	57
H(34)	5650	5965	7246	52
H(38)	9910	8175	7531	60
H(39)	12169	7547	7606	67
H(40)	12876	5863	7069	66
H(41)	11358	4714	6455	58

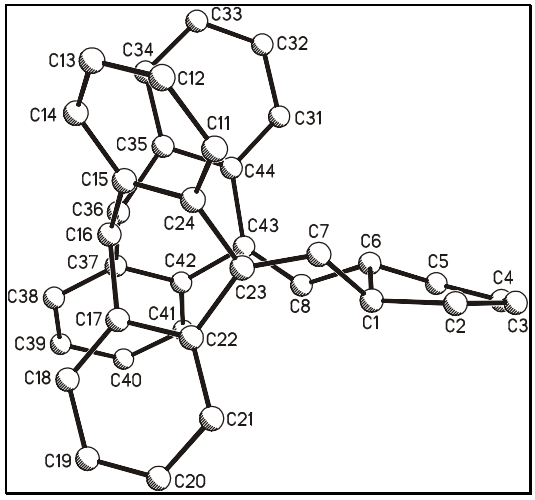

Geometrieparameter

Bindungslängen [Å]

C(1)	- C(7)	1.486	(3)	C(1)	- C(2)	1.510	(3)
C(1)	- C(6)	1.563	(3)	C(2)	- C(3)	1.320	(4)
C(3)	- C(4)	1.432	(4)	C(4)	- C(5)	1.315	(3)

C(5) - C(6)	1.504	(3)	C(6) - C(8)	1.492	(3)
C(7) - C(23)	1.333	(3)	C(8) - C(43)	1.337	(3)
C(11) - C(12)	1.382	(4)	C(11) - C(24)	1.401	(3)
C(12) - C(13)	1.367	(4)	C(13) - C(14)	1.373	(4)
C(14) - C(15)	1.385	(3)	C(15) - C(24)	1.396	(3)
C(15) - C(16)	1.481	(3)	C(16) - C(36)	1.351	(3)
C(16) - C(17)	1.498	(3)	C(17) - C(18)	1.381	(3)
C(17) - C(22)	1.417	(3)	C(18) - C(19)	1.396	(3)
C(19) - C(20)	1.365	(4)	C(20) - C(21)	1.385	(4)
C(21) - C(22)	1.388	(3)	C(22) - C(23)	1.484	(3)
C(23) - C(24)	1.476	(3)	C(31) - C(32)	1.377	(3)
C(31) - C(44)	1.387	(3)	C(32) - C(33)	1.377	(3)
C(33) - C(34)	1.398	(3)	C(34) - C(35)	1.382	(3)
C(35) - C(44)	1.414	(3)	C(35) - C(36)	1.493	(3)
C(36) - C(37)	1.485	(3)	C(37) - C(42)	1.390	(3)
C(37) - C(38)	1.392	(3)	C(38) - C(39)	1.381	(3)
C(39) - C(40)	1.369	(4)	C(40) - C(41)	1.382	(3)
C(41) - C(42)	1.403	(3)	C(42) - C(43)	1.477	(3)
C(43) - C(44)	1.493	(3)			

Bindungswinkel [°]

C(7) - C(1) - C(2)	110.1	(2)	C(7) - C(1) - C(6)	109.4	(2)
C(2) - C(1) - C(6)	111.1	(2)	C(3) - C(2) - C(1)	122.8	(2)
C(2) - C(3) - C(4)	120.5	(2)	C(5) - C(4) - C(3)	120.8	(2)
C(4) - C(5) - C(6)	122.7	(2)	C(8) - C(6) - C(5)	112.0	(2)
C(8) - C(6) - C(1)	109.5	(2)	C(5) - C(6) - C(1)	111.4	(2)
C(23) - C(7) - C(1)	130.8	(2)	C(43) - C(8) - C(6)	130.5	(2)
C(12) - C(11) - C(24)	119.0	(2)	C(13) - C(12) - C(11)	121.4	(2)
C(12) - C(13) - C(14)	119.7	(2)	C(13) - C(14) - C(15)	120.9	(2)
C(14) - C(15) - C(24)	119.3	(2)	C(14) - C(15) - C(16)	124.8	(2)
C(24) - C(15) - C(16)	115.9	(2)	C(36) - C(16) - C(15)	123.1	(2)
C(36) - C(16) - C(17)	120.5	(2)	C(15) - C(16) - C(17)	111.6	(2)
C(18) - C(17) - C(22)	120.0	(2)	C(18) - C(17) - C(16)	127.4	(2)
C(22) - C(17) - C(16)	112.4	(2)	C(17) - C(18) - C(19)	120.0	(2)
C(20) - C(19) - C(18)	119.9	(2)	C(19) - C(20) - C(21)	121.1	(2)
C(20) - C(21) - C(22)	120.2	(2)	C(21) - C(22) - C(17)	118.7	(2)
C(21) - C(22) - C(23)	124.1	(2)	C(17) - C(22) - C(23)	117.1	(2)
C(7) - C(23) - C(24)	118.9	(2)	C(7) - C(23) - C(22)	128.2	(2)

Bindungswinkel [°]

C(24) - C(23) - C(22)	112.1	(2)	C(15) - C(24) - C(11)	119.6	(2)
C(15) - C(24) - C(23)	115.2	(2)	C(11) - C(24) - C(23)	125.1	(2)
C(32) - C(31) - C(44)	119.8	(2)	C(33) - C(32) - C(31)	120.8	(2)
C(32) - C(33) - C(34)	120.5	(2)	C(35) - C(34) - C(33)	119.3	(2)
C(34) - C(35) - C(44)	119.9	(2)	C(34) - C(35) - C(36)	128.8	(2)
C(44) - C(35) - C(36)	111.2	(2)	C(16) - C(36) - C(37)	120.8	(2)
C(16) - C(36) - C(35)	121.5	(2)	C(37) - C(36) - C(35)	112.0	(2)
C(42) - C(37) - C(38)	120.4	(2)	C(42) - C(37) - C(36)	114.7	(2)
C(38) - C(37) - C(36)	124.8	(2)	C(39) - C(38) - C(37)	119.5	(2)

Torsionswinkel [°]

C(7) - C(1) - C(2) - C(3)	-145.9	(3)	C(6) - C(1) - C(2) - C(3)	-24.6	(4)
C(1) - C(2) - C(3) - C(4)	-0.9	(4)	C(2) - C(3) - C(4) - C(5)	14.4	(4)
C(3) - C(4) - C(5) - C(6)	1.4	(4)	C(4) - C(5) - C(6) - C(8)	-149.8	(2)
C(4) - C(5) - C(6) - C(1)	-26.8	(3)	C(7) - C(1) - C(6) - C(8)	-78.1	(2)
C(2) - C(1) - C(6) - C(8)	160.1	(2)	C(7) - C(1) - C(6) - C(5)	157.6	(2)
C(2) - C(1) - C(6) - C(5)	35.8	(3)	C(2) - C(1) - C(7) - C(23)	-138.7	(3)

C(6)	C(1)	C(7)	C(23)	98.9	(3)	C(5)	C(6)	C(8)	C(43)	-127.4	(2)
C(1)	C(6)	C(8)	C(43)	108.6	(2)	C(24)	C(11)	C(12)	C(13)	-0.2	(3)
C(11)	C(12)	C(13)	C(14)	0.0	(3)	C(12)	C(13)	C(14)	C(15)	0.7	(3)
C(13)	C(14)	C(15)	C(24)	-1.1	(3)	C(13)	C(14)	C(15)	C(16)	177.6	(2)
C(14)	C(15)	C(16)	C(36)	69.7	(3)	C(24)	C(15)	C(16)	C(36)	-111.6	(2)
C(14)	C(15)	C(16)	C(17)	-134.7	(2)	C(24)	C(15)	C(16)	C(17)	44.0	(2)
C(36)	C(16)	C(17)	C(18)	-70.0	(3)	C(15)	C(16)	C(17)	C(18)	133.7	(2)
C(36)	C(16)	C(17)	C(22)	104.9	(2)	C(15)	C(16)	C(17)	C(22)	-51.4	(2)
C(22)	C(17)	C(18)	C(19)	-0.7	(3)	C(16)	C(17)	C(18)	C(19)	173.8	(2)
C(17)	C(18)	C(19)	C(20)	-0.8	(3)	C(18)	C(19)	C(20)	C(21)	1.8	(3)
C(19)	C(20)	C(21)	C(22)	-1.3	(3)	C(20)	C(21)	C(22)	C(17)	-0.2	(3)
C(20)	C(21)	C(22)	C(23)	175.8	(2)	C(18)	C(17)	C(22)	C(21)	1.2	(3)
C(16)	C(17)	C(22)	C(21)	-174.1	(2)	C(18)	C(17)	C(22)	C(23)	-175.1	(2)
C(16)	C(17)	C(22)	C(23)	9.6	(2)	C(1)	C(7)	C(23)	C(24)	-165.7	(2)
C(1)	C(7)	C(23)	C(22)	2.9	(4)	C(21)	C(22)	C(23)	C(7)	53.8	(3)
C(17)	C(22)	C(23)	C(7)	-130.1	(2)	C(21)	C(22)	C(23)	C(24)	-137.0	(2)
C(17)	C(22)	C(23)	C(24)	39.1	(2)	C(14)	C(15)	C(24)	C(11)	0.8	(3)
C(16)	C(15)	C(24)	C(11)	-178.0	(2)	C(14)	C(15)	C(24)	C(23)	-175.6	(2)
C(16)	C(15)	C(24)	C(23)	5.6	(2)	C(12)	C(11)	C(24)	C(15)	-0.2	(3)
C(12)	C(11)	C(24)	C(23)	175.8	(2)	C(7)	C(23)	C(24)	C(15)	122.9	(2)
C(22)	C(23)	C(24)	C(15)	-47.4	(2)	C(7)	C(23)	C(24)	C(11)	-53.3	(3)
C(22)	C(23)	C(24)	C(11)	136.4	(2)	C(44)	C(31)	C(32)	C(33)	-0.7	(3)
C(31)	C(32)	C(33)	C(34)	0.3	(3)	C(32)	C(33)	C(34)	C(35)	0.1	(3)
C(33)	C(34)	C(35)	C(44)	-0.3	(3)	C(33)	C(34)	C(35)	C(36)	176.6	(2)
C(15)	C(16)	C(36)	C(37)	169.9	(2)	C(17)	C(16)	C(36)	C(37)	16.4	(3)
C(15)	C(16)	C(36)	C(35)	18.7	(3)	C(17)	C(16)	C(36)	C(35)	-134.8	(2)
C(34)	C(35)	C(36)	C(16)	-75.6	(3)	C(44)	C(35)	C(36)	C(16)	101.6	(2)
C(34)	C(35)	C(36)	C(37)	130.9	(2)	C(44)	C(35)	C(36)	C(37)	-51.9	(2)
C(16)	C(36)	C(37)	C(42)	-103.9	(2)	C(35)	C(36)	C(37)	C(42)	49.9	(2)
C(16)	C(36)	C(37)	C(38)	74.2	(3)	C(35)	C(36)	C(37)	C(38)	-132.1	(2)
C(42)	C(37)	C(38)	C(39)	0.1	(3)	C(36)	C(37)	C(38)	C(39)	-177.8	(2)
C(37)	C(38)	C(39)	C(40)	0.7	(4)	C(38)	C(39)	C(40)	C(41)	-0.8	(4)
C(39)	C(40)	C(41)	C(42)	0.1	(3)	C(38)	C(37)	C(42)	C(41)	-0.7	(3)
C(36)	C(37)	C(42)	C(41)	177.4	(2)	C(38)	C(37)	C(42)	C(43)	-178.2	(2)
C(36)	C(37)	C(42)	C(43)	0.0	(2)	C(40)	C(41)	C(42)	C(37)	0.6	(3)
C(40)	C(41)	C(42)	C(43)	177.7	(2)	C(6)	C(8)	C(43)	C(42)	-168.1	(2)
C(6)	C(8)	C(43)	C(44)	1.8	(3)	C(37)	C(42)	C(43)	C(8)	125.9	(2)
C(41)	C(42)	C(43)	C(8)	-51.4	(3)	C(37)	C(42)	C(43)	C(44)	-45.4	(2)
C(41)	C(42)	C(43)	C(44)	137.3	(2)	C(32)	C(31)	C(44)	C(35)	0.5	(3)
C(32)	C(31)	C(44)	C(43)	176.9	(2)	C(34)	C(35)	C(44)	C(31)	0.0	(3)
C(36)	C(35)	C(44)	C(31)	-177.5	(2)	C(34)	C(35)	C(44)	C(43)	-176.7	(2)
C(36)	C(35)	C(44)	C(43)	5.9	(2)	C(8)	C(43)	C(44)	C(31)	55.3	(3)
C(42)	C(43)	C(44)	C(31)	-134.1	(2)	C(8)	C(43)	C(44)	C(35)	-128.2	(2)
C(42)	C(43)	C(44)	C(35)	42.4	(2)						

7.4.5 X-ray structure of isomer 38

Kristall Daten:

Verbindung: $C_{36}H_{24}$

Formel: $C_{36}H_{24}$

Kristall-Farbe, -Habitus: Transparenter, farbloser Block

Kristallformat: 0.2 mm · 0.05 mm · 0.05 mm

Molekulargewicht: 456.55 g/mol

Raumgruppe: monoklin $P2_1/c$; IT – Nr.: 14

Berechnete Dichte: 1.242 g · cm^3

F(000): 960

Gitterparameter: Least-Squares-Verfeinerung von 3808 Reflexlagen im Winkelbereich zwischen $4.6° \leq 2\theta \leq 51.9°$

a = 8.9779 (5) Å α = 90.00
b = 29.007 (2) Å β = 94.090 (7) °
c = 9.3982 (5) Å γ = 90.0
V = 2441.3 (3) Å^3
Z = 4

Datensammlung

Gerät: STOE Imaging Plate Diffraction System (IPDS)

Strahlung: Mo-Kα; 71.073 pm; Graphit-Monochromator

Messtemperatur: 150 K

Messbereich: $3° \leq 2\theta \leq 45°$
$-9 \leq h \leq 9$
$-31 \leq k \leq 25$
$-9 \leq l \leq 10$

Messbereich in Phi: 0-120° (200 Bilder a 0.6°)

Belichtungszeit/Bild 20 min.

Phi-Messmodus: Oszillierend

Detektor-Abstand: 70 mm

Indizierung: 554 Reflexe

Mosaikbreite: 0.010

Integration: Dynamische Profile

Orientierungskontrolle: min.: 80/ max.: 300

Strukturlösung und Verfeinerung:

Reflexe:
7871 gemessene Reflexe
132 systematische ausgelöschte Reflexe
3150 unabhängige Reflexe
0 unterdrückte Reflexe
3140 unabhängige Reflexe zu Verfeinerung verwendet
1773 unabhängige Reflexe mit $Fo > 4\sigma(Fo)$

Durchschnittliches $I/\sigma(I)$ 5.78

$R_{int.}$: $\Sigma |F_o^2 - (F_o^2)\text{mean}| / [\Sigma F_o^2] = 0.0759$

Absorptionskorrektur: keine; $\mu = 0.07$ mm^{-1}

Strukturlösung: Direkte Methoden (SHELXS-97)

Strukturverfeinerung: Full-Matrix Least-Squares gegen F^2 (SHELXL-97)

Parameter:	In der asymmetrischen Einheit: 36 C-Atome anisotrope Auslenkungsparameter 24 H-Atome isotrope Auslenkungsparameter 326 Parameter full matrix verfeinert
Reflexe pro Parameter:	9.66
Wasserstoffatome:	Die Wasserstoffatome wurden geometrisch ideal positioniert (d_{C-H}(aromatisch) = 0.95) und mit festen isotropen Auslenkungsparametern [$U_{iso} = 1.2 \times U_{eq}(C_{aromatisch})$] nach dem Reitermodell verfeinert.
Atomformfaktoren:	Für Neutralatome
LP-Korrektur:	Ja
Extinktionskorrektur:	$F^* = F_c (k[1 + 0.001 \cdot x \cdot F_c^2 \cdot \lambda^3 / \sin(2\theta)]^{-0.25})$ x = 0.010 (2)
Gewichtung:	$w = 1/[\sigma^2(F_o^2) + (0.0719 \cdot P)^2 + 0.0 \cdot P]$; $P = (\mathrm{Max}(F_o^2,0) + 2 \cdot F_c^2) / 3$
Shift/Error:	≤ 0.001 im letzten Verfeinerungszyklus
Restelektronendichte:	Max.: 0.34 / Min.: -0.19 e/Å^3
R1 für 1773 Fo>4σ(Fo)	$R1 = \Sigma \lvert \lvert Fo \rvert - \lvert Fc \rvert \rvert / \Sigma \lvert Fo \rvert$ = 0.0599
R1 für alle 3150 Reflexe	= 0.1199
wR2 für 1773 Fo>4σ(Fo)	$wR2 = [\Sigma[w(F_o^2 - F_c^2)^2] / \Sigma[w(F_o^2)^2]]^{½}$ = 0.1278
wR2 für alle 3150 Reflexe	= 0.1488
Goodness of fit (Alle R.)	$S = [\Sigma[w(F_o^2 - F_c^2)^2] / (n-p)]^{½}$ = 0.0951
Restrained GoF (Alle R.)	= 0.0951
Restraints	0

Bemerkungen:

Datensammlung und Datenreduktion: STOE IPDS-Programmpaket; Graphik: SHELXTL PC XP;

Graphik: SHELXTL PC XP; Erstellung von Tabellen: SHELXL-97 CIFTAB

Es wurde eine zusätzliche Messung bis Phi = 52° mit 30 min. pro Bild und einem Phi-Inkrement von 0.4° durchgeführt und beide Datensätze aufeinander skaliert.

Atomkoordinaten [· 10^4] und äquivalente isotrope Auslenkungsparameter [$Å^2$· 10^3]

	X	Y	Z	U_{eq}
C(1)	6187 (4)	7025 (2)	7731 (5)	47 (1)
C(2)	6883 (5)	7015 (2)	6405 (5)	57 (2)
C(3)	8169 (6)	7251 (2)	6223 (5)	63 (2)
C(4)	9015 (6)	7514 (2)	7337 (6)	64 (2)
C(5)	10280 (5)	7346 (2)	8000 (6)	59 (2)
C(6)	10851 (5)	6903 (2)	7558 (6)	64 (2)
C(7)	10745 (5)	6500 (2)	8270 (6)	58 (1)
C(8)	10101 (4)	6452 (2)	9602 (6)	51 (1)
C(11)	4042 (4)	6287 (2)	6050 (4)	47 (1)
C(12)	3412 (5)	5882 (2)	5466 (5)	50 (1)
C(13)	3411 (4)	5487 (2)	6276 (5)	46 (1)
C(14)	4021 (4)	5482 (2)	7683 (4)	37 (1)
C(15)	4654 (3)	5883 (2)	8266 (4)	32 (1)
C(16)	5284 (4)	5928 (1)	9781 (4)	29 (1)
C(17)	4629 (4)	6344 (2)	10463 (4)	30 (1)
C(18)	4020 (4)	6356 (2)	11792 (4)	36 (1)
C(19)	3494 (4)	6767 (2)	12310 (4)	38 (1)
C(20)	3584 (4)	7168 (2)	11545 (4)	42 (1)
C(21)	4164 (4)	7160 (2)	10202 (5)	39 (1)
C(22)	4672 (4)	6747 (2)	9664 (4)	33 (1)
C(23)	5211 (4)	6713 (2)	8193 (4)	37 (1)
C(24)	4661 (4)	6288 (2)	7458 (4)	34 (1)
C(31)	10009 (4)	5417 (2)	8444 (5)	49 (1)
C(32)	9615 (4)	5013 (2)	7759 (5)	48 (1)
C(33)	8212 (4)	4819 (2)	7904 (5)	44 (1)
C(34)	7207 (4)	5042 (2)	8727 (4)	39 (1)
C(35)	7567 (4)	5454 (2)	9386 (4)	32 (1)
C(36)	6580 (4)	5733 (2)	10294 (4)	31 (1)
C(37)	7388 (4)	5868 (2)	11655 (4)	35 (1)
C(38)	6875 (4)	5803 (2)	13019 (4)	42 (1)
C(39)	7730 (5)	5941 (2)	14236 (5)	55 (1)
C(40)	9093 (5)	6159 (2)	14096 (5)	57 (1)
C(41)	9631 (4)	6219 (2)	12772 (5)	50 (1)
C(42)	8809 (4)	6071 (2)	11547 (5)	37 (1)
C(43)	9375 (4)	6076 (2)	10085 (5)	41 (1)
C(44)	9008 (4)	5652 (2)	9272 (5)	36 (1)

Äquivalente isotrope U berechnet als ein Drittel der Spur des orthogonalen U_{ij} Tensors

Anisotrope Auslenkungsparameter [$Å^2 \cdot 10^3$]

	U_{11}	U_{22}	U_{33}	U_{23}	U_{13}	U_{12}
C(1)	53 (2)	43 (3)	48 (3)	9 (2)	17 (2)	1 (2)
C(2)	58 (3)	64 (4)	51 (3)	1 (3)	16 (2)	4 (2)
C(3)	79 (3)	66 (4)	47 (3)	4 (3)	24 (3)	3 (3)
C(4)	80 (3)	49 (4)	67 (4)	2 (3)	30 (3)	-11 (3)
C(5)	50 (3)	52 (4)	77 (4)	-15 (3)	23 (3)	-14 (2)
C(6)	61 (3)	61 (4)	71 (4)	-10 (3)	19 (3)	-12 (3)
C(7)	56 (3)	54 (4)	66 (3)	-2 (3)	11 (3)	-1 (2)
C(8)	39 (2)	38 (3)	77 (4)	-5 (3)	5 (2)	6 (2)
C(11)	52 (2)	58 (4)	31 (3)	8 (2)	5 (2)	0 (2)
C(12)	51 (2)	71 (4)	26 (2)	-4 (3)	-1 (2)	-10 (2)
C(13)	44 (2)	57 (4)	37 (3)	-10 (3)	5 (2)	-11 (2)
C(14)	33 (2)	48 (3)	31 (3)	-3 (2)	3 (2)	-3 (2)
C(15)	26 (2)	42 (3)	28 (2)	-5 (2)	6 (2)	1 (2)
C(16)	31 (2)	28 (3)	28 (2)	2 (2)	5 (2)	-6 (2)
C(17)	27 (2)	36 (3)	26 (2)	-5 (2)	4 (2)	0 (2)
C(18)	36 (2)	41 (3)	30 (2)	5 (2)	0 (2)	3 (2)
C(19)	41 (2)	43 (3)	32 (2)	-4 (2)	7 (2)	2 (2)
C(20)	42 (2)	41 (3)	43 (3)	-12 (2)	9 (2)	5 (2)
C(21)	44 (2)	31 (3)	42 (3)	4 (2)	2 (2)	4 (2)
C(22)	30 (2)	37 (3)	31 (2)	-1 (2)	2 (2)	1 (2)
C(23)	39 (2)	38 (3)	34 (2)	7 (2)	4 (2)	3 (2)
C(24)	35 (2)	39 (3)	28 (2)	0 (2)	6 (2)	-1 (2)
C(31)	39 (2)	50 (4)	59 (3)	1 (3)	12 (2)	6 (2)
C(32)	46 (2)	43 (3)	55 (3)	-7 (3)	12 (2)	7 (2)
C(33)	49 (2)	35 (3)	47 (3)	-12 (2)	3 (2)	-1 (2)
C(34)	34 (2)	41 (3)	41 (3)	-3 (2)	2 (2)	-1 (2)
C(35)	29 (2)	32 (3)	35 (2)	-5 (2)	0 (2)	3 (2)
C(36)	33 (2)	30 (3)	31 (2)	-5 (2)	2 (2)	-4 (2)
C(37)	36 (2)	25 (3)	42 (3)	-7 (2)	-4 (2)	5 (2)
C(38)	46 (2)	47 (3)	32 (3)	-2 (2)	-4 (2)	8 (2)
C(39)	65 (3)	56 (4)	42 (3)	-8 (3)	-5 (2)	16 (3)
C(40)	63 (3)	54 (4)	50 (3)	-21 (3)	-23 (3)	12 (2)
C(41)	42 (2)	37 (3)	69 (4)	-9 (3)	-8 (2)	6 (2)
C(42)	37 (2)	30 (3)	43 (3)	-8 (2)	-10 (2)	6 (2)
C(43)	31 (2)	32 (3)	58 (3)	-2 (2)	-1 (2)	-1 (2)
C(44)	32 (2)	31 (3)	45 (3)	-2 (2)	2 (2)	1 (2)

Der Temperaturfaktorexponent hat die Form: $-2\pi^2(h^2 \cdot a^{*2} U_{11}+...+2hka^*b^*U_{12})$

H-Atomkoordinaten [· 10^4] und isotrope Auslenkungsparameter [$Å^2$· 10^3]

	X	Y	Z	U_{eq}
H(1)	6438	7277	8349	57
H(2)	6437	6839	5635	68
H(3)	8545	7244	5304	76
H(4)	8665	7809	7596	77
H(5)	10793	7515	8750	71
H(6)	11341	6896	6695	76
H(7)	11125	6230	7850	70
H(8)	10187	6710	10224	62
H(11)	4049	6560	5492	56
H(12)	2986	5879	4512	59
H(13)	2986	5213	5870	55
H(14)	4003	5208	8235	45
H(18)	3968	6082	12340	43
H(19)	3066	6772	13205	46
H(20)	3253	7450	11927	50
H(21)	4211	7436	9660	47
H(31)	10978	5541	8357	59
H(32)	10299	4864	7184	57
H(33)	7945	4537	7442	53
H(34)	6258	4907	8836	46
H(38)	5931	5662	13110	50
H(39)	7387	5888	15155	65
H(40)	9658	6267	14922	68
H(41)	10572	6362	12696	60

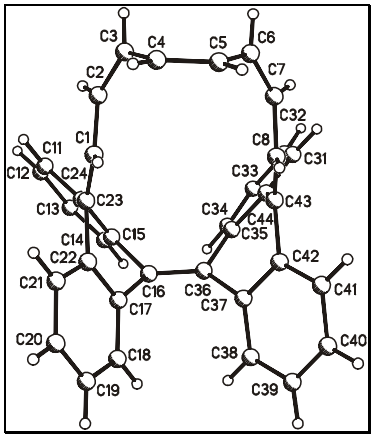

Geometrieparameter

Bindungslängen [Å]

C(1)	- C(23)	1.352	(6)	C(1)	- C(2)	1.433	(6)
C(2)	- C(3)	1.364	(7)	C(3)	- C(4)	1.463	(8)
C(4)	- C(5)	1.347	(8)	C(5)	- C(6)	1.455	(7)
C(6)	- C(7)	1.355	(8)	C(7)	- C(8)	1.422	(7)
C(8)	- C(43)	1.364	(6)	C(11)	- C(24)	1.399	(6)
C(11)	- C(12)	1.399	(7)	C(12)	- C(13)	1.374	(7)
C(13)	- C(14)	1.395	(6)	C(14)	- C(15)	1.388	(6)
C(15)	- C(24)	1.400	(6)	C(15)	- C(16)	1.500	(5)
C(16)	- C(36)	1.351	(5)	C(16)	- C(17)	1.505	(6)
C(17)	- C(22)	1.392	(6)	C(17)	- C(18)	1.399	(5)
C(18)	- C(19)	1.383	(6)	C(19)	- C(20)	1.373	(6)
C(20)	- C(21)	1.400	(6)	C(21)	- C(22)	1.392	(6)
C(22)	- C(23)	1.500	(5)	C(23)	- C(24)	1.481	(6)
C(31)	- C(32)	1.373	(7)	C(31)	- C(44)	1.406	(6)
C(32)	- C(33)	1.393	(6)	C(33)	- C(34)	1.389	(5)
C(34)	- C(35)	1.375	(6)	C(35)	- C(44)	1.426	(5)
C(35)	- C(36)	1.508	(5)	C(36)	- C(37)	1.477	(6)
C(37)	- C(38)	1.405	(6)	C(37)	- C(42)	1.415	(5)
C(38)	- C(39)	1.391	(7)	C(39)	- C(40)	1.391	(7)
C(40)	- C(41)	1.377	(7)	C(41)	- C(42)	1.391	(6)
C(42)	- C(43)	1.498	(6)	C(43)	- C(44)	1.474	(6)

Bindungswinkel [°]

C(23)	- C(1) - C(2)	126.7	(5)	C(3)	- C(2) - C(1)	121.6	(5)
C(2)	- C(3) - C(4)	125.0	(4)	C(5)	- C(4) - C(3)	121.3	(5)
C(4)	- C(5) - C(6)	119.3	(5)	C(7)	- C(6) - C(5)	125.6	(5)
C(6)	- C(7) - C(8)	124.5	(5)	C(43)	- C(8) - C(7)	127.2	(5)
C(24)	- C(11) - C(12)	119.7	(5)	C(13)	- C(12) - C(11)	119.9	(4)
C(12)	- C(13) - C(14)	121.2	(5)	C(15)	- C(14) - C(13)	119.2	(4)
C(14)	- C(15) - C(24)	120.4	(4)	C(14)	- C(15) - C(16)	124.4	(4)
C(24)	- C(15) - C(16)	115.1	(4)	C(36)	- C(16) - C(15)	124.0	(3)
C(36)	- C(16) - C(17)	122.4	(4)	C(15)	- C(16) - C(17)	110.0	(3)
C(22)	- C(17) - C(18)	119.2	(4)	C(22)	- C(17) - C(16)	114.6	(3)
C(18)	- C(17) - C(16)	126.2	(4)	C(19)	- C(18) - C(17)	120.1	(4)
C(20)	- C(19) - C(18)	120.8	(3)	C(19)	- C(20) - C(21)	119.8	(4)
C(22)	- C(21) - C(20)	119.6	(4)	C(17)	- C(22) - C(21)	120.4	(3)
C(17)	- C(22) - C(23)	117.9	(4)	C(21)	- C(22) - C(23)	121.7	(4)
C(1)	- C(23) - C(24)	127.6	(4)	C(1)	- C(23) - C(22)	120.8	(4)

C(24) - C(23) - C(22)	111.4	(3)	C(11) - C(24) - C(15)	119.6	(4)
C(11) - C(24) - C(23)	122.6	(4)	C(15) - C(24) - C(23)	117.5	(4)
C(32) - C(31) - C(44)	121.3	(4)	C(31) - C(32) - C(33)	120.2	(4)
C(34) - C(33) - C(32)	119.7	(4)	C(35) - C(34) - C(33)	121.0	(4)

Bindungswinkel [°]

C(34) - C(35) - C(44)	120.1	(3)	C(34) - C(35) - C(36)	126.4	(3)
C(44) - C(35) - C(36)	113.5	(4)	C(16) - C(36) - C(37)	123.7	(3)
C(16) - C(36) - C(35)	123.2	(4)	C(37) - C(36) - C(35)	111.1	(3)
C(38) - C(37) - C(42)	118.5	(4)	C(38) - C(37) - C(36)	125.6	(4)
C(42) - C(37) - C(36)	115.9	(3)	C(39) - C(38) - C(37)	120.9	(4)
C(38) - C(39) - C(40)	119.4	(4)	C(41) - C(40) - C(39)	120.6	(5)
C(40) - C(41) - C(42)	120.7	(4)	C(41) - C(42) - C(37)	119.7	(4)
C(41) - C(42) - C(43)	124.2	(4)	C(37) - C(42) - C(43)	115.9	(4)
C(8) - C(43) - C(44)	126.1	(4)	C(8) - C(43) - C(42)	121.0	(4)
C(44) - C(43) - C(42)	112.8	(4)	C(31) - C(44) - C(35)	117.8	(4)
C(31) - C(44) - C(43)	124.3	(3)	C(35) - C(44) - C(43)	117.9	(3)

Torsionswinkel [°]

C(23) - C(1) - C(2) - C(3)	-158.9	(5)	C(1) - C(2) - C(3) - C(4)	3.4	(9)
C(2) - C(3) - C(4) - C(5)	102.8	(6)	C(3) - C(4) - C(5) - C(6)	2.8	(7)
C(4) - C(5) - C(6) - C(7)	-103.8	(7)	C(5) - C(6) - C(7) - C(8)	-2.6	(9)
C(6) - C(7) - C(8) - C(43)	149.2	(5)	C(24) - C(11) - C(12) - C(13)	-0.3	(6)
C(11) - C(12) - C(13) - C(14)	0.4	(6)	C(12) - C(13) - C(14) - C(15)	-0.7	(5)
C(13) - C(14) - C(15) - C(24)	0.9	(5)	C(13) - C(14) - C(15) - C(16)	177.2	(3)
C(14) - C(15) - C(16) - C(36)	72.5	(5)	C(24) - C(15) - C(16) - C(36)	-111.1	(4)
C(14) - C(15) - C(16) - C(17)	-128.6	(3)	C(24) - C(15) - C(16) - C(17)	47.9	(4)
C(36) - C(16) - C(17) - C(22)	110.1	(4)	C(15) - C(16) - C(17) - C(22)	-49.2	(4)
C(36) - C(16) - C(17) - C(18)	-69.2	(5)	C(15) - C(16) - C(17) - C(18)	131.5	(4)
C(22) - C(17) - C(18) - C(19)	-1.1	(6)	C(16) - C(17) - C(18) - C(19)	178.1	(4)
C(17) - C(18) - C(19) - C(20)	-1.1	(6)	C(18) - C(19) - C(20) - C(21)	2.3	(6)
C(19) - C(20) - C(21) - C(22)	-1.2	(6)	C(18) - C(17) - C(22) - C(21)	2.2	(6)
C(16) - C(17) - C(22) - C(21)	-177.1	(3)	C(18) - C(17) - C(22) - C(23)	-174.9	(3)
C(16) - C(17) - C(22) - C(23)	5.8	(5)	C(20) - C(21) - C(22) - C(17)	-1.1	(6)
C(20) - C(21) - C(22) - C(23)	176.0	(4)	C(2) - C(1) - C(23) - C(24)	1.4	(8)
C(2) - C(1) - C(23) - C(22)	174.6	(5)	C(17) - C(22) - C(23) - C(1)	-135.2	(4)
C(21) - C(22) - C(23) - C(1)	47.7	(6)	C(17) - C(22) - C(23) - C(24)	39.0	(5)
C(21) - C(22) - C(23) - C(24)	-138.1	(4)	C(12) - C(11) - C(24) - C(15)	0.4	(5)
C(12) - C(11) - C(24) - C(23)	-173.8	(3)	C(14) - C(15) - C(24) - C(11)	-0.8	(5)
C(16) - C(15) - C(24) - C(11)	-177.4	(3)	C(14) - C(15) - C(24) - C(23)	173.7	(3)
C(16) - C(15) - C(24) - C(23)	-2.9	(4)	C(1) - C(23) - C(24) - C(11)	-52.3	(6)
C(22) - C(23) - C(24) - C(11)	133.9	(4)	C(1) - C(23) - C(24) - C(15)	133.3	(4)
C(22) - C(23) - C(24) - C(15)	-40.5	(5)	C(44) - C(31) - C(32) - C(33)	-1.7	(8)
C(31) - C(32) - C(33) - C(34)	1.0	(7)	C(32) - C(33) - C(34) - C(35)	0.9	(7)
C(33) - C(34) - C(35) - C(44)	-2.2	(7)	C(33) - C(34) - C(35) - C(36)	179.4	(4)
C(15) - C(16) - C(36) - C(37)	164.2	(4)	C(17) - C(16) - C(36) - C(37)	7.7	(6)
C(15) - C(16) - C(36) - C(35)	1.4	(6)	C(17) - C(16) - C(36) - C(35)	-155.0	(4)
C(34) - C(35) - C(36) - C(16)	-64.4	(6)	C(44) - C(35) - C(36) - C(16)	117.1	(4)
C(34) - C(35) - C(36) - C(37)	130.9	(5)	C(44) - C(35) - C(36) - C(37)	-47.6	(5)
C(16) - C(36) - C(37) - C(38)	66.4	(6)	C(35) - C(36) - C(37) - C(38)	-129.0	(4)
C(16) - C(36) - C(37) - C(42)	-115.0	(4)	C(35) - C(36) - C(37) - C(42)	49.6	(5)
C(42) - C(37) - C(38) - C(39)	1.1	(7)	C(36) - C(37) - C(38) - C(39)	179.7	(4)
C(37) - C(38) - C(39) - C(40)	1.8	(7)	C(38) - C(39) - C(40) - C(41)	-3.0	(8)
C(39) - C(40) - C(41) - C(42)	1.2	(8)	C(40) - C(41) - C(42) - C(37)	1.7	(7)
C(40) - C(41) - C(42) - C(43)	-173.3	(5)	C(38) - C(37) - C(42) - C(41)	-2.9	(6)
C(36) - C(37) - C(42) - C(41)	178.4	(4)	C(38) - C(37) - C(42) - C(43)	172.5	(4)
C(36) - C(37) - C(42) - C(43)	-6.2	(6)	C(7) - C(8) - C(43) - C(44)	-4.9	(8)
C(7) - C(8) - C(43) - C(42)	177.5	(5)	C(41) - C(42) - C(43) - C(8)	-45.4	(7)
C(37) - C(42) - C(43) - C(8)	139.4	(4)	C(41) - C(42) - C(43) - C(44)	136.7	(4)

C(37)	- C(42) -	C(43) -	C(44)	-38.5	(5)		
C(32)	- C(31) -	C(44) -	C(43)	177.3	(5)		
C(36)	- C(35) -	C(44) -	C(31)	-179.9	(4)		
C(36)	- C(35) -	C(44) -	C(43)	3.1	(6)		
C(42)	- C(43) -	C(44) -	C(31)	-136.8	(4)		
C(42)	- C(43) -	C(44) -	C(35)	40.0	(6)		
C(32)	- C(31) -	C(44) -	C(35)	0.5	(7)		
C(34)	- C(35) -	C(44) -	C(31)	1.5	(6)		
C(34)	- C(35) -	C(44) -	C(43)	-175.6	(4)		
C(8)	- C(43) -	C(44) -	C(31)	45.4	(7)		
C(8)	- C(43) -	C(44) -	C(35)	-137.8	(4)		

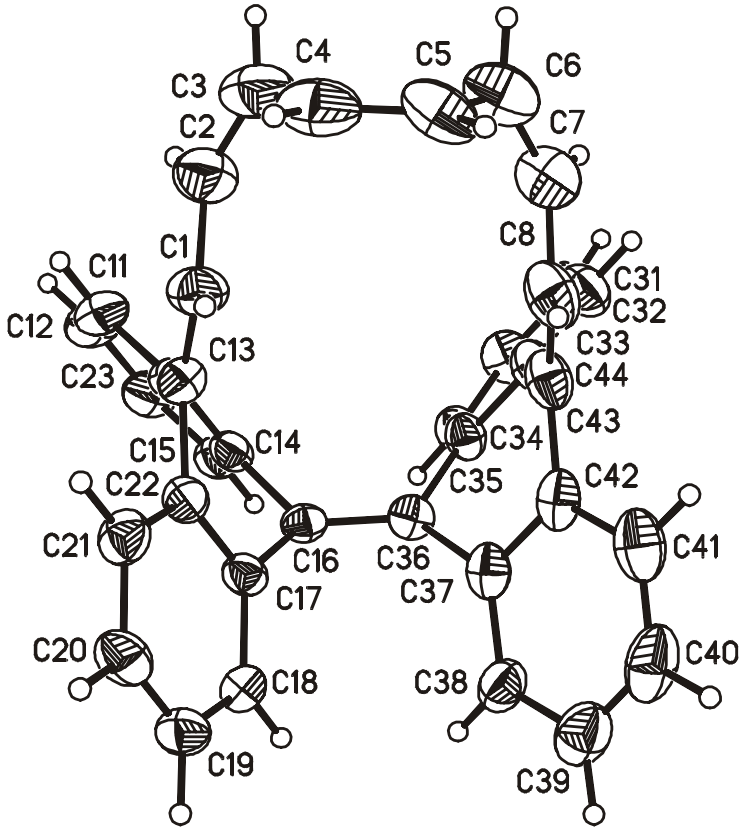

7.4.6 X-ray structure of the C_1 Möbius 39

Einkristallstrukturbestimmung von $C_{36}H_{24}$

Messprotokoll

Kristall Daten:

Verbindung:	$C_{36}H_{24}$
Formel:	$C_{36}H_{24}$
Kristall-Farbe, -Habitus:	Transparente, farblose Nadel
Kristallformat:	0.25 mm · 0.06 mm · 0.05 mm
Molekulargewicht:	456.55 g/mol
Raumgruppe:	monoklin $P2_1/c$; IT – Nr.: 14
Berechnete Dichte:	1.256 g · cm^3
F(000):	960

Gitterparameter Least-Squares-Verfeinerung von 8000 Reflexlagen im Winkelbereich
zwischen $8° \leq 2\theta \leq 54°$
a =9.6883 (7) Å α = 90.00
b = 16.545 (1) Å β = 100.90 (1) °
c =15.342 (1) Å γ = 90.0
V = 2414.7 (3) Å^3
Z = 4

Datensammlung

Gerät: STOE Imaging Plate Diffraction System (IPDS)

Strahlung: Mo-Kα; 71.073 pm; Graphit-Monochromator

Messtemperatur: 150 K

Messbereich: $3° \leq 2\theta \leq 52°$
$-11 \leq h \leq 11$
$-20 \leq k \leq 19$
$-17 \leq l \leq 18$

Messbereich in Phi: 0-104° (174 Bilder a 0.6°)

Belichtungszeit/Bild 20 min.

Phi-Messmodus: Oszillierend

Detektor-Abstand: 70 mm

Indizierung: 830 Reflexe

Mosaikbreite: 0.014

Integration: Dynamische Profile

Orientierungskontrolle: min.: 80/ max.: 300

Strukturlösung und Verfeinerung:

Reflexe: 10091 gemessene Reflexe
174 systematische ausgelöschte Reflexe
4658 unabhängige Reflexe
0 unterdrückte Reflexe
4658 unabhängige Reflexe zu Verfeinerung verwendet
2727 unabhängige Reflexe mit Fo>4σ(Fo)

Durchschnittliches I/σ(I) 7.67

$R_{int.}$: $\Sigma |F_o^2-(F_o^2)mean| / [\Sigma F_o^2] = 0.0771$

Absorptionskorrektur: keine; μ = 0.07 mm^{-1}

Strukturlösung: Direkte Methoden (SHELXS-97)

Strukturverfeinerung: Full-Matrix Least-Squares gegen F^2 (SHELXL-97)

Parameter: In der asymmetrischen Einheit:
36 C-Atome anisotrope Auslenkungsparameter
24 H-Atome isotrope Auslenkungsparameter
326 Parameter full matrix verfeinert

Reflexe pro Parameter: 14.3

Wasserstoffatome: Die Wasserstoffatome wurden geometrisch ideal positioniert (d_{C-H}(aromatisch) = 0.95) und mit festen isotropen

Auslenkungsparametern [$U_{iso} = 1.2 \times U_{eq}(C_{aromatisch})$] nach dem Reitermodell verfeinert.

Atomformfaktoren:	Für Neutralatome
LP-Korrektur:	*J*a
Extinktionskorrektur:	$F^* = F_c (k[1 + 0.001 \cdot x \cdot F_c^2 \cdot \lambda^3 / \sin(2\theta)]^{-0.25})$ x = 0.007 (2)
Gewichtung:	$w = 1/[\sigma^2(F_o^2) + (0.0639 \cdot P)^2]$; $P = (\mathrm{Max}(F_o^2,0) + 2 \cdot F_c^2) / 3$
Shift/Error:	≤ 0.001 im letzten Verfeinerungszyklus
Restelektronendichte:	Max.: 0.23 / Min.: -0.20 e/Å^3
R1 für 2727 Fo>4σ(Fo)	$R1 = \Sigma \lvert \lvert Fo \rvert - \lvert Fc \rvert \rvert / \Sigma \lvert Fo \rvert$ = 0.0542
R1 für alle 4658 Reflexe	= 0.1082
wR2 für 2727 Fo>4σ(Fo)	$wR2 = [\Sigma[w(F_o^2 - F_c^2)^2] / \Sigma[w(F_o^2)^2]]^{1/2}$ = 0.1184
wR2 für alle 4658 Reflexe	= 0.1397
Goodness of fit (Alle R.)	$S = [\Sigma[w(F_o^2 - F_c^2)^2] / (n-p)]^{1/2}$ = 0.959
Restrained GoF (Alle R.)	= 0.959
Restraints	0

Bemerkungen:

Datensammlung und Datenreduktion: STOE IPDS-Programmpaket; Graphik: SHELXTL PC XP;

Graphik: SHELXTL PC XP; Erstellung von Tabellen: SHELXL-97 CIFTAB

Atomkoordinaten [· 10^4] und äquivalente isotrope Auslenkungsparameter [Å^2· 10^3]

	X		Y		Z		U_{eq}	
C(1)	5486	(3)	6624	(2)	2740	(2)	34	(1)
C(2)	4893	(3)	6060	(2)	2041	(2)	40	(1)
C(3)	5478	(3)	5343	(2)	1919	(2)	41	(1)
C(4)	6899	(3)	5108	(2)	2338	(2)	40	(1)
C(5)	7971	(3)	5632	(2)	2412	(2)	32	(1)
C(6)	9448	(3)	5484	(2)	2790	(2)	36	(1)
C(7)	10471	(3)	5975	(2)	2607	(2)	37	(1)
C(8)	10135	(2)	6610	(2)	1926	(2)	32	(1)
C(11)	5973	(3)	7649	(2)	4426	(2)	34	(1)
C(12)	6466	(3)	8140	(2)	5148	(2)	37	(1)
C(13)	7136	(3)	8859	(2)	5047	(2)	38	(1)
C(14)	7410	(3)	9071	(2)	4220	(2)	32	(1)
C(15)	6972	(2)	8573	(1)	3484	(2)	26	(1)
C(16)	7230	(2)	8730	(1)	2574	(2)	22	(1)
C(17)	5874	(2)	8687	(1)	1915	(2)	23	(1)

C(18)	5391	(2)	9286	(2)	1300	(2)	30 (1)
C(19)	4105	(3)	9194	(2)	721	(2)	40 (1)
C(20)	3283	(3)	8517	(2)	781	(2)	41 (1)
C(21)	3725	(2)	7939	(2)	1415	(2)	35 (1)
C(22)	5015	(2)	8007	(2)	1998	(2)	28 (1)
C(23)	5522	(2)	7448	(2)	2755	(2)	28 (1)
C(24)	6178	(2)	7879	(2)	3572	(2)	28 (1)
C(31)	11905	(2)	7694	(2)	3436	(2)	32 (1)
C(32)	12385	(2)	8188	(2)	4155	(2)	35 (1)
C(33)	11646	(3)	8874	(2)	4298	(2)	34 (1)
C(34)	10385	(2)	9062	(2)	3729	(2)	29 (1)
C(35)	9858	(2)	8561	(1)	3014	(2)	24 (1)
C(36)	8527	(2)	8714	(1)	2357	(2)	21 (1)
C(37)	8783	(2)	8630	(1)	1428	(2)	23 (1)
C(38)	8329	(2)	9169	(2)	731	(2)	29 (1)
C(39)	8567	(3)	9020	(2)	-119	(2)	34 (1)
C(40)	9243	(3)	8323	(2)	-296	(2)	35 (1)
C(41)	9750	(2)	7795	(2)	387	(2)	31 (1)
C(42)	9558	(2)	7946	(1)	1256	(2)	25 (1)
C(43)	10152	(2)	7421	(1)	2017	(2)	26 (1)
C(44)	10645	(2)	7875	(1)	2850	(2)	24 (1)

Äquivalente isotrope U berechnet als ein Drittel der Spur des orthogonalen U_{ij} Tensors

Anisotrope Auslenkungsparameter [$Å^2 \cdot 10^3$]

	U_{11}	U_{22}	U_{33}	U_{23}	U_{13}	U_{12}
C(1)	29 (1)	39 (1)	35 (2)	5 (1)	9 (1)	0 (1)
C(2)	35 (1)	44 (2)	41 (2)	1 (1)	6 (1)	-9 (1)
C(3)	47 (2)	35 (1)	43 (2)	0 (1)	11 (1)	-15 (1)
C(4)	61 (2)	27 (1)	35 (2)	0 (1)	17 (1)	-5 (1)
C(5)	48 (2)	25 (1)	26 (2)	-1 (1)	11 (1)	2 (1)
C(6)	53 (2)	24 (1)	31 (2)	-1 (1)	9 (1)	9 (1)
C(7)	39 (1)	30 (1)	38 (2)	-4 (1)	-1 (1)	8 (1)
C(8)	29 (1)	32 (1)	33 (2)	-2 (1)	3 (1)	2 (1)
C(11)	26 (1)	45 (2)	32 (2)	8 (1)	9 (1)	10 (1)
C(12)	34 (1)	54 (2)	24 (2)	7 (1)	8 (1)	13 (1)
C(13)	35 (1)	52 (2)	27 (2)	-4 (1)	3 (1)	10 (1)
C(14)	30 (1)	42 (1)	25 (2)	-2 (1)	5 (1)	10 (1)
C(15)	22 (1)	32 (1)	23 (1)	4 (1)	5 (1)	11 (1)
C(16)	26 (1)	20 (1)	20 (1)	1 (1)	3 (1)	5 (1)
C(17)	21 (1)	28 (1)	21 (1)	-2 (1)	6 (1)	3 (1)
C(18)	25 (1)	40 (1)	26 (2)	8 (1)	6 (1)	9 (1)
C(19)	33 (1)	55 (2)	30 (2)	11 (1)	3 (1)	14 (1)
C(20)	20 (1)	70 (2)	32 (2)	-3 (1)	-1 (1)	4 (1)
C(21)	23 (1)	48 (2)	34 (2)	-3 (1)	6 (1)	-1 (1)
C(22)	19 (1)	36 (1)	28 (2)	-5 (1)	8 (1)	1 (1)
C(23)	18 (1)	32 (1)	35 (2)	3 (1)	11 (1)	2 (1)
C(24)	21 (1)	36 (1)	27 (2)	5 (1)	7 (1)	12 (1)
C(31)	21 (1)	41 (1)	34 (2)	6 (1)	5 (1)	5 (1)
C(32)	21 (1)	51 (2)	30 (2)	7 (1)	0 (1)	-3 (1)
C(33)	32 (1)	44 (2)	24 (2)	0 (1)	0 (1)	-11 (1)
C(34)	29 (1)	30 (1)	26 (2)	3 (1)	2 (1)	-5 (1)
C(35)	25 (1)	25 (1)	22 (1)	3 (1)	6 (1)	-3 (1)
C(36)	24 (1)	18 (1)	21 (1)	-1 (1)	2 (1)	-1 (1)
C(37)	18 (1)	26 (1)	23 (1)	-2 (1)	2 (1)	-5 (1)
C(38)	25 (1)	34 (1)	26 (2)	3 (1)	3 (1)	-2 (1)
C(39)	32 (1)	46 (2)	23 (2)	8 (1)	6 (1)	-2 (1)
C(40)	35 (1)	48 (2)	22 (2)	-1 (1)	8 (1)	-5 (1)
C(41)	28 (1)	36 (1)	34 (2)	-6 (1)	12 (1)	-4 (1)
C(42)	18 (1)	28 (1)	29 (2)	-1 (1)	6 (1)	-4 (1)
C(43)	16 (1)	31 (1)	32 (2)	2 (1)	7 (1)	-1 (1)
C(44)	20 (1)	27 (1)	26 (1)	6 (1)	6 (1)	0 (1)

Der Temperaturfaktorexponent hat die Form: $-2\pi^2(h^2 \cdot a^{*2} U_{11}+...+2hka^*b^*U_{12})$

H-Atomkoordinaten [· 10^4] und isotrope Auslenkungsparameter [$Å^2$· 10^3]

	X	Y	Z	U_{eq}
H(1)	5925	6375	3279	41
H(2)	4047	6206	1651	48
H(3)	4930	4965	1535	50
H(4)	7068	4574	2562	48
H(5)	7742	6161	2193	39
H(6)	9696	5033	3171	43
H(7)	11410	5910	2919	44
H(8)	9866	6420	1333	38
H(11)	5498	7160	4504	41
H(12)	6341	7979	5722	45
H(13)	7409	9208	5541	46
H(14)	7899	9558	4155	38
H(18)	5936	9760	1273	36
H(19)	3792	9595	286	48
H(20)	2412	8453	382	50
H(21)	3143	7484	1458	42
H(31)	12430	7229	3338	38
H(32)	13229	8056	4553	41
H(33)	11997	9218	4785	41
H(34)	9882	9535	3830	34
H(38)	7847	9648	841	34
H(39)	8263	9399	-580	41
H(40)	9361	8207	-884	41
H(41)	10235	7321	267	38

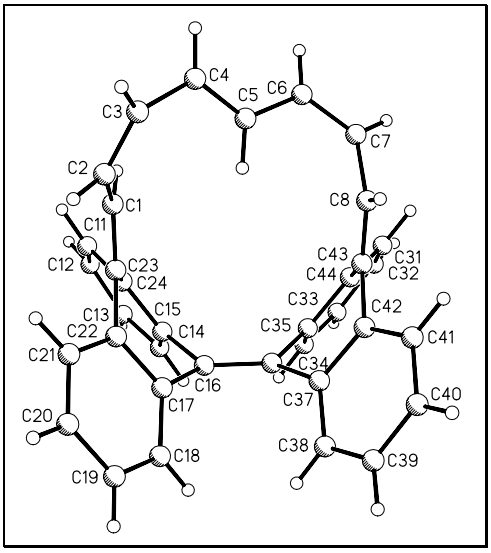

Geometrieparameter

Bindungslängen [Å]

C(1)	- C(23)	1.363	(4)	C(1)	- C(2)	1.455	(4)
C(2)	- C(3)	1.343	(4)	C(3)	- C(4)	1.458	(4)
C(4)	- C(5)	1.341	(4)	C(5)	- C(6)	1.459	(4)
C(6)	- C(7)	1.351	(4)	C(7)	- C(8)	1.476	(4)
C(8)	- C(43)	1.349	(3)	C(11)	- C(12)	1.384	(4)
C(11)	- C(24)	1.415	(4)	C(12)	- C(13)	1.377	(4)
C(13)	- C(14)	1.390	(4)	C(14)	- C(15)	1.397	(4)
C(15)	- C(24)	1.403	(3)	C(15)	- C(16)	1.488	(3)
C(16)	- C(36)	1.359	(3)	C(16)	- C(17)	1.500	(3)
C(17)	- C(18)	1.387	(3)	C(17)	- C(22)	1.419	(3)
C(18)	- C(19)	1.394	(4)	C(19)	- C(20)	1.388	(4)
C(20)	- C(21)	1.374	(4)	C(21)	- C(22)	1.397	(4)
C(22)	- C(23)	1.494	(4)	C(23)	- C(24)	1.477	(4)
C(31)	- C(32)	1.380	(4)	C(31)	- C(44)	1.405	(3)
C(32)	- C(33)	1.381	(4)	C(33)	- C(34)	1.396	(4)
C(34)	- C(35)	1.392	(4)	C(35)	- C(44)	1.417	(3)
C(35)	- C(36)	1.500	(3)	C(36)	- C(37)	1.499	(3)
C(37)	- C(38)	1.398	(3)	C(37)	- C(42)	1.411	(3)
C(38)	- C(39)	1.389	(4)	C(39)	- C(40)	1.378	(4)
C(40)	- C(41)	1.382	(4)	C(41)	- C(42)	1.402	(4)
C(42)	- C(43)	1.482	(4)	C(43)	- C(44)	1.481	(4)

Bindungswinkel [°]

C(23)	- C(1) - C(2)	131.3	(3)	C(3)	- C(2) - C(1)	123.4	(3)
C(2)	- C(3) - C(4)	124.3	(3)	C(5)	- C(4) - C(3)	121.1	(2)
C(4)	- C(5) - C(6)	127.7	(2)	C(7)	- C(6) - C(5)	121.3	(2)
C(6)	- C(7) - C(8)	120.2	(2)	C(43)	- C(8) - C(7)	129.7	(3)
C(12)	- C(11) - C(24)	119.7	(3)	C(13)	- C(12) - C(11)	121.1	(3)
C(12)	- C(13) - C(14)	119.7	(3)	C(13)	- C(14) - C(15)	120.5	(3)
C(14)	- C(15) - C(24)	119.6	(2)	C(14)	- C(15) - C(16)	125.2	(2)
C(24)	- C(15) - C(16)	115.2	(2)	C(36)	- C(16) - C(15)	123.6	(2)
C(36)	- C(16) - C(17)	124.5	(2)	C(15)	- C(16) - C(17)	110.1	(2)
C(18)	- C(17) - C(22)	120.0	(2)	C(18)	- C(17) - C(16)	124.4	(2)
C(22)	- C(17) - C(16)	115.5	(2)	C(17)	- C(18) - C(19)	120.0	(2)
C(20)	- C(19) - C(18)	120.1	(3)	C(21)	- C(20) - C(19)	120.2	(2)
C(20)	- C(21) - C(22)	121.2	(3)	C(21)	- C(22) - C(17)	118.4	(2)
C(21)	- C(22) - C(23)	124.7	(2)	C(17)	- C(22) - C(23)	116.7	(2)
C(1)	- C(23) - C(24)	120.2	(2)	C(1)	- C(23) - C(22)	127.0	(3)
C(24)	- C(23) - C(22)	112.7	(2)	C(15)	- C(24) - C(11)	119.0	(2)

C(15) - C(24) - C(23)	118.1	(2)	C(11) - C(24) - C(23)	122.8	(2)
C(32) - C(31) - C(44)	120.4	(2)	C(31) - C(32) - C(33)	120.5	(2)

Bindungswinkel [°]

C(32) - C(33) - C(34)	120.1	(3)	C(35) - C(34) - C(33)	120.5	(2)
C(34) - C(35) - C(44)	119.1	(2)	C(34) - C(35) - C(36)	124.8	(2)
C(44) - C(35) - C(36)	116.0	(2)	C(16) - C(36) - C(37)	124.2	(2)
C(16) - C(36) - C(35)	123.8	(2)	C(37) - C(36) - C(35)	110.3	(2)
C(38) - C(37) - C(42)	118.0	(2)	C(38) - C(37) - C(36)	125.7	(2)
C(42) - C(37) - C(36)	116.2	(2)	C(39) - C(38) - C(37)	121.3	(2)
C(40) - C(39) - C(38)	120.3	(3)	C(39) - C(40) - C(41)	119.6	(3)
C(40) - C(41) - C(42)	121.1	(2)	C(41) - C(42) - C(37)	119.5	(2)
C(41) - C(42) - C(43)	122.9	(2)	C(37) - C(42) - C(43)	117.6	(2)
C(8) - C(43) - C(44)	126.1	(2)	C(8) - C(43) - C(42)	120.4	(2)
C(44) - C(43) - C(42)	113.4	(2)	C(31) - C(44) - C(35)	119.2	(2)
C(31) - C(44) - C(43)	123.0	(2)	C(35) - C(44) - C(43)	117.6	(2)

Torsionswinkel [°]

C(23) - C(1) - C(2) - C(3)	144.7	(3)	C(1) - C(2) - C(3) - C(4)	-13.1	(5)
C(2) - C(3) - C(4) - C(5)	-41.2	(5)	C(3) - C(4) - C(5) - C(6)	-178.3	(3)
C(4) - C(5) - C(6) - C(7)	161.2	(3)	C(5) - C(6) - C(7) - C(8)	-8.2	(4)
C(6) - C(7) - C(8) - C(43)	112.1	(3)	C(24) - C(11) - C(12) - C(13)	1.1	(4)
C(11) - C(12) - C(13) - C(14)	-4.5	(4)	C(12) - C(13) - C(14) - C(15)	2.1	(4)
C(13) - C(14) - C(15) - C(24)	3.7	(3)	C(13) - C(14) - C(15) - C(16)	-178.7	(2)
C(14) - C(15) - C(16) - C(36)	67.2	(3)	C(24) - C(15) - C(16) - C(36)	-115.1	(2)
C(14) - C(15) - C(16) - C(17)	-127.6	(2)	C(24) - C(15) - C(16) - C(17)	50.0	(3)
C(36) - C(16) - C(17) - C(18)	-67.3	(3)	C(15) - C(16) - C(17) - C(18)	127.7	(2)
C(36) - C(16) - C(17) - C(22)	117.8	(2)	C(15) - C(16) - C(17) - C(22)	-47.2	(3)
C(22) - C(17) - C(18) - C(19)	-4.5	(4)	C(16) - C(17) - C(18) - C(19)	-179.2	(2)
C(17) - C(18) - C(19) - C(20)	2.4	(4)	C(18) - C(19) - C(20) - C(21)	0.6	(4)
C(19) - C(20) - C(21) - C(22)	-1.4	(4)	C(20) - C(21) - C(22) - C(17)	-0.7	(4)
C(20) - C(21) - C(22) - C(23)	174.4	(2)	C(18) - C(17) - C(22) - C(21)	3.6	(3)
C(16) - C(17) - C(22) - C(21)	178.8	(2)	C(18) - C(17) - C(22) - C(23)	-171.8	(2)
C(16) - C(17) - C(22) - C(23)	3.3	(3)	C(2) - C(1) - C(23) - C(24)	178.7	(2)
C(2) - C(1) - C(23) - C(22)	-4.6	(4)	C(21) - C(22) - C(23) - C(1)	46.4	(4)
C(17) - C(22) - C(23) - C(1)	-138.4	(2)	C(21) - C(22) - C(23) - C(24)	-136.7	(2)
C(17) - C(22) - C(23) - C(24)	38.4	(3)	C(14) - C(15) - C(24) - C(11)	-7.0	(3)
C(16) - C(15) - C(24) - C(11)	175.2	(2)	C(14) - C(15) - C(24) - C(23)	169.4	(2)
C(16) - C(15) - C(24) - C(23)	-8.4	(3)	C(12) - C(11) - C(24) - C(15)	4.6	(3)
C(12) - C(11) - C(24) - C(23)	-171.6	(2)	C(1) - C(23) - C(24) - C(15)	141.0	(2)
C(22) - C(23) - C(24) - C(15)	-36.1	(3)	C(1) - C(23) - C(24) - C(11)	-42.7	(3)
C(22) - C(23) - C(24) - C(11)	140.1	(2)	C(44) - C(31) - C(32) - C(33)	-1.1	(4)
C(31) - C(32) - C(33) - C(34)	1.7	(4)	C(32) - C(33) - C(34) - C(35)	0.1	(4)
C(33) - C(34) - C(35) - C(44)	-2.4	(3)	C(33) - C(34) - C(35) - C(36)	-179.1	(2)
C(15) - C(16) - C(36) - C(37)	161.5	(2)	C(17) - C(16) - C(36) - C(37)	-1.5	(4)
C(15) - C(16) - C(36) - C(35)	-2.0	(4)	C(17) - C(16) - C(36) - C(35)	-165.1	(2)
C(34) - C(35) - C(36) - C(16)	-63.6	(3)	C(44) - C(35) - C(36) - C(16)	119.6	(2)
C(34) - C(35) - C(36) - C(37)	130.9	(2)	C(44) - C(35) - C(36) - C(37)	-45.9	(3)
C(16) - C(36) - C(37) - C(38)	61.1	(3)	C(35) - C(36) - C(37) - C(38)	-133.5	(2)
C(16) - C(36) - C(37) - C(42)	-119.3	(2)	C(35) - C(36) - C(37) - C(42)	46.1	(3)
C(42) - C(37) - C(38) - C(39)	3.2	(3)	C(36) - C(37) - C(38) - C(39)	-177.1	(2)
C(37) - C(38) - C(39) - C(40)	1.0	(4)	C(38) - C(39) - C(40) - C(41)	-3.4	(4)
C(39) - C(40) - C(41) - C(42)	1.5	(4)	C(40) - C(41) - C(42) - C(37)	2.8	(3)
C(40) - C(41) - C(42) - C(43)	-176.4	(2)	C(38) - C(37) - C(42) - C(41)	-5.1	(3)
C(36) - C(37) - C(42) - C(41)	175.2	(2)	C(38) - C(37) - C(42) - C(43)	174.2	(2)
C(36) - C(37) - C(42) - C(43)	-5.4	(3)	C(7) - C(8) - C(43) - C(44)	5.6	(4)
C(7) - C(8) - C(43) - C(42)	-170.3	(2)	C(41) - C(42) - C(43) - C(8)	-40.6	(3)
C(37) - C(42) - C(43) - C(8)	140.1	(2)	C(41) - C(42) - C(43) - C(44)	143.0	(2)
C(37) - C(42) - C(43) - C(44)	-36.2	(3)	C(32) - C(31) - C(44) - C(35)	-1.2	(4)

C(32) - C(31) - C(44) - C(43)	173.3	(2)	C(34) - C(35) - C(44) - C(31)	3.0	(3)
C(36) - C(35) - C(44) - C(31)	179.9	(2)	C(34) - C(35) - C(44) - C(43)	-171.8	(2)
C(36) - C(35) - C(44) - C(43)	5.2	(3)	C(8) - C(43) - C(44) - C(31)	45.6	(3)
C(42) - C(43) - C(44) - C(31)	-138.2	(2)	C(8) - C(43) - C(44) - C(35)	-139.8	(2)
C(42) - C(43) - C(44) - C(35)	36.3	(3)			

7.4.7 X-ray Structure of the C_2 Möbius 40

Formula sum C_{144} H_{96}

Formula weight 1826.34

Crystal system monoclinic

Space group *C* 1 2/c 1 (no. 15)

Unit cell dimensions *a* = 16.280(2) Å

b = 10.959(1) Å

c = 14.373(2) Å

β = 110.41(2) °

Cell volume 2403.34(1789) $Å^3$

Density, calculated 1.262 g/cm^3

Pearson code mC240

Formula type N2O3

Wyckoff sequence f^{30}

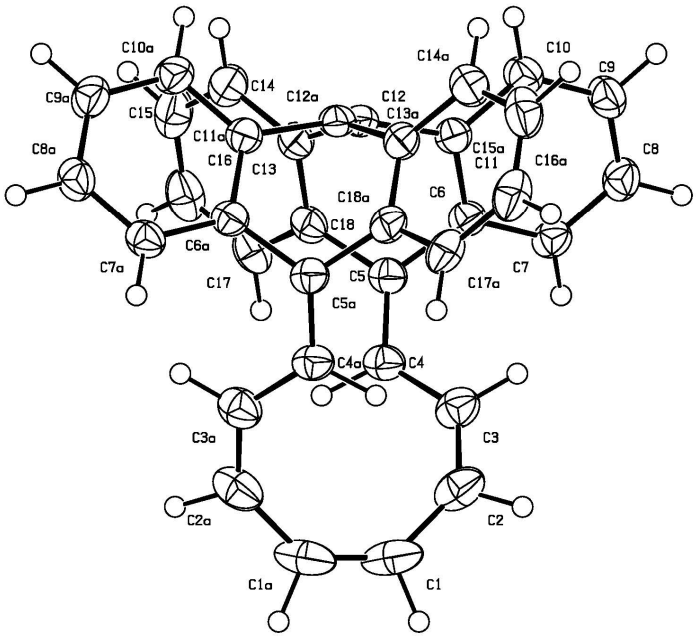
C10a
C14
C12a
C12
C14a
C10
C9
C9a
C15
C11a
C13a
C8a
C16
C13
C15a
C11
C16a
C8
C18a
C6
C18
C6a
C7a
C17
C5
C17a
C7
C5a
C4a
C4
C3a
C3
C2a
C2
C1a
C1

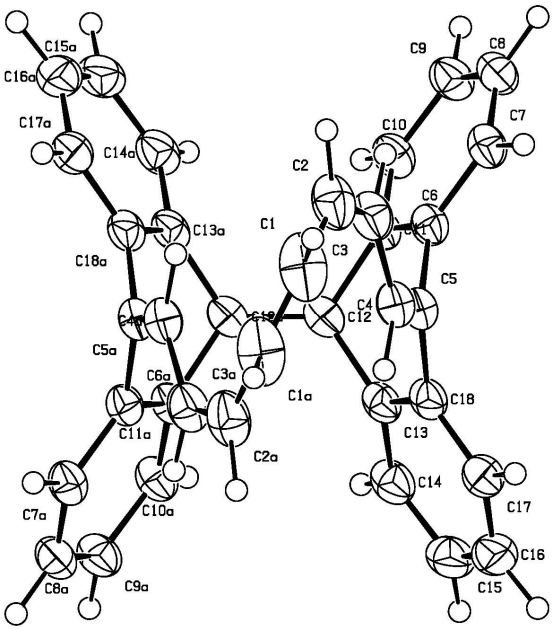
C15a
C16a
C17a
C14a
C13a
C18a
C5a
C6a
C11a
C7a
C8a
C9a
C10a
C2a
C1a
C3a
C1
C2
C3
C4
C12
C6
C5
C9
C8
C7
C10
C18
C13
C14
C17
C16
C15

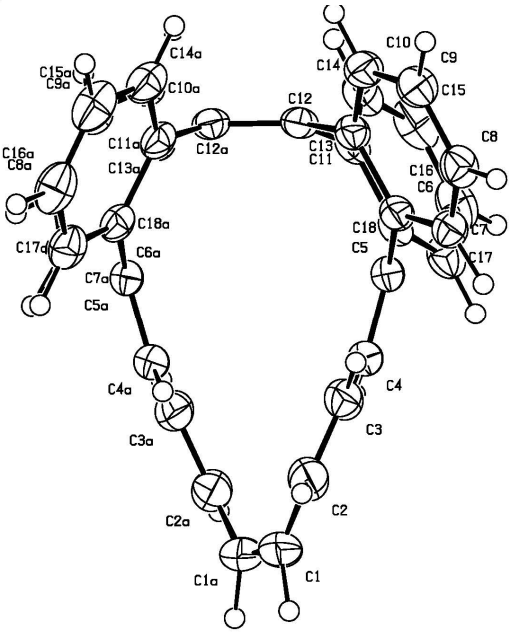
C14a
C15a
C9a
C10a
C11a
C12a
C12
C13
C11
C14
C10
C9
C15
C8
C16a
C8a
C13a
C16
C6
C18a
C18
C7
C17a
C6a
C5
C17
C7a
C5a
C4a
C4
C3a
C3
C2a
C2
C1a
C1

Bond distances (Angstroms)

Atom	A	B	Dist						
C1	H1	1.041	C1	C1′	1.337	C1	C2	1.454
C2	H2	1.040	C2	C3	1.347	C2	C1	1.454
C3	H3	1.027	C3	C2	1.347	C3	C4	1.453
C4	H4	1.063	C4	C5	1.354	C4	C3	1.453
C5	C4	1.354	C5	C6	1.486	C5	C18	1.486
C6	C7	1.397	C6	C11	1.410	C6	C5	1.486
C7	H7	0.979	C7	C8	1.386	C7	C6	1.397
C8	H8	0.998	C8	C9	1.385	C8	C7	1.386
C9	H9	0.976	C9	C8	1.385	C9	C10	1.391
C10	H10	0.969	C10	C9	1.391	C10	C11	1.393
C11	C10	1.393	C11	C6	1.410	C11	C12	1.488
C12	C12′	1.351	C12	C11	1.488	C12	C13	1.493
C13	C14	1.390	C13	C18	1.410	C13	C12	1.493
C14	H14	0.969	C14	C13	1.390	C14	C15	1.397
C15	H15	0.995	C15	C16	1.383	C15	C14	1.397
C16	H16	1.000	C16	C15	1.383	C16	C17	1.394
C17	H17	0.989	C17	C16	1.394	C17	C18	1.396
C18	C17	1.396	C18	C13	1.410	C18	C5	1.486
H1	C1	1.041	H2	C2	1.040	H3	C3	1.027
H4	C4	1.063	H7	C7	0.979	H8	C8	0.998
H9	C9	0.976	H10	C10	0.969	H14	C14	0.969
H15	C15	0.995	H16	C16	1.000	H17	C17	0.989

Bond angles (degrees)

Atom	A	B	C	Angle							
H1	C1	C1′	113.01	H1	C1	C2	112.08	C1	C1′	C2	134.83
H2	C2	C3	114.29	H2	C2	C1	112.87	C3	C2	C1	132.78
H3	C3	C2	115.49	H3	C3	C4	114.87	C2	C3	C4	129.60
H4	C4	C5	118.17	H4	C4	C3	118.33	C5	C4	C3	123.00
C4	C5	C6	124.39	C4	C5	C18	123.82	C6	C5	C18	111.43
C7	C6	C11	119.32	C7	C6	C5	123.98	C11	C6	C5	116.59
H7	C7	C8	119.75	H7	C7	C6	119.79	C8	C7	C6	120.36
H8	C8	C9	120.79	H8	C8	C7	119.04	C9	C8	C7	120.16
H9	C9	C8	119.71	H9	C9	C10	119.85	C8	C9	C10	120.42
H10	C10	C9	119.95	H10	C10	C11	120.09	C9	C10	C11	119.96
C10	C11	C6	119.75	C10	C11	C12	126.12	C6	C11	C12	114.09
C12	C12′	C11	122.86	C12	C12′	C13	122.84	C11	C12	C13	110.45
C14	C13	C18	119.86	C14	C13	C12	126.08	C18	C13	C12	114.06
H14	C14	C13	119.65	H14	C14	C15	120.45	C13	C14	C15	119.88
H15	C15	C16	121.89	H15	C15	C14	117.82	C16	C15	C14	120.28
H16	C16	C15	120.01	H16	C16	C17	119.53	C15	C16	C17	120.43
H17	C17	C16	120.1	H17	C17	C18	120.07	C16	C17	C18	119.78
C17	C18	C13	119.71	C17	C18	C5	123.72	C13	C18	C5	116.48

8. References

[1] H. W. Kroto, J.R. Heath, S. C. O'Brien, F.R. Curl, R.E. Smalley, *Nature* **1985**, 318, 162.

[2] S. Iijima, *Nature* **1991**, 354,56.

[3] P. J. F.Hariss, Carbon Nanotubes and Related structures New Materials for the Twenty-First century, cambrige university press 1999.

[4] M. Faraday, *Phil. Trans. Roy. London* **1825**, 440.

[5] A. Kekule', *Bull. Soc. Chim. Paris* **1865**, 3, 98.

[6] E. Erlenmeyer, *Ann*., **1866**, 327.

[7] P. Pascal, *Ann. Chim. Phys*., **1910**, 19, 5.

[8] J.W. Amirt, R. Robinson, *J. Chem. Soc*., **1925**, 127, 1604.

[9] E. Hückel, *Z. Physik* **1931**, 70, 310.

[10] L. Pauling, *J. Chem. Phys*., **1936**, 4, 673.

[11] F. London, *J. Phys. Radium* **1937**, 8, 397.

[12] J.A. Polpe, *J. Chem. Phys*., **1956**, 24, 1111.

[13] R. Heillborner *Tetrahedron*, **1964**.

[14] H. J. Dauben, J. D. Wilson, J. L. Laity, *J. Am. Chem. Soc*., **1968**, 90, 811.

[15] R.C. Benson, W. H. Flygare, *J. Am. Chem. Soc*., **1970**, 92, 7523.

[16] W. Kutzelnigg, *Isr. J. Chem*., **1980**, 19, 193.

[17] P.v.R. Schleyer, C. Maerker, A. Dransfeld, H. Jiao, N.J. Hommes, *J. Am. Chem. Soc*., **1996**, 118, 6317.

[18] R. Herges, D, Geuenich, *J. Phys. Chem.A*, **2001**, 105,3214.

[19] M. Bühl, A. Hirsch, *Chem. Rev*., **2001**, 101, 1153.

[20] K.M. Kadish, R.S. Ruoff, Fullerenes, Wiley Interscience 2000.

[21] N.S. Goroff, *Acc. Chem. Res*., **1996**, 29, 77.

[22] K. Jinno, Y. Sato, H. Nagashima, K. Itoh, *J. Microcolumn. Sep*., **1998**, 10, 79.

[23] L. T. Scott, M. M. Mcmahon, B. J. Hagen, J. Mack, J. Blank, H. Wagner, A. de Meijere, *Science*, **2002**, 295, 1500.

[24] J. W. Mintnire, B. I. Dunlap, C.T.White, *Phys. Rev. Lett.* , **1992**, 68, 631.

[25] G.Overney, W. Zhong, D. Tomanek, *Z. Phys. D*, **1993**, 27, 93.

[26] S. Iijima, T. Ichihashi, *Nature* **1993**, 363, 603.

[27] A. G. Rinzler, J. H. Hafner, P. Nikolaev, L. Lou, D. Tomanek, R. E. Smalley, *Science* **1995**, 269, 1550.

[28] A. Thess et al., *Science* **1996**, 273, 483.

[29] S.J. Tans, M.H. Devoret, H. Dai, R.E. Smalley, C. Dekker, *Nature* **1997**, 386, 377.

[30] A.C. Dilon, K.M. Jones, T.A. Bekkendahl, C.H. Kiang, D.S. Bethune, M.J. Heben, *Nature* **1997**, 386, 377.

[31] Z.F. Ren et al., *Science* **1998**, 282, 1105.

[32] B.W. Smith, M. Monthioux, D.E. Luzzi, *Nature* **1998**, 396, 323.

[33] S. Berber, Y.K. Kwon, D. Tomanek, *Phys. Rev. Lett.*, **2000**, 84, 4613.

[34] B. Vigolo te al. , *Science* **2000**, 290,1331.

[35] P. C. Collins, M.S. Arnold, P. Avouris, *Science* **2001**, 292, 706.

[36] M. Kociak et al., *Phys. Rev. Lett.*, **2001**, 86, 2416.

[37] N. Wang, Z.K. Tang, G.D. Li, J.S. Chen, *Nature* **2002**, 408, 51

[38] .S. Ihara, S. Itoh, J. Kitakami, *J. Phys. Rev. B*, **1993**, 47, 12908.

[39] S. Iijima, *Mat. Sci. Eng. B.*, **1993**, 19, 172.

[40] S. Amelinckx, B. Zhang, D. Bernaerts, V. Ivanov, *Science* **1994**, 265, 635.

[41] T. Guo, P. Nikoleav, A.G. Rinzler, R.E. Smalley, *J. Phys. Chem.*, **1995**, 99, 10, 694.

[42] W.K. Hsu, J.P. Hare, M. Terrones, P.F.J. Harries, H.W. Kroto, D.R.M. Walton, *Nature* **1995**, 377, 689.

[43] N. Hamada, S. Sawada, A. Oshiyama, *Phys. Rev. Lett.*, **1992**, 68, 1579.

[44] F. Vögtle, *Top. Curr. Chem.*, **1983**, 115, 157.

[45] R.W. Alder, R.B. Session, *J. Chem. Soc. Perkin. TransII*, **1985**, 1849.

[46] F.H. Kohnke, A.M.Z. Slawin, J.F. Stoddart, D.J. Williams, *Angew. Chem. Int. Ed. Engl.*, **1987**, 26, 892.

[47] S. Kammermeier, P.G. Jones, R. Herges, *Angew. Chem. Int. Ed. Engl.*, **1996**, 35, 2669.

[48] S. Kammermeier, P.G. Jones, R. Herges, *Angew. Chem. Int. Ed. Engl.*, **1997**, 36, 2200.

[49] T. Kawase, H.R. Darabi, M. Oda, *Angew. Chem. Int. Ed. Engl.*, **1996**, 35, 2664.

[50] Y. Kuwatani, T. Yoshida, A. Kusaka, M. Iyoda, *Tetrahedron Lett*., **2000**, 41, 359.

[51] D.E. Appletquist, R.L. Litle, E.C. Fridrich, R.E. Wall, *J. Am. Chem. Soc.,* **1959**, 81, 452.

[52] R.L. Vivattene, F.D. Greene, L.D. Cheung, R. Majeste, L.M. Tretonas, *J. Am. Chem. Soc.,* **1974**, 96, 4342.

[53] L.A. Carpino, *J. Am. Chem. Soc.,* **1960**, 82, 3133.

[54] H. Neumann, Ph.D. Thesis, Universität Erlangen, **1994**.

[55] K.B. Wiberg, M.G. Mattorro, P.J. Okarama, M.E. Jason, *J. Am. Chem. Soc.,* **1984**, 106, 2194.

[56] D.A. Hrovat, W.T. Borden, *J. Am. Chem. Soc.,* **1988**, 110, 4710.

[57] S. Kammermeier, H. Neumann, F. Hampel, R. Herges, *Liebigs Ann. Chem.,* **1996**, 1795.

[58] R. Herges, H. Neumann, *Liebigs Ann. Chem.,* **1995**, 1283.

[59] J.G. Welch, R.H. Magid, *J. Am. Chem. Soc.,* **1967**, 89, 5300.

[60] R. Herges, H. Neumann, F. Hampel, *Angew. Chem. Int. Ed. Engl.,***1994**, 33, 993.

[61] S. Kammermeier, P.G. Jones, R. Herges, *Angew. Chem. Int. Ed. Engl.,***1997**, 36, 2200.

[62] S. Kammermeier, R. Herges, *Angew. Chem. Int. Ed. Engl.,***1996** , 35, 417.

[63] S. Kammermeier, P.G. Jones, R. Herges, *Angew. Chem. Int. Ed. Engl.,***1996** 35, 2669.

[64] L.C. Qin, X. Zhao, K. Hirahara, Y. Miyamoto, Y. Ando, S. Iijima, *Natue* **2000**, 408, 50.

[65] C.P. Raj, N.A. Dhas, M. Chrekinski, A. Gedanken, S. Braverman, *Tetrahedron Lett*., **1998**, 39,5413.

[66] R.J. Giguere, T.L. Bray, S.M. Duncan, G. Majetich, *Tetrahedron Lett*., **1986**,27, 4945.

[67] P.A. Grieco, J.J. Nunes, M.D. Gaul, *J. Am. Chem. Soc.*,**1990**,112,4595.

[68] H. Parlar, R. baumann, *Angew. Chem. Int. Ed. Engl.*,**1981**,1, 14.

[69] P. Laszzlo, J. Lucchetti, *Tetrahedron Lett*., **1984**, 4, 387.

[70] M.P. Cava, A.A. Deana, K. Muth, **1959**, 81, 6458.

[71] H. Schmidbaur, *Angew. Chem. Int. Ed. Engl.* , **1997**, 24, 893.

[72] T. Yoshida, Y. Kuwatani, K. Hara, M. Yoshida, H. Matsuyama, M. Iyoda, S. Nagase, *Tetrahedron Lett*., **2001**, 42, 53.

[75] R. F. Heck, *Acc. Chem. Res*., **1979**, 12, 146.

[76] T. Jeffery, *Tetrahedron* **1996**, 52, 10113.

[77] M. Deichman, C. Näther, R. Herges, *Org. Lett*., **2003**, 5, 1269.

[78] R. Herges, M. Deichmann, J. Grunenberg, G. Bucher., *Chem. Phys. Lett*., **2000**, 327, 149.

[79] D.G. Whitten, J.C. Russell, R.H. Schmehl, *Tetrahedron* **1982**, 38, 2455.

[80] I.Kraljic, N. Barboy, J.P. Leicknam, *Photochem. Photobio.*, **1980**. 31. 351.

[81] E. Heilbronner, *Tetrahedron Lett.* , **1964**, 29, 1923.

[82] A. Frost, B. Musulin, *J. Chem. Phys*., **1953**, 21, 572

[83] H. E. Zimmerman, *J. Am. Chem. Soc.* ,**1966**, 88, 1564.

[84] H. E. Zimmerman, *J. Am. Chem. Soc.* ,**1966**, 88, 1566.

[85] R.W.A. Havrnith, J.H.V. Lenthe, L.W. Jenneskens, *International journal of Quantum Chemistry*, **2001**, 85, 52.

[86] S.M. Johanson, I.C. Paul, *J. Chem. Soc. B*, **1970**, 643.

[87] J.F.M. Oth, J.M. Gilles, *Tetrahedron Lett.*, **1968**, 6259.

[88] C. Castro, C.M. Isbron, W.L. Karney, M. Mauksch, P.v.R. Schleyer, *Organic Lett.* , **2002**, 4, 3431.

[89] B. W. Metcalf, F. Sondheimer, *J. Am. Chem. Soc.* , **1971**, 93, 6675.

[90] D. M. Walba, R. M. Richards, R. C. Haltiwanger, *J. Am. Chem. Soc.* , **1982**, 104, 3219.

[91] S. Tanda, T. Tsuneta, Y. Okajima, K. Inagaki, K. Yamaya, N. Hatakenaka, *Nature* **2003**, 417, 397.

[92]] H. Hopf, Classics in hydrocarbon chemistry, WILEY-VCH Verlag Gmbh, **2000**, 213.

[94] M. Avram, I. G. Dinulescu, E. Marica, G. Mateescu, E. Sliam, C. D. Nentizescu, *Chem. Ber*., **1964**, 97, 382.

[95] H.E. Zimmermann, *J. Am. Chem. Soc*., **1966**, 88, 1564.

i[96] T.M. Krygowski, M.K. Cyranski, *Chem. Rev.* , **2001**, 101, 1385.

Lebenslauf

Persönliche Daten

Name:	Dariush Ajami
Geburtsdatum:	01.03.1975, Teheran, Iran

Schulbildung

1980-1985	Grundschule Teheran,Iran
1985-1988	Orientierungsstufe, Teheran,Iran
1988-1992	Gymnasium, Teheran, Iran

Hochschulstudium

1993-1997	B.sc. (Chemie) Isfahan University, Isfahan, Iran
1997-1999	M.Sc. (Organische Chemie) Chemistry and Chemical Engineering Research Center of Iran, Teheran, Iran Betreuer: Prof.Dr. M.M.Heravi
Seit Feb. 2000	Promotionsarbeit am Institut für Organische Chemie der TU Braunschweig in der arbeitsgruppe von Prof. Dr. Rainer Herges
Apr. 2001	Wechsel mit Prof. Dr. Rainer Herges an das Institut für Organische Chemie der Christain-Alberchts-Universität Zu Kiel.